Optimization of high-density sludge process for maximum value recovery

By

Leo Folifac

A thesis submitted in fulfilment of the requirements for the degree

Doctor of Engineering: Chemical Engineering

In the Faculty of Engineering and Built environment

At the Cape Peninsula University of Technology

Supervisor: Tunde, V. Ojumu

Co-Supervisor: Prof Leslie, F. Petrik

Bellville Campus

November 2022

DECLARATION

I, Leo Folifac, declare that the contents of this thesis represent my own unaided work and that the thesis has not previously been submitted for academic examination towards any qualification. Furthermore, it represents my own opinions and not necessarily those of the Cape Peninsula University of Technology.

…… ……

Signed Date

ABSTRACT

The Republic of South Africa is one of the countries in the world that makes extensive use of its natural resources. Mining operators who are in charge of these heavy mining activities may abandon their mining sites when the mineral resources are depleted without following proper government procedures for mine closure. In this line of investigation, the abandoned pyritic rock tailings (in the abandoned mine) when exposed to water and air form a waste material known as acid mine drainage. The hazardous waste generated by mining activities is not limited to South Africa but is a global environmental issue. The South African government's policy for mining industries in the country encourages maximum exploitation of natural resources with near-zero waste discharge to the environment. The application of this policy entails the treatment of acid mine drainage (AMD), which is currently proving difficult due to the high costs associated with it. This challenge inspired this research, which aims to obtain a value-added material (nano-iron) from AMD and significantly cut down the amount of lime used for the neutralization of the pre-treated AMD as opposed to direct neutralization, thereby offsetting treatment costs. The field AMD samples used for beneficiation in this study were collected in South Africa and characterized both physically and chemically to determine the quality of the solutions. The physical characterization of the AMD samples revealed low pH, high electronic conductivity (EC), and total dissolved solids (TDS), whereas the chemical characterization revealed high dissolved metals and elevated sulphate concentration. These dissolved metals are toxic and include Fe, Ca, Mg, Al, Mn, and others. The complex chemical composition of acid mine drainage has exacerbated the problem of AMD treatment. Different approaches have been used to treat AMD, which could produce good-quality water even if it is unfit for human consumption. Chemical treatment is the most common and appropriate method for treating AMD, but it generates a large amount of sludge, which adds to treatment costs.

The South African mine water used for this research was collected from three mining sites of the Navigation coal mine in Mpumalanga Province: Penstock (P), Toeseep (T), and Kopseer (K). These AMD samples were elementally analyzed to determine if they were iron-rich AMD samples. The pH values of these AMD samples were P=2.14±0.02, T=2.20±0.03, and K=2.08±0.02 respectively. The AMD samples were classified as acidic with poor water quality by TWQR guidelines for potable water. The IC and ICP analyses revealed that all three mine water samples (P, T, or K) contained SO^{2-}_4, Al, As, Ba, Ca, Cd, Co, Cr, Cu, Fe, Na, Mg, Mn, Mo, Ni, Pb, Se, Be, B, Li, Hg, P, Sb, Si, Sr, Th, Y, and Zn in varying concentrations (see Table 4.6). As a reminder, the motivation for this study stemmed from the high cost of treating AMD, which contains toxic elements and has an acidic pH. Although the synthesis of nano-iron from

AMD using an unfriendly chemical reductant (sodium borohydride) has been reported in the literature, the synthesis of nano-iron particles from AMD using a chemical and an environmentally friendly reductant (green tea extract) prior to lime neutralization of their corresponding supernatant has not been reported. The production of nano-iron from AMD prior to lime neutralization reduces the amount of lime used to neutralize AMD by nearly half, lowering its treatment costs.

The aim of this study was achieved by first selecting which iron-rich field AMD sample from the three characterized Navigation coal mine AMD solutions was going to be utilized in this study. The choice was made due to the availability of the iron-rich AMD sample as well as economic considerations. In this case, the Penstock AMD was chosen as the iron-rich AMD sample used for this study. The production of nano-iron from the Penstock AMD solution using a chemical reductant (sodium borohydride) was optimized using time and concentration, whereas the production of nano-iron from AMD using an environmentally friendly reductant (green tea extract) was optimized using mass of extract, temperature, and time. Following that, the pre-treated AMD solutions were characterized using ion chromatography (IC) and inductively coupled plasma mass spectrometry (ICP-MS) prior to lime neutralization. The pre-treated AMD neutralization process was optimized by varying the amount of lime used to achieve a specific pH and gypsum product. In summary, the first phase of this study was carried out to remove iron as nano-iron from the AMD solution, and the second phase was carried out to neutralize the pre-treated AMD solution with lime. This experimental approach was devised in such a way that the traditional sludge generation process during AMD liming could be avoided, and the mass of lime used for the neutralization process could be cut in half compared to direct neutralization of the AMD solution, resulting in cost savings. In order to identify the nano-iron product synthesized from AMD using reductants, the following characterization was done X-ray Diffraction (XRD), scanning electron microscopy-energy dispersive spectroscopy (SEM/EDS), scanning transmission microscopy (STEM), and Fourier transform infrared (FTIR).

The pre-treated AMD neutralization process was optimized by varying the amount of lime used to achieve a specific pH and gypsum product. In summary, the first phase of this study was carried out to remove iron from the AMD solution, and the second phase was carried out to neutralize the pre-treated AMD, which was characterized using X-ray fluorescence (XRF) to determine the level of purity of the gypsum product. However, when neutralizing sodium borohydride pre-treated AMD with lime, the solid product contained more calcite than gypsum, and when neutralizing green tea pre-treated AMD with lime, the solid product contained more gypsum than calcite.

The nano-iron products synthesized from AMD were applied as solid catalysts in the decolourization of methylene blue. The ultraviolet visible (UV-vis) analytical technique was used to characterize the decolorized methylene blue solution.

KEYWORDS

Acid mine drainage

Reductant

Sodium borohydride

Green tea extract

Nano-iron

Pre-treated acid mine drainage

Lime neutralization

Characterization

Synthesis

Extraction

DEDICATION

This dissertation is dedicated to my closest family members for their unwavering support throughout the course of this study.

- Leo Folifac (Late Father)
- Juliana Ngimdou Folifac (Late Mother)
- Vivian Nguone Folifac (Late Sister)
- Bella-Rose Folifac (child)
- Wilson Tatianu Folifac (Brother)
- Quinta Tschafac Folifac (Sister)
- Christina Nzondia Folifac (Sister)
- Carolina Ebiaso (Sister)
- Philemon Nji Kum (Friend)

ACKNOWLEDGEMENTS

I would like to thank the Lord God in His supremacy for providing the strength, inspiration, and ability to complete this study, as well as His love and provision whenever I needed it.

My further acknowledgements go to the following people:

- Prof T.V Ojumu, my supervisor, for allowing me to complete my postgraduate studies under his supervision. I appreciate his ongoing support and insight throughout the project, as well as his advice, mentorship, and guidance, and for always being willing to listen. For being enthusiastic and always willing to help.

- Prof. L.F Petrik, my co-supervisor, for believing in me when I did not, for showing me love, care, and support, and for always being available when I needed her help. I would like to thank her for her inspiration, advice, courage, and, most importantly, the financial support she provided throughout the course of the study. I would like to thank her for her excellent supervision and insightful contributions throughout the research.

- Prof, J. Broadhurst, for giving me the opportunity to take part in the WRC project and for her technical and financial input throughout the course of my Ph.D.

- ENS Research Group, my second family, for their love, encouragement, and support, as well as all of the interactions that made my Ph.D. journey so interesting

- Water research commission of South Africa for their financial support and encouragement

- Emmanuel Ahmed for his help in lab work and encouragement. He believed in me, motivated me, and advised whereabouts.
- Alicia Botes from CAF, for her help in SEM and STEM analysis
- Charney Small from CAF for her help in the ICP-MS analysis
- Ilse Wells from UWC for her assistance with ICP-OES analysis.
- The staff at AL Abbotts and associates for their help in IC analysis.
- The Staff at Scientific services for their help in XRF and ICP analysis
- Randall J from CPUT for his help with FTIR analysis.
- My loved ones for their love, support, motivation, and advice.
- For my friends' support, aspiration, care, and love (Dr Juvet Malonda Shabani, Dr Awetunji, Joy Okoli, Bukhabane Serutla, and Njikum Philomon)

TABLE OF CONTENT

LIST OF FIGURES

LIST OF TABLES

PUBLICATION AND CONFERENCES

Journal manuscript under review for publication

Folifac, L., Ojumu T.V., and Petrik, L., (2022). Production of nanoparticles from South Africa acid mine drainage using reductants for the application in the degradation of methylene blue

Folifac, L., Ojumu T.V., and Petrik, L., (2022). Integrating Nano Iron production into the Neutralization process of Acid Mine Drainage

Published report

Folifac L, Broadhurst J, Petrik L, Ameh AE, J Jason A Jehoma, W Gitari. Integrating Nano Iron Production into the Acid Mine Drainage Neutralisation Treatment Process. Report to the water research commission of South Africa.

Published manuscript journal (Co-authoring)

Kimpiab, E., Kapiamba, K.F., Folifac, L., Oyekola, O. and Petrik, L., 2022. Synthesis of Stabilized Iron Nanoparticles from Acid Mine Drainage and Rooibos Tea for Application as a Fenton-like Catalyst. *ACS omega*, *7*(28), pp.24423-24431.

CHAPTER 1
INTRODUCTION

1.0 Introduction

This chapter presents the overall introduction of this study and an overview of the research topic. It also presents the background, problem statement, rationale and motivation of the research, aims and objectives, research questions, hypothesis, scope, delimitation of the study, research approach, and the dissertation framework.

1.1 Background

South Africa's water resources are under increasing strain, necessitating the development of integrated water management solutions and cross-sectoral partnerships. Acid mine drainage (AMD) is a major issue in South Africa, particularly in the Witwatersrand goldfields and the Mpumalanga coalfields. Acid mine drainage has a significant environmental and economic impact due to its corrosive nature and high salt and metal content. Several approaches and technologies have been identified and developed for the treatment of acid mine drainage, with neutralization with limestone and/or lime being the most used due to their simplicity and cost-effectiveness. The improved and widely used high-density sludge (HDS) process configuration produces denser and more stable sludge than traditional lime neutralization, reducing disposal space and costs (Bullen, 2006; Kuyucak et al., 1999). However, due to the scale of the AMD problem in South Africa, the HDS neutralization process generates significant amounts of sludge, while the treated effluent still contains elevated soluble sulphate salts and is generally unfit for consumption or use, as well as posing a risk to major water sources and the natural environment due to salinization (Lourenco & Curtis, 2021). In response to these concerns, as well as the growing recognition of mine water as a potentially valuable resource in a water-stressed country, South Africa's coal mining industry has successfully implemented two mine water reclamation plants in the Mpumalanga coalfields (Hutton et al., 2009a; Randall et al., 2011; Sekar et al., 2014).These plants employ multi-stage processes, including reverse osmosis (RO), to recover potable water, which is then used to supplement the local municipal water supply (Hutton et al., 2009a; Randall et al., 2011). A further paradigm shift has occurred in the treatment and management of HDS sludges and RO brines, with the recovery of useful and saleable byproducts being actively researched and, in some cases, pursued. For example, the sludge produced in the current HDS process at the eMalahleni Water Reclamation Plant (EWTP) is currently being used in the agricultural sector whereas Glencore

recently announced plans to recover salts and ice from RO brines using the eutectic freeze crystallisation (EFC) process developed at UCT. These mine water treatment plants, while progressive and integrated, are not without challenges, both operationally and economically. The treatment processes are relatively expensive, and the mixed sludge produced by the HDS process is of low quality and value. Variability in feed stream compositions also has an adverse effect on performance, making it difficult for treatment processes to achieve and maintain optimum efficiency. Although the EWTP has traditionally blended mine waters to produce a relatively consistent feed stream, the plant is currently being expanded and modified to treat high and low-acidity mine waters in separate circuits. However, preliminary commissioning trials have revealed the need for further research into the relationship between the chemical composition of the feed solution and plant operating conditions, particularly the interrelated parameters of lime dosage and pH, in order to optimize plant performance in terms of both output characteristics (effluent water and sludge) and economic efficiency.

The recovery of higher-end products from HDS process sludge has the potential to make treatment technologies more cost-effective and economically appealing while remaining consistent with sustainable development principles and related concepts such as resource efficiency, the circular economy, and industrial ecology. Because of the high iron content of acid mine drainage, the possibility exists of recovering iron products such as pigments and other industrial products. Iron oxides like magnetite and ferrite, as well as zerovalent iron (ZVF), have a wide range of applications, including water treatment and coal washing. Iron oxide and ZVF nanoparticles (100 nm) have been discovered to have several advantages over micrometric particles for wastewater treatment, with nanotechnology being one of the fastest-growing sectors of high-tech economies. Previous research (Wei & Viadero, 2007; Alexander & Ristow, 2010; Cheng et al., 2011; Akinwekomi et al., 2017; Alegbe et al., 2018) has demonstrated the feasibility of recovering iron oxides (magnetite and ferrite) and zerovalent nano-iron (ZVNF) from AMD and using it to remove metals. However, these studies have been relatively limited, with little emphasis placed on the integration of iron recovery into a multi-stage water management system that generates fit-for-purpose water and useful byproducts in a cost-effective manner. This is not a simple task; it necessitates a thorough understanding of the effects of key parameters on the performance of individual processes and their interactions with upstream and downstream processes, particularly in terms of output properties. This understanding, in turn, can serve to inform R&D campaigns to optimize the neutralisation process in terms of desirable output stream properties, as well as aid in the effective operation of an operating neutralisation operation by enabling the potential effects of variability in input stream compositions (AMD feed and neutralising reagents).

1.1.1 Production of acid mine drainage

Acid mine drainage is produced when waste rocks or tailings undergo pyritic oxidation in the presence of water. The typical elemental composition of AMD includes trace and major elements. As, Ba, Be, Ca, Cd, Co, Cu, Hg, Li, Mo, Ni, Pb, Se, Si, Ti, Zn, and Zr are examples of trace elements, while major elements include sulphate, chloride, nitrate, Al, Fe, Mn, Mg, and Na (Gitari et al., 2011a). Among the major elements found in AMD, iron (Fe) is the most dominant cation, while sulphate (SO^{2-}_4) is the most dominant anion (Azzie, 2002). AMD's physicochemical characteristics include a low pH, high electrical conductivity (EC), and a yellow colour (Blgham et al., 1990; Gaikwad & Gupta, 2008).

South Africa produces billions of litres of AMD each year. According to van Zyl et al. (2001), approximately 175 ML (mega liter) of AMD was produced per day, with 120 ML stored in the Pretoria area. According to this investigation, Witwatersrand produced 350 ML of AMD per day. The treated Witwatersrand water was estimated to supply 10% of Gauteng province's daily potable water for urban distribution at a cost of R3000/ML (CSIR, 2009). In general, the cost of treating acid mine drainage to meet the standard for release or any other purpose is high.

1.1.2 Nano-iron particles

Iron is a transition element in the periodic table's d-block due to its valence shell electrons in the d-orbital. It is also the fourth most abundant element on the planet. There are two types of iron: bulk zerovalent iron and nano zerovalent iron. Because of the small particle size and increased surface area of nano zerovalent iron, its physicochemical properties differ from those of bulk zerovalent iron. Iron nanoparticles are extremely reactive and can be measured on a nanoscale (1-1000 nm) (Alegbe et al., 2019). A variety of iron source materials can be used to create iron nanoparticles. Rocks, tailings, sand, and commercial reagents are examples of these materials, while its oxide form can be found in iron minerals such as wustite (Cornell & Schwertmann, 2003; Mohapatra & Anand, 2010), hematite, and magnetite, among others. Iron nanoparticles can be created using a variety of techniques. These methods include chemical precipitation, hydrolysis, electrochemical techniques, the sonotonic method, sol-gel, aerosol techniques, microemulsion methods, and surfactant mediated techniques (Wu et al., 2008; Mohapatra & Anand, 2010). The nano-iron synthesis methods described above are complex and expensive. The majority of techniques used in the extraction of Fe from its ores are designed to produce bulk or granular Fe with particle sizes in the micron-meter range

(Shoumkova, 2011). The purpose of this research is to use direct precipitation to generate nano-iron particles from AMD wastewater using low-cost, environmentally friendly reductants.

1.1.3 Treatment of acid mine drainage and wastewater

AMD can be treated using either active or passive technologies. Passive technologies are less expensive and have lower recurring costs than active technologies, which require machinery and maintenance and generate a large volume of sludge from the neutralization reaction with lime or caustic soda (Wei & Viadero, 2007; Menezes et al., 2010). AMD is actively treated with alkali reagents such as NaOH, Na_2CO_3, CaO, NH_3, or caustic soda. This raises the pH level and produces dissolved metal sludge in the form of hydroxide sludge. In general, chemical treatment can provide effective AMD remediation. However, this process incurs high treatment and disposal costs for the generated bulk sludge (Matlock et al., 2002; Johnson & Hallberg, 2005a; Skousen et al., 2013). In this line of research, a method for systematically extracting useful and significant elements such as Fe, Al, SO_4, etc., from AMD is required. The value of these extracted elements can affect the cost of AMD treatment while also being useful in other processes. The primary goal of this research is to selectively synthesize nano-iron particles from a specific iron-rich field AMD for the decolorization of methylene blue in solution. In keeping with recent research, iron-rich AMD has been reported as an alternative source of iron salt for chemically synthesizing nano-iron particles (Alegbe et al., 2019). However, studies have not shown that low-cost green reductants could be used to make nano-iron particles from AMD before neutralization to cut down on treatment costs.

The application of green reductants for the synthesis of nanomaterials (such as Fe nanoparticles) has been the focus of research. These nanoparticles have properties such as high reactivity, selectivity, large surface area, and strong affinity that can be used in wastewater treatment (Zhang et al., 2006; Müller and Nowack, 2010). Over the last decade, iron nanoparticles have attracted a lot of attention for their potential use in the treatment of groundwater and contaminated sites. Due to their small size and high reactivity, these particles can be used in the in-situ treatment of wastewater, as opposed to granular Fe, which can only be used for reactive barriers. Some research has suggested that zerovalent nano-iron particles (nZVI) can be used to transform halogenated organic contaminants and heavy metals (Zhang, 2003). It has also been demonstrated that zerovalent nano-iron particles synthesized from AMD using sodium borohydride can be used to treat AMD and other wastewater. These studies have shown that wastewater can be treated with zerovalent nano-iron particles while producing very little waste (Johnson & Hallberg, 2005a). Zerovalent nano-iron particles are less

expensive and have advantages over traditional treatment methods, such as reduced waste generation, treatment of organic and inorganic contaminants, and odour neutralization of sulfidic compounds (Alegbe et al., 2019). Because of their highly reactive, effective, and compatible nature, nano-iron particles have been shown in studies to be compatible with other treatments to produce non-hazardous end products (Gillham & O'Hannesin, 1994; O'Carroll et al., 2013). The main source of ferric iron used in the synthesis of nano-iron particles has been commercial iron salt (Wang and Zhang, 1997). These nano-iron particles are used in environmental cleanup and other processes.

This study's approach is to synthesize nano-iron particles from AMD in a cheap and cost-effective manner by using green reductants with a sufficiently high ferric-reducing antioxidant potential (FRAP) value that can act as reducing agents to ferric or ferrous iron salt in the AMD solution prior to neutralizing the generated supernatant. This study will also compare nano-iron particles synthesized from AMD using chemicals to nano-iron particles synthesized from AMD using green reductants. Finally, the AMD-based nano-iron will be used to decolourise methylene blue in solution.

1.1.4 Rationale and motivation of the research

Some communities in South Africa are still suffering from water scarcity as a result of contamination caused by the mining industry. This has drawn the attention of the public and private sectors to the need to find a long-term solution to the problem. The high cost of pumping water into and out of mines, as well as chemical treatment, has resulted in the abandonment of mining sites.

The rationale and motivation for this study stem from the fact that AMD should be investigated for beneficiation such as extracting valuable substances. Nanotechnology is a relatively new technology that can be used to beneficiate wastewater such as acid mine drainage. According to Wei et al. (2005) and Alegbe et al. (2019), iron-rich AMD is acid water that is rich in ferrous and ferric ions and can serve as an excellent source of iron salt. This can be used to produce nano-iron of comparable quality to that produced with reagent-grade chemicals (Wei & Viadero, 2007; Alegbe et al., 2019). Nano-iron made from AMD should also be cheaper than nano-iron made from reagent-grade chemicals (Alegbe et al., 2019). Even though using reagent-grade chemicals to generate nano-iron is expensive, it treats water with minimal waste (Zhang,

2003). In the presence of moderate reductants, nano-iron is a powerful catalyst that can be synthesized from reagent-grade ferric or ferrous iron salt.

1.1.5 Problem statement

The major issue confronting the mining industry and the South African government is the production of large amounts of acid mine drainage, caused by the dissolution of pyrite rocks in the presence of air and water. The South African government has established some regulatory mechanisms to monitor the activities of mining operators while also reducing environmental pollution. This has, however, resulted in the abandonment of some mining sites by some mining operators due to unfavourable government regulations or legislation. In this regard, mining operators have labelled the treatment of AMD generated by mining activities as costly. This is due to the chemicals used in AMD treatment and the production of a large amount of sludge for disposal. According to the CSIR (2009), AMD treatment costs approximately R3000/ML. This has become a financial burden for mining operators and opens the door to the abandonment of mining sites, which may result in more AMD polluting the environment. Secondly, water used for mining is not a free natural resource, so purchasing water from the government for this purpose raises the cost of mining and contributes to more acid mine drainage. The advantage of mining in South Africa is that it produces highly valuable commodities such as gold, diamonds, and coal, but it also produces AMD, which is a difficult and costly waste product to treat. The “pollute and pay” policy also puts a strain on mining operators because the Government imposes a hefty fine if mining operators do not follow the strict rules. This study aims to find a way to cut down on the cost of treating AMD by synthesizing value-added products from AMD that will offset AMD treatment costs.

1.2 Aims and Objectives

The aims of this study are as follows:

- To synthesize nano-iron particles from acid mine drainage (AMD)
- To treat AMD directly with reductants
- To treat AMD and iron depleted AMD with lime for comparative purposes

The objectives of this study are as follows:

- To produce nano-iron from AMD by utilizing chemical and environmentally friendly reductants.
- To compare the efficacy of chemical and green reductants in the decolourization of methylene blue.
- To treat AMD directly using chemical and environmentally friendly green reductants.
- To treat AMD with lime both before and after nano-iron extraction
- To compare the quality of sludge produced by neutralizing AMD both before and after nano-iron extraction using reductants.
- To characterize nano-iron particles produced from AMD, generated supernatants, and sludge produced from AMD after liming.
- To utilize AMD-based nano-iron particles in the decolourisation of methylene blue.

1.2 Research questions

- Is AMD water from South Africa's Mpumalanga region a good source of ferric or ferrous iron?
- Will applying chemical or green reductants directly to AMD be a good method of cleaning AMD?
- Is it possible to synthesize nano-iron particles out of AMD water?
- Is it possible to obtain high-quality nano-iron particles from AMD?
- What elements apart from Fe are associated with the chemically synthesized or green-synthesized nano-iron particles?
- Are the properties of nano-iron derived from AMD different from those derived from other sources?
- Is it possible to decolourise methylene blue contaminated water using AMD based nano-iron particles?
- Is the project environmentally friendly and cost-effective?
- Is the sludge produced after nano-iron synthesis from AMD completely iron-free?

1.3 Hypothesis of the study

AMD samples rich in iron can serve as a foundation for the synthesis of high-quality nano-iron particles using an environmentally friendly reductant with moderate ferric-reducing antioxidant potential (FRAP) and DPPH.

Nano iron particles synthesised from AMD can be used to decolourise methylene blue.

1.5 Purpose of this research

The primary goal of this research is to investigate if green extracts with moderate ferric-reducing antioxidant potential (FRAP) values can be used to synthesize high-quality nano-iron particles from AMD, which serves as a source of iron salt prior to post-liming. This method might be used to clean the acid water in a cost-effective manner. AMD water that has been treated could be reused for other purposes, such as irrigation and agriculture. The AMD-based nano-iron particles could be used in the treatment of water contaminated by methylene blue.

1.6 Scope of the study

The purpose of this research is to synthesize nano-iron particles from AMD prior to liming. For the synthesis of zerovalent nano-iron particles from AMD, chemical and green reductants were used. Lime was used to neutralize the iron-depleted AMD. The zerovalent nano-iron particles synthesised from AMD were used in the removal of nitrate from wastewater treatment.

1.7 Research approach

The experimental approach of this study used AMD and chemical or green reductants as feedstock materials for the synthesis of nano-iron particles prior to liming of the generated supernatant. Analytical techniques such as ion chromatography (IC), inductively coupled plasma mass spectrometry (ICP-MS), dissolved oxygen (DO), pH, electronic conductivity (EC), and total dissolved solid (TDS) were used to fully characterize the AMD solution. The iron from the AMD solution was reduced using chemical or green reductants to produce nano-iron particles. The synthesized nano-iron particles were analyzed using X-ray diffraction (XRD), scanning electron microscopy-electron dispersive spectroscopy (SEM-EDS), scanning transmission electron microscopy (STEM), and fourier transform infrared (FT-IR). The generated AMD supernatant after the removal of iron from AMD using reductants was analyzed using ion chromatography (IC) and inductively coupled plasma mass spectrometry (ICP-MS) before and after neutralisation with lime. The sludge generated after lime neutralisation of the AMD supernatant was characterized using X-ray fluorescence (XRF). Finally, the AMD-based nano-iron particles were applied in the treatment of methylene blue

contaminated water. The treated methylene blue contaminated water was analysed using ultraviolet visible (UV-vis).

1.8 Delineation of the research

Among the different types of South African acid mine drainage, the Navigation coal mine as-received field AMD samples were chosen as starting materials for this study. This was based on their high iron salt concentration. For the purpose of time and cost, this study only investigated the feasibility of green and chemical reductants that were used for the synthesis of nano-iron particles from AMD. This choice was motivated by the importance of synthesizing inexpensive, high-quality, and environmentally friendly nano-iron particles from AMD. The AMD-based iron nanoparticles were used in preliminary experiments for methylene blue decolorization.

1.9 Significance of the study

This study used a low-cost method to demonstrate that some plants can be used to synthesize high-quality nano-iron particles from AMD in an environmentally friendly manner. As a result, it served as a medium for both beneficiating AMD and offsetting its high treatment costs. Following the completion of this study, mining and wastewater treatment companies might benefit from the fact that AMD can provide cheap, high-quality, stable, and affordable nano-iron particles for wastewater treatment.

1.10 Structure of the thesis

This thesis consists of nine chapters. These include the introduction as chapter 1, literature review (chapter 2), research methodology (chapter 3), results and discussion (chapters 4-8) which comprise and reports on the characterization of AMD feedstock (chapter 4), characterization of AMD supernatant (chapter 5), characterization of nano-iron particles synthesized from AMD (chapter 6), characterization of neutralized supernatant and sludge generated (chapter 7), and application of the synthesized nano-iron particles in wastewater treatment. Lastly, chapter 9 presents the conclusion and recommendations to the study, followed by list of bibliographic references.

Chapter 1: Introduction

This chapter includes a general introduction to the study, background, study motivation, problem statement, aims and objectives, research question, hypothesis, the rationale of the study, scope, experimental approach, and thesis structure.

Chapter 2: Literature review

Chapter 2 provides a detailed review of AMD, including its sources, causes, composition, formation, characterization, treatment methods, and environmental impact. It will also review pertinent literature on nano-iron particles, including their sources, properties, structures, and synthesis. The use of nano-iron particles (nZVI) and nanotechnologies is covered. A brief summary of the chapter follows.

Chapter 3: Research methodology

This chapter contains detailed information about all the samples as well as the study area where samples were collected for analysis. The chemicals, equipment, and procedures utilized in this study are described. Finally, the instruments used and the operating parameters necessary for characterization are discussed.

Chapter 4: Characterisation of feedstock

The characterization of the as-received AMD, pretreated AMD, and plant extracts is presented and discussed in this chapter. The feedstock samples were characterized physically and chemically using pH, EC, DO, TDS, IC, CP-OES, FRAP, and DPPH.

Chapter 5: Characterization of AMD supernatant after treatment of AMD with reductants

The purpose of this chapter is to characterize the AMD supernatant produced after AMD was treated with chemical and green reductants. Characterization methods include ICP and ICP-OES analytical techniques.

Chapter 6: Characterization of nano-iron particles synthesized from AMD

This chapter describes the use of chemical and green reductants to treat AMD by synthesizing nano-iron particles from AMD. The obtained products were characterized using the following analytical techniques: XRD, SEM-EDS, Image J particle size analyzer, FTIR, and TEM for solid residues, and pH, EC, IC, and ICP for liquid supernatant.

Chapter 7: Neutralisation test work: AMD and pretreated AMD

This chapter presents and discusses the results of AMD neutralization using lime before and after iron extraction. The generated solid residues from the neutralization test work were characterized using XRD, IC, and ICP-OES, while the generated supernatant was characterized using IC and ICP-OES neutralisation.

Chapter 8: Application of synthesized nano-iron particles

This chapter describes and discusses the use of nano-iron particles synthesized from AMD in the treatment of water contaminated with methylene blue. The treated water was characterized using UV-vis.

Chapter 9: Conclusion and recommendations

The ninth chapter of this study contains its conclusion and recommendations. It will demonstrate the significance of using environmentally friendly and cost-effective antioxidants for the extraction of nano-iron particles from AMD and its application in the treatment of contaminated water .

CHAPTER 2
LITERATURE REVIEW

2.0 Introduction

Mine water has become a major hydrological and geochemical problem as a result of human exploitation of the earth's natural resources. The composition of mine water is determined by the type of ore mined and the chemical additives employed in the mineral and hydrometallurgical processing. It is the primary focus of this research to investigate the iron and sulphate-rich acid mine drainage that occurs in the Mpumalanga coalfields of South Africa.

This chapter presents an overview of published literature relevant to AMD and its treatment, with a special emphasis on the recovery of by-products, particularly nano-iron, as well as the treatment of AMD. An investigation into the prospective applications and standards for both gypsum and iron byproducts in the local context was carried out.

2.1 Background: sources, properties, effects, and prevention of acid mine drainage

2.1.1 Origin and sources of AMD

AMD is formed when weathered, naturally occurring sulphide minerals are exposed to air and water. Sulphide minerals found in rocks include pyrite (FeS_2), pyrrhotite ($Fe_{(1-x)}S$), arsenopyrite (FeAsS), bornite ($CuFeS_4$), chalcopyrite ($CuFeS_2$), chalcocite (Cu_2S), chalcocite (CuS), covellite (CuS), and galena (PbS) (Broadhurst et al., 2019a). For the most part, iron sulfides are the most common minerals that occur as unwanted (gangue) material in metallic ore coal deposits. The sulphides of iron, particularly pyrite, are the most common of these minerals. Aside from the fact that acid mine drainage can occur naturally, it is most often associated with anthropogenic activities such as construction and, in particular, the extraction and early beneficiation of sulfide-bearing hard rock ores and coal deposits. This is because the excavation of sulphide-bearing ores followed by mineral liberation exposes the surfaces of sulphide minerals to water and oxygen, causing them to corrode and decompose (Broadhurst et al., 2019a). Due to its status as a gangue mineral, exposed pyrite is separated from the targeted minerals as much as possible during the extraction and early processing stages, and the majority of it is deported to the mined rock face or to the large volume of waste generated during the subsequent processing steps of crushing, milling, and concentration of the run-of-mine ore. Point sources of AMD, on the other hand, are typically found in defunct mine shafts

with sulphide-bearing rock faces, mine waste impoundments (tailings, waste rock, discards, and overburden), and ore stockpiles, among other things. AMD pollution is a significant source of concern in South Africa, particularly in the Witwatersrand Basin and the Mpumalanga Province, where both the gold and coal mining industries operate. AMD pollution in South Africa is the subject of several previous Water Research Commission reports, which provide information on the causes and sources of AMD pollution (see for example Harrison et al., 2010a; Broadhurst et al., 2019b).

2.1.2 The mechanism of AMD formation

AMD is formed as a result of series of chemical events, which are depicted in equations 2.1 to 2.4 (Evangelou and Zhang, 2009; Stumm, 2012). Pyrite, the most common sulphide mineral, is oxidized in the presence of oxygen and water, resulting in the formation of ferrous iron, sulphate, and acid (equation 2.1).

$2FeS_2 + 7O_2 + 2H_2O \rightarrow 2Fe^{2+} + 4SO_4^{2+} + 4H^+$	(2.1)

In the presence of dissolved oxygen, the ferrous iron formed undergoes further oxidation, resulting in the formation of ferric iron and acid (Equation 2.2).

$4Fe^{2+} + O_2 + 4H^+ \rightarrow 4Fe^{3+} + 2H_2O$	(2.2)

Hydrolysis of Fe^{3+} at pH greater than 3.5 results in the precipitation of ferric hydroxide, Fe(OH)3, as well as the release of additional acid

$4Fe^{3+} + 12H_2O \rightarrow 4Fe(OH)_3 + 12H$	(2.3)

Equation 2.4 shows that at lower pH values, soluble ferric ions act as an effective pyrite oxidant, as shown by the results.

$FeS_2 + 14Fe^{3+} + 8H_2O \rightarrow 15Fe^{2+} + 2SO_4^{2-} + 16H^+$	(2.4)

Once the supply of Fe^{3+} or FeS_2 is depleted, the cyclic propagation of acid production will stop. Catalyzing micro-organisms plays an important role in the oxidation of mine tailings or wastes by catalyzing intermediate soluble sulphur forms and the oxidation of ferrous iron (Scheetz and Earle, 1998; Evangelou and Zhang, 2009; Johnson, 2003; Kucera et al., 2013; Dumett et

al., 2014). T. ferrooxidans (iron- and sulphur-oxidising bacteria), T. thiooxidans (sulfur-oxidising bacteria), and F. ferrooxidans (iron-oxidising bacteria) are the most prevalent microorganisms implicated in AMD production. In the presence of acid-consuming minerals such as carbonates, silicates, and clays, which may be found in pyrite ores, wastes, and the surrounding geology, the acid created by the oxidative breakdown of pyrite can be neutralized. In terms of neutralizing capacity and reaction rates, acid-neutralizing minerals can be distinguished by their wide range of properties. Carbonate minerals, the most common of which are limestone ($CaCO_3$) and dolomite ($CaMg(CO_3)_2$), weather quickly, whereas silicate minerals weather slowly and have lesser neutralizing properties. The net formation of AMD at any point source is ultimately a consequence of the relative rates and extent of the acid-generating and acid-neutralizing processes, which will differ depending on the mineralogy and geochemistry of the ores, wastes, and host ecosystems. Other elements that influence the rate and scope of AMD generation and dispersion in the natural environment include the hydrogeology of the area, the climate (temperature and rainfall), microbial populations, and waste and mine management procedures, among other things. Most of these characteristics are connected and entail protracted spatial and temporal scales that makes it challenging to predict AMD.

2.1.3 Characteristics of AMD

Mine water is often classified according to a number of characteristics (Lottermoser, 2007). The pH of mine water is an important property, with mine waters classified as acidic (pH<6), alkaline (pH > 8), or circumneutral (pH 6-8) (Morin & Hutt, 2001). Piper or trilinear diagrams are used to classify mine fluids according to their principal cations and anions. The major cations (Ca^{2+}, Mg^{2+}, Na^{+}, K^{+}) and anions (Cl^{-}, SO_4^{2-}, CO_3^{2}-, HCO^{3-}) are plotted on the diagrams. According to these diagrams, uncontaminated shallow groundwaters are often classified as calcium bicarbonate water, deep groundwaters as sodium bicarbonate water, and contaminated mine water as calcium sulphate water. Additionally, the percentage of transition metals and metalloids in mine water is of special importance in determining the overall quality of mine water. Contaminated mine water is usually enriched in metals and semi-metals, the concentrations of which are extremely dependent on both the geology of the area and the pH of the water in question. Ficklin diagrams are used to classify mine water in accordance with both pH and the total concentration of six dissolved heavy metals (Cd, Co, Cu, Ni, Pb, Zn) considered typical for mine waters (Ficklin et al., 1992). A common way to evaluate the overall concentration of cations, anions, metals, and semi-metals is by the total dissolved solids (TDS)

content of water, with "high quality" water having a TDS of less than 1000 mg/L and "poor quality" water having a TDS of more than 5000 mg/L. (MCA, 2014).

According to the International Network for Acid Prevention (INAP) (2009), there are three types of mine water:

i) Acid mine drainage (AMD) or acid rock drainage (ARD): AMD has an acidic pH of less than 6, a moderate to high metal content (Fe and Al > 100 mg/L, and Cu, Cr, Ni, Pb, and Zn > 10 mg/L), and elevated sulphate concentrations (greater than 1000 mg/L). Whenever the geological composition of the acid-forming mineral pyrite at the source exceeds that of the comparatively reactive acid-neutralising carbonate minerals (e.g., dolomite and limestone), acid mine/rock drainage (AMD/ARD) results.

ii) Neutral mine drainage (NMD): Neutral mine drainage is characterized by pH values that range from near neutral to alkaline (>6) and low to moderate concentration of metals and sulphate (TDS of less than 1000 mg/L).

iii) Mine drainage that is neutral in nature occurs when the geological composition of relatively reactive acid-neutralising carbonate minerals near its source is equal to or greater than the composition of the reactive acid metal pyrite.

Saline drainage (SD) is characterised as being neutral to alkaline (pH>6), having low pH, transition metal content, and a moderate concentration of the anions sulphate, calcium, and/or magnesium (TDS>1000 mg/L) in the drainage.

It is the primary focus of this research to examine the iron and sulphate-rich acid mine drainage that is commonly found in the Mpumalanga coalfields. Even though AMD varies considerably between places and over time, Table 2-1 summarizes AMD treated in water treatment plants in the Mpumalanga coalfields as well as the Witwatersrand goldfields.

In accordance with the findings in Table 2-1, AMD decant from coal mines has a low pH and a high TDS, as well as higher amounts of sulphate, calcium, magnesium, iron, manganese, and aluminium. The metals iron, manganese, and aluminum are particularly high in comparison to drinking water requirements (400-700 times higher). In line with previous research (for example Gunther, 2006; Annandale et al., 2009), mine water from collieries in Mpumalanga, the Free State, and the Limpopo Provinces includes increased amounts of metals and salts, even in cases where the pH is neutral or slightly acidic.

In the decant water from the Witwatersrand goldfields, similar trends are found, although the compositions of the decant water vary greatly depending on whether it is from the Western, Central, or Eastern basin. The presence of elevated quantities of uranium, as well as other potentially dangerous trace elements and semi-metals such as Ni, Cr, As, Cd, Zn, and Pb in AMD formed from obsolete mine workings and tailings dumps in the Witwatersrand goldfields, is of special concern (Broadhurst et al., 2019b). In gold ore deposits, several of these elements are coupled with the mineral pyrite, and thus migrate to the leachate during AMD formation.

Table 2. 1: Typical characteristics of AMD in the Witwatersrand goldfields (DWAF, 2013) and Mpumalanga coalfields (Gunther et al., 2006)

Water quality parameter	Units	Drinking water limits	Mpumalanga coalfields	Witwatersrand goldfields		
				Western basin	Central basin	Eastern basin
pH	@ 25°C	6.5-8.5	2.7	2.7	2.4	5.9
Acidity	mg/L as $CaCO_3$		1050	1255	34	560
Conductivity	mS/m @ 25°C		460	426	465	363
TDS	mg/L	500	4930	5388	5118	3358
Ca	mg/L	*32*	660	823	563	421
Mg	mg/L	*30*	230	-	258	166
Na	mg/L	*200*	130	243	171	264
SO_4	mg/L	400	3090	3410	3062	2289
Cl	mg/L	250	70	-	146	254
Fe	mg/L	0.3	210	799	108	227
Al	mg/L	0.1	40	-	193	2
Mn	mg/L	0.1	35	114	50	6
U	µg/L	30	_	100	695	470

Where: Drinking water limits are derived from IRMA (2016), except for values in italics which are from DWAF (1996)

2.1.4 Impacts and effects of AMD

Emissions of salt-laden and metal-enriched AMD from mine workings and waste dumps can contaminate and pollute the local environment, with negative consequences for natural ecosystems, human health, and local community livelihoods such as farming and fishing. Sections 2.1.4.1 – 2.1.4.4 summarize these interconnected impacts and effects (Broadhurst et al., 2019c)

2.1.4.1 Environmental pollution and degradation

Across the world, AMD is often regarded as the major surface water and groundwater water quality hazard associated with the mining sector. In South Africa, AMD is particularly common in the Witwatersrand goldfields and the Mpumalanga coalfields, among other places (Oelofse et al., 2007; Vermeulen et al., 2008). AMD also has the additional effect of degrading soil quality and fertility due to acidification, salinization, and the deposition of metal-rich secondary precipitates, among other things (Vermeulen et al., 2008).

An investigation by the South African Department of Water Affairs (now the Department of Water and Sanitation) found that coal mining around the Wilge, Bronkhorstspruit, Klein Olifants and Olifants Rivers was the most significant contributor to poor water quality and in-stream conditions (CER, 2016). It is also important to note the rise in salinization levels in the area's rivers, with elevated salt levels in the Witbank and Middleburg dams over the period 1972-2007 being directly linked to the coal mining industry (McCarthy, 2009). This is also a problem raised in the most recent Mine Water Atlas published by the South African Water Research Commission (WRC, 2017), which states:

> “When it comes to the main stem of the Olifants River and many of its tributaries, the upper Olifants watershed is generally in an undesirable state, although the situation improves to a bearable state at Loskop Dam. The salinity of the middle Olifants River is within a bearable range, while the salinity of the Lower Olifants River within the Kruger National Park improves to an acceptable level. Several tributaries, notably the Elands River, Wilge River, Steelpoort, and Ga-Selati, are in fair to acceptable condition in the upper reaches of the catchments but deteriorate to unacceptable salinity ranges in the lower reaches of the catchments before confluence with the Olifants River."

There have been numerous studies conducted in the Witwatersrand goldfields that have documented the contamination of water sources and soils as a result of AMD containing

elevated salt levels and high levels of metals (Pulles et al., 1992; Rösner and van Schalkwyk, 2000; Naicker et al., 2003; Tutu et al., 2008; Samuel, 2009; Durand, 2012; Taylor and Maphorogo, 2015). According to this prior research, the quantity of contaminants such as arsenic, cadmium, mercury, lead, and aluminium in the water surrounding defunct mine dumps in the region often exceeds international and national criteria in the water. As documented in reports by Kootbodien (2012), Samuel (2009), and a study conducted by the Federation for a Sustainable Environment (Cairncross et al., 2013), soils in the vicinity of defunct gold mines and tailings facilities are also contaminated with toxic metals such as arsenic, cadmium, cobalt, copper, mercury, manganese, nickel, zinc. In 2011, the National Nuclear Regulator of South Africa acknowledged that the radiation levels were 15 times greater than the levels permitted by the country's nuclear regulations (Cairncross et al., 2013)

2.1.4.2 Wellbeing of the ecosystem

AMD-contaminated ecosystems pose a significant threat to plants and living organisms due to acidity, dissolved metals, and secondary precipitate deposition (Merovich & Petty, 2007; Petty et al., 2010). A study by LeFevre and Sharpe (2002) found that when AMD is released into freshwater systems, it has an effect on the population of organisms and on the assemblages of invertebrates, algae, fish, and amphibians. Chemical pollutants such as acid and metals have negative toxicological effects on aquatic ecosystems, resulting in deformities, mortality, injuries, growth disorders, and low reproduction rates (Chadwick, 2013; Chibuike and Obiora, 2014), while the formation of secondary precipitates has an impact on organisms living at the bottom of streams by obstructing vision, contaminating food sources, and physically impairing breathing systems. According to Simate & Ndlovu (2014), fishing populations can be significantly decreased, if not completely eradicated, under certain conditions.

A detrimental impact on soil microbial activities is also caused by high concentrations of metals, which result in a reduction in soil microbial population and distribution, as well as poor microbial enzymatic activities (Sobolev and Begonia, 2008; Ngole-Jeme and Fantke, 2017). As a result of excessive levels of metals in soils, arthropod populations, as well as small and large mammals, have all suffered as a result of the contamination (Migliorini et al., 2004; Gall et al., 2015). According to research conducted by Eisler (2004), arsenic (As) dosages ranging from 17 mg/kg to 48 mg/kg body weight are fatal to birds, but doses ranging from 2.5 mg/kg body weight are harmful to some mammals following oral exposure (Mpode Ngole-Jeme and Fantke, 2017). Direct and indirect effects on plants have both been observed in the past. The contamination of soils by acid rock drainage (ARD) has negative consequences on the growth

and development of plants (Simate and Ndlovu, 2014). The toxicity and acidity (low pH) of the metals in ARD cause the soils to become waterlogged and compacted, which makes it hard for seeds to grow and for water and air to get into the soil system.

2.1.4.3 Wellbeing of the community

Aside from the health consequences, contamination of soils and water can lower soil productivity and have negative effects on the viability of crops and the health of livestock, reducing the land's ability to support agricultural and other farming activities. Contamination of soils and water can also cause soil erosion (Mangena and Brent, 2006; Simate and Ndlovu, 2014). As previously stated, exposure of soils to AMD through seepage, run-off, or irrigation can reduce soil fertility and productivity, thereby affecting the growth and quality of vegetables and other crops, as well as the productivity of other crops (IHRC 2016). Additionally, water that has come into contact with AMD is unsuitable for use as drinking water for animals and humans and can have a negative impact on livestock fertility and milk production, among other things (Bjureby et al., 2009; Simate and Ndlovu, 2014).

Hota and Behera (2015) conducted a study in Odisha to assess the impact of coal mining on agriculture and human health. They discovered that the costs incurred to the local communities, in terms of decreased agricultural production and increased medical expenses, were significant. The pollution of land and water caused by ARD resulting from coal mining resulted in a loss of livelihood from fishing and agriculture. Locally, according to a report by the Centre for Environmental Resources (CER, 2016), the impact of mining activities in the Mpumalanga region is so severe that farming activities cannot be sustained on the land in the majority of cases. The adverse effect of soil acidification from AMD on maize production was of particular concern, given that a large portion of the province's open-pit workings is located on the old maize triangle. According to the Benchmarks Foundation (2015), this has also had an impact on agricultural exports, as farmers have lost European clients.

2.1.4.4 Wellbeing of mammalian

In addition to the elevated concentrations of metals and semi-metals in water sources, soils, and food sources (such as crops and fish), AMD pollution can cause elevated concentrations of metals and semi-metals to accumulate in the environment. Some metals, such as iron, cobalt, and zinc, are essential nutrients, while others, such as the platinum group metals and gold, are relatively harmless. However, they may have physical or aesthetic effects, and at

high concentrations, they can become toxic. In addition to lead and arsenic, other metals (for example, cadmium, mercury, and arsenic) are extremely toxic, even at low concentration levels (Duruibe et al., 2007; Morais, 2012). Because these metals are not easily biodegradable, they can accumulate in vital organs and glands such as the heart, liver, kidney, and brain after ingestion, impairing their function and causing a variety of ailments depending on whether the exposure was acute or chronic (Demirezen and Aksoy, 2006; Rashid et al., 2008). There are a variety of ailments ranging from neurotoxic to carcinogenic actions, with poisoning caused by metal exposure affecting most major human physiological systems, such as the skeletal and nervous systems, as well as the respiratory, excretory, and digestive systems (Menezes et al., 2009; Jomova and Valko, 2011; Morais, 2012). In many cases, children are at greater risk of absorbing metals from the environment and subsequently suffering from associated health problems and contact with contaminated soil, and consumption of food grown in local vegetable gardens continues to be a source of concern for the public health community (IHRC, 2016).

2.1.5 AMD management and containment

Approaches to AMD mitigation can be divided into two categories: those that treat and contain AMD after it has been generated, and those that prevent AMD formation and/or subsequent generation. Sections 2.1.6.1 and 2.1.6.2 summarize these approaches. A more detailed review of AMD management and mitigation approaches and techniques is available on the International Network for Acid Prevention website.

2.1.6 AMD treatment techniques

Treatment strategies aim to prevent the transport and dispersion of AMD into the surrounding environment rather than preventing its generation at the source. Although end-of-pipe treatment is generally regarded as incompatible with cleaner production principles, treatment strategies may still be required as a temporary or permanent measure to prevent off-site contamination by AMD from previous operations and/or to be used in conjunction with AMD minimisation and prevention techniques. AMD treatment strategies are commonly classified as active or passive, though hybrid active-passive treatment processes are also available.

2.1.6.1 Active treatment techniques

Active treatment achieves better mine water quality through the application of technologies that require continual inputs of artificial energy, biochemical or chemical reagents. Active treatment solutions are becoming increasingly popular, and their methods of treatment entail the installation of a water treatment plant that is regularly monitored by trained personnel. Due to precise process control in the active treatment of AMD, it has the advantage of being able to handle any fluctuations in mine water quality and quantity. This is the most significant advantage of active treatment. If land availability is a constraint, active treatment is also preferable to passive treatment. However, because of the continuous input of electricity and reagents, as well as the requirement of experienced staff to operate and maintain AMD treatment units, this technique is both resource-intensive and expensive to implement. Furthermore, active treatment methods generate enormous volumes of waste, such as brines and sludge, which are difficult to dewater and are expensive to transport and dispose of after they have been processed. A number of active technologies are available, including neutralisation, chemical precipitation (which is frequently used in conjunction with neutralisation), membrane processes, ion exchange, and biological sulphate reduction. The most popular and well-developed active AMD treatment strategy involves the use of limestone and/or lime to neutralize acid mine drainage. Mine water treatment with limestone reduces acidity from mine water by generating alkalinity through the dissolution of limestone (Equations 2.5-2.7).

$CaCO_3 + H^+ \leftrightarrow Ca^{2+} + CO_2 + H_2O$	(2.5)

$CaCO_3+H_2O+CO_2 \leftrightarrow Ca^{2+}+2HCO$	(2.6)

$CaCO_3+H_2O \leftrightarrow Ca^{2+}+HCO^-+OH$	(2.7)

Metals such as Fe and Al are removed by the formation of hydroxide precipitates (see equations 2.8 and 2.9), whereas sulphate concentration in mine water is reduced by the reaction of Ca2+ ions from lime or limestone to form gypsum (Equation 2.10)

$Fe^{3+}(aq)+3HCO_3^-(aq) \rightarrow Fe(OH)_3(s)+3CO_2(g)$	(2.8)

$Al^{3+}(aq)+3HCO_3^-(aq) \rightarrow Al(OH)_3(s)+3CO_2(g)$	(2.9)

$Ca^{2+}(aq)+SO_4^2(aq)+H_2O \rightarrow CaSO_4.2H_2O(s$	(2.10)

Limestone has the ability to increase the pH to neutral or circumneutral levels (6-7). These pH values are not high enough to effectively remove several metals, including base metals, magnesium, and manganese. Due to the use of lime, the pH can be changed to alkaline levels (9-11), which aids in the removal of metals in the form of hydroxides or oxyhydroxides. It is also possible to employ limestone and lime as part of a two-stage neutralisation process that is integrated. The traditional method of lime/limestone neutralisation results in sludge with a low density (2-5% solids) that is difficult to thicken and filter. The high-density sludge (HDS) process is a refinement of the low-density treatment method, and it has the ability to significantly reduce sludge volume (by up to 95 percent) by significantly increasing the density of the sludge (normally to around 20-30%). A neutralizing agent (limestone or lime) and recycled sludge from a clarifier/thickener unit is added to the incoming effluent during the first stage of the HDS process. Following neutralization, this mixture is delivered into the main lime reactor, where a combination of aggressive aeration and high shear agitation ensures that the process chemistry and clarifier performance are at their best. The discharge from the lime reactor is then treated with flocculant in the flocculation tank in order to induce precipitation before being transferred to the clarifier/thickener unit for further treatment. The clarifier is responsible for separating the treated effluent from the sludge, with a portion of the sludge being recycled back to the beginning of the process. Due to the fact that the HDS technique is well established and relatively cost-effective, it is the most widely used method for treating AMD today. It is employed as a short-term remedy to manage AMD decant from closed gold mines in the Witwatersrand basin, with plants on the Western, Central, and Eastern limbs each having the ability to treat 35, 84, and 110 Mega litters per day respectively of AMD. Because sludge generation continues to be large, the disposal of this waste adds significantly to the overall operating costs of the facility.

Lime and limestone are both expensive and have large environmental impacts, making them unsuitable for many applications. As an alternative strategy, it is possible to use waste products that are relatively affordable and readily available in the local community as neutralizing reagents. Treatment of acid mine drainage with coal fly ash is one of the new approaches now being investigated for the long-term treatment of acid mine drainage in South Africa. Aluminosilicic acid (aluminosilicate) waste produced by the combustion of coal in the creation of electricity in coal-fired power plants is known as coal fly ash (CFA). The lime species found in the CFA is the one most commonly used for the neutralization and treatment of mine wastewater (Gitari et al., 2011a). Due to the fact that these power stations are generally located close to coal mines in South Africa, the transportation costs of CFA to the

treatment facilities are reduced significantly. High-energy mixing devices such as a jet loop reactor have also been shown to improve the dissolution of the fly ash matrix as well as improve the kinetics of reactions while simultaneously lowering the amount of fly ash utilized in the treatment process (Madzivire et al., 2010).

In spite of the fact that neutralisation processes such as the HDS process are effective in reducing most metals to levels that are safe for human consumption, sulphate concentrations in potable water typically remain above the required World Health Organisation (WHO) and Department of Water and Sanitation (DWS) limits for potable water (400 mg/L) due to the fact that gypsum is partially soluble in water. According to the composition and ionic strength of the solution, gypsum has a solubility range of 1500 mg/L to 2000 mg/L, and its solubility rises in the presence of ions such as Mg^{2+}, Na^{+}, and K^{+}. As a result, high density sludge (HDS) is most effective when used as a pre-treatment for AMD before further desalination. In a special report to the South African Inter-Ministerial Committee on Acid Mine Drainage (IMC, 2010), many techniques for desalinization of pre-treated AMD, as well as direct treatment of NMD and SD, have been proposed.

- Mintek, a South African research and development group, created the SAVMIN method, which is based on the selective precipitation of insoluble complexes at various phases of the treatment process, as well as the recycling of some of the chemicals employed in the process. This method results in the production of drinkable water and potentially marketable byproducts.
- In South Africa, Key Plan Pty (Ltd) successfully developed the high-pressure reverse osmosis (HiPRO) membrane process for converting saline water to potable water.
- SPARRO (slurry precipitation and recycle reverse osmosis) is a variation on the membrane desalination process. SPARRO is based on the concept of protecting membrane surfaces by supplying a slurry suspension onto which precipitation products can form. High water recoveries were achieved in a demonstration scale plant (Pulles et al. 1992).
- The Environmental and Remedial Technology Holdings (EARTH) (Pty) Ltd ion exchange process was used to purify mine water before discharge or re-use as potable water. It was developed by Environmental and Remedial Technology Holdings (Earth) (Pty) Ltd for the purification of mine water prior to discharge or re-use as agricultural, process, industrial, or potable water. As a result of the process, potable water is produced as well as valuable and marketable waste products such as ammonium

sulphate solution and mixed metal nitrate solution. A steady price environment and a stable product market are required for the feasibility of this technology.

- The Rhodes BioSURE process was developed in the early 1990s by the Environmental Biotechnology Group at Rhodes University in South Africa (EBRU). The process involves biological sulphate reduction using free waste feedstock, such as sewage sludge, rather than expensive carbon and electron donor sources, which would otherwise be required (ethanol and hydrogen). At the Grootvlei gold mine, the East Rand Water Care Company (ERWAT) has used BioSURE on a pilot plant scale to demonstrate its effectiveness

- The Magnesium-Barium-Alkali (MBA) Process, developed by the Tshwane University of Technology, is a chemical precipitation process that is based on the CSIR ABC Process. $Mg(OH)_2$ and $Ba(OH)_2$ are used as neutralizing and sulphate removal reagents in this process respectively. Sulphate is removed from solution in the form of $BaSO_4$.

- Treatment of 1000 L of acid mine drainage with coal fly ash in a jet loop reactor pilot plant was developed at the University of the Western Cape. The results showed that the concentration of major contaminants (sulphate, Al, Fe, Ca, Mg) and minor contaminants in treated AMD can be significantly reduced (by one to four orders of magnitude) compared to raw AMD. Depending on the degree of dewatering required for slurry pumping, the one-step treatment process recovered at least 66.6% (728.56 kg) of treated water (Kalombe et al., 2020)

Only the HiPRO process has been implemented on a commercial scale. The eMalahleni Water Reclamation Plant (EWRP) is one of the plants that uses a combination of lime neutralisation (HDS process), reverse osmosis (HiPRO process), and ultrafiltration to treat contaminated mine water from three operating Anglo mines and one defunct coal mine owned by South32 in Mpumalanga Province, removing 99% of the metals and salts. This plant, which was first operational in 2007, produced 30 ML/day of potable water, 25 ML/day of which was sold to the eMalahleni municipality. It has recently been expanded and modified to treat mine water from additional collieries and increase capacity to 50 ML/day. Following the success of the EWRP, a mine water reclamation demonstration plant was built at the Optimum opencast coal mine in Mpumalanga (Cogho & van Niekerk, 2009), which was followed by the construction of a second full-scale plant at Glencore's Tweefontein Colliery in 2016. When NMD is treated at

the Tweefontein plant to drinking water standards, the HiPRO desalination process is used. This results in the production of 15-20 ML/day of potable water, with a portion of this water being supplied to the local municipality at municipal rates.

The selection of appropriate treatment technology is influenced by a number of factors, including mine water composition, discharge rates and quantities, the end-use of the treated water, and legislative requirements for use, and the associated costs. In reality, there is no technical limit to the water quality that can be achieved using current available techniques; however, the cost and financial risk associated with the development and implementation of unproven technology is frequently the limiting factor. As a result, rather than technological limitations, the choice of a treatment technique is influenced by economic and environmental factors.

2.1.6.2 Passive treatment techniques

As previously stated, active treatment processes are costly, which has historically resulted in AMD being untreated or only partially treated, particularly when discharges have been from "orphan" or remote sites (Akcil & Koldas, 2006). Passive treatment strategies that require fewer resources could be an option. Although they are not perfect solutions, passive treatment refers to processes that do not necessitate regular human intervention, operations, or maintenance. As a result, they should ideally be designed to operate for many years without requiring a major retrofit to replenish materials and without requiring electrical power. Natural construction materials and processes should be used as much as possible in passive treatment strategies. Passive mine water treatment methods can be divided into two categories: biological and chemical. Biological passive treatment technologies typically involve channelling contaminated mine water through an environment containing sulphate-reducing bacteria or plants, such as constructed wetlands (Wieder, 1982; Hedin et al., 1994; Steed et al., 2000; Neculita et al., 2007). Wetlands are commonly used to treat low-flow, acidic streams or as a final polishing stage for pre-treated AMD. In practice, wetlands reduce acidity and remove metals and salts from mine water through a variety of physical, chemical, and biological processes such as adsorption, reduction, and oxidation. Passive chemical methods typically involve the use of drains filled with limestone gravel or a reactive barrier. Permeable reactive barriers are built in the latter case by excavating a portion of the aquifer ahead of the contaminated plume and replacing it with a reactive mixture. These reactive mixtures are typically organic carbon-based to promote bacterial sulphate reduction and metal sulphide precipitation at the same time.

Passive treatment methods for mine water have low operating costs and require little maintenance. Passive treatment systems are also more visually appealing and can be integrated into surrounding ecosystems. However, passive systems necessitate large areas of land to accommodate high flow and/or discharge highly contaminated mine water. These systems are unpredictable (particularly in terms of long-term sustainability) and provide limited options.

2.1.7 AMD prevention

Prevention strategies, in contrast to treatment strategies, are aimed at minimising or eliminating the formation of AMD at the source (for example, by preventing the exposure of pyrite surfaces to oxygen and/or water at the rock face or waste pile), or point of origin (for example, by generating wastes that are non-acid generating in the first instance), or both.

2.1.7.1 Generating benign mine waste

Desulphurization and waste blending are two strategies that can be used to generate non-acid generating wastes prior to disposing of them. Desulphurisation is the process of removing acid-forming sulphide minerals by employing physical separation techniques such as gravity separation or froth flotation. Regardless of the fact that flotation has not yet been applied on a commercial scale, laboratory studies have demonstrated that it can be used to effectively remove sulphur from base metal tailings and fine coal wastes, resulting in bulk waste streams that do not contain acid-generating substances (Harrison et al., 2010b). Encapsulation or conversion of the sulphide-enriched stream into valuable by-products are two options for dealing with this type of waste stream.

Mine waste composites which do not contain acid-generating materials can also be created prior to disposal by mixing or agglomerating mine waste with acid-neutralizing materials. For example, the blending of pyritic tailings (an acid-producing material) with coal fly ash (CFA) results in a composite material that causes the least amount of damage to the surrounding environment. The lime present in the CFA reacts with the liquid to form hydrated calcium silicate, which is highly resistant to corrosion and liquid ingress (Adriano et al., 1980; Halstead, 1986; Scheetz & Earle, 1998b). Additionally, kiln dust and steel slag have been used as alkaline blends.

2.1.7.2 Preventing exposure of sulphide surfaces

A variety of techniques has been developed to avoid exposing sulphide surfaces to air and oxygen within mine waste deposits and rockface surfaces, at both the bulk and particle levels:

Bactericides are detergent-based reagents that break down the greasy film on the surface of the acidophilic bacteria's cell wall. The use of anionic surfactants, such as sodium dodecyl sulphate (SDS), is both highly toxic to microorganisms and relatively inexpensive. However, the effect is only temporary, and thus the control of AMD is only temporary (Watzlaf, 1988; Schippers et al., 1998; Johnson & Hallberg, 2005b).

Micro-encapsulation entails the production of inert coatings, such as those produced by the reaction of AMD-producing mine waste with hydrogen peroxide and phosphate. During the process, hydrogen peroxide oxidizes pyrite, resulting in ferric iron precipitating as iron phosphate to coat the pyrite surfaces. Humic acid, oxalic acid, and sodium silicate are other coating agents that have been suggested.

Macro-encapsulation/capping involves the use of wet covers, dry covers (such as soils, geofabrics, and/or alkaline materials), or covers made of oxygen-consuming materials (such as peat, sewage sludge and composted municipal solid waste). These covers act as a barrier between mine waste and the elements (oxygen and/or water) that react with sulfide minerals. Tailings that have been mixed with alkaline materials can also be used as capping material. Agglomerates formed by mixing mine tailings with fly ash and Portland cement, for example, have been found to be effective in reducing AMD formation in base metal tailing impoundments (Misra et al., 1996; Benzaazoua et al., 2004)

Sub-aqueous deposition reduces sulphide oxidation in tailings because the oxygen diffusion coefficient in water is 10,000 times lower than in air and can be influenced by waste disposal into flooded open pits or subsurface workings, man-made or natural lakes or impoundments, or the marine environment. Disposal at natural lake and marine sites, on the other hand, may be restricted due to public and regulatory concerns. Furthermore, even if acid production is reduced, metal release may still be significant. This problem may be alleviated by a biologically active organic layer (wetland) and the presence of sulphate-reducing bacteria.

As with sub-aqueous tailings disposal, flooding and/or sealing can be used to reduce the formation of AMD in defunct underground shafts. Mineral-oxidizing microorganisms in mine water consume the dissolved oxygen present, and replenishment of dissolved oxygen via mass transfer and diffusion is hampered further when the mine is sealed (Johnson, 2003b).

Sealing underground mine shafts, adits, and stopes reduces AMD formation by preventing water and air ingress, as well as preventing polluted water from flowing out of flooded mine workings (Johnson & Hallberg, 2005b). The anticipated hydraulic pressure that the seal will have to withstand when the sealing process is completed is the primary factor that can affect the selection, design, and construction of underground mine seals.

Backfilling of defunct mine workings provides opportunities for reducing surface disposal of mine waste while also avoiding the formation of AMD in defunct mine workings. Backfill materials commonly used include waste rock, sand, or mine tailings, which are often blended with cement. Because coal combustion fly ash (FA) has pozzolanic properties, it can be used in place of cement in backfill applications. The permeability of CFA slurry backfill has been found to be lower than that of mine tailings or soils, resulting in less hazardous element leaching (Jorgenson and Crooke, 2003). Fly-ash residues from AMD treatment, combined with 3% cement, have also been proposed as a potentially suitable backfill material (Gitari et al., 2008; Gitari et al., 2009; Vadapalli et al., 2014). To effectively prevent AMD formation and dispersion, more than one approach or method will be required in many cases. For example, sulphide separation combined with water covers, elevated water table, and barrier covers may be the best-combined system for a specific tailings impoundment. While the costs and economic viability will vary depending on the site, preventative measures such as covers and mine sealing are typically expensive. Synthetic and complex multi-layer covers in particular can have application costs that are double those of soils and are thus only used at smaller sites.

2.2 Valuables recovery from AMD and their uses

2.2.1 Overview of potential valuables from AMD

AMD has traditionally been regarded as a waste emission, requiring treatment simply to ensure that it does not exceed the limits set by local legislation when discharged into the environment. These treatment techniques are expensive, and as laws become more severe, the costs increase even further. Sludge and brine generated by conventional treatment techniques can amount to between 25% and 30% of the entire costs of the operation, depending on how they are handled and disposed of. It is becoming widely recognized that AMD and/or the sludges created during AMD treatment are potentially useful, if not lucrative, by-products that can be recovered and used in other applications. More recently, the recovery of water as well as the recovery of additional commodities such as rare earth and base metals, sulphuric acid, iron salts and oxides, and gypsum-based products have received more

attention. Using AMD and AMD treatment sludges to recover valuable by-products can help reduce the cost on waste disposal while also offsetting the costs of the treatment and value recovery process. From Sections 2.2.1.1 through 2.2.1.6, different products that can be created from AMD are presented.

2.2.1.1 AMD as a valuable treatment agent

AMD has been discovered to be an effective flocculant for the removal of metals and harmful elements from wastewater. AMD containing Ca, Al, and Fe, in particular, can be used to remove phosphorous from wastewater from the industrial, agricultural, and domestic sectors. For example, research has shown that AMD can be used to treat or remove metals and phosphorous from dairy waste (Reddy et al., 1999), and mine water from a copper mine complex in Falun, Sweden, was used as a flocculating agent in the treatment of municipal sewage at Framby treatment plant (Banks et al., 2012).

2.2.1.2 Water as a valuable product

Water is, without a doubt, one of the most valuable products that can be produced from AMD. Many mining operations operate in water-stressed locations around the world, and although mines may be dealing with an excess of groundwater entering mine workings, the surrounding people are dealing with a scarcity of water on the surface. Exactly because of this quandary, the eMalahleni Water Reclamation Plant (EWRP) in the Mpumalanga Province of South Africa was built to treat AMD from coal mines in the region. Since its construction, this plant has produced roughly 25 ML/day of potable water for the local municipality, meeting approximately 12% of the city's daily water requirements and successfully providing drinking water for approximately 60 000 people. A second AMD treatment plant in the vicinity, which uses the HiPRO desalination method to produce 15-20 ML/day of potable water, is now under construction. Energy demanding and expensive, the treatment of AMD to meet potable water standards is a time-consuming and expensive endeavour, and the expense of supplying drinking water to local towns in Mpumalanga is mainly subsidized by the mining industry. AMD could yield water of lower quality that would require less substantial treatment and could be used for agricultural or even industrial purposes. As a result, AMD treatment costs, energy usage, and sludge creation can be lowered while still delivering water that is fit for purposes other than human consumption. A demonstration project on 60 ha of allocated land on the

Mafube Colliery in the Mpumalanga Province is being carried out by the Mine Water Coordinating Body (MWCB), the South African Water Research Commission (WRC), Anglo Coal, Exxaro, and South32, which is using poor quality NMD (neutral mine drainage) and SD (saline drainage) to cultivate salt-tolerant crops such as soybean and wheat (Mining Review, 2017).

2.2.1.3 High-value metals

Several processes have been developed to recover potentially valuable metals (such as Cu, Zn, and Co) from AMD, for example sulphide precipitation, copper cementation with metallic iron, direct electrowinning, ion exchange, solvent extraction, as well as combinations of these technologies. Sulphuric acid has also been recovered using diffusion dialysis from AMD. Previous authors, such as Bowell et al. (2016), have discussed these processes in depth.

2.2.1.4 Valuable salts

Desalination processes such as nanofiltration and reverse osmosis generate large amounts of salt-laden brine, which is typically disposed of in the ocean or large evaporating ponds. The simultaneous recovery of potable quality water and individual monovalent and divalent metal sulphate salts, such as $CaSO_4.2H_2O$, $MgSO_4$, $Na2SO_4$, and K_2SO_4 from these brines via evaporative or freeze Crystallisation is possible (Randall et al., 2011b; Randall & Nathoo, 2015). At the Tweefontein Colliery in Mpumalanga, the world's first commercial plant for EFC of brines from the reverse osmosis treatment of AMD was commissioned in 2017. Glencore purchased the unit, which Prentec built and designed based on technology developed at the University of Cape Town's Department of Chemical Engineering. This plant recovers 5 ML of desalinated water per day, as well as potentially usable salts from hypersaline brines (Nicolson, 2017).

2.2.1.5 AMD sulphur-based products

Processes for the treatment of AMD are rarely intended to recover sulphur as a major product, in part due to the low monetary value of sulphur and the difficulties in acquiring adequate purity of sulphur. However, a number of techniques offer the possibility of at least partial sulphur recovery as well as the production of gypsum products.

(i) Gypsum product

The main component of the sludge produced by lime or limestone neutralisation of AMD is gypsum or calcium sulphate dehydrate ($CaSO_4 2H2O$). It has a variety of potential applications, particularly in agriculture and construction. Gypsum can be used as a physical soil improver, increasing workability and moisture retention, and as a sulphate source for alkaline soils. It is especially beneficial for crops such as alfalfa, corn, wheat, and peanuts that require a high sulphate content. Gypsum is also widely used in the construction industry as a primary component of plaster and in the production of gypsum board, which is used in wall, ceiling, and partition systems in residential, institutional, and commercial structures. Finally, gypsum can be converted into elemental sulphur, which can then be further processed into sulphuric acid. In the South African context, a number of applications for synthetic gypsum from AMD and other industrial sources has been investigated and these are discussed further in Sections 2.2.2.

(ii) Sulphur and sulphuric acid

Elemental sulphur can be recovered from AMD either directly through biological processes or indirectly through the conversion of sulphate compounds precipitated from AMD in chemical processes, such as barium sulphate and gypsum. Elemental sulphur is used to make a variety of products such as fungicides, matches, gunpowder, and synthetic rubber. The main application, however, is in the production of sulphuric acid and, to a lesser extent, phosphatic and nitrogenous fertilizers (MoDiselle M, 2012).

Biosulphate reduction removes sulphate via microbial reduction to hydrogen sulphide while also producing hydroxide ions that neutralize acid. Hydroxide ions react with trivalent metals (Al(III) and Fe(III)) to form oxyhydroxide/hydroxide precipitates, resulting in a mixed metal residue with metal recovery potential. Biological AMD treatment processes, such as the Paques SULFATEQ process, the BioSURE process, and the VitaSOFT process, typically involve two stages. Sulphate is anaerobically converted to sulphide by sulphate-reducing bacteria in the first stage, with metals removed in the form of metal sulphides. The residual sulphide in the effluent from the first stage is converted to high purity elemental sulphur in the second stage by sulphur-oxidizing bacteria, with further alkalinity production (Munnik & Pulles, 2009; IMC, 2010; Mogashane et al., 2020)

Elemental sulphur can also be recovered from AMD chemically by converting barium sulphate or gypsum. Barium salts such as barium hydroxide or barium carbonate are used in barium processes such as the CSIR Alkali-Barium CalciumTM (ABC) Process and the modified

Magnesium-Barium-Alkali (MBA) Process developed by Tshwane University of Technology (Akinwekomi et al., 2017; Munnik & Pulles, 2009; IMC, 2010; Mogashane et al., 2020). Pre-treatment of AMD with limestone and/or lime to remove metals in the form of a mixed metal oxide/gypsum sludge prior to the addition of barium to form a relatively pure barium sulphate precipitate is common in barium treatment processes. Due to the high cost and toxicity of barium salts, barium treatment processes typically include a barium recovery step. The thermal conversion of barium sulphate into barium sulphide and carbon dioxide occurs in this step. After that, barium sulphide is treated with water and carbon dioxide to produce barium carbonate and hydrogen sulphide, which is then converted into elemental sulphur. While the technical viability of ABC technology was demonstrated at a gold mine in 2007/2008, barium processes are reportedly three times more expensive than lime neutralization (DWAF, 2013).

Elemental sulphur can also be produced as a byproduct of gypsum. In a three-step process developed and patented by South Africa's Council for Scientific and Industrial Research (Mbhele et al., 2009; de Beer et al., 2014), elemental sulphur is generated from waste gypsum ($CaSO_4.2H_2O$):

• Conversion of gypsum to calcium sulphide and carbon dioxide via thermal reduction with carbon at temperatures ranging from 900 to 1100°C (Equation 2.11)

$CaSO4\ (s) + 2C\ (s) \rightarrow CaS\ (s) + 2CO2\ (g)$	(2.11)

• Direct aqueous carbonation of CaS to produce hydrogen sulphide (H2S) as a byproduct and low-grade $CaCO_3$ as a byproduct (Equation 2.12):

$CaS(s)+H2O+CO2(g)\rightarrow H2S\ (g) + CaCO3$	(2.12)

• Elemental sulphur recovery from H_2S using the commercially available PiPco process (Equation 2.13):

$2H2S(g)+O_2(g)\rightarrow 2S(s)+2\ H_2O\ (l)$	(2.13)

This process was tested in a laboratory setting with waste gypsum from Stage 2 of the eMalahleni Water Reclamation Plant and FOSKOR. Sulphur produced from stripped H_2S had a purity of between 95 and 96%, with a recovery of 76 to 81%, compared to 91% recovery from pure gypsum. The calcium carbonate (limestone) produced was of low quality, with a $CaCO_3$ content of 90%. Apatite ($Ca5(PO_4)_3OH$) and anhydrite were the major contaminants ($CaSO_4$). In a subsequent study, de Beer et al. (2014) carbonated CaS in two stages to produce both "low purity" (99%) and "high purity" >99% $CaCO_3$, with the latter accounting for

12-23% of total calcium carbonate recovery. The combined metal-rich gypsum sludge from both stages 1 and 2 of the eMalahleni Water Reclamation Plant is converted into elemental sulphur, low purity limestone ($CaCO_3$), and magnesite in a modified version of this patented process known as the Gyp-SliM process ($MgCO_3$). This process (shown in the simplified diagram in Figure 2-1) includes an additional crystallisation step to separate magnesium carbonate from the carbonation sludge, which is a mixture of calcium carbonate, magnesium bicarbonate, and metal-bearing ash (Gunther and Naidu, 2008).

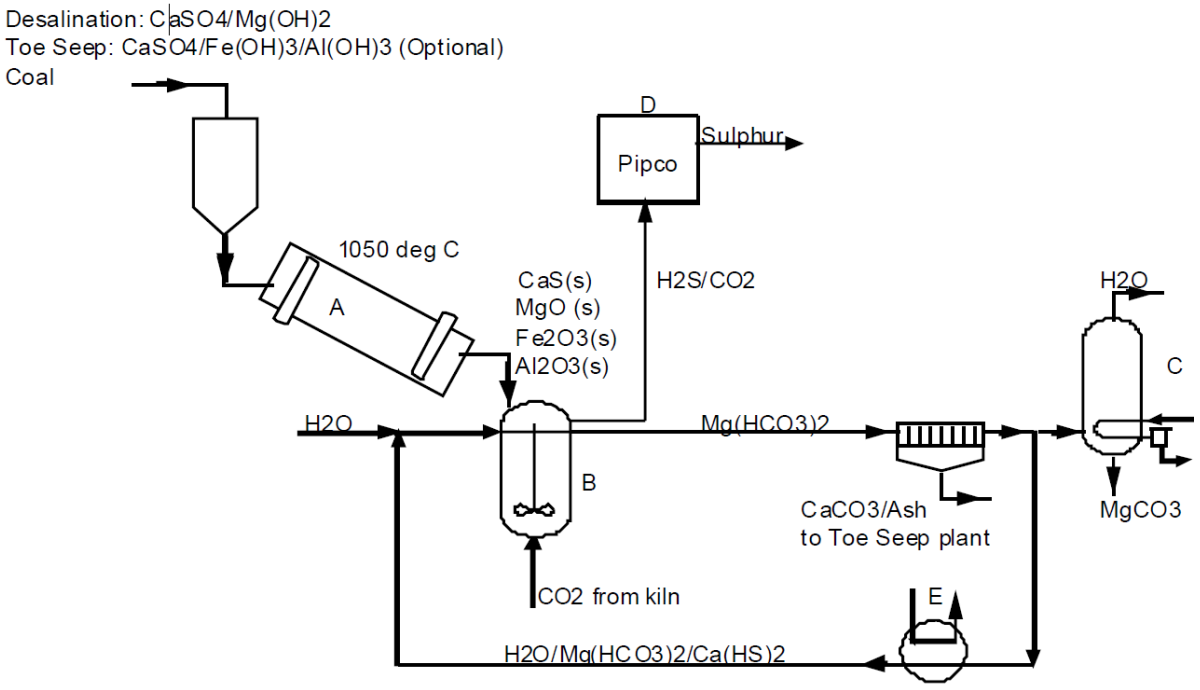

Figure 2. 1: Simplified process flow diagram of the Gyp-SLiM process (Gunther and Naidu, 2008)

2.2.1.6 Iron-based materials (products)

Iron-rich AMD can be used to produce a variety of potentially useful iron products.

(i) Goethite and haematite pigment production

Goethite and hematite are iron oxides that can be used as pigments (yellow and red pigments respectively) in the production of paint, ceramics, resins, and other materials (Hedin et al., 2003; de Almeida Silva et al., 2017; Silva et al., 2019). Iron is initially precipitated from AMD as ferric hydroxide at pH 3.6, using alkali metal hydroxide (e.g NaOH or KOH) in the method proposed in various studies (Hedin et al., 2003; de Almeida Silva et al., 2017; Silva et al., 2019). The ferric hydroxide precipitate is then redissolved with nitric acid before crystallization

of goethite with potassium hydroxide at pH 12. The produced goethite can then be converted to hematite via thermal dehydration, dehydroxilation, or oxidation/reduction (Silva et al., 2012; de Almeida Silva et al., 2017).

(ii) Magnetite

Magnetite has a wide range of industrial applications, including wastewater treatment, ore processing, and use as a magnet in navigational devices. Although magnetite is typically produced from pure ferric or ferrous chlorides and sulphates, Silva et al. (2012) and Akinwekomi et al. (2017) have shown that it can also be produced from AMD using a chemical precipitation process. In both cases, Fe(II) rich solutions were converted to magnetite by forming mixed Fe(II)/Fe(III) hydroxides. Silva et al. (2012) created the Fe(II) rich solutions through a series of steps that included precipitation of ferric hydroxide, re-dissolution of ferric hydroxide in sulphuric acid, and subsequent photoreduction of ferric to ferrous iron using UV radiation. This method recovered more than 96% of the iron.

(iii) Ferrous sulphate heptahydrate (menlanterite)

By reducing ferric iron in AMD to ferrous under UV radiation, ferrous sulphate heptahydrate can be produced (Vigânico et al., 2011). The reduction of iron with UV results in the formation of an OH radical, which has a bactericidal effect and slows the formation of ferric iron (see Equation 2.14)

$4\mathrm{Fe}^{2+} + \mathrm{O}_{2(\mathrm{aq})} + 4\mathrm{H}^{+} \rightarrow 4\mathrm{Fe}^{3+} + 2\mathrm{H}_2\mathrm{O}$	(2.14)

Melanterite (FeSO4.7H2O) crystals are formed as a result of subsequent evaporation and can be used in agricultural applications. Vigânico et al. (2011) created commercial-grade melanterite (99.5% purity) by leaching pyrite-rich coal processing wastes in an acidic solution.

(iv) Ferric sulphate coagulant

Ferric sulphate is one of many reagents commonly used in industrial effluent treatment and domestic water supply (Colling et al., 2011). Menezes et al. (2009b) and Colling et al. (2011) investigated the production of ferric sulphate via bioleaching of pyrite in coal tailings. After that, the solutions were evaporated to produce a coagulant containing 12% iron (w/w). The ferric sulphate-rich coagulant was found to be as effective in wastewater treatment as commercial poly-ferric sulphate made from iron scraps (Colling et al., 2011).

(v) Nano-iron particles

Given the high reactivity of zerovalent nano-iron compared to micro and macro iron, it has a variety of benefits over the latter in water treatment applications. A preliminary investigation

conducted by Alegbe et al. (2018) revealed that treatment of AMD with sodium borohydride results in the production of zerovalent nano-iron (ZVNF), which can be employed for the in-situ removal of metals. In line with this investigation, the iron content of AMD was reduced from 3400 to 1 mg/L, while the concentration of cadmium, selenium, and mercury was also reduced. When it comes to water treatment, ZVNF is the most commonly used compound. Section 2.2.3 has a more in-depth explanation of the ZVNF applications and their implications.

2.2.2 Products recovery and the eMalahleni Water Treatment Plant (EWRP)

2.2.2.1 An overview of the EWRP

As discussed in Section 2.2.5, the eMalahleni Water Reclamation Plant (EWRP) in South Africa's Mpumalanga coalfields was specifically designed to recover potable water for local consumption from AMD and NMD emanating from the surrounding coal mines and dumps, using a three-stage process of lime neutralisation (HDS), reverse osmosis (HiPRO), and ultrafiltration (see Figure 2-2). The HDS process is neutralized in stage 1 water by using slaked lime or limestone, which precipitates the majority of the sulphate and metals in the form of gypsum sludge, which is removed by clarification. Ultrafiltration (UF) is used as a pre-treatment for reverse osmosis (RO), with a permeate recovery rate of 65%. The RO retentate is transported to stage 2, where precipitation is followed by hydrocyclones, clarification, and membrane processes similar to those used in stage 1 (permeate recovery 65%). The RO retentate is further treated in stage 3, which is similar to stage 2, with the formation of a final liquid brine containing the residual salts that were not removed during the neutralisation steps in stages 1 and 2 (Hutton et al., 2009b).

Overall, the EWRP plant effectively removes 99% of the metals and salts from the contaminated mine water in the form of waste, with waste from each stage differing in quantity, form, and composition. In stage 1, the HDS neutralisation process produces a metal-rich gypsum sludge composed of gypsum and oxyhydroxides of Fe, Al, Mg, Mn, and Zn. The sludge, also known as clay-based gypsum, has been found to have high concentrations of Ba, Cu, Ni, Ti, and Zr (Gunther and Naidu, 2008). The neutralization of the RO retentate in stage 2 of the plant produces additional gypsum sludge. This gypsum, which accounts for 20% of total gypsum generated by the EWRP, contains fewer metals than stage 1 gypsum sludge and is also known as white gypsum. It is also said to contain traces of Mg, Al, Cr, Cu, Fe, Mn, Sr, Ti, Zn, and Zr (Gunther and Naidu, 2008). Finally, the liquid brine reject produced in stage 3 is primarily composed of salts, specifically, Na, K, Ca, sulphate, and chloride, as well as Mg,

ammonium, chloride, and bicarbonate (Randall et al., 2011c). Other metals such as Fe, Li, Mn, and Sr have been found in trace concentrations in brine waste (Gunther and Naidu, 2008).

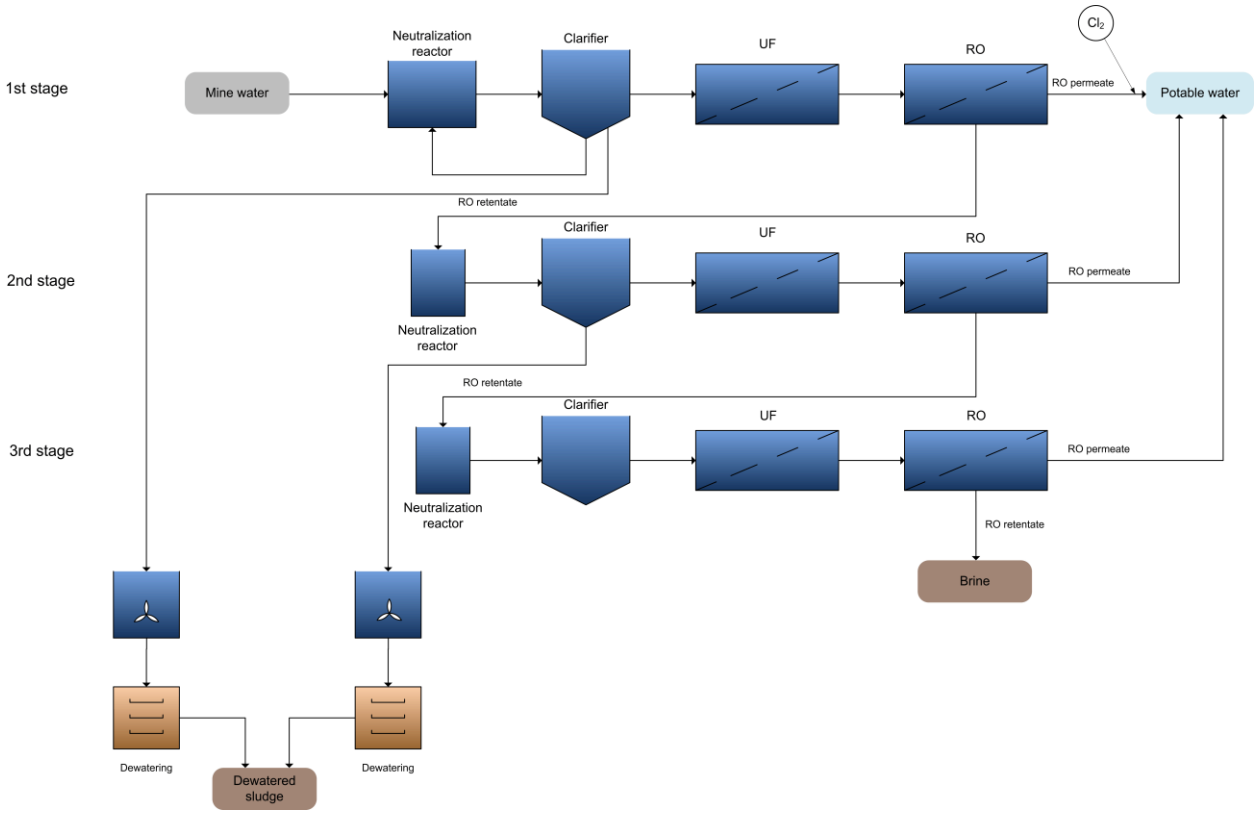

Figure 2. 2: The eMalahleni Water Reclamation Plant (modified from Hutton et al., 2009**)**

According to Gunther and Naidu (2008), the EWRP produces 4-5 tons of gypsum waste (dry basis) and 6-8 m^3/day of liquid (brine) waste per 1000 cubic meters (i.e., 1 ML) of potable water produced. In an effort to reduce waste disposal costs (which typically account for 25% to 30% of total water reclamation costs) and potentially generate additional income to cover water treatment costs, the EWRP has investigated a number of options for converting gypsum and brines into useful downstream products. Anglo Coal funded the Gyp-BuMP (Gypsum converted into Building and Mining Products) project to develop processes for converting gypsum waste into building products (such as bricks, plasterboard, paint extenders, fire-resistant doors, etc.) or mining products (such as stone dust for underground combustion prevention) (Gunther and Naidu, 2008). Despite the fact that approximately 29 potential building and mining products were identified, the Gyp-BuMP project's primary focus has been on housing (Gunther and Naidu, 2008). In 2010, 66 houses were built in a pilot project using gypsum from the second stage of the EWRP plant. While it has been suggested that stage 1 gypsum sludge could be used to replace river sand in conventional brickmaking for housing purposes, this sludge is currently sold to SA Lime and Gypsum for agricultural purposes. A second project, dubbed Gyp-SLiM (gypsum processed into sulphur, limestone, and

magnesite), investigated the use of technology from Anglo Coal, the CSIR, and Sulphide Tech for the conversion of waste gypsum from the EWRP (stages 1 and 2) into sulphur, limestone ($CaCO_3$), and magnesite ($MgCO_3$). The project provided funding for 18 months of laboratory testing and market research. While a pilot project was planned, there is no evidence that this process has been demonstrated on a larger scale than in the laboratory.

For the potential recovery of potable water and usable salts from the HiPRO brines generated in stage 3 of the EWRP, two options have been identified: algal brine beneficiation using algae to produce by-products such as spirulina and beta-carotene, and eutectic freeze crystallization (EFC) for the selective recovery of individual salts (Gunther and Naidu, 2008). Randall et al. (2011c) conducted laboratory tests on EWRP brine and discovered that EFC could recover potable water (80% by volume of the brine generated), as well as the salts Na_2SO_4 (96.4% purity) and $CaSO_4.2H_2O$ (96.4% purity), each amounting to approximately 13 kg per m^3 of brine. However, the brine waste generated at the EWRP is still disposed of in two evaporation ponds, which require a significant amount of land and cost upwards of R100 million each to build. Furthermore, the life of such ponds is only about five years.

2.2.2.2 A model or conceptual approach for incorporated value recovery

While the discussion in Section 2.2.2.1 demonstrates that efforts have been made to recover value from AMD within the EWRP in ways that go beyond potable water, the options explored to date have been limited, and few of these opportunities have been realised beyond the sale of gypsum for agricultural purposes.

It is hypothesized that additional opportunities could be realised by taking a more holistic approach to value recovery that considers the integration of waste streams throughout the entire coal deposit-energy mechanistic chain. Figure 2-3 depicts such an approach.

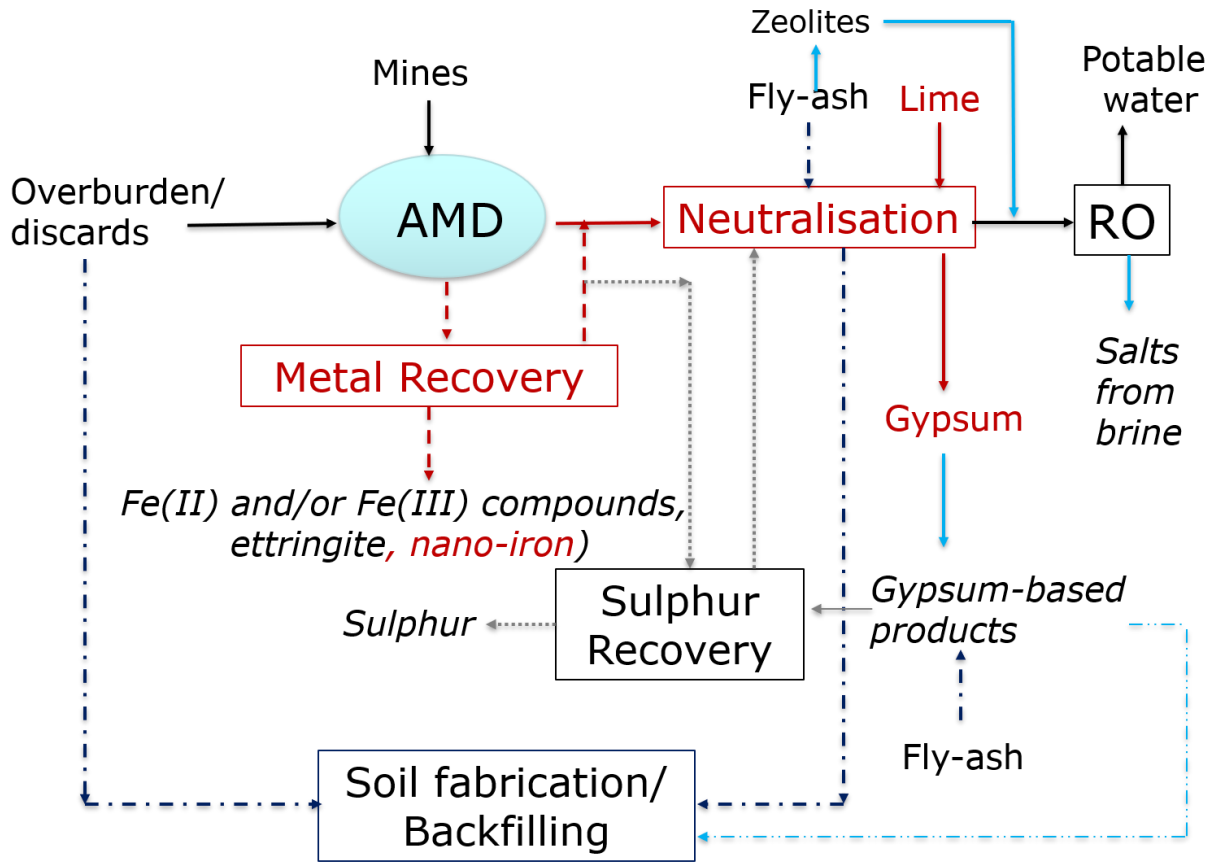

Figure 2. 3: Model approach for the integration of value recovery from coal production and combustion waste.

The use of limestone and/or lime in the HDS neutralisation process causes co-precipitation of several metals, including Fe, Al, Mg, and, to a lesser extent, Zn and Mn, which are typically present in AMD from coal mines, resulting in gypsum sludge containing significant amounts of metal hydroxides. Prior removal of iron, in the form of Fe(III), Fe(II), Fe(II)/Fe(II), or zerovalent nano-iron (see discussions in 2.3.1.6), allows for the recovery of usable iron products while also improving the quality and thus the potential value of the gypsum sludge generated in the subsequent neutralisation stage. The incorporation of a sulphur recovery circuit, as outlined in Section 2.3.1.5., could provide an opportunity to recover higher value elemental sulphur for sulphuric acid production. Alternatively, elemental sulphur and metal carbonates could be extracted from gypsum using the Gyp-Slim or a modified version of it (see Section 2.3.1.5). In addition to recovering iron and sulfur-based products, salts could be recovered from HiPRO brines using processes such as EFC.

However, additional opportunities for maximum value recovery may be realized by taking a more holistic approach that integrates wastes from the entire coal value chain, including wastes from primary extraction, coal processing or washing, and coal combustion. As

discussed in Section 2.2.5.1, laboratory studies have shown that fly ash generated from coal-fired power plants, which are mostly located within 25 kilometers of Mpumalanga's coal mines, is a potentially suitable replacement for lime in the treatment of AMD (Madzivire et al., 2010; Gitari et al., 2011b), capable of effectively neutralizing acid while simultaneously removing sulphate and metals from a variety of feed AMD solutions. Petrik et al. (2006) have also demonstrated that the fly-ash/gypsum residue generated during the fly-ash neutralisation process has the potential to be used as backfill material for mine voids or to generate zeolite products. Petrik et al. (2006) generated a relatively pure faujasite zeolite with high cation exchange capacity through the hydrothermal conversion of solid waste sludge generated from the neutralisation of a coal AMD sample with fly-ash from a local power station, based on previous studies using fly-ash as a source of silicate and aluminium for the synthesis of zeolites aluminium. The zeolite prepared from fly ash/gypsum residue was found to be more efficient at toxic element removal than the commercial resin (LewatitTp207) and to have a similar capacity for metal removal as a commercial faujasite. Petrik et al. (2006) proposed that the zeolite could be used in the EWRP to remove residual metals (either to replace or improve the performance of the HiPRO process) and/or sold as a by-product.

As an alternative to zeolite production, the fly ash/gypsum sludge generated by fly-ash neutralization could be used as a replacement for cement to increase the strength of the solid residues (Petrik et al., 2006). Petrik et al. (2006) discovered in laboratory-scale studies that the sludge-cement mixture had high compressive strength and appeared to be suitable for the confinement of mined-out areas. Aside from cement, fly ash has been used in backfill applications in conjunction with lime, or with both lime and gypsum as binders, due to its pozzolanic properties (Mishra and Karanam, 2006). Other authors (Palarski, 1993; Chugh et al., 2002) have used binders and mixtures of fly ash and coal mine waste to create consolidated backfill material for coal mines. Thus, there is the possibility of combining wastes from coal extraction and processing (overburden, discards, and tailings), coal AMD neutralization, and coal combustion (fly ash) in the production of backfill material for coal mine voids. In a similar manner, waste materials such as fly ash, lime, and gypsum can be used as a partial replacement or alternative for sand or cement in the production of clay or cement bricks (Ali et al., 2011; Naik et al., 2014; Karthikeyan et al., 2019). According to Ali et al. (2011), while lime improves the compressive strength of fly-ash mixtures, gypsum accelerates the strength gain for these lime-stabilized fly ashes, especially during the initial curing period.

Soil conditioning or fabrication is another potential application involving multiple waste streams from coal production and combustion. According to studies, the properties of fly ash make it potentially suitable as an ameliorant for improving soil quality (Tchuldjian et al., 1994; Skousen

et al., 2013; Ram and Masto, 2014). Silt-sized particles, low bulk density, higher water holding capacity, alkaline pH, and a significant presence of potential plant nutrients are examples of such properties (Ram and Masto, 2014). Fly ash combined with organic and inorganic materials (lime, gypsum, animal manure, sewage sludge, compost, soil and rocks, biochar, etc.) produced better results than fly-ash alone in most cases (Ram and Masto, 2014). Similarly, soil amendment and fertiliser are two of the most important and widely used applications of gypsum (Koralegedara et al., 2019). Gypsum is commonly used as an ameliorant to improve the quality of sodic soils, water infiltration, porosity, and particle aggregation. Gypsum also contains Ca and S, which are essential for plant growth (Koralegedara et al., 2019). The feasibility of using the desulphurised fraction of coal processing slurry waste, along with organic matter and nutrients such as compost and anaerobic sludge, as the main substrate for the manufacture of fabricated soils has been demonstrated by studies at the University of Cape Town (Amaral Filho et al., 2020). The use of mixtures of soil, coal waste, and additional organic matter and nutrients, according to their study, can reduce the amount of topsoil used in coal mine restoration while also significantly reducing the amount of fine coal disposed of in dump deposits. According to the reported land applications of fly ash, gypsum, and coal processing waste, it may be possible to combine these wastes in the replacement or conditioning of soils for coal mine site rehabilitation.

While numerous opportunities for integrating downstream applications of wastes from coal production, coal AMD treatment, and coal combustion have been proposed here, the technical feasibility of the technologies and their integrated application must still be demonstrated, either in the laboratory or on a pilot scale. Even if these technologies have been demonstrated, commercial implementation will necessitate the creation of a more rigorous business case that takes into account the environmental, economic, socio-technical, and regulatory aspects of the proposed options.

As stated in the previous chapter, the focus of this study is primarily on the technical feasibility of generating nano-iron from AMD, as well as the effects of this on downstream neutralisation process parameters and outputs, particularly gypsum, which is one of the major wastes from the EWRP. In keeping with this theme, Sections 2.3.3 and 2.3.4 provide a more detailed overview of the applications of nano-iron and gypsum.

2.2.3 Summary of applications

Nanotechnology has attracted a great deal of attention as a result of its capacity to manipulate fundamentally desirable properties of nanomaterials such as reactivity, catalysis, strength,

photo-activity, and selectivity (Cayuela et al., 2016; Sun et al., 2017). The use of nanoparticles (less than 100 nm in size) in the environment has numerous advantages, including greater performance, decreased energy consumption, and a reduction in the amount of residual trash. Zerovalent nano-iron (ZVFN), also known as zerovalent iron nanoparticles (nZVF), is one of the most investigated and effective nanomaterials for the mineralisation of a wide range of contaminants in contaminated water, soil, and aquifers (Cao et al., 2005; López-Téllez et al., 2011; Yaacob et al., 2012; Bae et al., 2016; Pullin et al., 2017)

Iron-based compounds are commonly utilized in the treatment of wastewater, pharmaceuticals, medicine, food manufacturing, and other manufacturing processes because of their low toxicity, biodegradability, and economic effectiveness (Adeleye et al., 2016).

When it comes to water treatment, ZVNF is the most commonly used compound. Granular iron has been employed in the form of permeable reactive barriers (PRBs) at several locations for many years (Nowack, 2010; Mueller., 2010), and PRBs are still considered to be the most up-to-date technology in the field. Their most significant disadvantage is that they can only deal with toxins that pass through the barrier. Zerovalent iron nanoparticles have recently become very attractive for applications such as adsorption (Lopes et al., 2016) or recovery of metal ions from industrial wastes or natural water streams, owing to a large number of active sites for adsorption and the consequent reduction in the quantity needed for each litre of solution (Parbs and Birke, 2005). Furthermore, the high surface area to mass ratios of nanoparticles has the potential to significantly increase the adsorption capabilities of sorbent materials. To go along with their large specific surface areas, nanoparticles also have distinct adsorption properties, which are related to the varied distributions of reactive surface sites and disordered surface regions on their surfaces (Tiwari et al., 2008). ZVNF has successfully removed a wide range of pollutants from water, including metals (Ba, Cd, Cu, Pb, Hg, U, and Zn), semi-metals (As, Se), anions (nitrogen dioxide, perchlorate, and sulphate), and organic compounds (Li et al., 2010; Cundy et al., 2008).

2.3 Synthesis of iron nanoparticles

The special properties of iron nanoparticles can be used because of the simplicity with which different methods are utilized in synthesising the nanomaterials. In recent decades, researchers have shown a lot of interest in the synthesis of nanoparticles, and several studies have been conducted and developed to that end. Nanoparticles (NPs) are solid particles that

exist between the states of atoms and clusters. NPs have unique physical properties such as small particle size, a large specific surface area (SSA), and quantum effects (Wu et al., 2008). Recent approaches to the synthesis of nanoparticles aim to produce iron nanoparticles with stable, controlled sizes, shapes, biocompatibility, and monodispersity. Because naked iron nanoparticles are highly unstable, they exhibit high reactivity, allowing them to be easily oxidized. For example, magnetite can be oxidized to maghemite when exposed to air, resulting in a decrease or loss of magnetism and dispersibility (Wu et al., 2008). Nano-iron particles of various sizes and structures are typically synthesized using various methods and reaction conditions. The morphology of iron oxide nanoparticles is determined by the particle processes used: growth, nucleation, aggregation, and impurity adsorption. Iron nanoparticles have properties that differ greatly from their bulk form.

Iron nanoparticle synthesis has been divided into two categories: physical and chemical methods (Li et al., 2006; Tavakoli et al., 2007). Iron nanoparticles are synthesised by chemical or green methods, by precipitation from ferrous chloride or ferric chloride using sodium borohydride, or plant extracts respectively (Wang and Zhang, 1997; Lu et al., 2007), or by reduction of iron, oxide particles or by physical means using severe plastic deformation (Azushima, 2003; Azushima et al., 2008). Because of differences in the methods and conditions of synthesis, the iron particles synthesized using these methods differ from one another, yielding different particle sizes, morphology, particle distribution sizes, surface area, and agglomeration.

2.3.1 Physical synthesis

Some physical methods for the synthesis of nanocrystalline materials have been developed over the last two decades, including severe plastic deformation (SPD), inert gas condensation and consolidation, electrodepositing, ball milling, and consolidation (Setman et al., 2008). At the nanoscale, these methods are used to synthesise well-defined iron particles with varying particle sizes and shapes.

2.3.2 Chemical synthesis

The chemical synthesis method can be used to generate iron nanoparticles of various sizes, shapes, and conditions via various routes. For the synthesis of nanomaterials, this method necessitates the use of chemical reagents derived from either natural or commercial sources

(Alegbe et al., 2019). Using a sequential reductive reaction, Fe, FeO, and Fe_3O_4 can be synthesized from Fe_2O_3. Iron nanoparticles can be synthesized using a variety of techniques, including (i) chemical precipitation, (ii) sol gel and force hydrolysis, (iii) electrochemical technique, (iv) precipitation by anhydrous solution, (v) sonotonic technique, (vi) aerosol / vapour technique, (vii) microemulsion technique, (viii) surfactant mediated / template technique, (ix) flow injection technique, and (x) biomimetric technique. Using a chemical precipitation method, (Alegbe et al., 2019) precipitated zerovalent nano-iron particles from a chemical reagent iron salt solution and AMD solution using sodium borohydride as a chemical reductant, at room conditions. The properties of the zerovalent nano-iron particles were similar and were used in the treatment of AMD.

2.3.3 Green synthesis

Over the recent decades, the synthesis of iron nanoparticles from iron salt solutions has shifted from using chemical reductants to using environmentally friendly green reductants. Stable nano-iron particles of different sizes, surface area and shapes has been synthesized from different plant extracts due to its low cost that acts as a stabilising agent (Herlekar et al., 2014)**.** Magnetic nanoparticles are synthesized at room temperature or via the hydrothermal route by combining the plant extract in a fixed ratio with the metal salt solution (Herlekar et al., 2014)**.** Tea extract is the most used plant resource for the synthesis of iron nanoparticles.

Hoag et al. (2009) produced nZVI by reacting C. sinensis (green tea) extract with 0.1 M $FeCl_3$ solution. These nanoparticles were created in a matter of minutes at room temperature, with tea polyphenols acting as a reducing and capping agent. When compared to two commonly used iron chelates for bromothymol blue degradation, the activity of these nanoparticles was found to be higher.

In another study, the synthesis was carried out at room temperature with different volumes of tea extract and $Fe(NO_3)_3$ solution to examine the effect of tea extract concentration on the size of the nanoparticles formed; it was shown that the particle size decreased as the concentration of tea extract increased. Using the borohydride reduction process, it was demonstrated that the size of the nanoparticles generated varied between 50 nm and 500 nm. The biocompatibility of nZVI produced using green tea or borohydride as the reducing agent was evaluated by exposing cell lines to nZVIs for 24 to 48 hours and then performing a methyl tetrazolium (MTS) and lactate dehydrogenase (LDH) assay. The amount of LDH leaked increased as the particle size grew, putting additional strain on the cellular membrane. As a

result, compared to nanoparticles manufactured using the borohydride reduction technique, nZVI created using green tea were shown to be harmless to human keratinocytes (Nadagouda et al., 2010). This was due to the fact that they were substantially smaller in size.

Green tea extracts (Shahwan et al., 2011) were used to synthesize iron nanoparticles from metal salts GT-Fe NPs (which are primarily composed of iron oxide/oxohydroxide). It was shown that these nanoparticles were effective in the degradation of cationic dyes like methylene blue (MB) as well as anionic dyes like methyl orange (MO).

Using three different tea extracts, namely green tea (GT), oolong tea (OT), and black tea (BT), Kuang et al. (2013) synthesized iron nanoparticles. These nanoparticles were evaluated for their ability to act as a catalyst in the Fenton-like oxidation of monochlorobenzene (MCB). The results were promising. The GT-Fe NPs were the most effective at removing MCB, followed by the OT-Fe NPs at 53 percent and the BT-Fe NPs at 39 percent after 180 minutes of exposure.

Shahwan et al. (2011) developed a method for synthesizing polydispersed iron nanoparticles using eucalyptus leaf extract obtained from the leaves of the plant. nZVI, Fe_3O_4, and Fe_2O_3 were the three different types of nanoparticles that were synthesized during the procedure.

Rao et al. (2013) demonstrated that pomegranate leaf extract can be used to successfully synthesize Fe0/Fe3O4 nanoparticles. Y. lipolytica cells, which are a good biosorbent, were coated with these nanoparticles on two strains (NCIM 3589 and NCIM 3590) of heat-killed yeast cells. The bionanocomposite was tested for its ability to remove hexavalent chromium from the environment.

Venkateswarlu et al. (2013) synthesized magnetite nanoparticles using plantain peel extract as a low-cost bioreducing agent, which they found to be effective. Iron salt solution was hydrolyzed, resulting in the formation of ferric hydroxide, which was then reduced by various biomolecules to form Fe_3O_4 nanoparticles as a result of the reaction. The possible involvement of polyphenols and other biomolecules in nanoparticle synthesis has been considered based on the results of FTIR analysis. The as-prepared nanoparticles have a large surface area (11.31 m^2 /g) and a high saturation magnetization (15.8 emu/g), indicating that they are highly magnetic. BET surface area and pore volume measurements revealed that the nanoparticles had a mesoporous structure, as determined by the BET surface area and pore volume.

Kumar et al. (2013) synthesized stable iron oxide (Wuestite) from an aqueous extract of the pericarp of T. chebula dry fruit using an aqueous extract of the fruit's pericarp. The

nanoparticles were found to be pure iron oxide (as determined by energy dispersive X-ray spectroscopy (EDS)) and stable for up to 21 days after being synthesized. The phytoche is a plant.

According to previous research, the synthesis of nano-iron particles from a chemical reagent iron salt solution using chemical or plant extracts proves that plant extracts have moderate ferric reducing antioxidant power (FRAP) and diphenyl picryl hydrazyl (DPPH) values compared to the high FRAP and DPPH values of sodium borohydride, a traditional chemical reductant of iron. Using previous research findings, this study used green tea extract to generate nano-iron particles of varying sizes from iron-rich AMD before neutralizing the supernatant with lime. This process produced a value-added product from AMD and a sludge product containing a mixture of calcite and gypsum. The process also reduced the amount of lime used by nearly half than when the AMD solution was neutralized with lime directly, hence lowering the cost of the neutralization process.

2.4 Overview of local gypsum applications

2.4.1 Gypsum applications

Natural gypsum is widely employed in a wide range of applications, including construction (see Section 2.3.1.5). For the most part, synthetic gypsum, such as phosphogypsum (PG) and flue-gas desulphurization (FGD) gypsum, can be utilized as a replacement material in these applications. Aside from its use in construction as an additive in cement and floor screed, gypsum is also used to make plasterboards, cornices, and other moulded items. It is also used in agriculture as a soil conditioner and plant nutrition supplement (DMRE, 2009, OTM, 2009). In all three of these applications, the gypsum market in South Africa has a longstanding history. Construction and building applications appear to be dominated by the companies OMV, Gyproc, and Etex, while agricultural gypsum products are dominated by Kalkor and SA Lime & Gypsum, which are also large national suppliers. Additional information about gypsum product applications and requirements can be found in the sub-sections that follow this one.

(i) Cement additive

Uncalcined gypsum is added to cement at a rate ranging from 2 percent to 6 percent to operate as a retarder, delaying the setting time of the cement and improving the grinding qualities of the clinker, among other things. Relatively low-grade gypsum (95%) is generally deemed suitable for use as a cement ingredient because of its low toxicity. The typical purity of natural

gypsum used in cement manufacturing ranges from 88 to 92% (OTM, 2009), but Schutte (2018) reported that low-grade gypsum with 82% purity (in some cases even less) can be used. Gypsum is used in this application accounting for 50–60% of global gypsum use (Schutte, 2018). According to statistics available for 2006–2008 (DMRE, 2018; OTM, 2009), the annual application of gypsum as a cement addition in South Africa averaged between 500 and 600 kt/a (approximately 60% of total gypsum consumption).

(ii) Gypsum plasterboard

Gypsum plasterboard is used for ceilings, drywall partitioning in offices and homes, and fire-resistant assemblies all over the world. Gypsum plaster and plasterboard are made by drying and calcining gypsum ($CaSO_4.2H_2O$) to monohydrate ($CaSO_4.H_2O$) and then to hemihydrate ($CaSO_4.0.5H_2O$). In a form mould, the hemihydrate gypsum (also known as plaster, plaster of Paris, or stucco) is mixed with water, a foaming agent, and various binders and catalysts. When rehydrated, the hemihydrate plaster forms needle-like crystals of $CaSO_4.2H_2O$ that interlock with one another to form a firm, fire-resistant material (DMRE, 2009). Plasterboard requires a relatively high purity (> 95%) gypsum because soluble salts such as P_2O_5, MgO, F, and K_2O cause efflorescence on plasterboard surfaces. OMV, which supplies roughly 60% of South Africa's gypsum demand, reportedly limits the P_2O_5 and F content in gypsum to 0.01% for both cement and plaster production. Gyproc, another local supplier, will accept up to 6% impurities as long as soluble salts account for less than 0.1% of this 6% (i.e., 0.02% of total soluble salts). Non-soluble salt content of 2.5% is also specified, as insoluble inclusions act as inert fillers and reduce gypsum's compressive strength when calcined for plasterboard (OTM, 2009). Appendix A contains additional information on the specifications for synthetic (FDG) gypsum used in plasterboard applications. According to available data (OTM, 2009), plasterboard accounted for approximately 17% of total gypsum consumption in South Africa in 2007.

(iii) Land applications

Gypsum is widely used in agriculture to improve the chemical and physical conditions of soils, acting as an ameliorant as well as a fertiliser (see reviews by Koralegedara et al., 2019).

Reducing surface soil acidity;

Supplying Ca and S as nutrients, thereby improving plant growth and yield;

Improving physical properties of clay soils by improving flocculation of soil particles and keeping the soil crumbly, thereby increasing water penetration;

Alleviating sodic soils by displacing sodium through cation exchange reactions.

Aside from agriculture, gypsum has been used in the remediation of degraded and contaminated land. The use of gypsum (alone or in combination with compost) in the remediation of a coal mine was found to reduce soil acidity as well as the bioavailability of contaminants such as Pb, P, and Ba through the formation of insoluble salts (Koralegedara et al., 2019). Gypsum used in land applications, like gypsum used as a cement additive, does not require pre-calcination and can be used in relatively low-grade products (as low as 70% purity) (Schutte, 2018). In fact, some contaminants, such as Mg, K, Fe, and Se, may be beneficial because they act as extra nutrients. The metal-rich gypsum sludge from stage 1 of the EWRP is currently sold to SA Lime and Gypsum for agricultural purposes, as stated in Section 2.2.2.1. According to communications with this company's representatives, the EWRP gypsum is blended with lime in varying ratios depending on the requirements. As a result, there appears to be little benefit in providing purer gypsum for agricultural purposes. According to data from 2007 and 2008, the agricultural sector in South Africa consumed between 200 and 210 kt/a of lime (OTM, 2009).

(iv) Manufacture of downstream products

As discussed in Section 2.2.1.5, gypsum can be further processed into downstream products such as sulphur, limestone, and magnesite by using Gyp-SLiM or similar technologies. Sulphur is primarily used to produce sulphuric acid in South Africa, but the single largest end-user of sulphur globally is the production of phosphate fertilizers (DMRE, 2018). Cement producers have traditionally been the largest consumers of limestone in South Africa (accounting for 75%), followed by metallurgical and agricultural applications, which account for 10% and 6% respectively (DMRE, 2018). However, significant amounts of limestone will be required for the planned flue-gas desulphurisation (FDG) units that were scheduled to be installed at the Kusile and Madupi power plants between 2021 and 2025. Magnesite is primarily used in the production of refractory bricks after it has been converted to magnesium oxide.

2.5 Summary

There are several options for recovering iron and sulphur from coal-related AMD that have been identified by this review. In particular, nano-iron (NI) is a potentially valuable iron product that has applications in the water treatment industry. Traditional nano-iron production uses pure Fe(III) solutions, and the production of nano-iron from AMD is still largely unexplored territory. Additionally, the removal and recovery of iron prior to lime neutralisation provide the opportunity to reduce costs. Using previous research findings, this study used green tea extract (an environmentally friendly reductant) to generate nano-iron particles of varying sizes from iron-rich AMD before neutralizing the supernatant with lime. This process produced a value-added product from AMD and a sludge product containing a mixture of calcite and gypsum. The process also reduced the amount of lime used by nearly half when compared to directly neutralizing the AMD solution with lime, lowering the cost of the neutralisation process.

CHAPTER 3

SAMPLING, EXPERIMENTAL AND ANALYTICAL TECHNIQUES

3.0 Introduction

Chapter 2 of the current study presented a review of relevant literature. Chapter 3 presents the experimental approach, protocols and analytical techniques that were employed in this study.

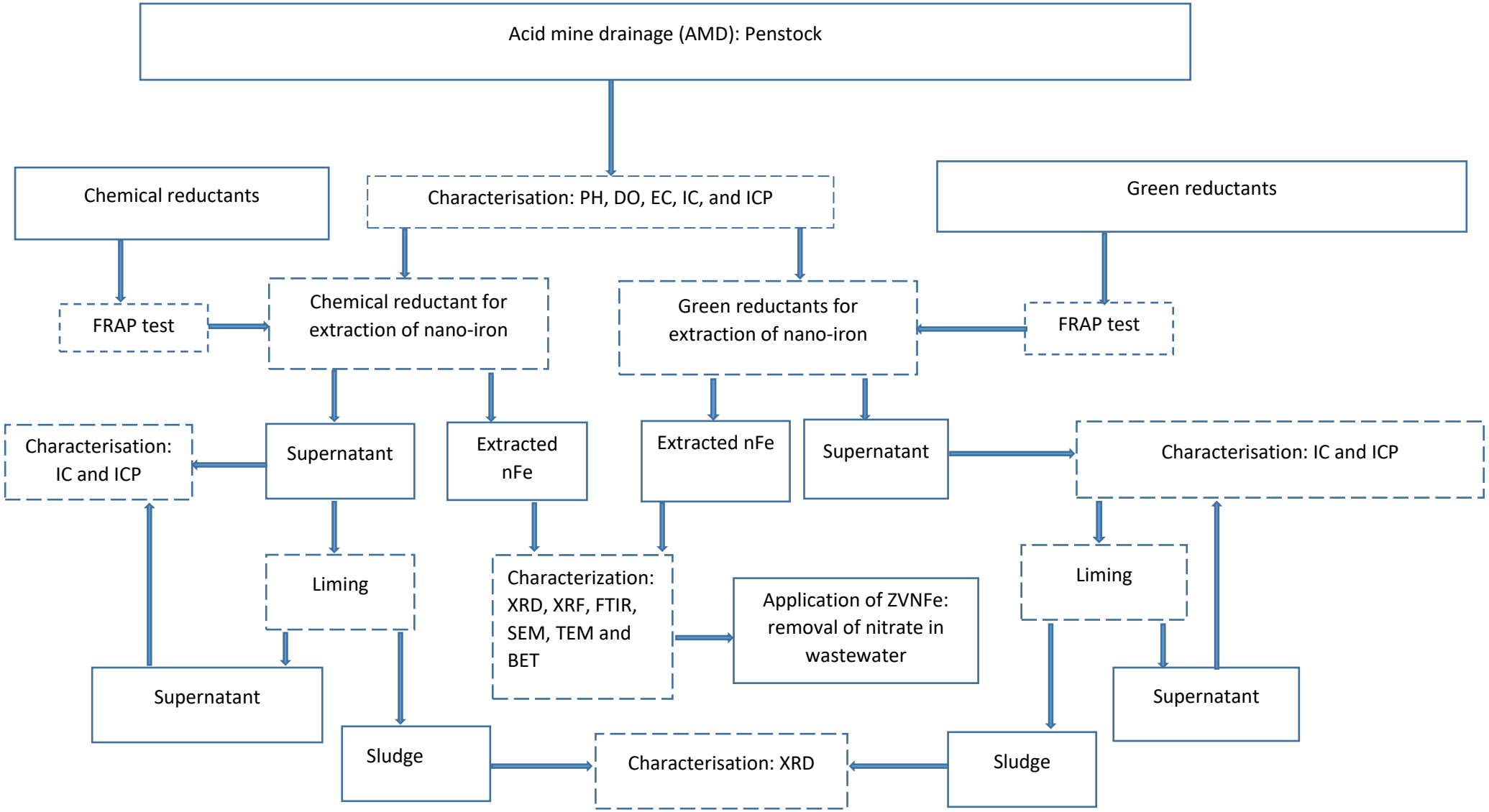

Figure 3. 1: Schematic diagram for nano-iron synthesis from AMD and post neutralisation

3.1 Study Area

This section presents the location from which the liquid waste material used for beneficiation purposes in this study was collected and stored. Acid mine drainage samples were collected from the Navigation coal mine in the Mpumalanga Province. For mine industries to attain a waste discharge that is close to zero, a novel and environmentally friendly way to convert the mine waste (environmental burden) to value-added products was investigated. The choice of field mine water used in this study was based on its availability, convenience, composition, and economic reasons, and to investigate the application of AMD based nano-iron particles produced from the mine water. This will provide an alternative medium to commercial-grade nano-iron particles for the same application.

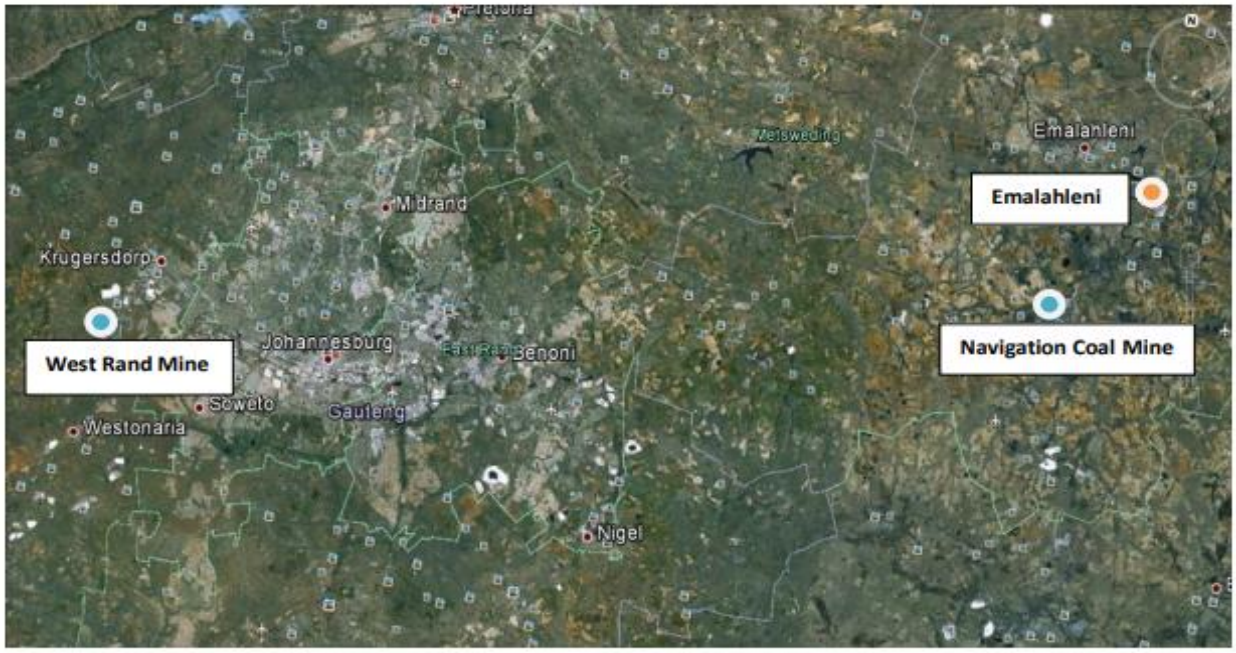

Figure 3. 2: Geography of AMD sampling source in in South Africa, Mpumalanga Province.

The liquid waste materials used in this study were as-received field AMD samples collected from the Navigation coal mine in the Mpumalanga province (see Figure 3.2). The choice of mine water was due to its accessibility and concentration of iron in the solution.

Table 3. 1: Materials and sampling source

Sample	Label	Source
Penstock AMD	P	Navigation Coal Mine, Mpumalanga
Toeseep AMD	T	Navigation Coal Mine, Mpumalanga
Kopseer AMD	K	Navigation Coal Mine, Mpumalanga

3.2 Materials

3.2.1 Sampling

This section presents the storage of field AMD samples that were used in the production of nano-iron particles using reductants such as sodium borohydride and green tea.

3.2.1.1 Acid mine drainage sample storage

The AMD samples used in this study were collected from the Mpumalanga coalfields located in the Mpumalanga province. These AMD samples were then stored in an airtight container so that the oxidation of ferrous iron to ferric iron were prevented. Prior to the physico-chemical analysis of the AMD samples, the samples were filtered with 0.45 µm pore size membrane filter paper to eliminate suspended solids. Physical characterisation of the AMD samples included pH, EC, TDS and DO, while the chemical characterisation of the AMD samples involved the determination of cations and anions. During this process, the filtered AMD samples were divided into two portions. One portion was used for the cationic analysis using ICP-OES analytical technique while the other portion was used for the anionic analysis using IC analytical technique. The AMD sample used for cationic analysis was preserved with 2 or 3 drops of nitric acid for each 100 mL AMD sample that was stored at 4 ^{o}C.

3.2.2 Chemicals used

This section presents the chemicals utilized in this study, their percentage purity and from what company they were purchased. The chemicals utilized in this study are tabulated in Table 3.2.

Table 3. 2: List of chemical reagents

Chemical	Formula	Supplier	% Purity
Nitric acid	HCL	Kimix	99.9
Sodium borohydride	$NaBH_4$	Kimix	99.8
Ethanol	CH_3CH_2OH	Kimix	99
Green tea	/	/	/
Ferric chloride	$FeCl_3.6H2O$	Kimix	99
Lime	$Ca(OH)_2$	Kimix	95

3.2.3. Equipment used

Table 3.3 presents the list of equipment used in this study

Table 3. 3: List of equipment

Equipment	Model and specifications
Laboratory oven	Scientific series 2000 (maximum T =250 ^{O}C)
Tube furnace	Labofurn (maximum T=1000 ^{O}C)
Hot plate	Lab smart MS-H-Pro (maximum T=340 ^{O}C)
Laboratory centrifuge	Sigma microcentrifuge 1-14 series, unrefrigerated (speed=200-14800)
Sonicator	Branson ultrasonic CPX2800H-J, 2.8 L, 40 KHz

3.3 Methodology

The methods used to synthesize nano-iron particles from the as-received AMD samples and the neutralization of the pre-treated AMD sample are described in detail in this section. The overall experimental procedure is illustrated in Figure 3.3.

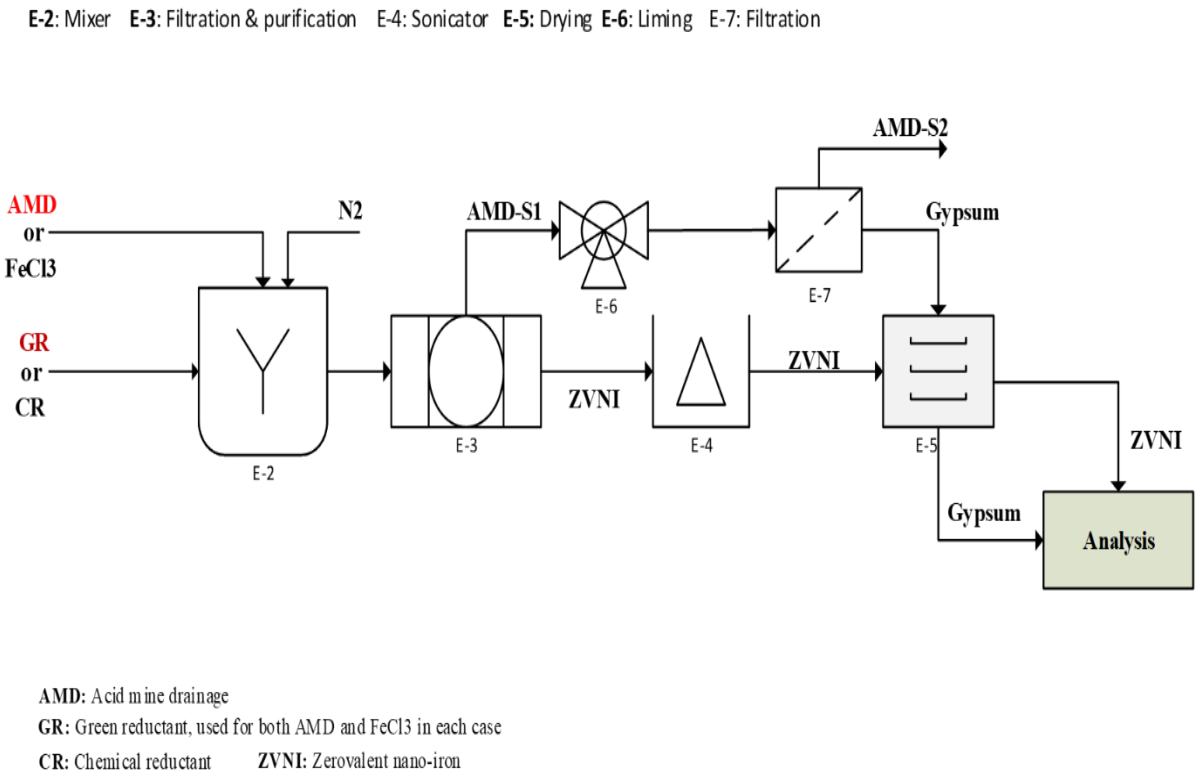

Figure 3. 3: Block flow diagram for the production of nano-iron particles and gypsum product from South African AMD (GR = green tea reductant, CR = chemical reductant, AMD = acid mine drainage, AMDS = acid mine drainage supernatant, ZVNI = zerovalent nano-iron, N_2 = nitrogen)

3.3.1 Preparation of reductants

Chemical and green reductants were prepared and used for the synthesis of nano-iron particles from AMD.

3.3.1.1 Preparation of chemical reductant: Sodium borohydride solution

5.674 g (0.6 M) of sodium borohydride was weighed using a plastic boat and transferred into a 250 mL volumetric flask. 100 mL of de-ionized water was transferred into the volumetric flask and shaken vigorously for appropriate mixing. Thereafter, the volume was made up to the mark with de-ionized water. The same procedure was used to prepare 0.1 M, 0.2 M, 0.3 M, 0.4 M, 0.5 M, 0.6 and 0.7 M sodium borohydride solution that corresponds to 0.945, 1.891, 2.837, 3.783, 4.728

g, 5.674 g and 6.620 g in 250 mL of deionized water. Sodium borohydride was chosen as a reagent grade reductant in this study due to its high FRAP value compared to other reagent grade reductants and because it can be used to reduce and precipitate nano-iron from AMD.

3.3.1.2 Preparation of green reductant: Plant extracts

As a proof-of-concept study, extracted polyphenols from different tea plants were used to prepare environmentally friendly reductants (green reductants) that could act as alternatives to chemical reductants used to produce nano-iron from AMD. These tea plants included *C. Sinensis* (green tea)*, A. Linearis* (green rooibos tea or green tea), and *Aspalathus linearis* (rooibos tea). After the collection of the plant polyphenolic part, the content was extracted using Sharma & Lall's (2014) method with slight modification. In this line of investigation, 60 g of tea leaves were weighed and ground mechanically. The ground tea was then immersed into 300 mL of deionized water and 30 mL of aqueous ethanol (25%). Subsequently, the tea mixture was agitated for 1 hour at 60 ^{o}C at a speed of 250 rpm. After the set time had elapsed, the mixture was allowed to cool prior to the evaporation of the ethanolic content using a rotor vaporiser set at 65 ^{o}C. Finally, the water content in the tea mixture was removed using a freeze dryer to obtain an amorphous powder. The obtained amorphous powder was then stored in an airtight container at 20 ^{o}C to prevent the ingress of air that could affect its antioxidant capabilities. These green extracts together with the reagent grade reductant were analysed for their scavenging activity (DPPH) and ferric reducing antioxidant power (FRAP) as outlined in section 3.3.7 and 3.3.8 respectively.

The tea extract solutions were prepared by dissolving their respective distinct masses of 0.1, 0.2, 0.3, 0.4, or 0.5 g in 50 mL of deionized water that corresponded to 2, 4, 6, 8, or 10 g/L. Thereafter, the solutions were then centrifuged for 5 minutes at 5000 rpm. The respective centrifuged supernatants of green tea extract were then physically characterised using pH, EC, or ORP prior to using it to extract stable nano-iron from AMD. Collected field Penstock AMD was utilized as a feedstock solution to produce stable nano-iron particles using aqueous green tea extract.

3.3.2 Synthesis of nano-iron particles from South African field AMD solutions

This section presents the synthesis of nano-iron particles from AMD solutions using reductants such as sodium borohydride and green tea solution extract.

3.3.2.1 Chemical synthesis

Sodium borohydride was selected as a chemical reductant that was used for the extraction of nano-iron particles from field Penstock AMD samples (see Table 3.1). Sodium borohydride was selected as a choice of chemical reductant due to its very high FRAP value and its capacity as a reducing agent. 500 mL of 0.6 M sodium borohydride solution was prepared by dissolving 11.348 g of sodium borohydride in deionized water. Afterwards, in each case, 50 mL of sodium borohydride solution was then transferred in a burette and titrated against 100 mL of nitrogen-purged field Penstock AMD samples in a round-bottomed flask. The sodium borohydride solution in the burette was added to each of the field AMD solutions in a dropwise manner to precipitate nano-iron particles for 80 minutes at 250 rpm. Thereafter, the mixture was filtered using 0.45 µm filter paper, washed three times with 100 mL of deionized water, and one time with 50 mL of 50% ethanol prior to sonication for 15 minutes to prevent agglomeration and to ensure even distribution of nano-iron particles. The sonicated mixture was then subjected to filtration and the nano-iron particles were washed with 100 mL of deionised water and 50 mL of 50 % ethanol. The nano-iron particles obtained were then dried in an inert environment to avoid oxidation, and the weight of the particles was recorded. The supernatant generated because of iron removal from AMD was collected and stored at 4 ^{o}C. Finally, the synthesized nano-iron particles were characterized using XRD, SEM/EDS and Image J for particle size analyser, FTIR, and STEM analysis while the supernatant was characterised using ICP-MS and IC analytical techniques.

Equation of reaction:

Fe^{3+} (aq) $+BH_{4-}$ (aq) $+H_2O \rightarrow Fe^{o}$ (s) $+B(OH)_3$ (aq) $+H_2$ (g	(3.1)

Half equation:

Fe^{3+} (aq) $+ 3e \rightarrow Fe^{0}$ (s) $E = -0.036$ V	(3.2)

Half equation:

H^{+} (aq)$+ 2e \rightarrow H_2$ (g) $E = -0.00$ V	(3.3)

Half equation:

$B(OH)_3\ (aq)+7H^+\ (aq)+\ 8e \rightarrow BH^{-4}\ (aq)+10.5H_2\ (g)\ E_{BH4}= 0.481\ V$	(3.4)

Overall equation:

$Fe^{3+}\ (aq)+\ 3BH^{-}_4\ (aq)+\ 9H_2O(l) \rightarrow F\ e\ (s)+\ 3B(OH)_3\ (aq)+10.5H_2\ (g)$	(3.5)

3.3.2.2 Chemical synthesis: concentration optimisation

Sodium borohydride was chosen as the reductant for the baseline experiments because it has a high capacity to reduce iron from solution. In this line of investigation (see Table 3.4), 100 mL of varying concentrations of sodium borohydride (0.1-0.7 M) were prepared by dissolving their corresponding masses of 0.945, 1.891, 2.837, 3.783, 4.728, 5.674, or 6.620 g in 250 mL deionized water. Subsequently, in each case, 50 mL of the prepared solution was transferred in a burette and titrated against 100 mL of field Penstock AMD nitrogen purged solution in a round-bottomed flask. The sodium borohydride solution in the burette was then added to the AMD solution in a dropwise manner. As a result, effervescence occurred with the evolution of a colourless gas (hydrogen) and the formation of a black precipitate. The solution was then left to mix for a total time of 80 minutes. Afterward, in each case, the precipitate was filtered and washed three times with 100 mL of deionized water followed by rinsing with 50 mL of 50% ethanol prior to sonification for 15 minutes to prevent agglomeration of the nano-iron particles. The sonicated particles were then filtered, washed with 100 mL of deionized water followed by 50 mL of 50% ethanol, and dried in an inert environment to prevent oxidation while the generated supernatant after the removal of Fe was collected and stored at 4 ^oC prior to characterisation. Finally, the nano-iron particles obtained were subjected to characterisation. The characterisation techniques used included: XRD, SEM/EDS and Image J for particle size analysis, FTIR, and STEM while the iron-depleted supernatant was analysed using IC and ICP-OES.

Table 3. 4: Experimental conditions of nano-iron synthesis from AMD using $NaBH_4$

Samples	Variable parameter	Fixed parameters
	Conc of $NaBH_4$ (M)	
SBNI 1	0.1	
SBNI 2	0.2	
SBNI 3	0.3	Vol. of $NaBH_4$ (50 mL), vol. of AMD (100 mL), speed (250 rpm),
SBNI 4	0.4	and optimum reaction time (80 minutes)
SBNI 5	0.5	
SBNI 6	0.6	
SBNI 7	0.7	

The effect of sodium borohydride concentration on the properties of zerovalent nano-iron particles synthesized from South African field AMD samples and their corresponding effluents are investigated and discussed in chapter 5.

3.3.2.3 Green synthesis

Green tea was selected as a green reductant used for the extraction of nano-iron particles from field Penstock AMD sample. Green tea was selected as a green reductant due to its high antioxidant properties and its capacity as a reducing agent (See Table 4.17). 50 mL of green tea solution was prepared by dissolving 0.6 g of green tea extract in deionized water. The tea solution was then centrifuged and filtered. Afterward, the tea solution was then transferred in a burette and titrated against 100 mL of nitrogen-purged field Penstock AMD solution in a round-bottomed flask. The tea extract in the burette was added to the AMD solution drop by drop to precipitate nano-iron particles and then mixed for 24 hours at 35 ^{0}C. Thereafter, the mixture was allowed to cool, filtered obtained using 0.45 µm filter paper, washed three times with 100 mL of deionized water, and rinsed with 50 mL of 50% ethanol prior to drying the nano-iron particles in an inert environment. The supernatant generated after the removal of Fe was collected and stored at 4 ^{o}C before characterisation. Finally, the synthesized nano-iron particles were characterized using XRD, SEM/EDS and Image J for particle size analysis, FTIR, and STEM while the generated Fe-depleted supernatant was characterised using ICP-MS and IC analytical techniques.

Proposed mechanism of green tea synthesized nano-iron particles from iron solution

Hao et al. (2021) proposed a mechanism of synthesised green tea-based nano-iron particles (*n*Fe). They proposed that if biomolecules that are present in green tea extract such as 1,3,5-benzenetriol, 1,2,3-benzenetriol, caffeine and bis(2-ethylhexyl) phthalate are extracted into solution and mixed with an iron salt compound, it leads to the emergence of core shell structured nano-iron particles. The shell is made up of FeOOH and the core comprises nano-iron. In this scenario, all the major biomolecules in the green tea extract act simultaneously as reducing and capping agents that function to reduce iron from higher oxidation state (Fe^{2+}) to lower oxidation state (Fe^{0}) nano-iron particles.

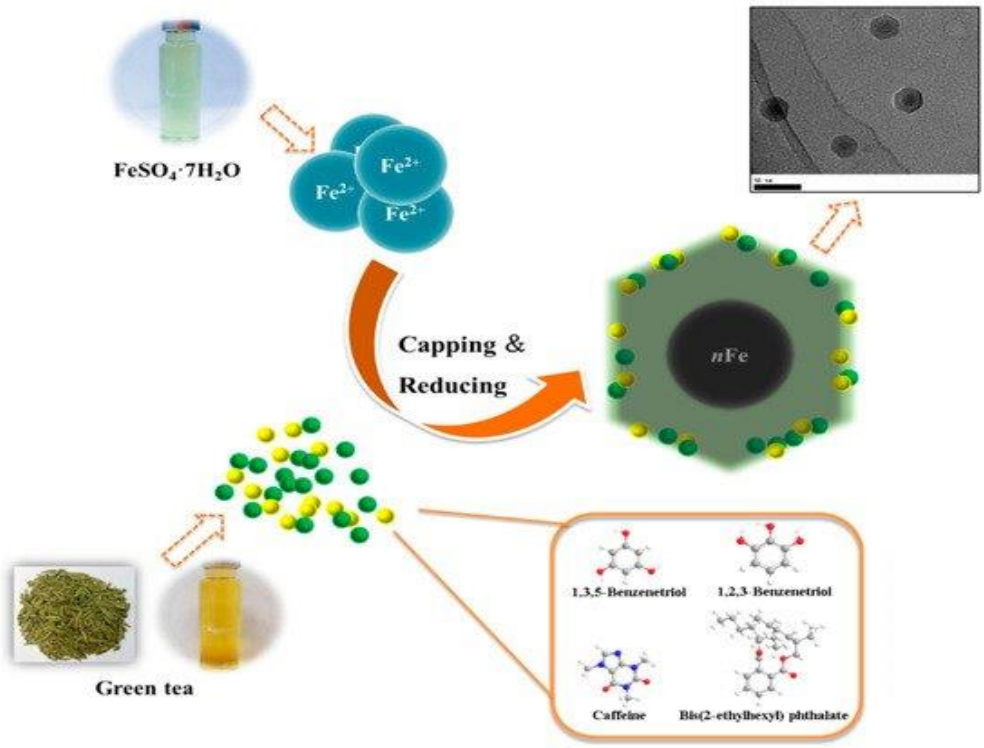

Figure 3. 4: Proposed mechanism of green tea by (Hao et al., 2021)

3.3.2.4 Green tea optimisation

This section presents and discusses the parameters that were used for the optimisation of nano-iron production from field AMD P solution using green tea as a reductant. The main aim of this optimisation technique was to achieve the optimum yield of nano-iron particles with the lowest amount of reductant. Three conditions (mass, temperature, and time) were examined in the production of nano-iron particles from field Penstock AMD.

Mass Optimisation

50 mL of field Penstock AMD solution was measured and poured into a 250 mL round-bottomed flask. Nitrogen gas was bubbled through the Penstock AMD solution for approximately 15 minutes to eliminate oxygen in the AMD solution. The field Penstock AMD was subjected to stirring at 300 rpm using a magnetic stirrer. 50 mL of green tea solution was prepared by dissolving the respective masses of green tea extract that corresponded to 0.1, 0.2, 0.3, 0.4, 0.5, 0.6, and 0.7 g in deionized water (see Table 3.5). The tea solution was then centrifuged and filtered. In each case, the prepared solution was poured into a burette and titrated against 50 mL of nitrogen-bubbled field Penstock AMD in a round-bottomed flask. The solution in the burette was added to the field AMD solution in a dropwise manner to precipitate green nano-iron particles and stirred for 24 hours at 35 ^{0}C. Subsequently, the mixture was allowed to cool, filtered, and washed three times with 100 mL of deionized water and once with 50 mL of ethanol. The trapped residue (nano-iron particles) on the filter paper was then collected and dried in an inert environment while the generated supernatant after the removal of Fe was then collected and stored at or lower than 4 ^{0}C prior to characterisation. Finally, the solid product (nano-iron particles) was characterised using XRD, SEM/EDS and Image J for particle size analysis, FTIR, and STEM while the generated Fe-depleted supernatant was characterised using ICP-MS and IC analytical techniques.

The tabular presentation of mass optimization of green tea extract during the synthesis of nano-iron particles from AMD is shown in Table 3.5.

Table 3. 5: Mass optimisation of green tea for the synthesis of nano-iron from AMD

Samples	Variable parameter	Fixed parameters
	Mass of green tea (g)	
GTNI 1	0.1	
GTNI 2	0.2	
GTNI 3	0.3	Vol. of AMD (50 mL), vol. of green tea (50 mL), speed (300 rpm),
GTNI 4	0.4	reaction time (24 hours), temperature (35 ^{o}C)
GTNI 5	0.5	
GTNI 6	0.6	
GTNI 7	0.7	

The effect of green tea dry mass in 50 mL deionized water on the properties of nano-iron particles synthesized from South African field AMD samples and their corresponding effluents is investigated and discussed in chapter 5.

Temperature optimisation

50 mL of field Penstock AMD solution was measured and poured into a 250 mL round-bottomed flask. Nitrogen gas was bubbled through the Penstock AMD solution for approximately 15 minutes to eliminate oxygen in the AMD solution and prevent oxidation of the synthesized nano-iron particles. The field Penstock AMD solution was stirred at 300 rpm using a magnetic stirrer. 50 mL green tea solution containing 0.5 g of green tea extract was measured with a pipette and added in a dropwise manner into five different 50 mL aliquots of field Penstock AMD solutions at different temperatures of 30, 35, 40, 45, or 50 ^{0}C respectively and stirred for 24 hours. A change in colour from yellow to black of the AMD solution was observed that indicated the precipitation of nano-iron particles. In each case, temperature optimisation was done in the same manner.

The tabular presentation of temperature optimisation of green tea extract during the synthesis of nano-iron particles from AMD is shown in Table 3.6.

Table 3. 6: Temperature optimisation of green tea for the synthesis of nano-iron from AMD

Samples	Variable parameter	Fixed parameters
	Temperature (35 ^{o}C)	
GTNI 8	30	
GTNI 9	35	Vol. of AMD (50 mL), vol. of green tea (50 mL), speed (300 rpm),
GTNI 10	40	reaction time (24 hours), mass of green tea (0.5 g)
GTNI 11	45	
GTNI 12	50	

Contact time optimisation

50 mL of field Penstock AMD solution was measured and poured into a 250 mL round-bottomed flask. Nitrogen gas was bubbled through the Penstock AMD solution for approximately 15 minutes to eliminate oxygen in the AMD solution and prevent oxidation of the synthesized nano-iron particles. The field Penstock AMD was subjected to stirring at 300 rpm using a magnetic stirrer. 50 mL of green tea solution containing 0.5 g of green tea extract was measured with a pipette and added in a dropwise manner into five different 50 mL aliquots of field Penstock AMD solutions and stirred for different reaction times of 4, 8, 12, 16, 20 or 24 hours at 35 ^{o}C. A change in colour from yellow to black of the AMD solution was observed that indicated the precipitation of nano-iron particles. In each case, mass of green tea extract and temperature optimisation was done in the same manner.

The tabular presentation of contact time optimisation of green tea extract during the synthesis of nano-iron particles from AMD is shown in Table 3.7.

Table 3. 7: Time optimisation of green tea extract during the synthesis of nano-iron from AMD

Samples	Variable parameter	Fixed parameters
	Time (hours)	
GTNI 13	4	Vol. of AMD (50 mL), vol. of green tea (50 mL), speed (300 rpm), temperature (35 ^{o}C), mass of green tea (0.5 g)
GTNI 14	8	
GTNI 15	12	
GTNI 16	16	
GTNI 17	20	
GTNI 18	24	

3.3.3 Neutralisation of AMD

This section presents the neutralisation of field Penstock AMD solution using slaked lime. The neutralization test work was conducted to determine the effect of lime dosage, redox potential, and pH on the compositions of AMD treated effluent and sludge generated. 95% pure industrial grade slaked lime was used as a neutralization agent during the treatment of AMD in a jar test method.

3.3.3.1 Direct neutralisation of field Penstock AMD

After a careful optimisation of time and mass of lime, two masses of lime ($Ca(OH)_2$) were selected for the neutralisation test work of 500 mL Penstock AMD solution for 120 minutes. The selected masses of lime that were utilized for the neutralisation test work were 5.5 g and 6 g. Thereafter, 5.5 g and 6 g of lime were transferred into separate jars containing 500 mL of field Penstock AMD solution. In each case, the mixture (AMD and lime) was steadily mixed for 120 minutes at 250 rpm. During this time, the pH and redox potential (ORP) of the neutralisation mixture was measured using a pH and redox potential (ORP) probe after every 10 minutes for 120 minutes. Subsequently, the treated mixture was filtered, and the obtained sludge sample (residue) was dried in an oven set at 70 ^{o}C for 24 hours. The generated AMD supernatant (treated effluent) was collected and stored at 4 ^{o}C prior to analysis. Finally, the sludge sample was subjected to XRF to identify elemental components whereas the treated effluent was subjected to ion chromatography

(IC) and Inductive coupled plasma-mass spectroscopy spectrometry (ICP-MS) for analysis on anions and element concentration respectively.

Table 3. 8: Experimental conditions for direct neutralisation of field Penstock AMD solution

Samples	Variable parameter	Fixed parameters
	Mass of lime (g)	
5.5 g	5.5	Vol. of AMD (500 mL), mixing time (120 min), speed (300 rpm)
6 g	6	

The image of the experimental setup for the direct neutralisation of field Penstock AMD is shown in Figure 3.5

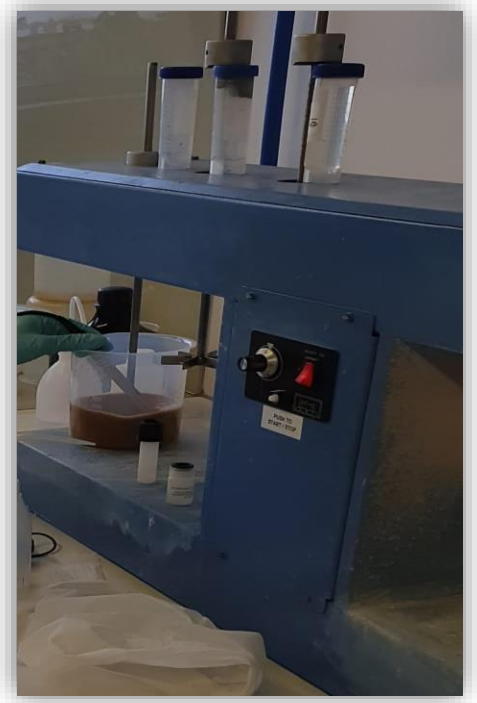

Figure 3.5: Experimental setup for direct neutralisation of field Penstock AMD

3.3.3.2 Neutralisation of field Penstock AMD pre-treated with sodium borohydride.

The obtained iron-depleted supernatant generated because of the production of zerovalent nano-iron particles from field Penstock AMD using sodium borohydride was subsequently subjected to the lime neutralisation process. After careful optimization of the mass of lime and time, 1.5 g and 2 g of lime was selected for the treatment of 250 mL of field Penstock AMD solution pre-treated with sodium borohydride for the removal of iron from solution. Thereafter, 1.5 g or 2 g of lime was transferred into a test jar containing 250 mL of iron-depleted field Penstock AMD and the mixture was allowed to mix for 120 minutes at 250 rpm at room temperature. During this time, the pH and redox potential (ORP) of the agitating neutralisation mixture was measured using a pH and redox potential (ORP) probe after every 10 minutes for 120 minutes. Subsequently, the treated mixture was filtered, and the obtained sludge sample was dried in an oven set at 70 ^{o}C for 24 hours. The treated effluent was also collected and stored at 4 ^{o}C prior to analysis. Finally, the sludge sample was subjected to XRF to identify elemental components whereas the treated effluent was subjected to ion chromatography (IC) and Inductive coupled plasma-mass spectroscopy (ICP-MS) for anion analysis and element concentration respectively.

Table 3. 9: Experimental conditions for the neutralization of Penstock AMD pre-treated with sodium borohydride (b)

Samples	Variable parameter	Fixed parameters
	Mass of lime (g)	
1.5 g	1.5	Vol. of AMD (250 mL), mixing time (120 min), speed (300 rpm)
2 g	2	

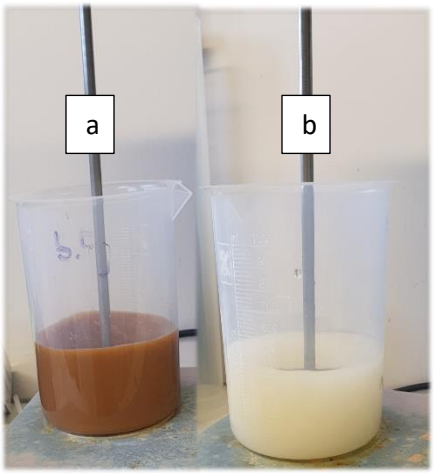

Figure 3. 5: Experimental setup for (a) direct lime neutralization of the as-received AMD and (b) lime neutralisation of AMD pre-treated with sodium borohydride.

3.3.3.3 Neutralisation of field Penstock AMD pre-treated with green tea extract.

In this study, AMD that had been pre-treated with green tea to remove iron from the solution was neutralized with varying amounts of lime. The amounts of lime ($Ca(OH)_2$) that were selected for the neutralisation of 250 mL of the pre-treated AMD solution were 1.25 g, 1.75 g, 2.25g, or 2.75 g. Thereafter, 1.25 g, 1.75 g, 2.25 g, or 2.75 g of lime were transferred into separate test jars containing 250 mL of the pre-treated AMD solutions. In each case, the pre-treated AMD and lime mixture was steadily mixed for 120 minutes at 250 rpm at room temperature. During this time, the pH and redox potential (ORP) of the agitated neutralisation mixture was measured using a pH and ORP probe after every 10 minutes for 120 minutes. Subsequently, the treated mixture was filtered, and the obtained sludge sample was dried in an oven set at 70 ^{O}C for 24 hours. The generated AMD supernatant (treated effluent) was also collected and stored at 4 ^{o}C prior to analysis. Finally, the sludge sample was submitted for XRF to obtain its elemental composition whereas the treated effluent was submitted for ion chromatography (IC) and Inductive coupled plasma-optical emission spectrometry (ICP-OES) for the analysis of anions and element concentration respectively.

Table 3. 10: Experimental conditions for the neutralisation of Penstock AMD pre-treated with green tea (T=time)

Samples	Variable parameter	Fixed parameters
	Mass of lime (g)	
1.25 g	1.25	Vol. of AMD (250 mL), mixing T (120 min), speed (300rpm)
1.75 g	1.75	
2.25 g	2.25	
2.75 g	2.75	

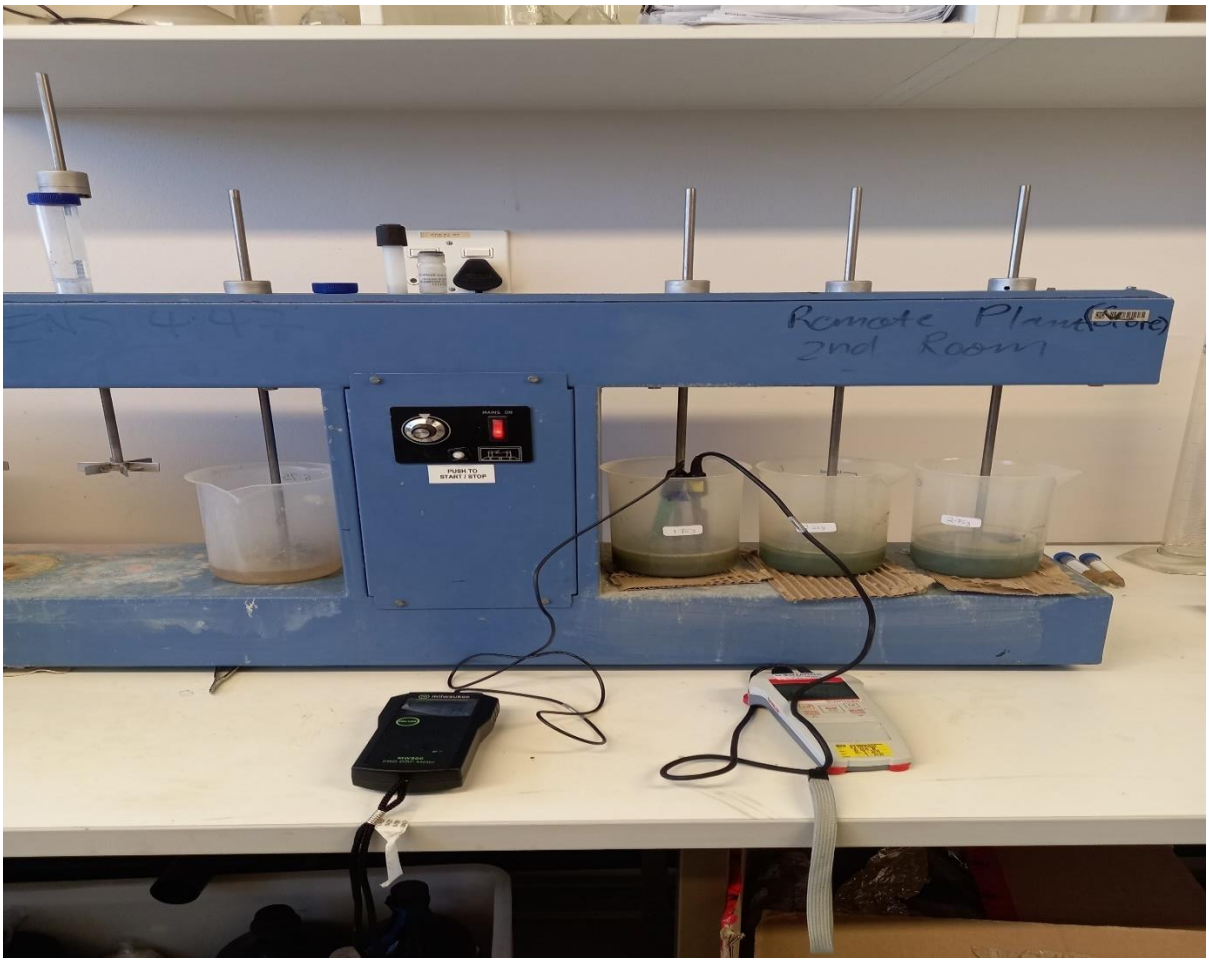

Figure 3. 6: Experimental setup for lime neutralisation of pre-treated Penstock AMD using green tea.

3.3.4 Catalytic testing of nano-iron particles synthesised from AMD.

100 mL of 10 ppm methylene blue (MB)-contaminated solution was measured using a measuring cylinder and transferred into three separate 250 mL beakers. In each case, the pH of the MB-contaminated solution was adjusted to pH=3 using a 0.001 M HCl solution, and 5 drops of hydrogen peroxide were also added. Thereafter, 5 mg of nano-iron particles synthesized from AMD using sodium borohydride (SBNI 0.6) or green tea (GTNI 0.5) were measured and transferred into two of the pH-adjusted contaminated MB solutions. The control solution was prepared by adding 5 mg of green tea extract (GTE) into the third pH-adjusted contaminated MB solution. Finally, all the contaminated MB solutions were subjected to 2 hours of mixing. When the mixing time had elapsed, the mixtures were removed and filtered using 0.45 µm filter paper. The obtained supernatant in each case was analysed using a UV-vis analytical technique to obtain the removal efficiency of MB from the solution.

3.4 Analytical method

This section presents the various analytical techniques that were used to characterise liquid and solid samples in this study.

3.4.1 pH measurement

This sub-section presents the measurement of the degree of acidity of the as-received field AMD solutions, treated AMD effluents, and tea solutions. The degree of acidity of these samples depended on their concentration of hydrogen ions. In this regard, a more acidic sample had a higher concentration of hydrogen ions and vice versa.

Procedure

The pH of field AMD solutions, treated AMD effluents, and tea solutions were measured using a portable HI 991301 pH meter with portable pH/EC/TDS/ DO/Temperature probe. Prior to sample measurements, the pH meter was calibrated with buffer solutions of 4.01 and 7.01. Thereafter, the samples were measured in triplicate to minimise error.

3.4.2 Electrical conductivity (EC)

This sub-section presents the measurement of electrical conductivity (EC) of field AMD (K, T, or P) solutions, treated AMD effluents, and tea solutions.

Procedure

The EC measurements of the AMD solutions and treated effluents were obtained by using an HI 991301 pH meter with a portable pH/EC/TDS/ DO/Temperature probe. The EC meter was calibrated with 12.88 mS/cm at room temperature. Thereafter, the samples were measured in triplicate for accuracy.

3.4.3 Dissolved oxygen (DO)

This sub-section presents the measurement of dissolved oxygen in the as-received field AMD solutions.

Procedure

The DO measurement of the AMD sample was obtained by using an HI 991301 pH meter with a portable pH/EC/TDS/ DO/Temperature probe. Triplicate DO measurements were obtained on the AMD samples.

3.4.4 Oxidation reduction potential (ORP)

This sub-section presents the ORP measurements of the as-received field AMD solutions, treated effluents, and green tea solutions.

Procedure

The ORP measurement was done using the HI 991301 pH meter with portable pH/EC/TDS/ DO/Temperature probe. The pH meter was industrially calibrated for ORP measurements.

3.4.5 Ion chromatography (IC): AMD and treated effluents

This section presents the use of the ion chromatography (IC) analytical technique in the measurement of anions in the as-received field AMD (K,T or P) samples and treated AMD (K, T, or P) effluents (supernatant generated after nano-iron removal and post liming).

Procedure

The as-received AMD samples and their corresponding treated AMD effluents were filtered using a 0.45 µm filter paper. The filtered samples were then diluted with deionised water to obtain a suitable electronic conductivity (EC) value (that was lower than 100 µS/cm) required for sample measurement. Subsequently, a small volume of the filtered solution (mobile phase) was forced through a column designed with packed particles, and the time the ion took to pass through the packed column was recorded. The ion retention time depended on its physico-chemical interaction with the packed column. Standards of known concentration were then used to approximate sample concentrations. In this line of investigation, the IC technique was used to analyse anions in field the field Penstock AMD sample and its corresponding treated effluents. These anions included sulphate (SO^{2-}_4), nitrate (NO^{2-}_3), and chloride (Cl^-). Prior to anion analysis, a suitable stock solution was developed by weighing and dissolving 1.6485 g NaCl in 1000 mL of demineralised and degassed water to make an equivalent of 1000 mg/L chloride solution. Calibration standards of 1 mg/L to 10 mg/L were also prepared. SO_4-S and NO_3-N were prepared in triplicate as calibration standards.

3.4.6 Inductively coupled plasma-optical emission spectroscopy (ICP-MS): AMD and treated effluents.

This section presents the use of the inductively coupled plasma-optical emission spectroscopy (ICP-MS 7900 by Agilent) analytical technique used for the measurement of cations found in field AMD (K, T or P) samples and treated AMD effluents.

Procedure

The as-received Penstock AMD solutions and their corresponding treated effluents were filtered using 0.45 µm filter paper to remove any solid particles that could interfere with the analysis. These solutions were then diluted to obtain a suitable EC value between 50-100 µS/cm. Subsequently, the samples were submitted and subjected to inductive coupled plasma-optical

emission spectroscopy (ICP-MS 7900 by Agilent) for the analysis of dissolved trace metals, minor metals, and major metals (Al, Fe, Ca, Mg, K, Na, Mn). Prior to dissolved metal analysis, the equipment was checked for accuracy against certified standards.

3.4.7 DPPH antioxidant assay: plant extracts

This section presents the radical scavenging activity of plant extracts against the stable 2,2-diphenyl-1-picrylhydrazyl organic compound.

Procedure

The DPPH test involves the reaction of an organic compound (DPPH) with hydrogen-donating compounds in a process that can be monitored using a spectrometer at a 517 nm wavelength as the DPPH compound changes colour from violet to light yellow (Brand-Williams et al., 1995). In line with this investigation, a stock solution of 200 mg/L of plant extracts was prepared by weighing and dissolving 10 mg of the dry plant extract in 50 mL of solvent (methanol). Thereafter, further dilutions were prepared from the plant stock solution to make ready lower concentrations of the plant stock solution (that included 100, 50, 25, 12.5, 0.4 mg/L). In a similar manner, stock solutions of ascorbic acid were prepared and successionally diluted to lower concentrations. Also, blank solutions were made from 100 µL and 50 µL of diluted extract solution and methanol solvent respectively, while the negative control was made from 100 µL and 50 µL of DPPH and methanol respectively. Subsequently, 50 µL of 150 mg/L of DPPH in methanol was added to 100 µL of plant extract solution in a microplate. This mixture was then kept in the dark for 30 minutes. The absorbance of successively diluted extracts, ascorbic acid, blanks, and controls was determined using a Biotek Power-wave XS Multi Well reader (Analytical and Diagnostic Products, Johannesburg, South Africa). The experiments were run in triplicate and the obtained values were transformed to percentage inhibition using the formula in equation 3.1

$$\% \text{ Inhibition } = \frac{(\text{Abs. Blank} - \text{Abs. Sample}) \text{ X } 100}{\text{Abs. Blank}} \quad (3.1)$$

3.4.8 Ferric reducing antioxidant power (FRAP) assay: plant extracts.

This section presents the ferric-reducing antioxidant power (FRAP) analytical technique that was used to determine the antioxidant strength of reductants used in this study.

Procedure

The FRAP activity was determined by using the method that was developed by Benzie and Strain (1996) with minor modifications. A buffer acetate solution (of 300 mM, pH 3.6) and a solution of 10 Mm TPTZ (2,4,6-tripyridyl-s-triazine) was mixed in the presence of 0.1M HCl and $FeCl_3 \cdot 6H_2O$ (20 mM) in a ratio of 10 :1:1 in order to obtain an active FRAP. Thereafter, in each case, 2 mg/L of ascorbic acid (standard) and plant extract were prepared in a careful manner and immediately subjected to 5 minutes of agitation using a vortex mixer (Dragon LAB MX-S). The agitated mixture was then centrifuged using an Eppendorf centrifuge 5810R for 5 minutes at 1000 rpm to permit the formation of clear solutions of the test samples. Subsequently, 100 mL of the tea extract solution was separately mixed with 300 mL of the prepared active FRAP reagent. The absorbance of the sample was then measured at a wavelength of 593 nm using a Multiskan spectrum (Thermo Electro Corporation). The calibration curve of known Fe^{2+} concentration was created by using methanol solutions of $FeSO_4 \cdot 7H_2O$ ranging from 100 to 2000 μM. The parameter equivalent concentration is defined as the concentration of antioxidant having a Ferric-TPTZ reducing ability equivalent to that of 1Mm $FeSO_4 \cdot 7H_2O$.

3.4.9 X-ray fluorescence spectroscopy (XRF): nano-iron intermediate products

This section presents the elemental composition of sludge from field Penstock AMD solution using the XRF analytical technique. The Philips 1404 Wavelength Dispersive spectrometer was set up for operational use at 40 mA and 50 kV.

Procedure

The sludge samples produced from South African field AMD were dried in an oven for 12 hours at 60 °C. The dried samples were then mixed with a binder composed of 10 % of C-wax and 90 % EMU powder. Subsequently, the sample-binder mixture was milled, moulded into pellets, and inserted in the sample holder compartment of the instrument. The X-ray fluorescence spectroscopy technique reports its data as % oxide for major elements and mg/L (mg/kg) for minor and trace elements respectively.

3.4.10 X-ray diffraction (XRD): neutralisation/HDS sludge and nano-iron products

This section presents the X-ray diffraction technique used to access the mineral phase of the synthesized nano-iron product. The conditions used for the XRD operation are also stated.

Procedure

The samples (nano-iron and gypsum) were oven dried at 60 ^{o}C for 12 hours to remove traces of moisture. Thereafter, the samples were ground to a fine powder before being loaded onto an alcohol-cleaned rectangular polypropylene holder using an alcohol-cleaned spatula. The loaded sample was then inserted and clipped into the instrument. Analytical data was collected from 10^{o} to 90^{o} 2Ɵ. Table 3.7 details the instrumental conditions of a Phillip X'Pert Pro MPD X-ray diffractometer that was used to obtained analytical data.

Table 3. 11: Phillip X'Pert Pro MPD XRD operation settings

Parameter	Settings
X-ray detector	Vantec 1
Generator voltage	40 kV
Generator current	40 mA
Scanning range angle	10^{o}-80^{o}
Scanning type	Locked couple
Scan speed per step	2θ/min and step size of 0.02o Theta
Scan time	0.5 sec per step
Scan size	0.03^{o}
Synchronous rotation	Copper Kα (alpha) at 1.540598

3.4.11 Scanning electron microscopy (SEM-EDS): Nano-iron products

This section presents the surface morphology and elemental composition of nano-iron particles and green zerovalent nano-iron particles obtained from AMD using SEM-EDS analytical techniques.

Procedure

During mounting of nano-iron samples, an adhesive carbon tape was placed onto aluminium stubs. An alcohol-cleaned spatula was then used to collect a tiny amount of nano-iron particles to spread onto the carbon adhesive tape. Thereafter, the samples were coated with carbon for 10 seconds to make them conductive and suitable for analysis. Finally, the samples were inserted into the analyser and micrograph images of each sample were captured. The EDS route was used to obtain the elemental composition of the samples. Table 3.8 details the instrumental set up for STEM that was used for analysis.

Table 3. 12: Electron microscopy (SEM) instrumental set up.

Parameter	Settings
Accelerating voltage	30 kV
Current	10 nA
Emitter	Thermal field emission type
Aperture	0.4 mm
Resolution	1 nm
Standard detector	ESB with filtering grid
Magnification	900K

3.4.12 Transmission electron microscopy (TEM): nano-iron products

This section presents the use of transmission electron microscopy (TEM) in analysing the morphology, crystallinity, and particle size of synthesized nano-iron particles from AMD.

Procedure

A small amount of the synthesized nano-iron particles was transferred into a sample bottle containing 5 mL of methanol solvent. The sample mixture was then placed in a sonicator for five minutes to allow vigorous mixing. This process was done for proper dispersion of particles.

Thereafter, a drop of the nano-iron-methanol mixture was deposited on a nickel grid and allowed to dry at room temperature. Table 3.10 details the instrumental set up of TECNAI G2 F20 X Twin Mat FEG used for HRTEM analysis.

Table 3. 13: Instrumental set up operating parameters for G2 F20 X Twin Mat FEG

Parameter	Settings
High tension	200 kV
Extraction voltage	3950 V
FEG emission current	54 µA
Condenser aperture	3 mm
Objective aperture	2 mm
Gun lens	1 nm
Spot size	3 nm

3.4.13 Fourier transforms infrared spectroscopy (FTIR): plant extracts and nano-iron.

This section presents the Fourier transforms infrared spectroscopy (FTIR) analytical technique used to provide information about functional groups, chemical bonding, and molecular structure of the samples (green extract and nano-iron samples)

Procedure

The synthesised nano-iron samples were dried for 12 hours at 60 ^{o}C, whereas the green tea extract solutions were freeze-dried to obtain an amorphous powder. Thereafter, the samples were submitted for analysis. Prior to analysis, the analytical surfaces of the equipment (Perkin Elma 1600 FTIR analyser) were cleaned with acetone to remove contaminants and then background trials were run. Afterwards, an alcohol-cleaned spatula was used to collect about 1 mg of the sample in each case and spread it over the analytical surface perpendicular to the shoe. The shoe in each case was then used to apply a gentle force on the sample and infrared red (IR) spectra were obtained between a range of 4000-400 cm^{-1}. The obtained data provided information as mentioned above.

3.5 Summary

Chapter 3 describes the location where the feed (raw AMD) was collected. This chapter also discusses the chemicals, equipment, and experimental methods used in this study. Finally, detailed information was provided about the analytical techniques used to characterize both solid and liquid products generated during this study. The following chapter (Chapter 4) will provide information about the physicochemical properties of the feed (raw AMD and its corresponding supernatants) and reductants (green tea extract and sodium borohydride) used to synthesize nano-iron from the feed (raw AMD).

CHAPTER 4

CHARACTERIZATION OF FEEDSTOCK

4.0 Introduction

This chapter presents and discusses the characterization results of various feedstock samples used in this study. These include acid mine drainage (AMD) samples (Kopseer, Toeseep and Penstock), pre-treated acid mine drainage samples (supernatant 1 and supernatant 2), plant extracts (green tea, green rooibos tea, rooibos tea), and lime. The different field AMD samples were analysed to determine how rich their concentration of iron was in the solution. Following that, the iron-rich AMD sample was then selected as an alternative source of iron that substituted reagent-grade iron salt used for the synthesis of nano-iron particles. The AMD feedstock samples that were collected from the Navigation coal mine and the feedstock AMD P pre-treated samples (supernatant 1 and supernatant 2) were characterised for their physical properties using pH, electronic conductivity (EC), total dissolved solids (TDS) dissolved oxygen (DO) and oxidation-reduction potential (ORP) analytical techniques, whereas IC and ICP were used to access their chemical properties. Thereafter, the green reductants used in this study were physically characterised using the pH, EC and ORP analytical techniques. Their corresponding antioxidant capabilities were analysed using ferric reducing antioxidant power (FRAP) and 2, 2-diphenyl-1-picrylhydrazyl (DPPH) analytical techniques. These green reductants were structurally analysed for their molecular vibrations of polyphenolic compounds using the Fourier transform infrared spectroscopy (FTIR) analytical technique. In line with this investigation, tea extract with a higher antioxidant strength was used to synthesize nano-iron particles from field AMD sample that were compared with nano-iron particles synthesised from field AMD samples using sodium borohydride.

4.1 Characterisation of field Penstock AMD feedstock samples

This section presents and discusses the characterisation results of field AMD samples after various analyses. These AMD samples were collected from the Penstock (P), Toeseep (T), and Kopseer (K) Navigation coal mine sites. The quality of the field AMD feedstocks was assessed using various physico-chemical characterisation techniques prior to using it for lime treatment and the production of nano-iron and gypsum.

4.1.1 Physical characterisation of field AMD samples

Field Penstock, Toeseep, and Kopseer AMD samples were characterised using pH, EC, TDS, DO or ORP analytical techniques. The obtained results provide knowledge about the physical state of the field AMD solutions prior to utilizing the samples for preparing nano-iron, feedstock supernatants and gypsum production.

4.1.1.1 pH Measurement of field AMD samples

The pH values of the as-received field AMD samples were measured to determine the extent of acidity. The technique used to characterise the degree of acidity has been detailed in 3.3.1. Prior to pH measurements, the pH meter was calibrated with buffer solutions of 4.01 and 7.01. The obtained results are presented in Table 4.1.

Table 4. 1: pH values of AMD samples

Name of AMD samples	pH Value
Kopseer	2.08±0.02
Penstock	2.14±0.02
Toeseep	2.20±0.03

Table 4.1 presents the pH results of field AMD samples that were measured in the laboratory (see Table 4.1). The obtained pH values of the as-received field AMD samples used in this study were in the acidic range with Kopseer (pH=2.08) being the most acidic followed by Penstock (pH=2.14) and then Toeseep (pH=2.20). This observation is similar to the results of past studies (Feng et al., 2000). The pH value of AMD coupled with other parameters can be used to determine the quality of the mine water (Okamoto et al., 2006). The pH level of an iron-rich AMD has the ability to precipitate iron and as a result, lower the concentration of iron in the AMD solution (Wei et al., 2005; de Almeida Silva et al., 2019; Akcil & Koldas, 2006). The low pH values of the field mine water samples indicate that all the AMD solutions are of poor quality and do not meet potable water quality standards.

4.1.1.2 Electronic conductivity of AMD samples

The measure of free ions in solution that are capable of conducting electricity is termed electronic conductivity (EC). The electrical conductivity of the AMD samples used in this study was measured in the lab and not on site. The measurement was conducted to determine the concentration of free ionic species present in the as-received field AMD feedstock samples. This analysis was performed using the characterisation technique described in section 3.3.2. The electronic conductivity (EC) analytical results of the AMD solutions are presented in Table 4.2 below.

Table 4. 2: Electronic conductivity of the as-received AMD feedstock samples

Name of AMD samples	Electronic Conductivity (Ms/cm)
Kopseer	47±0.09
Penstock	23±0.02
Toeseep	15±0.04

Table 4.2 presents the EC results of the as-received AMD feedstock samples. It was observed that the EC value of the Kopseer AMD was higher than that of Penstock and Toeseep AMD samples (see Table 4.2). This indicates that the Kopseer feedstock AMD contained more free ions in solution compared to its Penstock and Toeseep feedstock AMD counterparts. This could be attributed to the fact that the low pH of the Kopseer AMD (2.08) favoured the dissolution of pyrite ores into solution thereby producing more free ions in the AMD solution. However, the low EC value of the Toeseep AMD sample compared to the Kopseer and Penstock AMD samples could be attributed to the precipitation of iron in the form of ferric hydroxide that in turn reduces the concentration of ferric ions in solution and thus its corresponding EC value. This fact was corroborated by similar results from literature (Akcil & Koldas, 2006). There are some factors that can influence the consumption and the rate of precipitation of certain metals in AMD solution. These includes the type of metal, pH, and EC of the solution. The pH value of the AMD feedstock solution has the strongest influence on its corresponding EC value. This is because at a certain pH, metal from pyrite rocks goes into solution and releases ions, which consequently affects the EC of the solution, and the reverse in this case was true.

4.1.1.3 Total dissolved solids

The TDS analysis was used to quantify the total amount of dissolve salts in the as-received feedstock AMD samples. The TDS analytical technique was detailed in section 3.3.3.

Table 4. 3: Total dissolved solids of Kopseer, Penstock, and Toeseep AMDr

Name of AMD samples	Total Dissolved Solid (mg/L)
Kopseer	78±0.08
Penstock	55±0.05
Toeseep	29±0.06

Table 4.3 presents the total dissolved solids (TDS) of the feedstock AMD samples. It was observed that the total dissolved solid of Kopseer AMD was higher than that of Penstock and Toeseep AMD. This can be attributed to the fact that the pH and EC value of the Kopseer AMD sample favoured the dissolution of pyrite with little precipitation of pyrite metal in the form of iron hydroxide. The decrease in the TDS value from Kopseer>Penstock>Toeseep could be attributed to the fact the pyrite in the Toeseep AMD may have been in contact with atmospheric oxygen that initiated precipitation of pyrite as ferric hydroxide, thus decreasing its TDS value. Some studies have corroborated the evidence that a decrease in TDS value in an AMD sample could be a result of the sample's physical characteristics, such as pH and EC, favouring the precipitation of iron in the form of ferric hydroxide in the presence of oxygen (Akcil & Koldas, 2006).

4.1.1.4 Dissolved oxygen of field AMD samples

Dissolved oxygen is one of the parameters that is used to measure or assess the quality of water. The amount of oxygen molecules that is dissolved in water is termed dissolved oxygen (DO). This test is used to evaluate the water treatment process and level of pollution. There are some activities that affect the amount of dissolved oxygen in the field AMD samples. These activities include physical, chemical, and biochemical activities. The DO values of field AMD samples used in this study were measured in the laboratory and not on site. The technique used in assessing the amount of dissolved oxygen in the as-received AMD samples is detailed in section 3.3.4 and the obtained values are presented in Table 4.4

Table 4. 4: Dissolved oxygen (DO) of feedstock AMD samples

Name of AMD samples	Dissolved Oxygen (mg/L)
Kopseer	1.2±0.04
Penstock	1.5±0.01
Toeseep	1.8±0.03

Table 4.4 presents the DO results of the as-received AMD samples used in this study

The amount of DO in the AMD solutions depends on the samples' exposure to air. The air started oxidising ferrous iron to ferric iron, as tiny precipitates were observed at the bottom of the container. From Table 4.4, it can be observed that the DO of the Toeseep AMD was higher than that of the Penstock and Kopseer AMD, and their corresponding water quality was arranged in a descending manner T>P>K. Literature has also supported that a decrease in DO may be attributed to the oxidation of ferrous iron to ferric iron that in turn produces AMD rich in hydrogen ion and which consequently reduces the pH of the solution with the metal ions being released (Akcil & Koldas, 2006). Previous investigations have also shown that dissolved oxygen can impact the oxidation of ferrous to ferric iron (Akcil & Koldas, 2006). Studies reported that oxidation of iron in acid mine water depends more on the availability of dissolved oxygen as gravity and mechanical aeration might not provide sufficient oxygen for iron precipitation (Akcil & Koldas, 2006). A higher DO of the Toeseep AMD signifies that it had better water quality. Barrie & Hallberg (2005) reported that an increase in DO may be caused by effective aeration and the procedure of sampling and storage. Due to the ongoing dynamic interactions that are constantly taking place in the AMD solution, it is difficult to provide a constant prediction of the quality of the AMD solution.

4.1.1.5 Oxidation reduction potential (ORP)

The ORP analytical technique was used to measure the extent to which a substance can oxidise or reduce another substance. This technique was employed to measure the ORP value of the as-received field AMD samples. The ORP analytical technique is detailed in section 3.3.4 and its corresponding results are presented in Table 4.4.

Table 4. 5: ORP of AMD feedstock samples

Name of AMD samples	ORP (mV)
Kopseer	458±0.04
Penstock	448±0.03
Toeseep	425±0.01

Table 4.5 shows the ORP results of the AMD feedstock samples. It was observed that the ORP value of the Kopseer AMD solution was higher than the ORP value of the Penstock and Toeseep AMD solutions. However, their ORP values were quite similar (see Table 4.5). The more positive the reduction potential of a solution, the more that solution has a tendency to gain electrons from a new specie and consequently be reduced while oxidising it. Among the AMD samples presented in Table 4.4, the Kopseer AMD possessed a slightly higher affinity for electrons than the Penstock and Toeseep AMD samples due to a more positive redox potential. In this line of investigation, a mixture of the feedstock AMD samples (having similar positive ORP values) with a chemical or green reductant indicated that electron transfer from the reductant to the metals in solution would occur, hence precipitating them. It is also important to know that different metals possess different electron affinity. Measurement of the feedstock ORP values was done in triplicate to minimise error.

Summary

The pH, electronic conductivity, total dissolved solids, and the oxidation reduction potential of acid mine drainage samples varied from site to site depending on the chemical composition, geological composition, rate of oxidation, and the available pyrite ores. The pH of the AMD solution impacted other variables such as TDS and EC as these variables depend on pH. Meanwhile the dissolved oxygen (DO) had a strong influence on the pH of the AMD sample (Johnson & Hallberg, 2005b). The dependence of the pH on the DO can be ascribed to the fact that oxidation of Fe originating from the pyrite rock in solution would produce an acidic solution. The more pyrite ores in mine water undergo oxidation, the lower the corresponding pH, and the more metals go into solution to form their different ions. In line with this investigation, the TDS was also influenced by pH due to an increase in the rate of dissolution of elements, but above a certain point of dissolution, precipitation started to occur.

4.1.2 Chemical characterisation of the as-received AMD samples

This section presents and discusses the chemical composition of the as-received field AMD samples that were collected from the Navigation coal mine. This investigation was carried out to evaluate the quantity of chemical species that are in solution in the as-received AMD samples. The characterisation techniques that were used to quantify the chemical species in solution of the as-received AMD samples include inductively coupled plasma-optical emission spectroscopy (ICP-OES) and ion chromatography (IC). It is noteworthy that the results of the chemical species found in the AMD samples were determined in the laboratory and not on site. The results are not thus absolute as dynamic interactions such as pH, EC, TDS, or DO will influence the onsite and offsite measurement.

4.1.2.1 Elemental composition of the as-received AMD samples

This section presents and discusses the elemental composition of the as-received field AMD samples. This investigation was performed so that each AMD sample could be assessed for its richness in iron content that was intended for use in the production of nano-iron particles. The analytical techniques that were used for this measurement were IC and ICP-OES as detailed in section 3.3.5 and 3.3.6 respectively. The IC and ICP-OES results are presented in Table 4.6 and 4.7 respectively.

Table 4. 6: Properties of field AMD samples used for laboratory test work

Parameters	Unit	Field AMD K	Field AMD T	Field AMD P
pH		2.08 ± 0.03	2.20 ±0.02	2.14 ± 0.06
Electrical conductivity (EC)	mS/cm	3200 ± 1.27	2500± 2.30	2900± 4.10
Redox potential	mV vs SHE	458± 1.1	425± 0.91	448± 0.72
Major metals				
Fe	mg/L	4420 ± 14.3	1930 ± 10.8	4002 ± 22.1
Ca	mg/L	527 ± 22.4	508 ± 19.3	503 ± 18.9
Mg	mg/L	575± 8.21	414 ± 4.46	465± 15.2
Al	mg/L	460 ± 18.2	246 ± 3.58	367 ± 21.2
Mn	mg/L	126 ± 1.21	48.3 ± 0.95	85.4 ± 3.8
Minor metals				
Na	mg/L	33.5 ± 1.21	64.2± 0.21	33.1± 0.92
Si	mg/L	33.8± 2.55	12.0± 0.08	28.1± 1.02
Zn	mg/L	13.1 ± 0.07	6.10 ± 0.05	9.8 ± 0.01
Trace metals				
As	mg/L	0.16± 0.07	0.21± 0.01	0.32± 0.02
B	mg/L	0.11± 0.02	0.17± 0.04	0.14± 0.03
Be	mg/L	0.15 ± 0.08	0.13± 0.05	0.14± 0.04
Cd	mg/L	0.001 ± 0.01	0.001 ± 0.03	0.001 ± 0.01
Co	mg/L	1.84 ± 0.08	0.52 ± 0.02	1.11 ± 0.05
Cr	mg/L	0.42± 0.22	0.51± 0.09	0.34 ± 0.07
Cu	mg/L	0.11±0.04	0.18± 0.01	0.11± 0.02
Hg	mg/L	0.01±0.01	0.01±0.04	0.01±0.02
Li	mg/L	BDL	BDL	BDL
Mo	mg/L	0.08 ± 0.01	0.09 ± 0.01	0.08 ± 0.06
Ni	mg/L	1.87 ± 0.02	0.97 ± 0.03	1.12 ± 0.07
P	mg/L	0.35± 0.08	0.20 ± 0.01	0.001± 0.03
Pb	mg/L	0.02± 0.05	0.04± 0.03	0.16 ± 0.01
Sb	mg/L	0.02± 0.02	0.02± 0.02	0.02± 0.03
Sr	mg/L	0.36 ± 0.01	0.38 ± 0.09	0.84 ± 0.05
Th	mg/L	0.02 ± 0.01	0.001±0.03	0.01±0.01
Ti	mg/L	0.10±0.04	0.10±0.07	0.1±0.05
V	mg/L	0.11± 0.04	0.12± 0.01	0.22± 0.09
Y	mg/L	2.34±0.04	1.07±0.08	1.91±0.06
Zr	mg/L	0.01±0.02	BDL	0.01±0.03

Where: BDL= Below Detection Limit

Table 4.6 shows the results of the chemical composition of Kopseer, Penstock, and Toeseep AMD samples that were collected from the Navigation coal mine sites. These results prove that the major elements in the AMD solutions were Fe, Ca, Mg, Al, or Mn, while the minor elements in the AMD solutions were Na, Si, or Zn, and the rest of the elements detected were trace elements. The Kopseer AMD recorded the highest concentration of major and minor elements followed by the Penstock AMD and Toeseep AMD. The concentration of the target element (Fe) was highest in the Kopseer AMD and followed this order K(4420 mg/L) >P(4002 mg/L)>T(1930 mg/L). As could be observed from Table 4.4, the AMD samples had similar concentrations of calcium above 500 ppm. There are similarities in the Fe concentration found in the Kopseer and Penstock AMD samples compared to the iron concentration found in the Toeseep AMD sample (see Table 4.6). Among the major elements found in the AMD samples, Fe had the highest concentration. In line with this investigation, it was shown that all three AMD solutions can be used as alternative sources of iron for the synthesis of nano-iron particles, even though their recovery may differ. Alegbe et al. (2019) has reported on the use of sodium borohydride to synthesize zerovalent nano-iron particles from an iron rich AMD sample. However, the use of an environmentally friendly reductant to synthesize zerovalent nano-iron particles from an iron rich AMD as an alternative source of iron has not been reported or investigated in detail. This study seeks to exploit that route. Among the different AMD samples characterized in this section, the Penstock AMD was chosen as a source of iron-rich AMD for the green route synthesis of nano-iron particles for economic reasons. These reasons include its bulk availability and comparable Fe concentration to the Kopseer AMD. It is also important to note that radioactive elements such as Th and Y were determined in the AMD solutions, which is harmful to humans and the ecosystem.

Anion analysis

This section presents and discusses ion analysis of the as-received field AMD samples using ion chromatography (IC) analysis. This technique was discussed in section 3.3.5. The obtained data is presented in Table 4.7

Table 4. 7: IC analysis of raw AMD samples n= 3

Samples	Units	SO_4^{2-}	NO_3^-	Cl^-
Kopseer	mg/L	13200±72.3	3.89±1.0	15.3±0.2
Penstock	mg/L	11500±29.0	2.13±0.2	10.2±1.2
Toeseep	mg/L	9910±68.1	2.20±0.20	10.1±1

Table 4.7 shows the concentration of anions found in the different as-received AMD samples that were collected from the Kopseer, Toeseep and Penstock sites. The concentration of sulphate ions found in the AMD samples was arranged in descending order: Kopseer (13200 mg/L)>Penstock(11500 mg/L)>Toeseep(9910 mg/L). The concentration of nitrate ions observed for the different AMD samples was 3.89, 2.13, and 2.20 mg/L for Kopseer, Penstock, or Toeseep AMD respectively. Similarly, the concentration of nitrate ions in the AMD samples were 3.89, 2.13, and 2.20 mg/L for the Kopseer, Penstock, or Toeseep sample respectively. The anionic results showed that there was a significant gap between the sulphate (SO^{2-}_4) ions found in the different AMD samples compared to other detected anions (NO_3^-, Cl^-), making sulphate ions the dominant anion in the different AMD samples. This analysis is in line with what has been reported by other scholars (Costa et al., 2008). The concentration of sulphate ions in mine water acts as an indicator in assessing the acidity of the mine water (Masindi et al., 2018). This was corroborated by the pH value recorded in Table 4.1. Sulphate is the target anion specie in AMD due its acidic nature and high concentration compared to other anions (Zaal & Sheridan, 2015). The expected high concentration of sulphate ions in AMD can be attributed to the high concentration of sulphur that is associated with pyritic ores associated with coal (Mativenga et al., 2018). Such a high concentration of sulphate ions in mine water poses a great threat to water quality.

Summary

Acid mine drainage (AMD) contains both cations and anions in varying degree. The cations are determined using inductive coupled plasma-optical emission spectroscopy (ICP-OES) while the anions are determined using ion chromatography (IC). The cations found in AMD are mostly found in three levels such as major, minor and trace elements. In this case study, the major elements included Fe, Ca, Mg, Al, and Mn, minor elements included Na, Si, and Zn, whereas trace elements included As Cr, Co,Y, Ni and Cu, etc. It is important to note that among the cations found in the AMD samples used in this study, Fe was the most dominant metal while sulphate (SO^{2-}_4) was the most dominant anion. It is from this finding that the experimental approach to synthesise nano-

iron particles from AMD was derived. It is also from this finding that the experimental protocol to lime AMD before or after iron removal was devised. The purpose was to produce a cleaner gypsum product. AMD P was the choice of AMD used for the green route synthesis of nano-iron particles because of its high concentration of iron, its availability, and for economic reasons. In the next subsection results are given for Supernatant 1 and supernatant 2.

Supernatant 1 (Penstock AMD pre-treated with sodium borohydride) and supernatant 2 (Penstock AMD pre-treated with green tea extract) were characterised physically by using pH and ORP analytical techniques. Further characterisations were conducted on their chemical composition using the ICP-OES and IC analytical techniques. The results obtained provided knowledge about the physical and chemical state of the pre-treated AMD solutions prior to utilizing the samples for the neutralisation test work (liming).

4.2 Characterization of pre-treated Penstock AMD

This section presents and discusses the characterization results of pre-treated Penstock AMD samples using sodium borohydride or green tea as a reductant to remove iron from the solution. The quality of the pre-treated AMD feedstocks was assessed using various physico-chemical characterization techniques prior to using the feedstock for lime neutralization.

4.2.1 Physical characterisation of pre-treated AMD feedstock: supernatant 1 and 2

Supernatant 1 (sodium borohydride pre-treated AMD) and supernatant 2 (green tea pre-treated AMD) feedstock samples were characterised using pH and ORP analytical techniques. These analytical techniques provided physical knowledge about the pre-treated samples.

4.2.1.1 pH of pre-treated Penstock AMD feedstock: supernatant 1 and supernatant 2

The pH of supernatant 1 and supernatant 2 was measured to assess the degree of acidity or basicity of their corresponding solution. The analytical technique used in this measurement was detailed in section 3.3.1. The obtained pH results are presented in Table 4.8.

Table 4. 8: pH values of feedstock supernatants

Name of supernatant	pH Value
Supernatant 1	8.58±0.41
Supernatant 2	1.81 ±0.12

Table 4.8 presents the pH results of supernatant 1 and 2. As a reminder, feedstock supernatant 1 was generated as a result of the pre-treatment of field Penstock AMD solution with sodium borohydride, whereas feedstock supernatant 2 was generated as a result of pre-treatment of field Penstock AMD with green tea extract. The pH of supernatant 1 (pH=8.58) was highly basic, which was the complete opposite of supernatant 2 (pH=1.81), which was acidic. This could be attributed to the fact that the pre-treatment mechanism of field Penstock AMD solution to generate supernatant 1 had an acid-consuming and base-generating process, thus increasing the pH of the solution; however, in the case in supernatant 2, the mechanism of pre-treatment had an acid-generating and base-consuming process that led to a decrease in pH.

4.2.1.2 ORP of pre-treated Penstock AMD feedstock: supernatant 1 and supernatant 2

The oxidation reduction potential (ORP) analytical technique was used to measure the extent to which a substance can oxidise or reduce another substance. This technique was employed to measure the ORP values of supernatant 1 and supernatant 2 that were obtained from the pre-treatment of the as-received field Penstock AMD solution with sodium borohydride or green tea extract respectively. The ORP analytical technique was detailed in section 3.3.4 and its corresponding results presented in Table 4.9.

Table 4. 9: Oxidation Reduction Potential (ORP) of pre-treated AMD P sample

Name of AMD samples	ORP (mV)
Supernatant 1	133±2.1
Supernatant 2	177±1.4

Table 4.9 shows the ORP results of supernatant 1 and 2 samples. It can be seen that the ORP value of the supernatant 1 (133 mV) is lower than the ORP value of supernatant 2 (177 mV). The more positive the reduction potential of a solution, the higher the tendency of the solution to gain electrons from a new specie and consequently be reduced while oxidising the new specie. A less

positive reduction potential of a solution means that the solution has a higher tendency to lose electrons to a new specie and consequently be oxidised while reducing the new specie. In this case, supernatant 1 will more easily loose electrons than supernatant 2 due to the difference in their redox potential.

4.2.2 Chemical characterisation of pre-treated Penstock AMD feedstock: supernatant 1 and supernatant 2

This section presents and discusses the chemical composition of supernatant 1 and 2 samples. As a reminder, supernatant 1 and supernatant 2 were generated as a result of pre-treatment of field Penstock AMD samples with sodium borohydride and green tea extract respectively. The chemical analysis was carried out to evaluate the quantity of chemical species that are in the different recovered supernatant solutions. The characterization techniques that were used to quantify the chemical species in the supernatant solutions included inductively coupled plasma-optical emission spectroscopy (ICP-OES) and ion chromatography (IC).

4.2.2.1 Elemental characterization of field Penstock AMD P feedstock: supernatant 1 and 2

The elemental compositions of pre-treated field Penstock AMD samples (supernatant 1 and supernatant 2) were determined using IC and ICP-OES analytical techniques. This analysis was conducted to confirm the extent to which iron and other elements had been depleted from field Penstock AMD after its treatment with sodium borohydride or green tea extract. Thereafter, Penstock AMD pre-treated samples were used for the neutralisation test work with lime. The IC and ICP-OES analytical techniques used in this study were detailed in section 3.3.5 and 3.3.6 respectively and presented in Table 4.10 and 4.11 respectively.

Table 4. 10: Elemental composition of pre-treated field Penstock AMD with sodium borohydride: Supernatant 1

Parameters	Units	AMD P Supernatant 1
Major Metals		
Fe	mg/L	0.06
Ca	mg/L	313
Mg	mg/L	338
Mn	mg/L	23.6
K	mg/L	0.59
Na	mg/L	5005
B	mg/L	2194
Minor metals		
Si	mg/L	4.03
Zn	mg/L	0.00
Al	mg/L	0.53
Trace elements		
As	mg/L	0.00
Ba	mg/L	0.00
Cd	mg/L	BDL
Co	mg/L	BDL
Cr	mg/L	BDL
Cu	mg/L	BDL
Hg	mg/L	0.00
Mo	mg/L	BDL
Ni	mg/L	0.01
Pb	mg/L	BDL
Sb	mg/L	0.00
Sr	mg/L	0.37
Se	mg/L	0.00
Sn	mg/L	BDL
V	mg/L	0.00

Where ND= not determined and BDL=Below detection limit

Table 4. 11: Elemental composition of pre-treated field AMD with green tea: supernatant 2

Parameters	Units	AMD P Supernatant 2
Major metals		
K	mg/L	242
Fe	mg/L	800
Ca	mg/L	178
Mg	mg/L	142
Al	mg/L	120
Mn	mg/L	13.0
Na	mg/L	19.0
Si	mg/L	10.0
Zn	mg/L	1.30
Trace elements		
As	mg/L	BDL
Be	mg/L	BDL
Cd	mg/L	BDL
Cr	mg/L	BDL
Cu	mg/L	0.05
Li	mg/L	BDL
Mo	mg/L	0.04
Ni	mg/L	0.3
P	mg/L	1.20
Pb	mg/L	BDL
Sr	mg/L	0.08
Th	mg/L	BDL
Ti	mg/L	BDL
Y	mg/L	BDL
Zr	mg/L	BDL

BDL = Below detection limit

Table 4.10 and 4.11 showed feedstock samples after pre-treatment of field AMD P sample with sodium borohydride or green tea extract respectively. It was observed that supernatant 1 was depleted in Fe (0.06 mg/L) and other major elements (Ca=313 mg/L, Mg=338 mg/L, Al=0.53, Mn=23.6); supernatant 2 was depleted in Fe (420 mg/L) and other major elements (Ca=178 mg/L, Mg=142 mg/L, Al=120, Mn=13), compared to the raw AMD P (Fe=4002 mg/L, Ca=503 mg/L, Mg=465 mg/L, Al=367, Mn=85.4). The field Penstock AMD sample (supernatant 1), pre-treated with sodium borohydride, had a much lower concentration of Fe (0.06 mg/L) than the green tea pre-treated Penstock AMD sample (supernatant 2) (Fe=420 mg/L). This investigation indicated that sodium borohydride is a stronger reducing agent of Fe than green tea. The elevated elements in the AMD solutions pre-treated Penstock with sodium borohydride were B and Na (2194 mg/L or 5005 mg/L) whereas the elevated element in the pre-treated AMD solution with green tea extract was K (242 mg/L). These elements (B, Na, or K) were leached out from the reductants that were used to treat AMD P solution in order to generate the feedstock supernatants for the neutralisation test work. This can be corroborated by the fact that in the raw as-received field Penstock AMD solution that was used as a feedstock to generate the supernatant feedstocks, the concentration of boron (B), sodium (Na) and potassium (K) were 0.14 mg/L, 33.1 mg/L, and 0.0 mg/L respectively. After the treatment of the as-received Penstock AMD feedstock solution with sodium borohydride or green tea as reductants, the B (2194 mg/L) and Na (5005 mg/L) concentration were elevated significantly. In feedstock supernatant 1 (sodium borohydride pre-treated Penstock AMD), Na and B were high while K concentration was significantly elevated in feedstock supernatant 2 (green tea pre-treated Penstock AMD). It can also be seen in Table 4.10 and 4.11 that some trace elements that were found in the raw AMD solution could not be detected in the AMD solutions after treatment (supernatant 1 and supernatant 2), thus the trace metals were precipitated.

Anion analysis

This section presents and discusses anion analysis of Penstock AMD pre-treated with sodium borohydride (supernatant 1) and Penstock AMD pre-treated with green tea (supernatant 2) using ion chromatography (IC) analysis. This technique was detailed in section 3.3.5. The data obtained is presented in Table 4.12.

Table 4. 12: IC analysis of pre-treated Penstock AMD solution using reductants

Sample	Units	$SO^{2-}4$	NO3 –	Cl-
AMP Raw	mg/L	11500	2.13	10.2
AMD P Supernatant 1	mg/L	10400	ND	ND
AMD P Supernatant 2	mg/L	7820	1.4	11.2

Supernatant (AMD pre-treated with sodium borohydride (1) or green tea(2)) and ND (not detected)

Table 4.12 shows the concentration of anions found in the feedstock Penstock AMD supernatants (1 and 2). The sulphate content in the raw field Penstock AMD solution that was pre-treated with sodium borohydride or green tea was analysed by IC to be 11500 mg/L. After pre-treatment, the sulphate concentration only decreased to 10400 mg/L in supernatant 1 and to 7820 mg/L in supernatant 2 (see Table 4.12). The analysed results in Table 4.12 also show that there is high concentration of sulphate ions compared to other detected anions (NO_3^-, Cl^-), thus making sulphate ions the dominant anion in supernatant 1 and 2. It is worth noted that the sulphate ions in supernatants 1 and 2 were still high; the sulphate content in supernatant 1 was close to that of the raw Penstock AMD, showing that the reductants did not remove sulphate effectively. This is useful, as then the iron precipitate is less contaminated.

4.3 Characterisation of plant extracts

This subsection presents and discusses the physico-chemical characterisation of tea extracts used in this study. These plant extracts were obtained from green tea, green rooibos tea and rooibos tea leaves.

4.3.1 Physical characterisation

Green tea, rooibos tea, and green rooibos tea samples were characterised using pH, EC, or ORP techniques. The results obtained provide knowledge about the physical state of the tea solutions prior to utilizing the samples for nano-iron production from AMD

4.3.1.1 pH of tea extracts

The pH of the tea extracts was measured to assess their degree of acidity or basicity in solution. The analytical technique used in this measurement is described in section 3.3.1. The obtained pH results are presented in Table 4.13.

Table 4. 13: pH results of different tea solutions. Extraction conditions: mass of tea leaves = 60 g, ethanol=50 mL, H_2O=300 mL, temperature=70 ^oC, agitation speed = 300rpm and Time = 1 hour

		Mass of green tea in 40 mL deionised water				
Sample	**Parameter**	**0.1 g**	**0.2 g**	**0.3 g**	**0.4 g**	**0.5 g**
Green tea	pH	5.42	5.39	5.34	5.33	5.33
Rooibos tea	pH	5.09	5.05	5.20	5.23	5.22
Green rooibos tea	pH	4.98	4.98	5.00	4.99	5.10

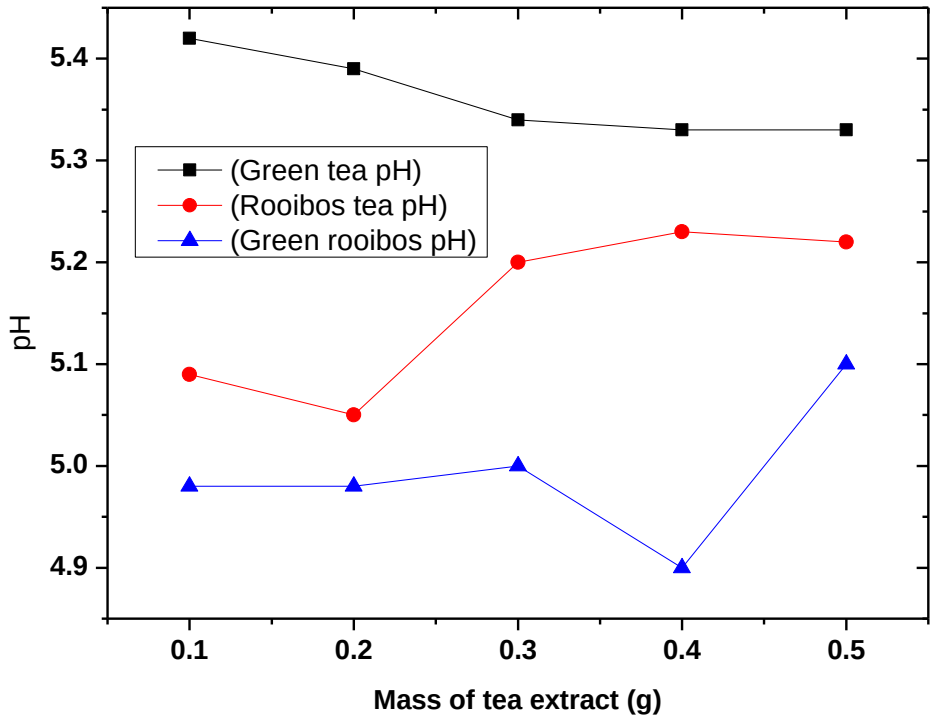

Figure 4. 1: Graphical presentation of pH values of different concentrations of tea extracts. Extraction conditions: mass of tea leaves=60 g, ethanol=50 mL, H_2O=300 mL, temperature=70 ^oC, agitation speed=300rpm and time=1 hour

Table 4.13 and Figure 4.1 presents the pH results of different tea leaf extracts in solution with deionised water. Prior to analysis, different masses of tea extracts (green tea, green rooibos tea, or rooibos tea) was dissolved in 40 mL of deionised water and mixed to obtain a homogenous solution. Thereafter, a portable pH/EC/TDS/ DO/Temperature probe was used to measure the pH of the solution in each case. From Table 4.13 and Figure 4.1, it was observed that the pH values of the tea extracts fall in the acidic range. It could also be observed that the pH values of the tea solutions did not vary much, as even the mass of tea extract in solution increased from 0.1-0.5 g (see Table 4.13). Among the tea extracts, green tea was the most basic, with a pH of up to 5.33, while green rooibos tea was the most acidic with a pH up to 5.10. Even though the pH value of green tea and green rooibos tea were closely similar compared to that of rooibos tea, they all have similar pH values. Previous studies have reported a pH range between 4.6, 4.1, 4.8 or 5.6 for rooibos tea, rosehip tea, Black Assam tea and Green Mee tea respectively (Jaganyi & Wheeler, 2003). This corroborates the pH data presented in Table 4.13 for green tea, rooibos tea and green rooibos tea.

4.3.1.2 Electronic conductivity (EC) of tea extracts

Electronic conductivity (EC) is the potential of free ions in a solution to conduct electricity. The electronic conductivity of tea extracts used in this study was tested. The EC technique was conducted on the tea extract solutions in order to measure the concentration of free ions in the solutions. The EC analytical technique was detailed in section 3.3.2. The obtained EC results of tea extracts are reported in Table 4.14.

Table 4. 14: Electronic conductivity (EC) results of tea extract solutions. Extraction conditions: mass of tea leaves= 60 g, ethanol=50 mL, H_2O=300 mL, temperature=70 ^oC, agitation speed=300rpm and time=1 hour

		Mass of green tea in 40 ml deionised water				
Sample	**parameter**	**0.1 g**	**0.2 g**	**0.3 g**	**0.4 g**	**0.5 g**
Green tea	EC (µS)	190	310	560	700	800
Rooibos tea	EC (µS)	150	250	450	580	700
Green rooibos tea	EC (µS)	170	280	505	640	750

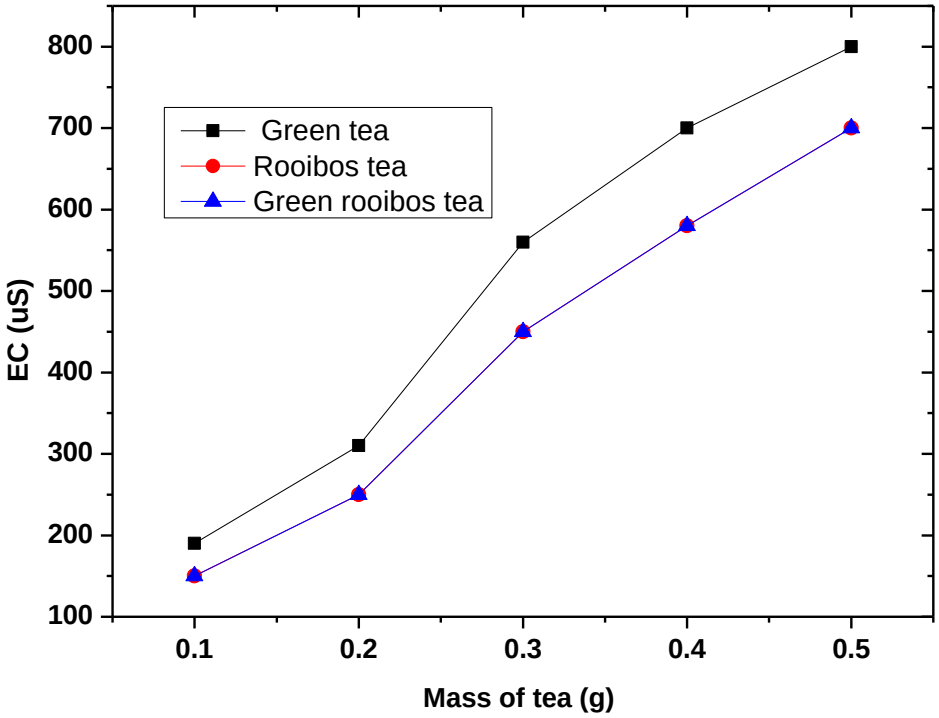

Figure 4. 2: Graphical presentation of electronic conductivity (EC) values of different tea extracts (green tea, rooibos tea and green rooibos tea). Extraction conditions: mass of tea leaves=60 g, ethanol=50 mL, H_2O=300 mL, temperature=70 ^oC, agitation speed=300rpm

Table 4.14 and Figure 4.2 present the EC measurements of different tea extracts (green tea, rooibos tea, and green rooibos tea). As can be observed in Table 4.14 and Figure 4.2, the electronic conductivity (EC) of the tea samples increased with an increase in the mass of tea extract in solution as expected. This could be attributed to the fact that as the dissolved mass of green tea extract increased, more free ionic species were released to the tea solution. It was also observed that green tea solution had the highest electronic conductivity compared to rooibos tea and green rooibos tea solutions. It was finally observed that the EC of rooibos tea and green rooibos tea solution were closely similar.

4.3.1.3 Oxidation reduction potential (ORP) of tea extracts

The oxidation reduction potential (ORP) of different tea extracts was measured to determine the extent to which the tea extracts would lose (and become oxidised) or gain electrons (and become

reduced) during a chemical reaction. In this section, the oxidation reduction potential of the various tea extracts was obtained after dissolution of the tea extracts in deionised water. The type of liquid media used for dispersion also affects the ORP value as the redox species in solution can interact with ease with the Pt electrode of the ORP probe (Shi et al., 2011). In this study deionised water was selected as the choice of liquid media used for dispersion of redox species to avoid the influence of ions on the ORP values of the tea extracts. The analytical technique used in this investigation is detailed in section 3.3.4. The obtained results are presented in Table 4.8 and Figure 4.3.

Table 4.15: Oxidation reduction potential (ORP) results of various tea extract solutions. Extraction conditions: mass of tea leaves=60 g, ethanol=50 mL, H_2O=300 mL, temperature=70 ^oC, agitation speed=300rpm and time=1 hour

		Mass of green tea in 40 ml deionised water				
Sample	**parameter**	**0.1 g**	**0.2 g**	**0.3 g**	**0.4 g**	**0.5 g**
Green tea	ORP (mV)	223	213	207	192	179
Rooibos tea	ORP (mV)	239	230	217	219	205
Green rooibos tea	ORP (mV)	241	235	221	223	210

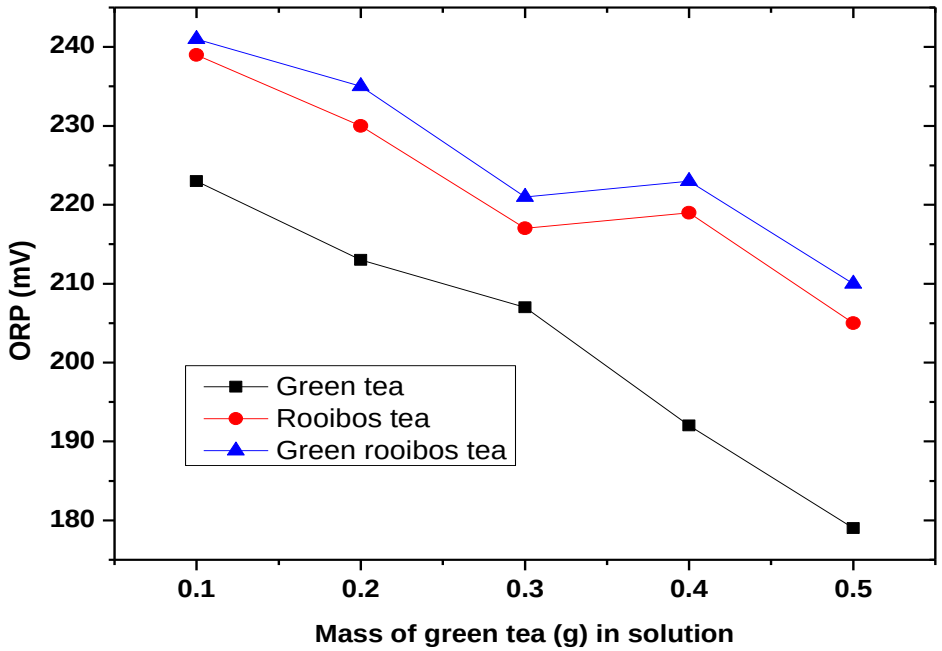

Figure 4. 3: Graphical presentation of ORP values of different tea extracts (green tea, rooibos tea and green rooibos tea). Extraction conditions: mass of tea leaves=60 g, ethanol=50 mL, H_2O=300 mL, temperature=70 ^oC, agitation speed = 300 rpm and time = 1 hour

Table 4.15 and Figure 4.3 showed the measured ORP data and its trends for the various tea extract solutions that were used in this study. Prior to analysis, different masses of tea extracts (green tea, green rooibos tea, or rooibos tea) were dissolved in 40 mL of deionised water and mixed to obtain a homogenous solution. Thereafter, a portable ORP probe was used to measure the ORP of the solutions. From the obtained ORP data, it was observed that the ORP values of the tea extracts decreased as the mass of tea extract in solution increased, indicating a stronger reducing agent correlation with mass of tea. It was also observed that among the tea extracts (green tea, rooibos tea or green rooibos tea), green tea was the stronger reducing agent as its ORP values were lower than those of rooibos tea and green rooibos tea (see Table 4.8 and Figure 4.3). This is because the green tea-extracted polyphenolic content contained more redox species in solution, thus showing its ORP value to be more strongly reducing (Vishnoi et al., 2018). The redox potential of green tea or green rooibos tea solution showed similar behaviour as the mass of tea in solution increased. As could be observed, their corresponding ORP values went up slightly from when 0.3 g of green tea extract was dissolved in solution to when 0. 4 g of green tea extract was dissolved in solution. Thereafter, a significant drop was observed in the ORP value (refer to Table 4.14 and Figure 4.3). Understanding the ORP data coupled with other parameters, the choice of the green reductant used in this study was established.

4.3.2 Chemical characterisation of tea extract solutions

This section presents and discusses the chemical composition of extracted tea samples that were dissolved in deionised water. This investigation was carried out to evaluate or measure the quantity of chemical species in solutions of the tea extracts. The characterisation techniques that were used to quantify the chemical species in solution of the tea samples included ICP-OES and IC as detailed in section 3.3.5 and 3.3.6 respectively.

4.3.2.1 Elemental composition of tea extracts

The elemental composition of the liquid tea extracts was obtained by identifying and measuring the concentration of elements in solution using the ICP-OES analytical technique. The results are presented in Table 4.16.

Table 4. 16: Elemental composition of different tea extracts. Extraction conditions: mass of tea leaves = 60 g, ethanol=50 mL, H_2O=300 mL, temperature=70 ^oC, agitation speed=300 rpm and time=1 hour

Parameter	Unit	Green tea	Rooibos tea	Green rooibos tea
Elements				
Al	mg/L	12.0	11	13
Mn	mg/L	9.01	9.30	8.97
Fe	mg/L	0.90	0.12	0.89
Ni	mg/L	0.15	0.28	0.19
Cu	mg/L	0.12	0.02	0.19
Zn	mg/L	0.29	0.41	0.43
Sr	mg/L	0.02	0.01	0.31
Ba	mg/L	0.04	0.03	0.4
Ca	mg/L	4.32	8.21	7.10
Na	mg/L	1.44	3.21	2.21
P	mg/L	62.0	73.1	71.4
Si	mg/L	2.41	2.17	2.56
K	mg/L	281	311	297
Co	mg/L	0.008	0.07	0.87
Ba	mg/L	0.04	0.09	0.01
Sr	mg/L	0.03	0.12	0.03
Zn	mg/L	0.3	0.5	0.9
Cu	mg/L	0.1	0.4	0.1
Ni	mg/L	0.1	0.21	0.3
Se	mg/L	0.001	0.02	0.004

Table 4.16 showed the elemental composition of green tea, rooibos tea, and green rooibos tea. These results prove that the major elements in the tea extracts were Al, Mn, P, Si, or K while the rest were minor elements (See Table 4.16). The concentration level of the major and minor elements found in the tea extracts were similar. Among the major elements (Al, Mn, P, Si, or K) found in the tea samples, as corroborated by various studies (Fernandez et al., 2002; Ashraf & Mian, 2008; Welna et al., 2013; McKenzie et al., 2010; Chen et al., 2009), K (GT=218 mg/L, RT=311 mg/L, or GRT=297 mg/L) > P(GT=62 mg/L, RT=73.1 mg/L or GRT=71.4 mg/L) > Al(GT=12.0 mg/L, RTE=11 mg/L, or GRTE=13 mg/L) > Mn (GT=9.01 mg/L, RTE=9.30 mg/L, or GRTE=8.97 mg/L) > Ca(GTE=4.31 mg/L, RTE=8.21 mg/L or GRTE=7.10 mg/L) > Si(GTE=2.41 mg/L, RTE=2.17 mg/L, GRTE=2.56 mg/L) > Na(GTE=1.44 mg/L, RTE=3.21 mg/L, or GRTE=2.21 mg/L) and the rest were trace and minor elements (Fernandez et al., 2002; Ashraf & Mian, 2008; McKenzie et al., 2010; Pohl & Prusisz, 2007; Malik et al., 2008). The most abundant trace elements found in teas are Fe, Cu and Zn (Ashraf & Mian, 2008; Welna et al., 2013; Ferrara et al., 2001; Han et al., 2005; Shen & Chen, 2008). In line with this investigation, it was also revealed that all three tea extracts can be used as reductants for the synthesis of nano-iron particles depending on their antioxidant power to reduce Fe. The use of tea extract as a reductant to produce nano-iron from AMD will have some elements elevated in solution. These elements will originate from the tea extract during its use as a reductant to produce nano-iron from AMD.

4.3.3 Ferric reducing antioxidant property (FRAP)

After the extraction of polyphenolic compounds from green tea, green rooibos tea and rooibos tea, the antioxidant activity of the extracts was measured using ferric reducing antioxidant property (see table 4.17). The ferric ion was reduced to ferrous ion by the polyphenolic substances in tea. This process occurred at a low pH with the formation of a coloured compound (ferrous-tripyridyltriaz). FRAP values were then recorded by comparing the change in absorbance at 593 nm in the test reaction mixtures with those containing ferrous ions per dry weight of the tested sample as displayed in Table 4.17. In this study, green tea extract was chosen as a choice of reductant for the synthesis of nano-iron particles because of its higher FRAP and DPPH values. This indicates its high antioxidant and reductant strength that is needed to reduce iron from solution.

Table 4. 17: Antioxidant power of polyphenolic compounds extracted from different tea species as recorded from ferric reducing antioxidant (FRAP) assay. Extraction conditions of tea species: mass of tea= 60 g, ethanol=50 mL, H_20= 300 mL, temperature= 70 ^oC, agitation speed and time = 300 rpm, for 1 hour. COV (coefficient of variation).

Plant and Chemical reductants	FRAP per dry weight of sample (µmol FeII/g)	COV (%) for triplicate measurement
Green tea extract	888	1.89
Green rooibos tea extract	804	2.41
Rooibos tea extract	756	2.39
Sodium borohydride	6013	2.72

From Table 4.17, the FRAP values of the aqueous-ethanolic extracts of green tea, green rooibos tea, rooibos tea and sodium borohydride were 888, 804, 756 or 6013 µmol/g respectively. The sodium borohydride FRAP test value revealed in Table 4.17 was for comparative purposes with the antioxidant strength of the green reductants. It was observed that as expected sodium borohydride had the highest FRAP value to reduce iron from a higher oxidation state to a lower oxidation state. Even though sodium borohydride had a higher FRAP value, the antioxidant values of the tea reductants were comparable (see Table 4.17). It was further observed that among the green reductants, green tea had the highest FRAP value. This was an indication that green tea has the capability to reduce iron from a higher oxidation state to a lower oxidation state. However, the aqueous-ethanolic polyphenolic tea extracts did not show large discrepancies in their FRAP values. Therefore, all the tea extracts had reducing capability for iron (see Table 4.17). The FRAP test current findings are in accordance with the findings by Oakes (2013) that the tea extracts contain sufficiently high amounts of polyphenolic compounds with the potential to act as a reducing agent. On this note, it was expected that compounds that donate electrons for the reduction of Fe^{3+} to Fe^{2+} can also quench free radicals. In this line of investigation, the radical scavenging activity of the tea extracts was determined against the stable free radical DPPH antioxidant activities.

4.3.4 Characterisation of tea extracts by 2,2-diphenyl-1-picrylhydrazyl (DPPH*)*

Following the extraction of polyphenols from green tea extracts (green tea, green rooibos tea, and rooibos tea), the scavenging activity of the tea extracts was investigated against the stable free

radical 2, 2-diphenyl-1-picrylhydrazyl (DPPH). Table 5.2 presents the DPPH results of the tea extracts using ascorbic acid as a reference reductant against DPPH.

Table 4. 18: Antioxidant activities of aqueous-ethanolic tea extracts as recorded by 2, 2-diphenyl-1-picrylhydrazyl (DPPH). Extraction conditions of tea extract: mass of tea=60 g, ethanol=50 mL, H20=300 mL, temperature=70 ^{o}C, agitation speed=300rpm and time=1 hour. (T=time).

			% Inhibition	
Antioxidant (mg/l)	**Ascorbic acid**	**Green T**	**Green rooibos T**	**Rooibos T**
3.12	25.3±0.23	2.71±0.91	4.63±1.21	1.57±0.02
6.25	41.83±1.48	3.16±0.06	7.12±1.42	2.86±1.11
12.5	66.84±2,67	17.38±0.21	11.37±0.98	1.31±0.71
25	96.52±0.98	24.49±0.9	19.41±1.42	8.94±1.71
50	96.97±1.21	40.92±1.1	40.11±2.41	17.81±2.11
100	97.01±0.72	65.65±1.4	71.92±3.1	34.40±1.98

The tea extracts (green tea, green rooibos tea and rooibos tea) showed a high percentage of inhibition at 100 mg/L on DPPH (see Table 4.18). However, ascorbic acid as a reference standard (reductant) proved to have a higher percentage inhibition that was greater than 97% at 100 mg/L for DPPH (see Table 4.18). The percentage inhibition of ascorbic acid as a reference reductant was close to 100% but the percentage inhibition values of the tea extracts were still significant, although somewhat lower compared to that of ascorbic acid as a reference reductant. These results are in line with the finding in literature (Badmus et al., 2018a). Consequently, green tea, green rooibos tea, and rooibos tea extracts can inhibit oxidative processes by significant reaction in a biological matrix. In this line of investigation, the structural vibrations of polyphenolic compounds were also analysed.

4.3.5 Fourier transform infrared spectroscopy (FTIR)

This subsection presents and discusses the FTIR results of aqueous-ethanolic extracts of green tea, green rooibos tea, and rooibos tea. The purpose of this analysis was to investigate the structural properties of the various tea extracts. The FTIR analytical technique has been detailed in section 3.3.13 and the obtained results presented in Figure 4.4.

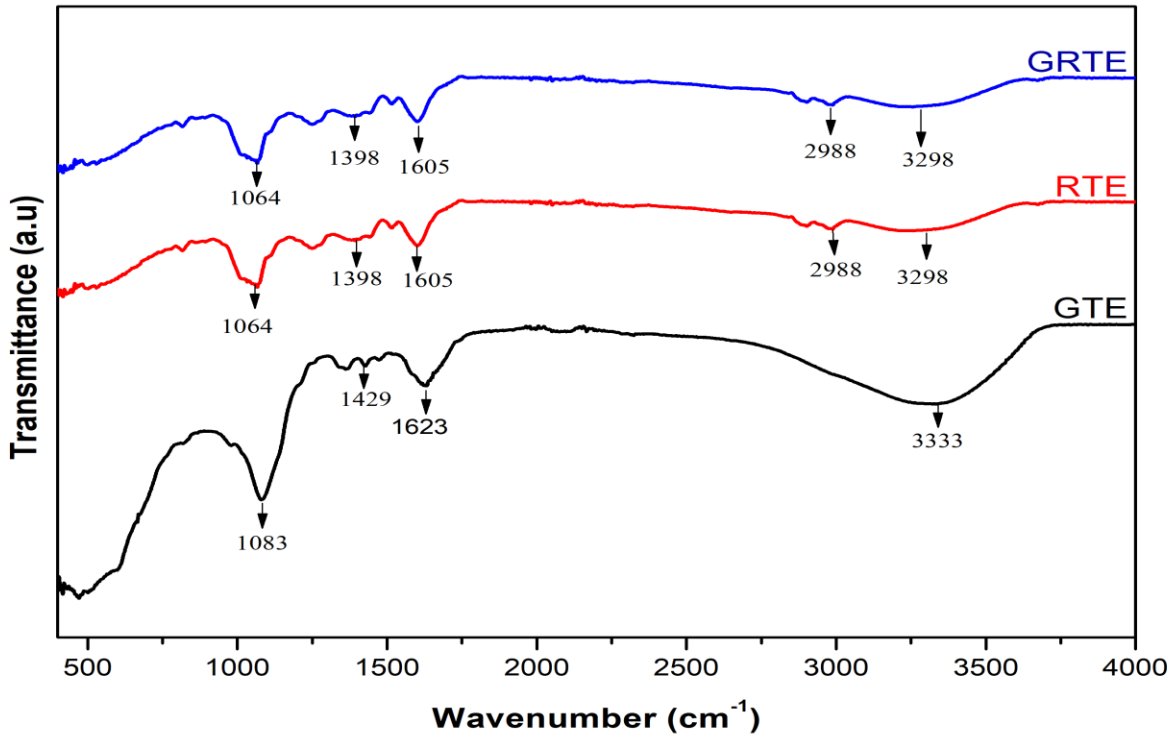

Figure 4. 4: FT-IR transmittance spectrum of green tea (GTE), green rooibos tea (GRTE) and rooibos tea (RTE) extracts. Extraction condition of tea extracts: mass of tea= 60 g, ethanol=50 mL, H_20=300 mL, temperature=70 ^oc, agitation speed=300 rpm, time=1 hour.

From Figure 4.4, the stretching vibrations of polyphenolic compounds could be observed. The stretching vibration at 3298 cm^{-1} for green rooibos tea (GRTE) and rooibos tea (RTE) and at 3333 cm^{-1} for green tea (GTE) could be assigned to O-H stretching (Suresh et al., 2014). The intense O-H vibration of green tea extract (GTE) could be attributed to the high contribution of benzylic OH from its polyphenol content, which is higher than it is in green rooibos tea and rooibos tea (Badmus et al., 2018a). The apparent peak found on GRTE, RTE and GTE at 1605, and 1623 cm^{-1} respectively could be assigned to C=C aromatic skeletal vibrations (Lin et al., 2017). The presence of this peak confirms the presence of aromatic compounds in the polyphenolic extracts of tea. Its broad intensity in GTE among others confirms a higher concentration of the aromatic compound. The symmetric, asymmetric, and carbonyl peaks for GRTE and RTE are found at 1206, 1398, and 1064 cm^{-1} peak points while the symmetric, asymmetric and carbonyl peaks shifted to a higher wavelength for green tea extract (GTE) to peak points at 1400, 1429, and 1083 cm^{-1}. It was also observed that C-H vibrations were present in GRTE and RTE but absent in the GTE extract.

4.3.6 Scanning electronic microscope (SEM): morphological analysis of tea extracts

This section presents and discusses the morphology of dried tea extract samples (green tea, rooibos tea, and green rooibos tea). The morphological interpretation of the tea extracts also includes elemental analysis. The analytical technique used to determine the morphology and elemental analysis of the tea extracts is scanning electron microscopy-energy dispersive spectroscopy (SEM-EDS) as detailed in section 3.3.11. The obtained SEM-EDS qualitative results are presented in 4.19.

Table 4. 19: EDS of powdered tea extracts, Extraction condition of tea extracts: mass of tea= 60 g, ethanol=50 mL, H_20=300 mL, temperature=70 ^oC, agitation speed=300 rpm, time=1 hour

Elements	Weight % of GTE	Weight % of RT	Weight % of GRTE
O	89.62	65.02	67.99
Na	0.00	7.35	7.33
Mg	0.00	2.50	2.93
Cl	0.00	27.83	12.58
K	12.38	11.28	9.17
Total	100.00	100.00	100.00

From Table 4.19 the variance in the elemental composition between green tea extract (O or K) and rooibos extracts (O, Na, Mg or Cl) can be observed. This can be attributed to the geographical origin of the tea, the number and the frequency of pesticide and fungicide sprays, as evidenced in Indian, Iranian and Sri Lankan teas (Mehra & Baker, 2007; Moghaddam et al., 2008; Mossion et al., 2008; Seenivasan et al., 2008). The variation in elemental composition in tea could also be attributed to the concentration of the elements in the soil type and their uptake capacity of the given elements to the leaves of the tea plants (Mehra & Baker, 2007). However, the elemental composition of tea extracts using the EDS analytical technique cannot be solely relied upon since it only scans the surface of the material to be tested.

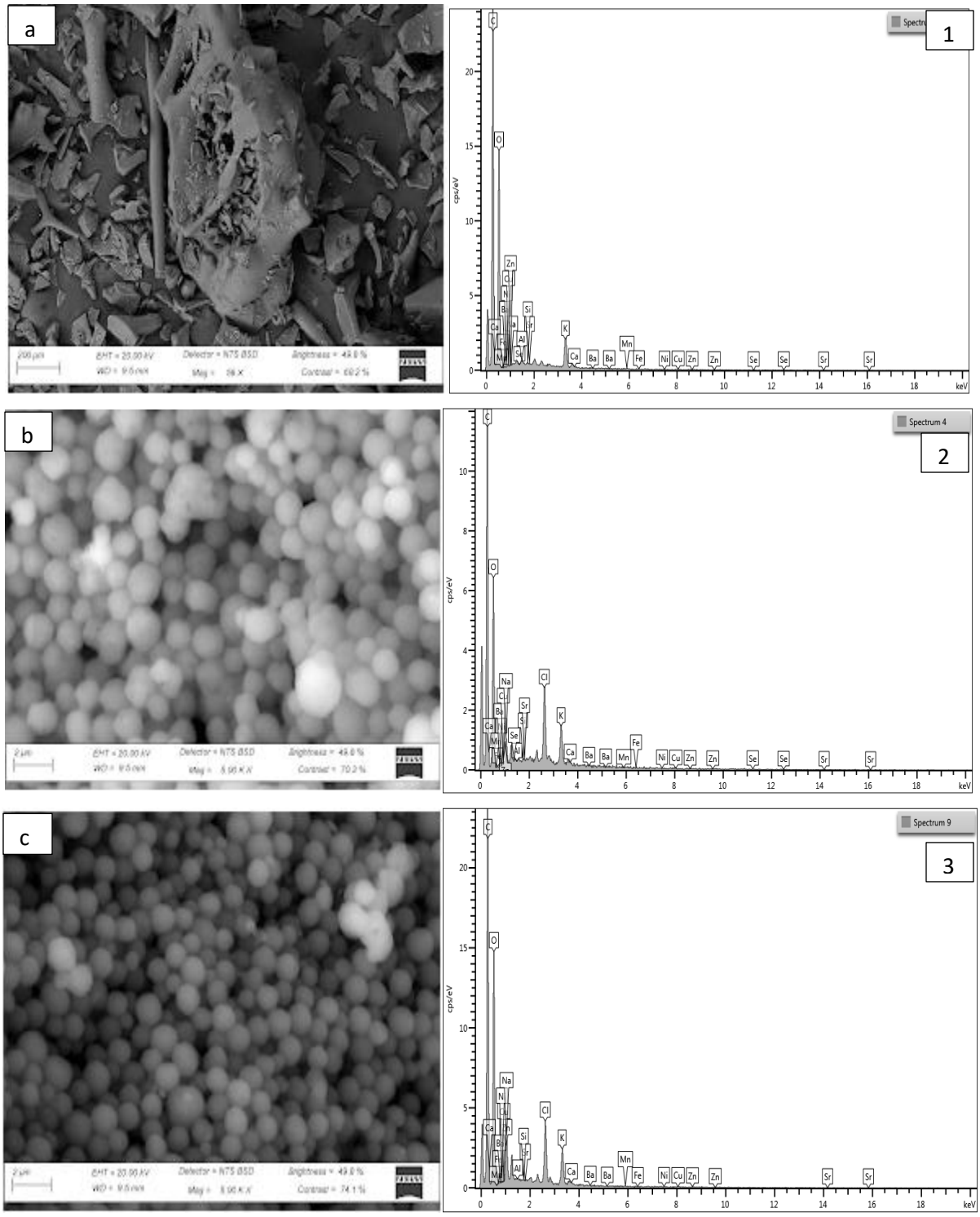

Figure 4. 5: SEM images of powdered tea extracts (a) GTE, (b) GRTE and (c) RTE extracts

The SEM images and EDS spectrum of tea extracts (green tea, rooibos tea or green rooibos tea) that was extracted from their various tea leaves and then dried are presented in Figure 4.5. After

observation of the tea extracts micrograph, it was observed that the particles of the green tea extract were irregularly shaped, whereas the particles of rooibos tea and green rooibos tea extracts were spherically shaped particles in the low µm size range.

Particle size interpretation of tea extracts

The particle size distribution of tea extracts measured from their corresponding SEM images.

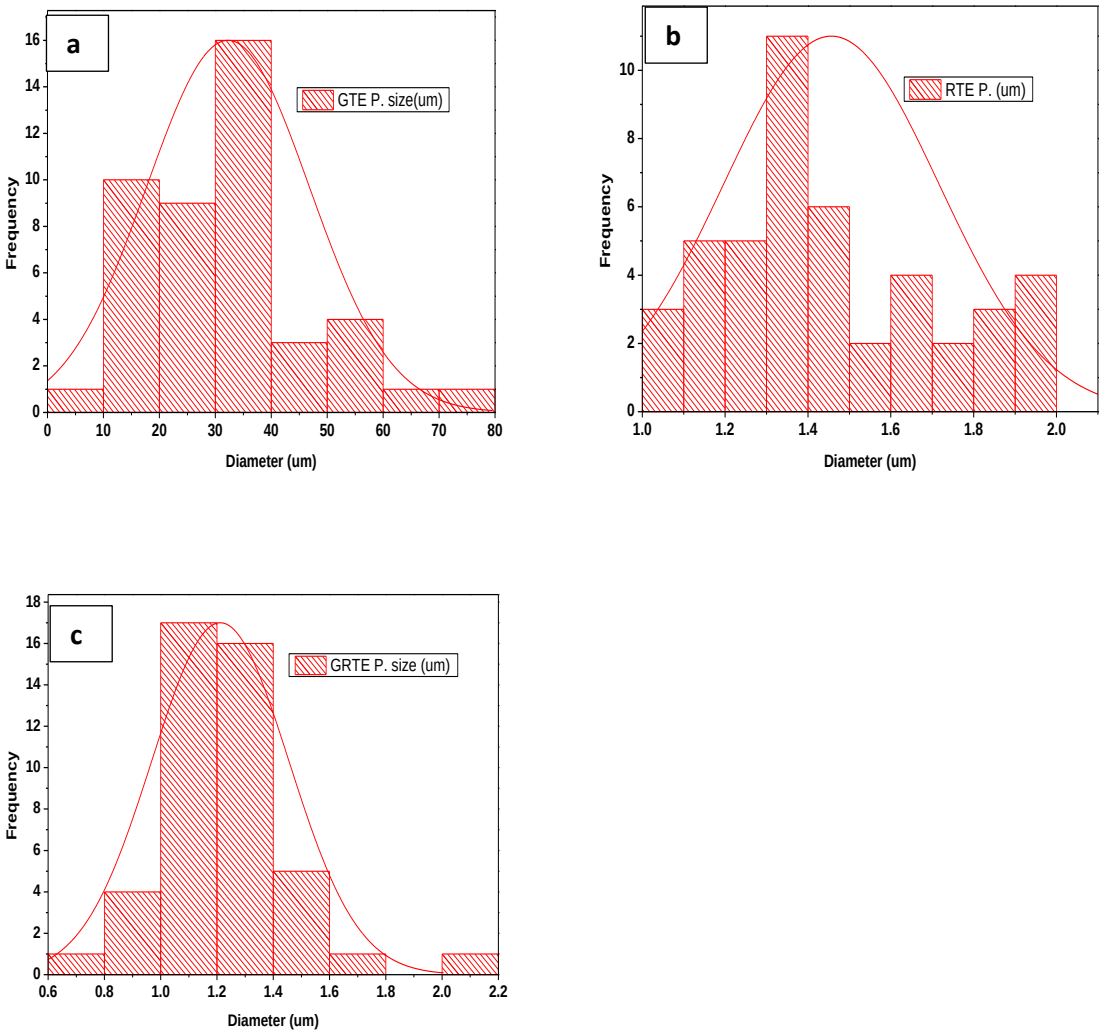

Figure 4. 6: Particle size distribution of dried extracts of (a) green tea (b) rooibos tea and (c) green rooibos tea. Extraction conditions: Mass of tea= 60 g, ethanol=50 mL, H_20=300 mL, temperature=70 ^oC, agitation speed=300 rpm, and time=1 hour. (GTE=green tea extract, RTE=rooibos tea extract, GRTE=green rooibos tea extract).

Graphical representation of the size distribution of particles of tea extracts (GTE, RTE, or GRTE) could be seen in Figure 4.6. It was observed that the average particle sizes for GTE, RTE or GRTE were approximately 32.261, 1.456 g or 1.212 µm respectively. The average particle size of green tea extract was about 30 times greater than those of rooibos and green rooibos extract, even though the same method of extraction was used on all tea leaves. In this line of investigation, Makanjuola (2017) reported bigger particle sizes of 0.425 mm, 0.710 mm, or 1.180 mm for tea (*Camellia sinensis*), ginger (*Zingiber officinale*) and tea ginger blend. This indicates that the particle sizes of rooibos tea extracts obtained in this study were smaller than particle sizes obtained from past studies.

4.3 Choice of AMD and choice of reductant used for nano-iron synthesis in this study

Various South Africa as-received field AMD samples (Kopseer, Toeseep or Penstock) and various South Africa tea extracts (green tea, rooibos tea, or green rooibos tea) were characterised using different analytical techniques in this study. The analytical techniques used to characterise the South Africa AMD samples included pH, EC, TDS, DO, ORP, ICP, or IC, whereas the analytical techniques used to characterise the tea extracts as reductants included pH, ORP, FRAP, DPPH, FTIR, or SEM-EDS. These techniques were used to characterise the feedstock samples in order to access their quality for research purposes. In this line of investigation, the AMD samples were all acidic, and conducted electricity with various concentrations of cations and anions. The most dominant cation and anion found in the AMD samples were iron (Fe) and sulphate (SO^{2-}_4) respectively. However, the concentration of iron and sulphate in the AMD samples differed. The Kopseer AMD had the highest concentration of iron and sulphate followed by Penstock AMD and then Toeseep AMD. In this regard, the Kopseer AMD was the most suitable South Africa AMD to be utilized for nano-iron synthesis using reductants, followed by the Penstock AMD with a comparable concentration of iron. The iron content in the Kopseer and Penstock AMD was twice as much the concentration of iron in the Toeseep AMD solution. Since all the AMD samples had a reasonable concentration of iron, they could all be utilized as feedstock samples for the synthesis of nano-iron particles using a chemical reductant (sodium borohydride) or green reductant. However only the Penstock (P) AMD was used to produce nano-iron particles from AMD. The reason for the choice of feedstock AMD was because it was readily available in bulk, had comparable iron (Fe) concentration (4002 mg/L) to that of the Kopseer AMD (4420 mg/L), and its physico-chemical characteristics at the time of usage to produce nano-iron were almost the same.

After establishing the choice of feedstock AMD, the choice of green reductant for nano-iron synthesis from the feedstock AMD was also established. In this case it was green tea extract. This is because after assessing the antioxidant power and structural analysis of green tea, rooibos tea and green rooibos tea extract using ferric reducing antioxidant power (FRAP), 2, 2-diphenyl-1-picrylhydrazyl (DPPH), and scanning electronic microscope (SEM), the green tea extract had the highest FRAP and DPPH values, indicating that it was a stronger reducing agent of iron (Fe) than its counterparts (rooibos tea and green rooibos tea extract). In summary, South Africa field AMD P and South Africa green tea extract were feedstock samples for the synthesis of nano-iron particles using a chemical and a green reductant for comparative purposes.

CHAPTER 5

APPLICATION OF REDUCTANTS FOR THE EXTRACTION OF NANO-IRON PARTICLES

5.0 Introduction

The current chapter describes and discusses the use of chemical and environmentally friendly reductants for the extraction of nano-iron particles from acid mine drainage (AMD). The present section is subdivided into two sections. The first section (5.1) introduces and discusses the use of sodium borohydride ($NaBH_4$) as a reductant in the extraction of nano-iron particles from mine water (AMD). The second section (5.2) presents and discusses the use of green tea to extract nano-iron particles from AMD. These reductants were chosen for comparative purposes.

5.1 Treatment of AMD using sodium borohydride as a chemical reductant

This section presents and discusses the results obtained after applying sodium borohydride to Penstock AMD collected from the Navigation coal mine. The concentration of sodium borohydride used for the extraction of nano-iron from AMD was optimized to reduce reductant mass, cost, and time wastage.

5.1.1. Sodium borohydride ($NaBH_4$) concentration optimization

The optimization process of sodium borohydride as a reductant was carried out by making different concentrations of sodium borohydride solutions 0.1 M, 0.2 M, 0.3 M, 0.4 M, 0.5 M, 0.6 M, and 0.7 M corresponding to dosages of 3.8 g/L, 7.6 g/L, 11.3 g/L, 15.1 g/L, 18.9 g/L, 22.7 g/L or 26.5 g/L to extract nano-iron from the collected Penstock AMD.

.

5.1.2. Effect of borohydride (M) on the pH and composition of the treated AMD solutions

The results in Table 5.1 show the pH values of Penstock AMD and pre-treated Penstock AMD using sodium borohydride.

Table 5. 1: pH values of raw AMD and treated AMD using sodium borohydride ($NaBH_4$)

$NaBH_4$ Conc (M)	pH of $NaBH_4$ treated AMD
Raw AMD	2.14
0.1	4.96
0.2	5.51
0.3	5.88
0.4	6.24
0.5	7.11
0.6	8.63
0.7	8.95

Table 5.1 shows that increasing the concentration of sodium borohydride that was used to treat AMD from 0.1 M to 0.7 M raises the pH of the pre-treated field Penstock AMD solution from 4.98-9.14.

5.1.3 Effect of sodium borohydride concentration on the removal metals and sulphate

All experimental parameters that were used to produce nano-iron from AMD using sodium borohydride were used at the applied conditions (see Table 5.2).

Table 5. 2: Extraction of nano-iron from Penstock AMD solution: Effect of initial concentration of sodium borohydride on the composition of the AMD solutions (AMD pH=2.14, room temperature=25 ^{o}C, contact time=120 minutes, $NaBH_4$ volume=50 mL, and AMD volume=100 mL).

Parameter	**Initial concentration (mg/L)**	The concentration of elements (mg/L) in AMD as a function of the initial concentration of sodium borohydride						
		0.1 M	0.2 M	0.3 M	0.4 M	0.5 M	0.6 M	0.7 M
Fe	4000	1096	1084	700	645	3.8	0.06	0.05
Al	367	245	53	2	0.1	0.01	0.53	0.01
Ca	503	360	345	330	319	315	313	298
Mn	85	62	60	60	56	35	23	23
Mg	376	157	143	125	108	103	101	101
Si	28	24	18	8	5	5	4	1
Cu	0.1	0.03	0.01	0.001	0.001	0.001	0.001	0.001
Zn	9.8	7	7	1.7	0.5	0.007	0.002	0.001
Mo	0.1	0.0001	0.0001	0.0001	0.0001	0.0001	0.0001	0.0001
Ni	1.2	0.3	0.4	0.5	0.3	0.02	0.01	0.01
Co	1.1	0.4	0.4	0.3	0.2	0.01	0.002	0.001
Sr	0.8	0.19	0.19	0.3	0.3	0.26	0.25	0.21
K	0.98	0.18	0.17	0.2	0.44	0.76	0.46	0.58
Se	ND	0.0006	0.0003	0.0001	0.0002	0.0002	0.0002	0.0002
Na	33	408	807	1923	2685	3715	5005	5500
B	0.14	149	301	663	904	1211	2194	2550
Sb	0.02	0.00003	0.00002	0.00001	0.00002	0.0005	0.0004	0.00002
Cd	0.001	0.0065	0.0063	0.00018	0.00005	0.00002	0.00002	0.00001
Chloride	10.2	10	10	10	10	10	10	10
Nitrate	2.13	0.27	0.2	0.2	0.33	0.28	0.27	0.2
Sulphate	11500	8582	8250	8403	8356	8571	8300	8450

Table 5.2 shows that increasing the concentration of sodium borohydride in the AMD solution significantly precipitated redox-sensitive elements but had less effect on precipitating low redox-sensitive elements. Redox-sensitive elements in the AMD solution included Fe, Al, Mn, Mg, Si, or Zn, whereas low redox-sensitive elements included Ca, Cu, Mo, Sr, or Se

5.1.4 Effect of sodium borohydride concentration on the removal of Fe from AMD

Figure 5.1 presents the results of the effect of sodium borohydride on the removal of iron from the Penstock AMD. The experimental conditions used to carry out this plan are as follows: AMD pH=2.14, room temperature=25 ^{o}C, Contact time= 20 minutes, $NaBH_4$ volume = 50 mL, AMD volume = 100 mL, (n = 3)

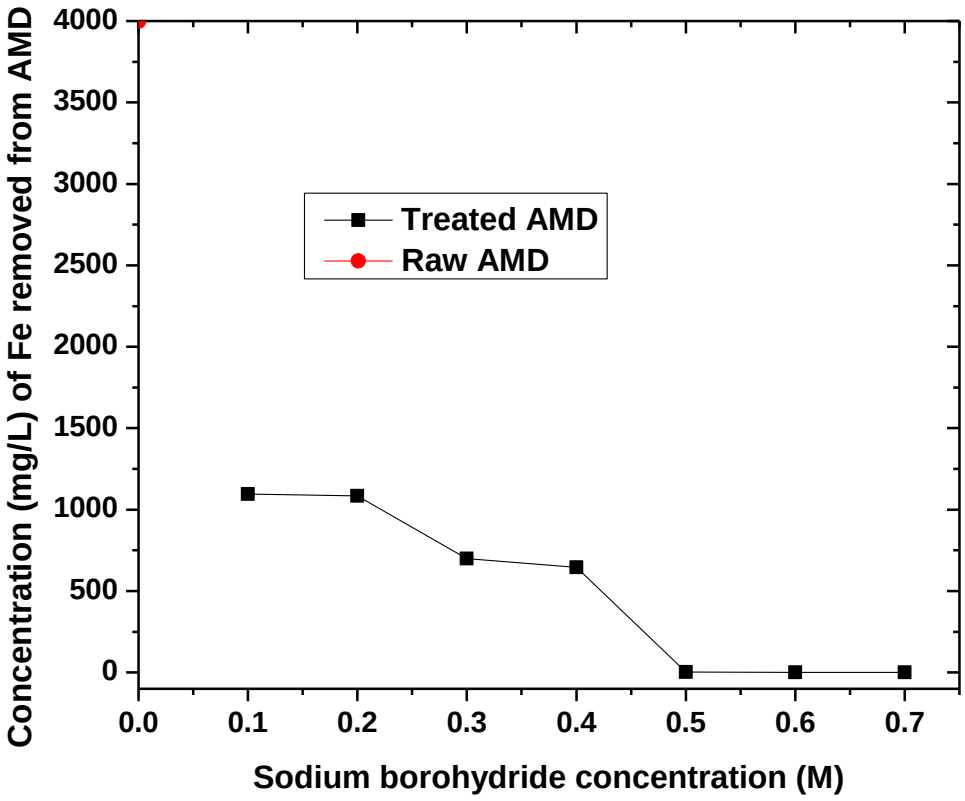

Figure 5. 1: Extraction of nano-iron from AMD solutions: effect of sodium borohydride dosage on the extent of Fe extraction. Experimental conditions: AMD volume=100 mL, AMD pH=2.14, $NaBH_4$ volume= 50 mL, temperature=25 ^{o}C and contact time=120 minutes, n=3.

Table 5.1 presents the initial concentration of iron (Fe=4000 mg/L) and other elements found in the Penstock AMD solution. The Penstock mine water was treated using different concentrations (0.1 M to 0.7 M) of sodium borohydride solution to remove Fe. From Figure 5.1, the removal of Fe from the AMD solution increased as the concentration of sodium borohydride increased from

0.1-0.6 M. In this regard, a 0.6 M solution of sodium borohydride was considered the optimum reductant concentration used to remove Fe from AMD. When the optimum dosage of sodium borohydride (0.6 M) solution was used to treat the Penstock AMD, the concentration of Fe decreased from 4000 mg/L to 0.06 mg/L (see Table 5.2 and Figure 5.1).

Equation 2.4 summarizes the method used to reduce ferric ions in an iron salt solution during its treatment with sodium borohydride as described in the literature (Glavee et al., 1995; Wang and Zhang, 1997; Xinchao and Viadero, 2007). The redox reaction between sodium borohydride and ferric ions produced hydrogen gas, which prevented the synthesized nano-iron particles from oxidizing.

$4Fe^{3+} + 3BH_4^- + 9H_2O \rightarrow 4Fe^0 + 3H_2BO_3 + 12H^+ + 6H_2$	(2.4)

5.1.5 Effect of sodium borohydride concentration on the removal of Al, Ca, and Mg from AMD

The concentration of Al, Ca, or Mg removed from the field Penstock AMD using sodium borohydride as a reductant is shown in Figure 5.2. The initial concentrations of these elements were Al (367 mg/L), Ca (503 mg/L), and Mg (376 mg/L).

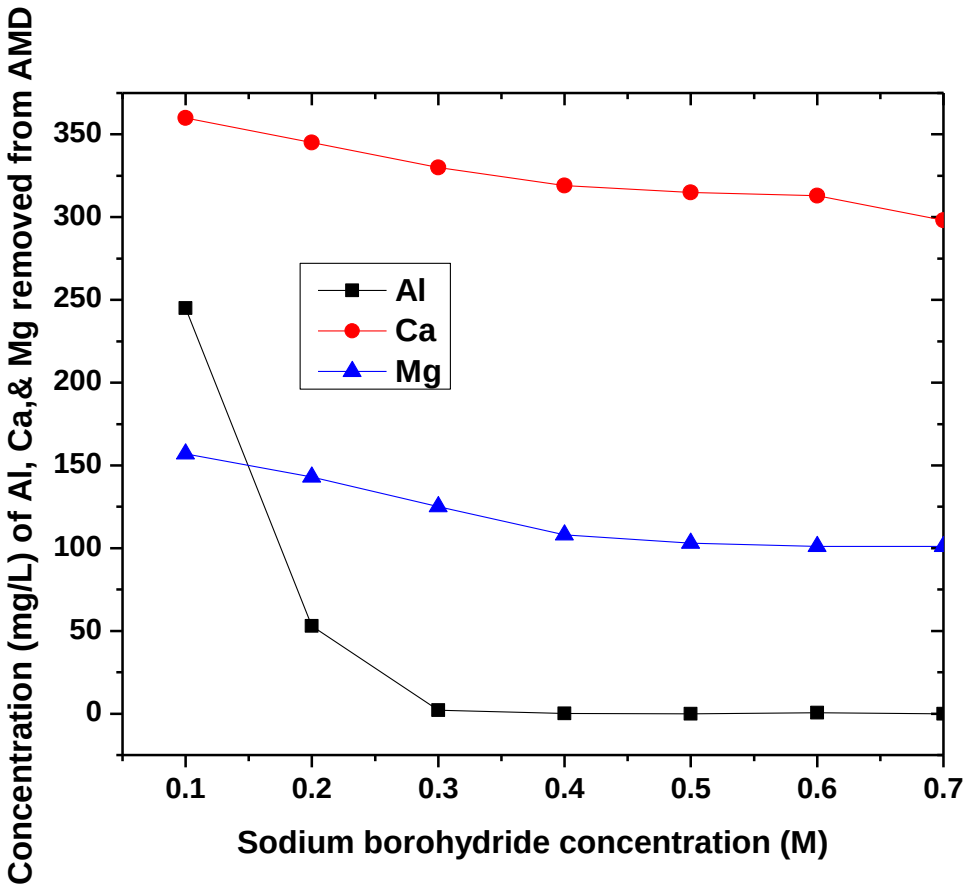

Figure 5. 2: Concentration of Al, Ca, or Mg removed from AMD using sodium borohydride as a reductant. Experimental conditions: AMD volume=100 mL, AMD pH=2.14, $NaBH_4$ volume= 50 mL, temperature=25 ^oC and Contact time=120 minutes (n = 3).

Figure 5.2 demonstrated that the removal of Al, Ca, and Mg increased as the concentration of sodium borohydride increased from 0.1 to 0.3 M, but was slowly removed between 0.4 and 0.7 M. The lowest concentrations of Al, Ca, and Mg in AMD after the treatment of AMD with sodium borohydride were 0.01 mg/L, 298 mg/L, and 101 mg/L respectively. This demonstrates that Al, Ca, and Mg co-precipitated with Fe during the removal of Fe from AMD.

5.1.6 Effect of sodium borohydride concentration on the removal of Si, Mn, and Zn from AMD

Figure 5.3 presents the concentration of Si, Mn, or Zn that was removed from the Penstock AMD solution using sodium borohydride as a reductant. The initial concentrations of these elements were Si (28 mg/L), Mn (85 mg/L), and Zn (9.8 mg/L).

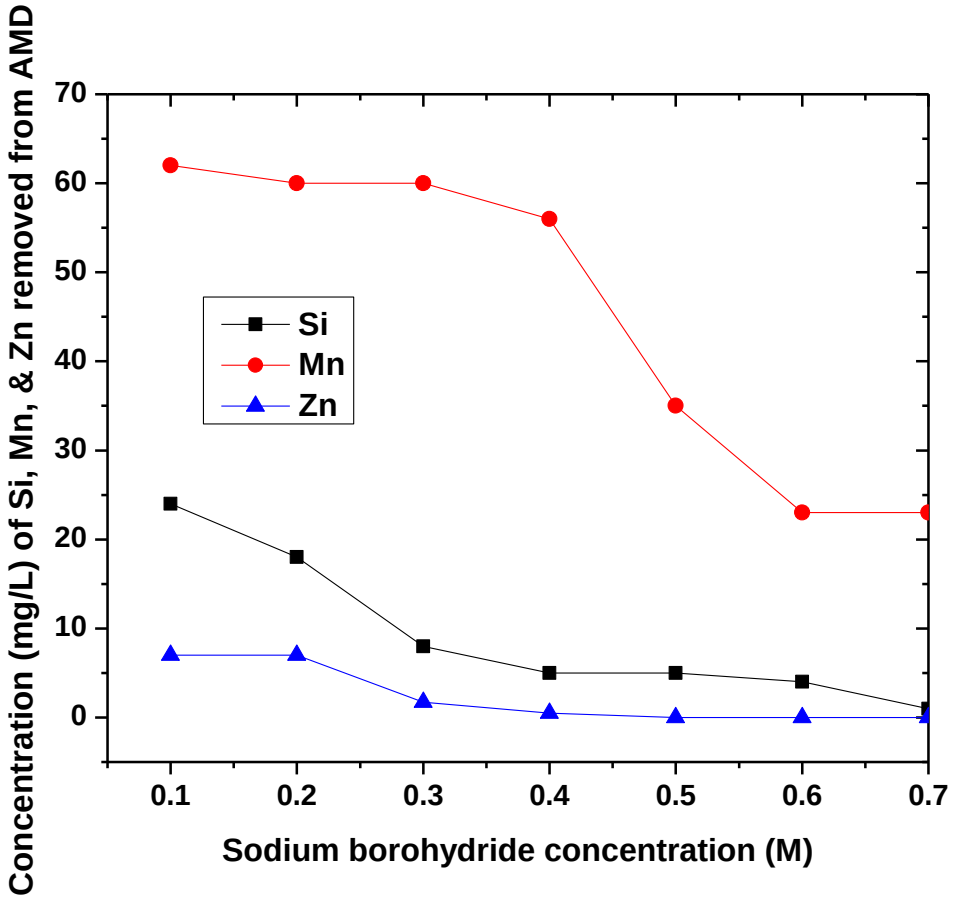

Figure 5. 3: Concentration of Si, Mn, or Zn removed from AMD using sodium borohydride as a reductant. Experimental conditions: AMD volume=100 mL, AMD pH=2.14, $NaBH_4$ volume= 50 mL, temperature=25 ^oC and contact time=120 minutes (n=3)

The removal of Si, Mn, or Zn from AMD increased as the concentration of sodium borohydride increased from 0.1 to 0.6 M in most cases. The lowest concentrations of these elements in the AMD solution after treatment with sodium borohydride were recorded as Si (4 mg/L), Mn (23 mg/L), and Zn (0.02 mg/L). When 0.6 M or 0.7 M of sodium borohydride solution was used to treat

AMD, a constant slope was maintained for Mn and Zn, whereas the concentration of Si decreased (see Figure 5.3).

5.1.7 Effect of sodium borohydride concentration on the removal of Ni, Co, Sr, K, and Cu from AMD

Figure 5.4 demonstrates the removal of Ni, Co, Sr, K, and Cu from AMD. The initial concentrations of these elements in the AMD solution were Ni (1,2 mg/L), Co (1.1 mg/L), Sr (0.8 mg/L), K (0.98 mg/L), or Cu (28 mg/L).

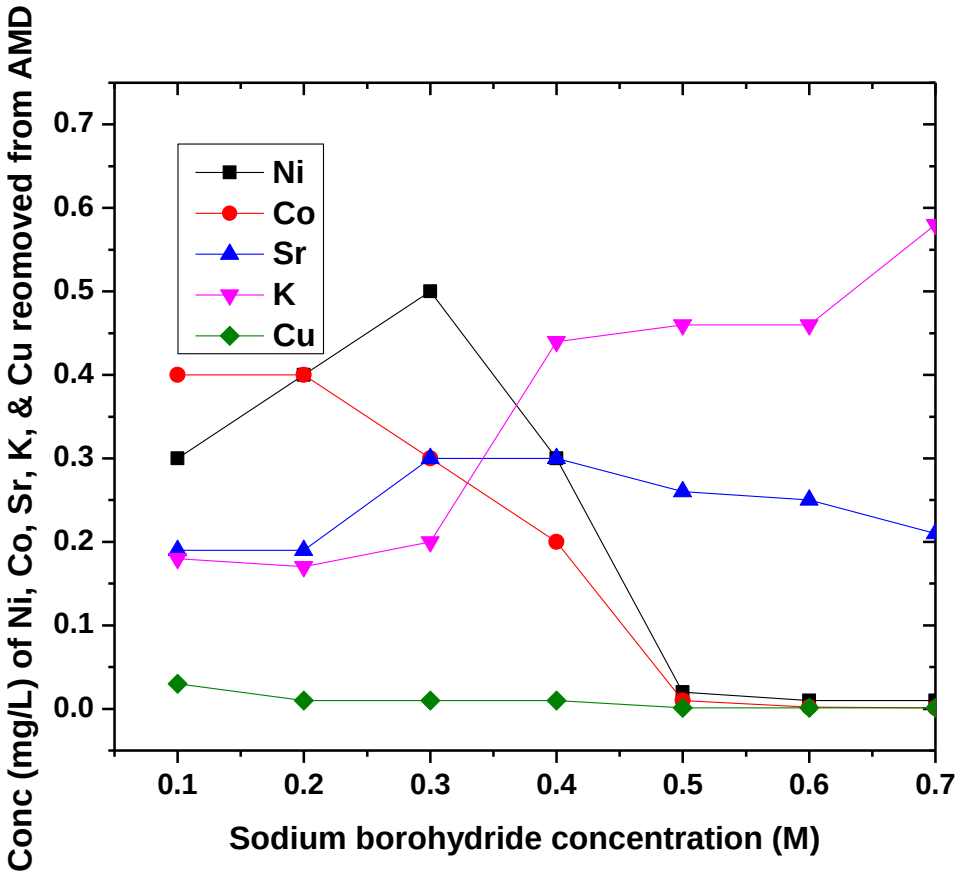

Figure 5. 4: Concentration of Ni, Co, Sr, K, Cu removed from AMD using sodium borohydride as a reductant, Experimental conditions: AMD volume=100 mL, AMD pH=2.14, $NaBH_4$ volume= 50 mL, temperature=25 ^oC and contact time=120 minutes (n=3)

Figure 5.4 demonstrated that when a 0.1 M solution of sodium borohydride was used to treat the Penstock AMD, the concentration of Ni, Co, Sr, or Cu in the AMD solution decreased significantly in most cases. Thereafter, the removal of these elements fluctuated. In the case of Co, as the concentration of sodium borohydride in the AMD solution increased from 0.1 to 0.5 M, its concentration in the AMD solution decreased, whereas K was the contrary. This is because K could have been leached out as a contaminant from the sodium borohydride reductant during AMD Fe precipitation since it was not 100% pure.

5.1.8 Effect of sodium borohydride concentration on Na and B in the AMD solutions

This section presents the concentration of Na and B in the Penstock AMD solution when the concentration of sodium borohydride used to precipitate Fe increased from 0.1 to 0.7 M. The results of the effect of sodium borohydride concentration on the initial concentration of Na (33 mg/L) and B (0.14 mg/L) in the Penstock AMD solution are presented in Figure 5.5.

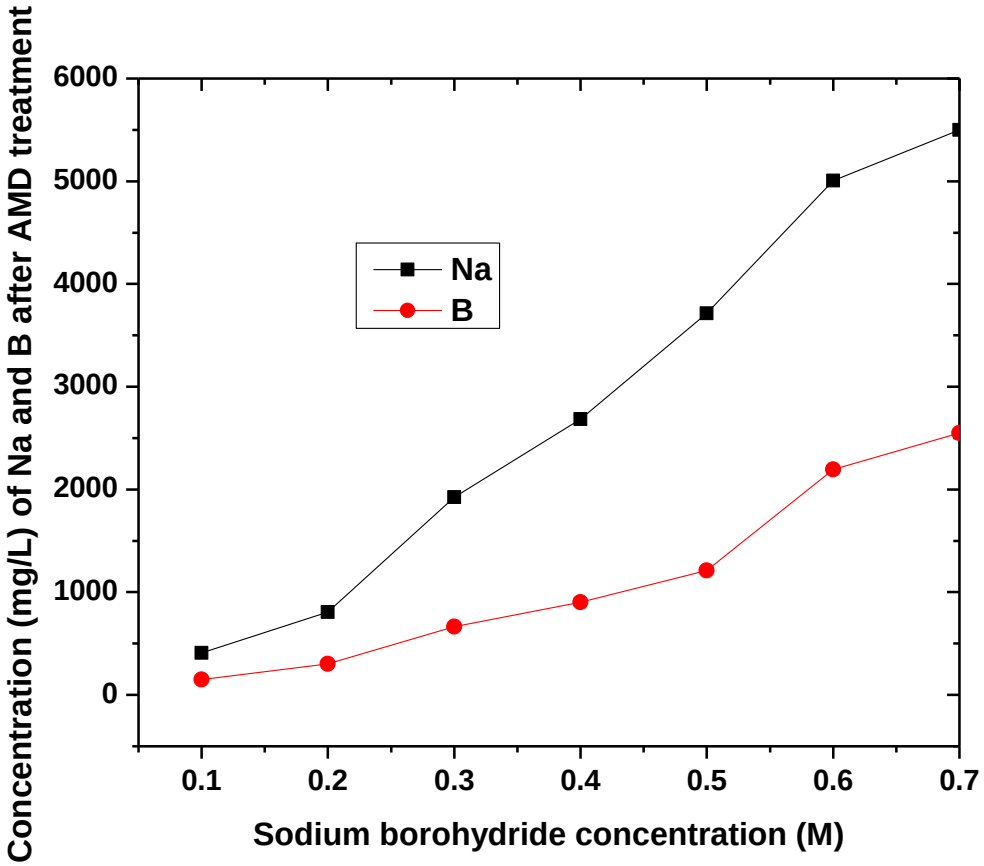

Figure 5. 5: Concentration of B and Na in AMD using sodium borohydride as a reductant, Experimental conditions: AMD pH = 2.14, room temperature = 25 ^{o} C, optimum Contact time = 120 minutes optimum $NaBH_4$ volume = 50 mL, optimum AMD volume = 100 mL, (n = 3).

Figure 5.5 demonstrates that the concentration of Na and B increased significantly when the concentration of sodium borohydride increased in the AMD solution. The highest concentrations of Na (5500 mg/L) and B (2550 mg/L) were observed when a 0.7 M solution of sodium borohydride was used to treat AMD. In summary, the concentration of Na and B increased in the AMD solution as the concentration of sodium borohydride increased. The high Na and B concentrations in the AMD solution were coming from the sodium borohydride reductant that was used to treat AMD.

5.1.9 Effect of sodium borohydride concentration on the removal of SO^{2-}_4 from AMD

To observe the trend of sulphate removal in the Penstock AMD solution during its treatment with sodium borohydride, the concentration of sodium borohydride was varied. As shown in Table 4.1, the initial concentration of sulphate in the AMD sample was 11500 mg/L.

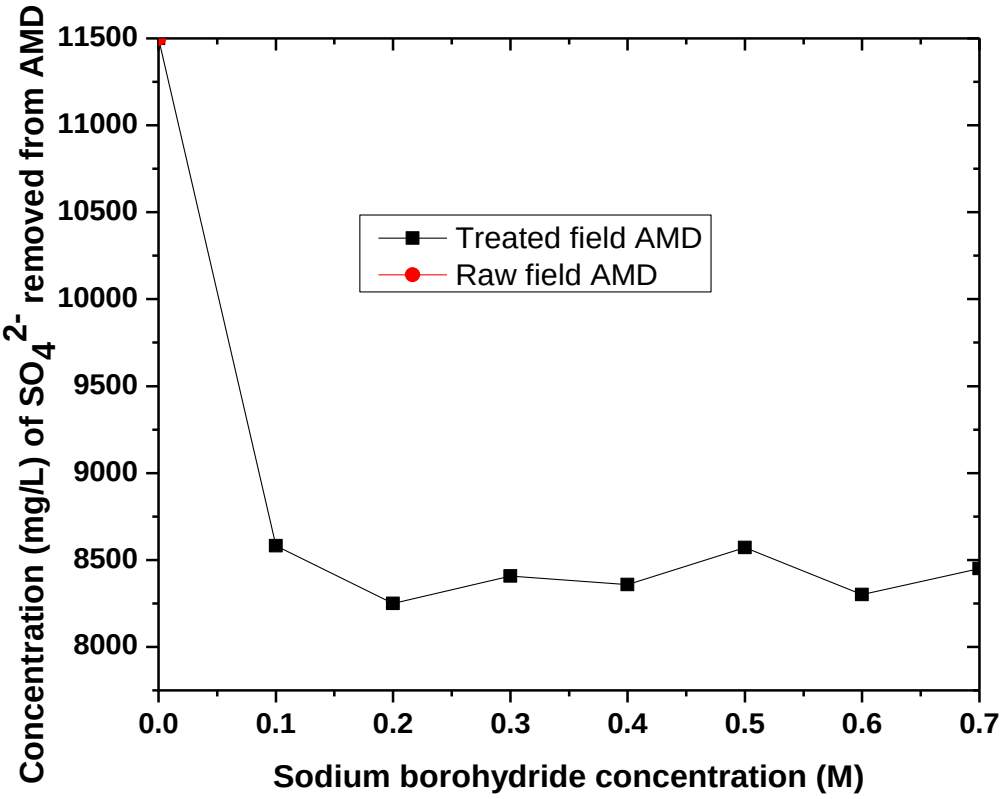

Figure 5. 6: Sulphate (SO^{2-}_4) removal from Penstock AMD using various concentration of sodium borohydride as a reductant: AMD pH=2.14, room temperature=25^{o}C, optimum contact time=120 minutes, optimum $NaBH_4$ volume=50 mL, optimum AMD volume=100 mL (n = 3).

Figure 5.6 depicts the trend of removing sulphate from AMD by varying the concentration of sodium borohydride as a reductant. Figure 5.6 demonstrates that when a 0.2 M sodium borohydride solution was used to treat AMD, the concentration of sulphate in the AMD solution decreased from 11500 mg/L to 8250 mg/L, which was the highest removal of sulphate from the AMD solution. As the concentration of sodium borohydride increased, the removal of sulphate from AMD solution fluctuated (see Figure 5.6).

5.1.10 Percentage removal of elements from AMD

This section revisits Table 5.2, but this time the data is presented as a percentage removal of elements from AMD in Table 5.3.

Table 5.3 presents the percentage removal of elements from AMD using sodium borohydride as a chemical reductant.

Table 5. 3: The effect of sodium borohydride concentration (M) on the percentage removal of cations and anions from field Penstock AMD solution (AMD pH=2.14, NaBH4 volume=50 mL, AMD volume= 100 mL, room temperature = 25 ^{o}C, contact time= 120 minutes, speed=250 rpm).

Parameter	Percentage removal of elements (mg/L) from AMD as a function of the initial concentration of sodium borohydride (M)						
	0.1 M	0.2 M	0.3 M	0.4 M	0.5 M	0.6 M	0.7 M
Fe	72	73	83	84	99.9	99.9	99.9
Al	33	85	99	99.9	99.9	99.9	99.9
Ca	28	31	34	36	37	37	40
Mn	27	29	29	34	58	73	73
Mg	63	70	71	75	76	77	77
Si	14	25	71	82	82	85	95
Cu	70	90	99	99	99	99	99
Zn	29	29	82	95	99.9	99.9	99.9
Mo	99.9	99.9	99.9	99.9	99.9	99.9	99.9
Ni	75	66	66	75	98	99	99
Co	64	64	72.8	82	99	98	99.9
Sr	76	76	63	63	68	69	74
K	82	83	80	55	22	53	40
Sb	99.9	99.9	99.9	99.9	99.9	99.9	99.9
Chloride	2	2	2	2	2	2	2
Nitrate	87	90	90	85	87	87	91
Sulphate	25	28	27	27	25	28	27

5.1.11 The percentage removal of major and minor elements from AMD

The percentage removal of major and minor elements (Fe, Al, Ca, Mg, Mn, Si, or Zn) from the Penstock AMD solution using sodium borohydride as a reductant is depicted in Figure 5.7. The

initial concentrations of these elements are shown in Table 5.2: Fe (4000 mg/L), Al (367 mg/L), Ca (503 mg/L), Mg (376 mg/L), Mn (85 mg/L), Si (28 mg/L) and Zn (9.8 mg/L).

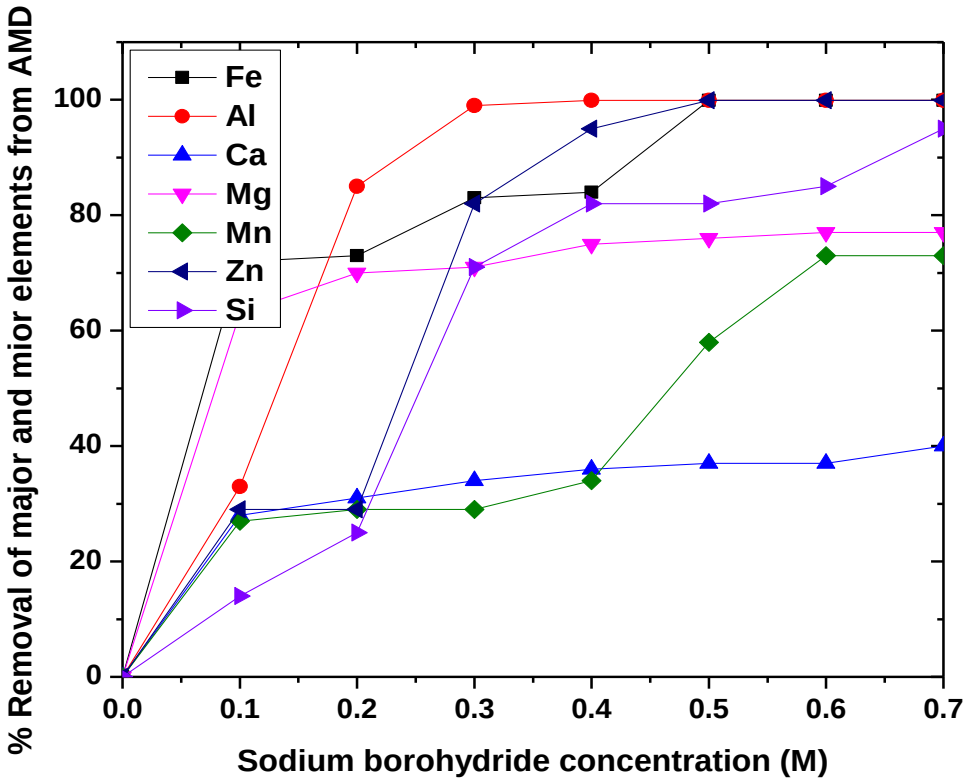

Figure 5. 7: Percentage removal of Fe, Al, Ca, Mg, Mn, Si, or Zn from AMD using sodium borohydride as a reductant, Experimental conditions: AMD pH=2.14, room temperature=25 ^{o}C, optimum contact time=120 minutes, optimum $NaBH_4$ volume=50 mL, optimum AMD volume=100 mL (n = 3).

Figure 5.7 shows the trend of percentage removal of major and minor elements (Fe, Al, Ca, Mg, Mn, Si, or Zn) from the AMD sample using sodium borohydride solution as a reductant. It also shows the maximum percentage removal of major and minor elements from the raw AMD sample as Fe (99.9%), Al (99.9%), Zn (99.9%), Si (96%), Mg (76%), Mn (72%), or Ca (40%). In most cases, as the concentration of sodium borohydride in the raw AMD solution increased from 0.1 to 0.6 M, so did the percentage removal of the major and minor elements that co-precipitated with Fe (see figure 5.7). This suggests that sodium borohydride was extremely effective at removing Fe and other major elements from AMD, such as Al, Ca, Mg, Mn, Si, or Zn. These elements can

be expected to co-precipitate with Fe as they are affected by the reducing environment created by sodium borohydride ($NaBH_4$).

5.1.12 The percentage removal of trace elements from AMD

The removal of Ni, Co and Sr from AMD treated with sodium borohydride reductant is depicted in Figure 5.8. The initial concentrations of these elements, as shown in Table 4.1 are Ni (1.2 mg/L), Co (1.1 mg/L), Sr (0.8 mg/L), and Ni (3.47 mg/L).

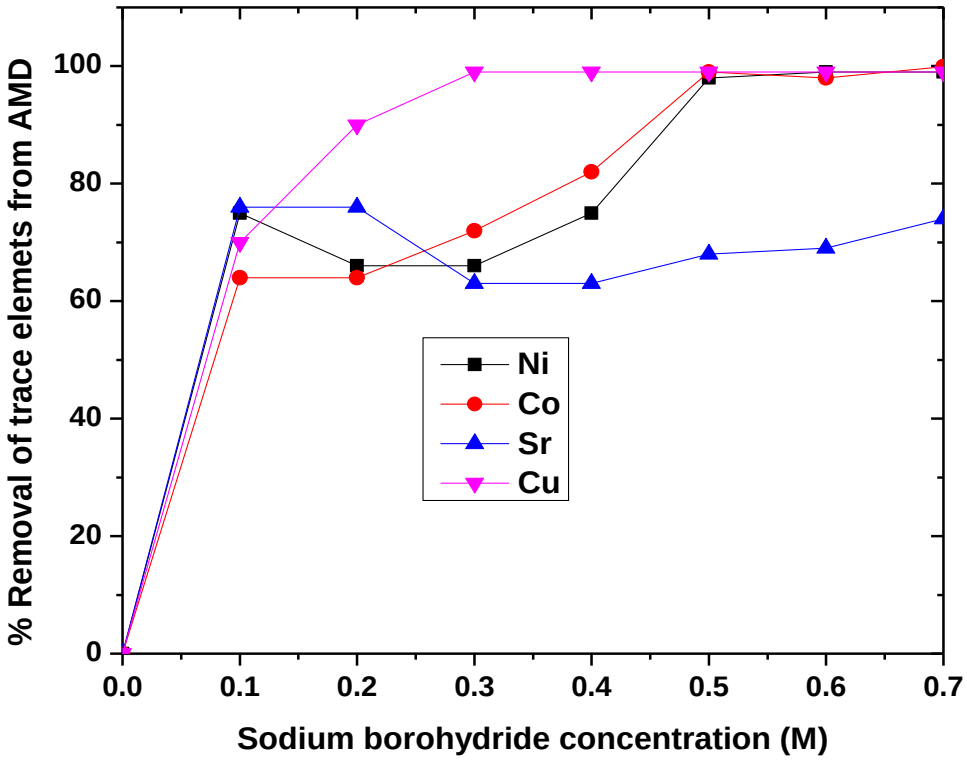

Figure 5.8: Percentage removal of Ni, Co, and Sr from AMD using sodium borohydride as a reductant. Experimental conditions: AMD pH = 2.14, room temperature = 25 ^{o}C, optimum Contact time = 120 minutes optimum $NaBH_4$ volume = 50 mL, optimum AMD volume = 100 mL (n = 3).

It can be seen in Figure 5.8 that as the concentration of sodium borohydride increased, so did the percentage removal of Ni, Co, and Sr from AMD. The optimum percentage removal of Ni (99%), Co (99%) and Sr (76%) from AMD was noted when 0.5 M of sodium borohydride was used to

treat Penstock AMD, except for Sr whose optimum removal from AMD was observed when 0.7 M of sodium borohydride was used to treat AMD.

5.1.13 The percentage removal of sulphate, chloride, and nitrate from AMD

Figure 5.9 depicts and discusses the results of using sodium borohydride as a reductant upon removal of anions such as sulphate, nitrate and chloride ions from Navigation Penstock AMD.

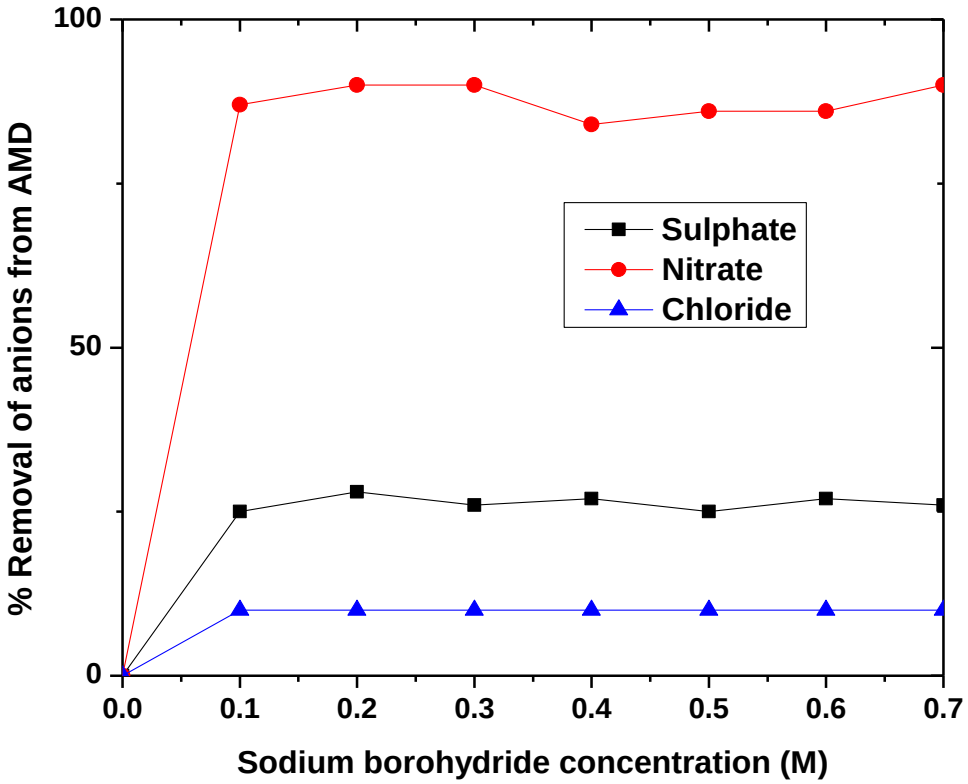

Figure 5. 9: Percentage removal of sulphate, nitrate or chloride from AMD using sodium borohydride as a reductant. Experimental conditions: AMD pH = 2.14, room temperature = 25 ^{o}C, optimum contact time = 120 minutes, optimum $NaBH_4$ volume = 50 mL, optimum AMD volume = 100 mL (n = 3).

As shown in Figure 5.9, sulphate and chloride were only slightly removed from AMD, whereas nitrate percentage removal was nearly complete using sodium borohydride as a reductant. The

percentage removal of these anions in the Penstock AMD fluctuated except for chloride as the concentration of sodium borohydride increased from 0.1 M to 0.7 M. The highest percentage removals of sulphate, nitrate and chloride were 28%, 91% and 2% respectively.

5.2 Treatment of AMD using green tea as a green reductant

This section presents the results obtained after applying different dosages of aqueous green tea extract (*C. sinensis*) to remove Fe from the Penstock AMD solution. This process was optimized in order to reduce the mass of reductant (*C. sinensis*), cost, and wastage of time.

5.2.1. Green tea dosage (g) optimization

The optimization process of green tea extract was carried out by using different dosages of green tea extract (0.1 g, 0.2 g, 0.3 g, 0.4 g, 0.5 g, 0.6 g, or 0.7 g) in their aqueous form to synthesize nano-iron particles from the Penstock AMD solution after mixing for 24 hours.

5.2.2 Effect of green tea dosage on the pH and composition of the treated AMD solutions

Table 5.4 shows the pH values of treated AMD using different dosages of aqueous green tea extract. Experimental conditions applied: AMD volume=50 mL, dosage (of green tea extract)=50 mL containing 0.1-0.7 g extract, AMD pH=2.14, agitation speed=250 rpm, temperature=35 ^{o}C, and contact time=24 hours (n=3).

Table 5. 4: pH values of raw AMD and AMD treated with varying dosages of green tea extract

Mass of green tea extract in (40 mL deionized H_2O)	pH of AMD supernatant generated after treatment with green tea
AMD	2.14
0.1 g	1.92
0.2 g	1.91
0.3 g	1.90
0.4 g	1.90
0.5 g	1.89
0.6 g	1.82
0.7 g	1.80

According to Table 5.4, increasing the dosage of green tea extract (from 0.1 to 0.7 g) to produce nano-iron particles from AMD slightly reduced the pH of their corresponding AMD supernatant (see Table 5.4). In line with this investigation, the pH of the AMD supernatants was more acidic than the pH of the as-received AMD. This could be attributed to the dissolution of acid-forming polyphenolic compounds that were leached out of green tea extract during AMD treatment.

5.2.3 Dosage effect of green tea extract on the removal of anions and cations

Table 5. 5: Extraction of nano-iron from the Penstock AMD solution: effect of the initial dosage of green tea extract on the composition of elements in the AMD solution. Experimental conditions applied: AMD volume=50 mL, AMD pH=2.14, dosage=50 mL solution of 0.1-0.7 g green tea extract, agitation speed=250 rpm, temperature=35 ^{o}C, and contact time=24 hours (n=3).

Parameter

	Initial concentration (mg/L)	Final concentration of elements (mg/L) in AMD as a function of initial dosage of green tea extract						
		0.1 g	0.2 g	0.3 g	0.4 g	0.5 g	0.6 g	0.7 g
Fe	4002	1800	1284	894	678	550	551	553
Al	367	263	205	190	146	120	120	116
Ca	503	275	253	239	206	178	176	174
Mn	85	41	32	28	18	13	13	11
Mg	376	257	226	190	152	142	141	133
Si	28	19	16	14	11	10	10	9.0
Cu	0.1	0.06	0.06	0.06	0.05	0.05	0.04	0.04
Zn	9.8	3.6	3.0	2.0	1.6	1.3	1.0	0.4
Mo	0.1	0.01	0.01	0.03	0.03	0.04	0.05	0.05
Ni	1.2	0.3	0.4	0.4	0.3	0.3	0.4	0.3
Co	1.1	0.1	0.1	0.1	0.1	0.1	0.1	0.1
Sr	0.84	0.2	0.2	0.2	0.1	0.08	0.08	0.08
K	0.98	127	142	187	243	259	352	360
Se	ND	0.1	0.2	0.3	0.3	0.3	0.3	0.4
P	ND	0.5	0.7	0.9	1.0	1.2	1.3	1.5
Na	33.1	27	26	24	22	19	18	18
Sulphate	11500	7995	7990	7650	7694	7817	8175	8201

5.2.4 Dosage effect of green tea extract on the removal of Fe from AMD

Figure 5.1 shows the effect of dosing AMD with green tea extract on the removal of Fe from the AMD solution.

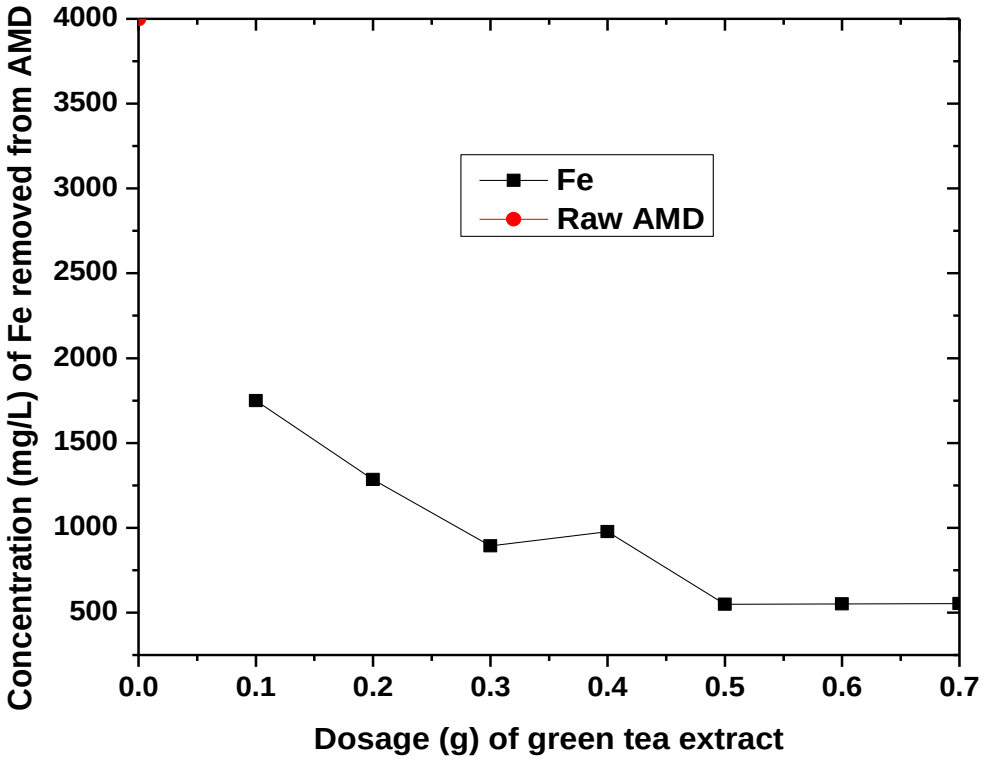

Figure 5. 10: Concentration of iron (Fe) removed from AMD using dried green tea in 40 mL of deionised water. Experimental conditions applied: AMD volume=50 mL, AMD pH=2.14, dosage =50 mL solution of 0.1-0.7 g green tea extract, agitation speed=250 rpm, temperature=35 ^{o}C, and contact time=24 hours (n=3).

The results of the initial concentration of Fe (4000 mg/L) and other elements found in AMD are shown in Table 4.1. These results were obtained from the IC and ICP-MS analysis of AMD. Following that, the Penstock AMD solution was treated with solutions made from powdered green tea extract (0.1–0.7 g) to produce nano-iron particles. The extraction began with a solution made from 0.1 g of powdered green tea extract, which decreased the concentration of Fe in the AMD solution from 4000 mg/L to 1800 mg/L. When the Penstock AMD was treated with solutions made from higher masses of green tea extract (0.1–0.5), the concentration of Fe in the AMD solution decreased from 1800 mg/L to 550 mg/L. It was also observed that when solutions containing 0.5–0.7 g of green tea extract were used to treat the Penstock AMD, the concentration of Fe in the AMD solution remained nearly constant. Based thereon, it was clear that a solution made from

0.5 g of powdered green tea extract was a sufficient dosage required for adequate iron removal from the Penstock AMD.

Reduction mechanism of green tea to produce nano-iron

To produce nano-iron particles from AMD, solutions made from powdered green tea extract were chosen as the reductant. This is due to the high content of polyphenols and organics in green tea, as well as the fact that green tea is a powerful antioxidant with high FRAP and DPPH values. There are approximately 4,000 species of green tea, with approximately one-third of the total containing polyphenolic compounds that can act as a reducing agent on salt precursors to produce nano-iron particles. Flavonoids and catechins are among the polyphenolic compounds found in green tea. Because the standard potential of Fe is -0.036 V, the active catechins, primarily epigallocatechin gallate (EGCG), act as electron donors (reducing agents) that can reduce Fe^{2+} or Fe^{3+} to a lower oxidation state, Fe^0. The reduction mechanism of green tea works in two stages. When the green tea reductant is added to the salt precursor, the OH bond is broken and a partial bond with the metal ion is formed, resulting in the formation of a complex. Secondly, when electrons are released, the partial bond is broken. This converts Fe^{2+} or Fe^{3+} nanoparticles to Fe^0 nanoparticles, which oxidize on their own to form ortho-quinone.

$EGCG + 3Fe^{n+} \rightarrow EGCG3Fe^{n+}$ (chelate complex)	(5.1)

$EGCG3Fe^{n+} + e's \rightarrow\rightarrow 3Fe^0 + quinone$	(5.2)

EGCG (Epigallocatechin Gallate)

EGCG3Fe (Catechin gallate chelate complex)

Overall equation

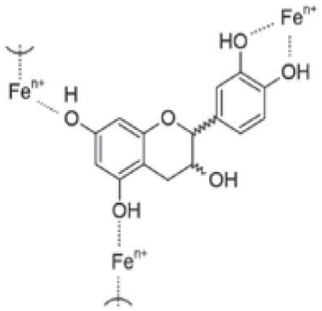

(±)-catechin

$3Fe^0 + quinone$…….5.3

5.2.5 Dosage effect of aqueous green tea extract on the removal of Al, Ca, Mg and K

This section presents the results of the effect of dosing AMD with aqueous green tea extract on the initial concentrations of Al (367 mg/L), Ca (5.3 mg/L), Mg (376 mg/L), and K (0.98 mg/L). The following are the experimental conditions applied: AMD volume=50 mL, AMD pH=2.14, dosage =50 mL solution of 0.1-0.7 g green tea extract, agitation speed=250 rpm, temperature=35 ^{o}C, and contact time=24 hours (n=3). Figure 5.11 presents the concentration removal of Al, Ca, Mg, and K.

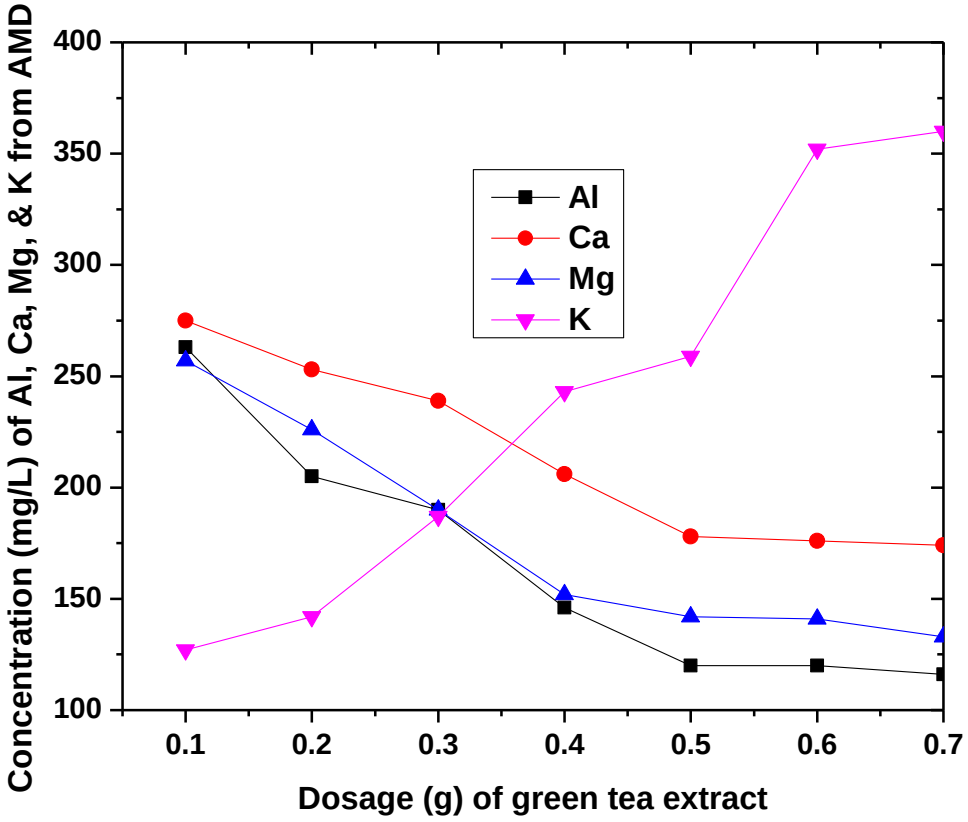

Figure 5. 11: Concentration of Al, Ca, Mg, or K removed from AMD using green tea extract. Experimental conditions applied: AMD volume=50 mL, AMD pH=2.14, speed=250 rpm, temperature=35 ^{o}C, and contact time=24 hours (n=3).

Figure 5.11 depicts the results of varying the dosage of green tea extract during the treatment of Penstock AMD. The concentration of Al (367 mg/L), Ca (5.3 mg/L), and Mg (376 mg/L) in the AMD sample decreased to Al (120 mg/L), Ca (178 mg/L), and Mg (142 mg/L), while the concentration of K increased from 0.98 to 360 mg/L. The reduction in the concentration of these elements in the AMD solution indicated that these elements co-precipitated with Fe during its extraction. The increased concentration of K in the AMD solution was caused by the high content of K in the green tea extract that was used to extract Fe from AMD.

5.2.6 Dosage effect of aqueous green tea extract on the removal of Si, Mn, Zn, and Na

The concentration of Si, Mn, Zn, or Na removed from AMD using green tea extract is shown in Figure 5.12. The initial concentrations of these elements were Si (28 mg/L), Mn (85 mg/L), and Zn (9.8 mg/L).

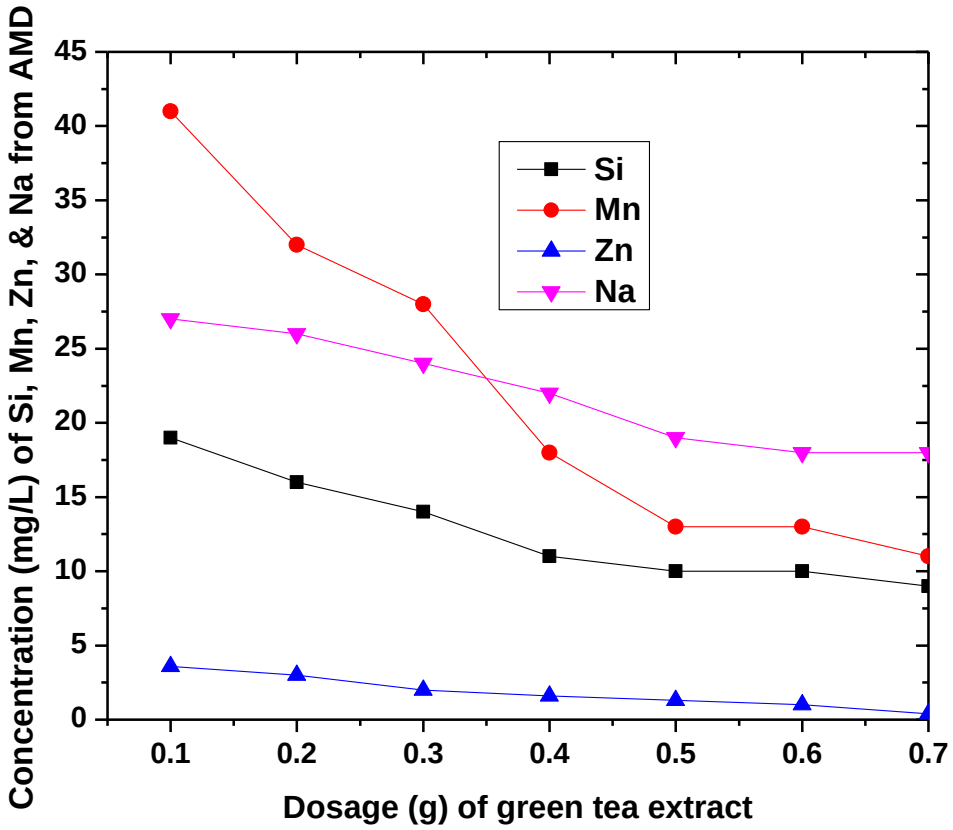

Figure 5. 12: Concentration of Al, Ca, Mg, or K removed from AMD using green tea extract. Experimental conditions applied: AMD volume=50 mL, AMD pH=2.14, dosage (of green tea extract)=50 mL solution of 0.1-0.7 g tea extract, agitation speed=250 rpm, temperature=35 ^{o}C, and contact time=24 hours (n=3).

The removal of Si, Mn, Zn or Na from AMD increased as the dosage of green tea extract in the AMD solution increased. The lowest concentration of these elements was recorded as Si (9 mg/L), Mn (13 mg/L), Zn (1 mg/L) and Na (18 mg/L) (see F igure 5.12).

5.2.7 Dosage effect of green tea extract on the removal of Ni, Co, Sr, K, and Cu

The removal of Si, Mn, Zn, and Na from AMD increased as the dosage of green tea extract in the AMD solution increased. The lowest concentrations of these elements in the AMD solution were recorded as Si (10 mg/L), Mn (11 mg/L), Zn (1 mg/L), and Na (18 mg/L) (see Figure 5.12).

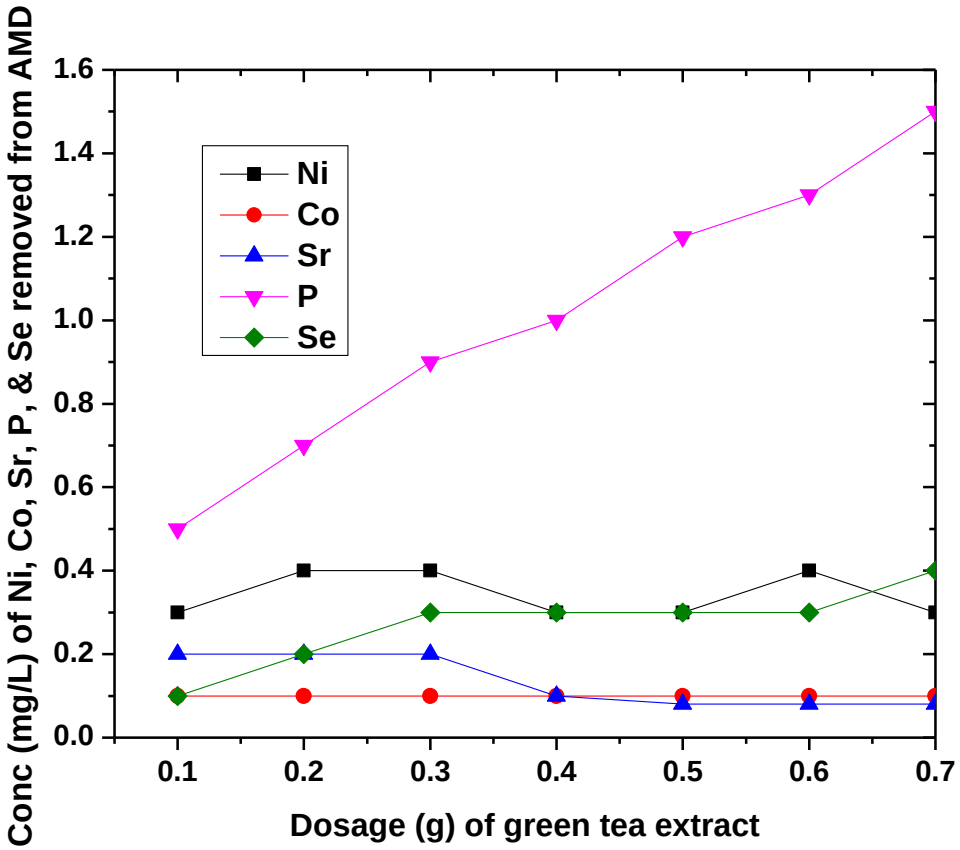

Figure 5. 13: Concentration of Ni, Co, Sr, P, or Se removed from AMD using green tea extract. Experimental conditions applied: AMD volume=50 mL, AMD pH=2.14, dosage (of green tea extract)=50 mL solution of 0.1-0.7 g green tea extract, agitation speed=250 rpm, temperature=35 ^{o}C, and contact time=24 hours (n=3).

Figure 5.13 shows the removal of Ni, Co, Sr, Se, K, or Cu from AMD that was treated with green tea extract. However, the concentration of P and Se in the AMD solution increased. This is because green tea extract used to treat AMD contained a reasonable amount of Se and P, which went into the solution with AMD.

5.2.8 Dosage effect of green tea extract on the removal of SO^{2-}_4

The dosage of green tea extract was optimized during the treatment of AMD to produce nano-iron particles. In this line of investigation, the trend of sulphate removal from AMD was observed. The initial concentration of sulphate in the AMD solution prior to treatment was 11500 mg/L, as shown in Table 4.1. The effect of green tea dosage on the removal of sulphate from AMD was analysed using the IC and ICP analytical techniques described in sections 3.5.5 and 3.5.6 respectively. The trend of sulphate removal from AMD is shown in Figure 5.14.

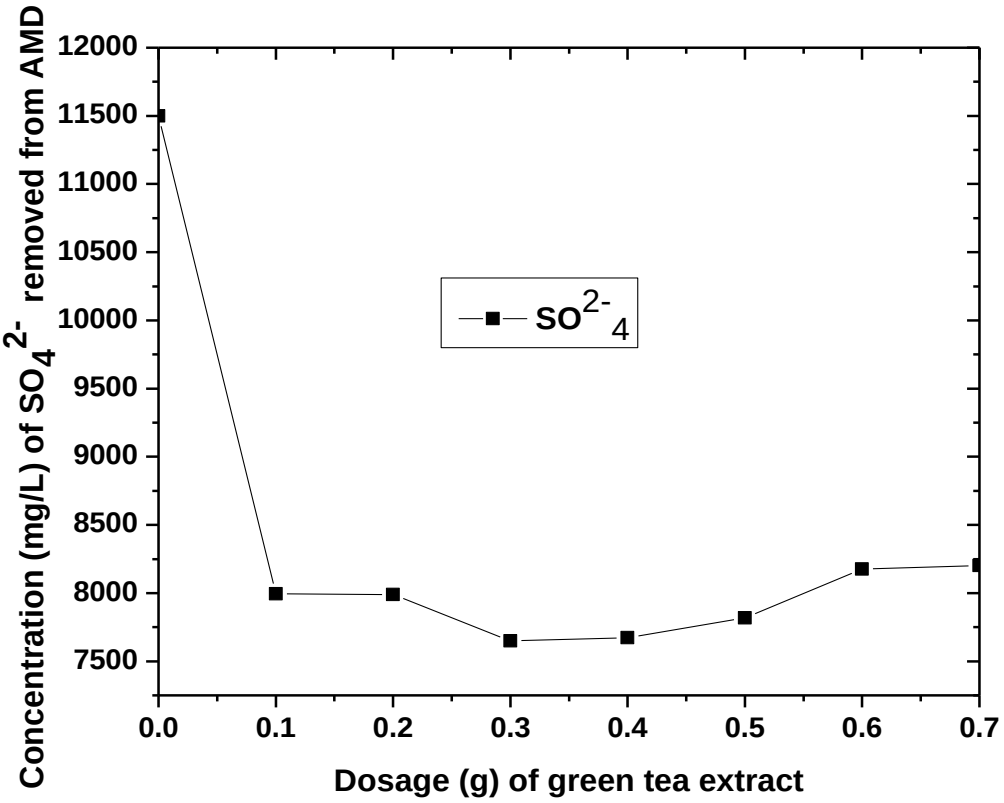

Figure 5. 14: Concentration of SO^{2*}_4 removed from AMD using green tea. Experimental conditions applied: AMD volume=50 mL, AMD pH=2.14, dosage (of green tea extract)=50 mL solution of 0.1-0.7 g green tea extract, agitation speed=250 rpm, temperature=35 ^{o}C, and contact time=24 hours (n=3).

Figure 5.14 shows the trend of sulphate removal from AMD by varying the dosage of green tea extract that was used to treat AMD. The highest removal of sulphate from AMD was observed when a tea solution that contained 0.3 g of green tea extract was used to treat AMD. At this dosage, the sulphate concentration in the AMD solution decreased from 11500 mg/L to 7,650 mg/L. At higher doses of green tea extract (0.4–0.7 g), the removal of sulphate from AMD was less favoured.

5.2.9 Percentage removal of elements from AMD

This section revisits Table 5.5, but the data is now presented in Table 5.6 as percentage removal of elements from AMD.

Table 5. 6: The dosage effect of green tea extract on the percentage removal of cations and anions from field Penstock AMD solution. AMD volume=50 mL, AMD pH=2.14, dosage (of green tea extract)=50 mL solution of 0.1-0.7 g green tea extract, agitation speed=250 rpm, temperature=35 ^{o}C, and contact time=24 hours (n=3).

Parameter	Percentage removal of elements from AMD as a function of initial concentration of green tea extract (in 40 mL deionised water)						
	0.1 g	0.2 g	0.3 g	0.4 g	0.5 g	0.6 g	0.7 g
Fe	55	67	77	83	89	89	89
Al	29	40	48	60	67	67	68
Ca	45	49	52	61	64	65	65
Mn	52	62	67	78	84	84	85
Mg	31	39	49	59	62	62	64
Si	33	42	50	60	64	64	68
Cu	42	40	40	50	50	60	60
Zn	63	69	79	83	86	89	88
Mo	87	87	62	62	50	37	37
Ni	73	64	64	73	73	64	73
Co	90	90	90	90	90	90	90
Sr	76	76	76	88	90	90	90
K	n.a.	n.a.	n.a.	n.a.	n.a.	n.a.	n.a.
Se	n.a.	n.a.	n.a.	n.a.	n.a.	n.a.	n.a.
P	n.a.	n.a.	n.a.	n.a.	n.a.	n.a.	n.a.
N/a	18	21	27	33	42	45	45
Sulphate	30	30	33	33	32	28	29

n/a=not applicable

5.2.10 The percentage removal of major and minor elements from Penstock AMD

Figure 5.15 depicts the percentage removal of major and minor elements (Fe, Al, Ca, Mg, Mn, Si, or Zn) from AMD using green tea extract as a reductant. The initial concentrations of these elements in AMD were Fe (4000 mg/L), Al (367 mg/L), Ca (503 mg/L), Mg (376 mg/L), Mn (85 mg/L), Si (28 mg/L), and Zn (9.8 mg/).

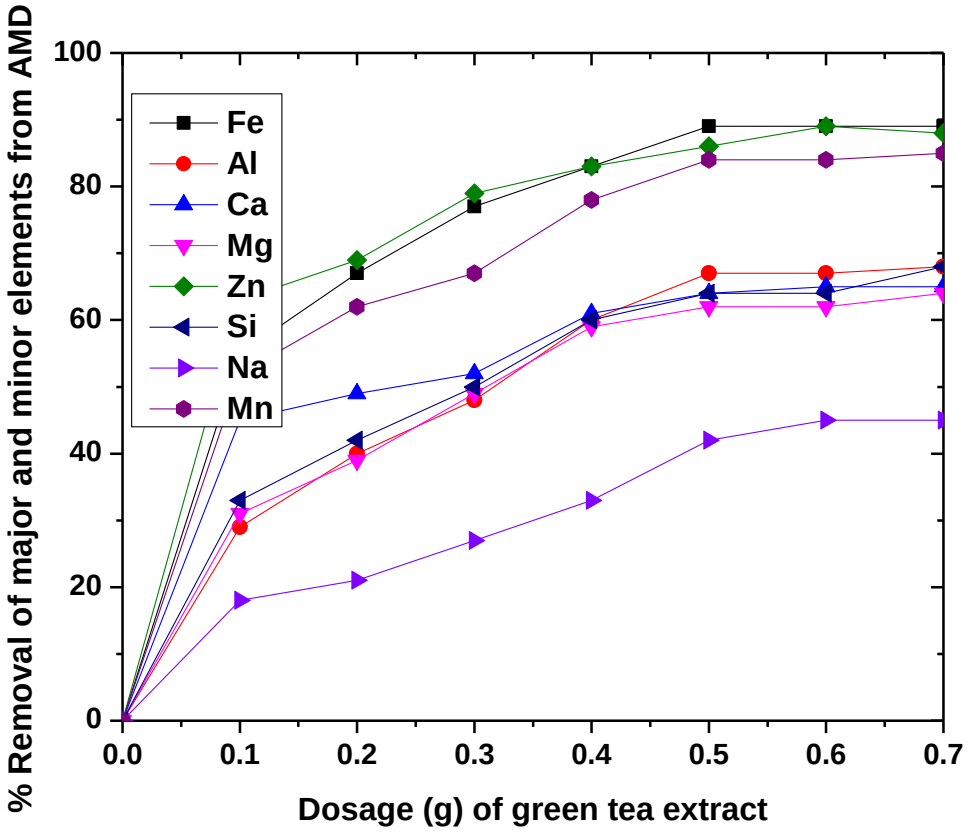

Figure 5. 15: Percentage removal of major and minor elements from AMD using green tea extract as a reductant. Experimental conditions applied: AMD volume=50 mL, AMD pH=2.14, dosage (of green tea extract)=50 mL solution of 0.1-0.7 g green tea extract, agitation speed=250 rpm, temperature=35 ^{o}C, and contact time=24 hours (n=3).

Figure 5.15 shows the percentage removal trend of major and minor elements such as Fe, Al, Ca, Mg, Zn, Si, Na, or Mn from AMD solution using green tea extract as a reductant. It also shows the highest percentage removal of these elements from the AMD solution: Fe (89%), Al (67%), Ca (64%), Mg (62%), Zn (86%), Si (64%), Na (42%), and Mn (84%). In most cases, increasing the dosage of green tea extract in the raw AMD solution from 0.1 to 0.5 g increased the percentage removal of these elements from AMD. This shows that Fe and other major elements (Al, Ca, Mg, Mn, Si, or Zn) could be removed from AMD by using green tea extract as a reductant.

5.2.11 The percentage removal of trace elements from AMD

The percentage removal of Ni, Co, and Sr from AMD treated with green tea as a reductant is shown in Figure 5.4. The initial concentrations of these elements were Ni (1.2 mg/L), Co (1.1 mg/L), Sr (0.8 mg/L), and Ni (3.47 mg/L). Experimental conditions applied: AMD volume=50 mL, AMD pH=2.14, dosage (of green tea extract)=50 mL solution of 0.1-0.7 g green tea extract, agitation speed=250 rpm, temperature=35 ^{o}C, and contact time=24 hours (n=3).

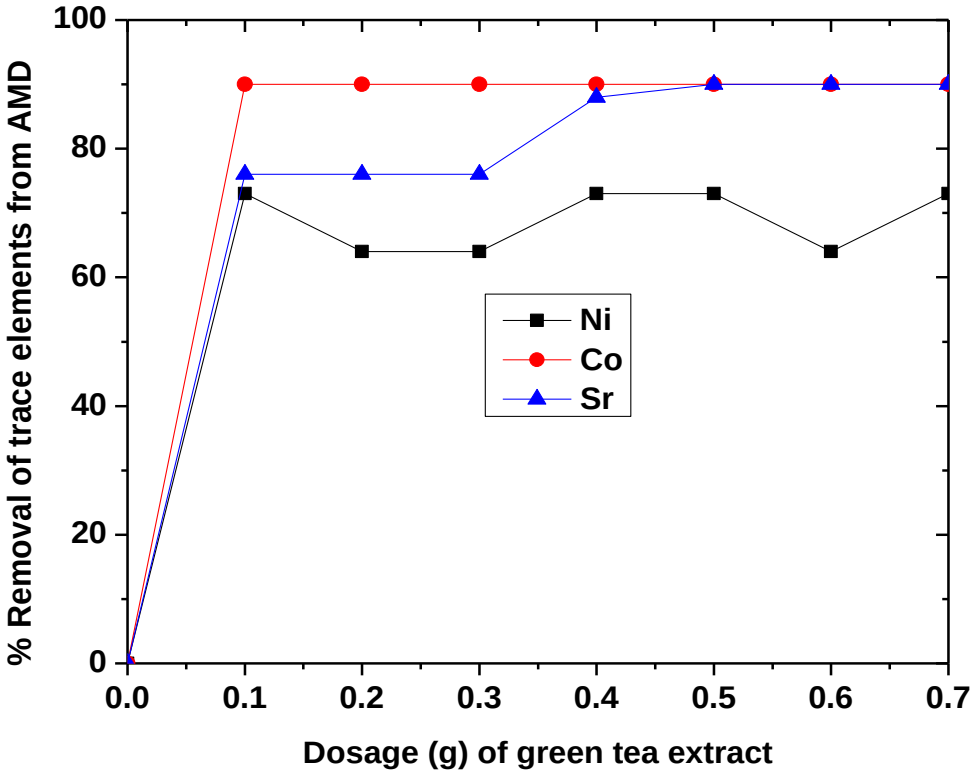

Figure 5. 16: Percentage removal of trace elements from AMD using green tea extract as a reductant. Experimental conditions applied: AMD volume=50 mL, AMD pH=2.14, dosage (of green tea extract)=50 mL solution of 0.1-0.7 g green tea extract, agitation speed=250 rpm, temperature=35 ^{o}C, and contact time=24 hours (n=3).

Figure 5.16 shows the percentage removal of each of these elements from the AMD sample: Ni (73%), Co (90%), and Sr (90%). The removal of Ni, Co, or Sr was comparable when an increasing

dose of green tea extract was used to treat AMD. This shows that increasing the amount of green tea extract in the AMD solution during the removal of Fe as nanoparticles did not significantly affect the simultaneous removal of Ni, Co, or Sr from AMD.

5.2.12 The percentage removal of sulphate from AMD

During the treatment of the Penstock AMD with green tea extract, the dosage of green tea extract was optimized in order to observe the sulphate removal trend from AMD. The initial concentration of sulphate in the AMD solution was 11500 mg/L, as shown in Table 5.5. IC and ICP-MS were used to characterize the treated AMD solution.

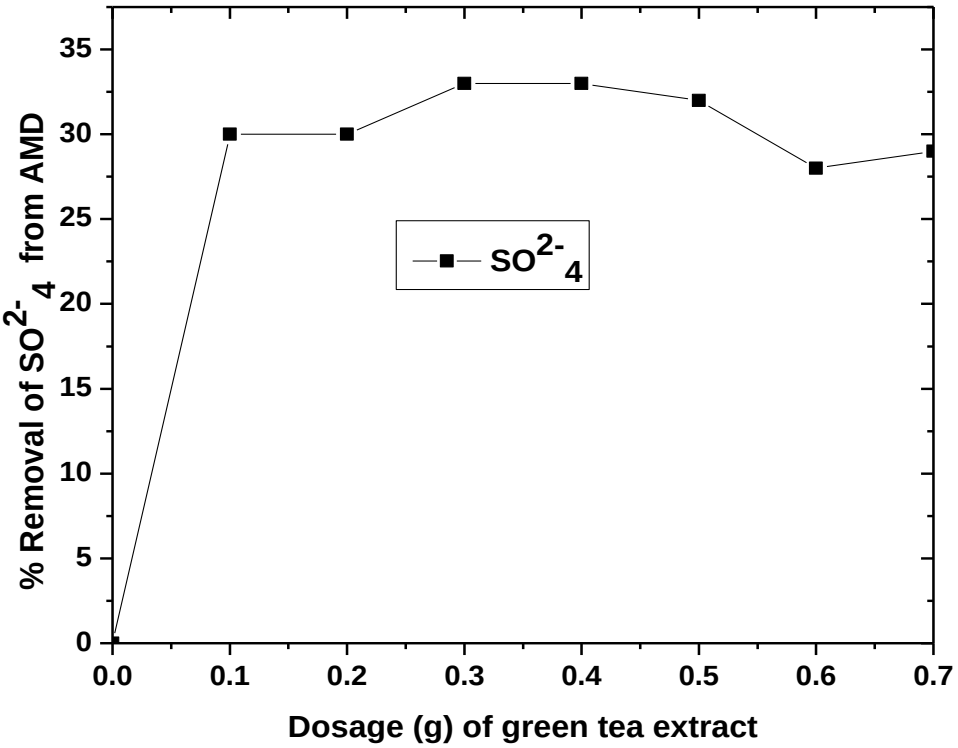

Figure 5. 17: Percentage removal of sulphate from AMD using green tea extract as a reductant. Experimental conditions applied: AMD volume=50 mL, AMD pH=2.14, dosage (of green tea extract)=50 mL solution of 0.1-0.7 g green tea extract, agitation speed=250 rpm, temperature=35 ^{o}C, and contact time=24 hours (n=3).

Figure 5.17 depicts the percentage removal of sulphate from the Penstock AMD solution. The percentage removal of sulphate from the Penstock AMD solution was not significantly improved by increasing the dose of green tea extract (refer to Figure 5.17).

5.2.13 Temperature optimisation

To investigate the effect of reaction temperature on the removal of cations and anions from the Penstock AMD solution, varying reaction temperatures (30 ^{o}C, 35 ^{o}C, 40 ^{o}C, 45 ^{o}C, and 50 ^{o}C) and 0.5 g of green tea extract were used to treat AMD. This is because, at room temperature, Fe did not precipitate from AMD. It is also worth knowing that 0.5 g of green tea extract was the optimum dosage to remove Fe from AMD and thus was selected for this process.

Table 5.7 and Figure 5.18 show the effect of temperature on the concentration of metals and sulphate in AMD.

5.2.14 Effect of temperature on metal and sulphate removal from AMD

Table 5. 7: Extraction of nano-iron from AMD solution: Effect of temperature on the composition of the supernatants generated from AMD treatment with green tea extract. AMD volume=50 mL, AMD pH=2.14, dosage (of green tea extract)=50 mL solution of 0.5 g green tea extract, temperature=30-50 ^{O}C, agitation speed=250 rpm, and contact time=24 hours (n=3).

Component	Feed (mg/L)	Final concentration (mg/L) as a function of temperature				
		30°C	35 °C	40 °C	45 °C	50 °C
Fe	4002	500	450	400	378	379
Al	367	131	120	99	90	94
Ca	503	230	182	168	168	152
Mn	85	18	14	14	25	14
Mg	376	139	142	150	160	132
Si	28	10	10	10.5	11	10.5
Cu	0.1	0.06	0.05	0.05	0.05	0.04
Zn	9.8	1.9	1.4	1.8	1.6	1.7
Mo	0.1	ND	0.05	ND	ND	ND
Ni	1.2	0.28	0.33	0.30	0.28	0.28
Co	1.1	0.1	0.07	0.2	0.1	0.1
Sr	0.8	0.08	0.08	0.08	0.07	0.1
K	ND	261	259	272	285	242
Na	33	22	20	20	19	19
Sulphate	11500	7400	7750	7700	7700	7500

Where: ND = not determined

5.2.15 Effect of temperature on the removal of Fe from AMD

Figure 5.18 shows the results of the effect of temperature on iron removal from the Penstock AMD using green tea as a reductant. The experimental conditions applied are as follows: AMD volume=50 mL, AMD pH=2.14, dosage (of green tea extract)=50 mL solution of 0.5 g green tea extract, temperature=30-50 ^{O}C, agitation speed=250 rpm, and contact time=24 hours (n=3).

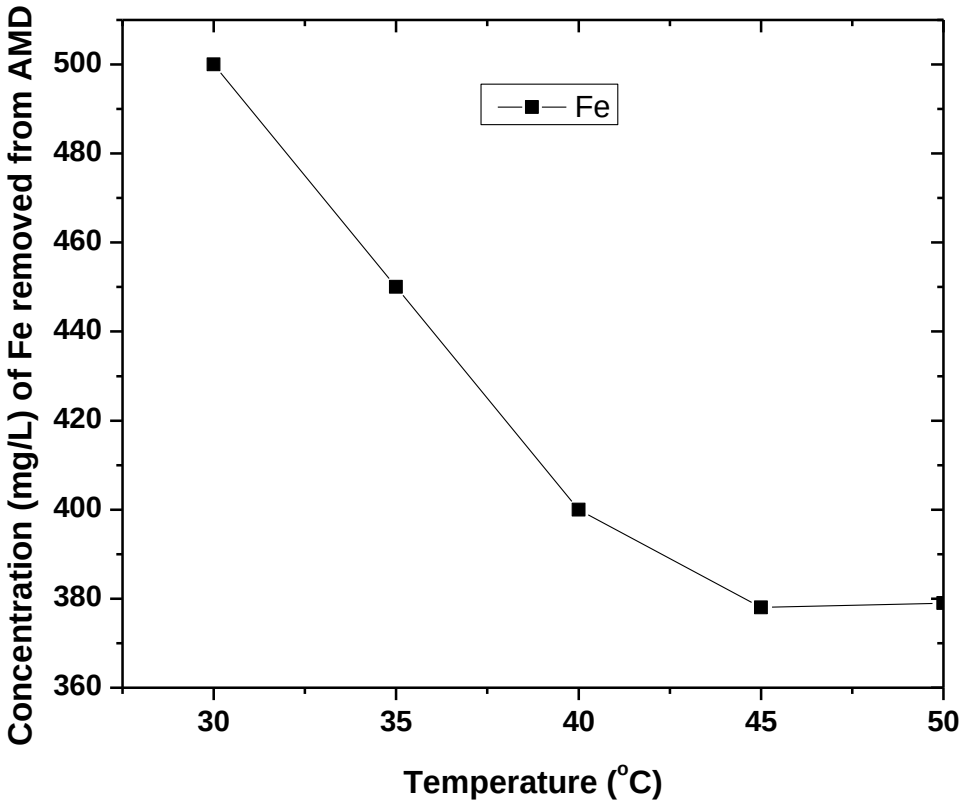

Figure 5. 18: Effect of temperature on the composition of the supernatant arising from the treatment of Penstock AMD solution with green tea extract. Experimental conditions applied: AMD volume=50 mL, dosage of green tea=0.5 g of dried green tea extract (in 50 mL deionised water), AMD pH=2.14, agitation speed=250 rpm and contact time=24 hours

The results of varying temperatures during the treatment of AMD with green tea as a reductant are shown in Figure 5.18. The initial concentration of Fe (4000 mg/L) in the AMD solution decreased to 379 mg/L during this process. The optimum temperature for removing Fe from the Penstock AMD solution was observed at 45 °C, since a similar result was observed when the temperature was raised to 50 °C.

5.2.16 Effect of temperature on the removal of Al, Ca, Mg and K from AMD

Figure 5.19 depicts the effect of temperature on the initial concentrations of Al (367 mg/L), Ca (5.3 mg/L), Mg (376 mg/L), and K (0.98 mg/L) in the Penstock AMD. Experimental conditions applied: AMD volume=50 mL, dosage of green tea=0.5 g of dried green tea extract (in 50 mL deionised water), AMD pH=2.14, agitation speed=250 rpm and contact time=24 hours

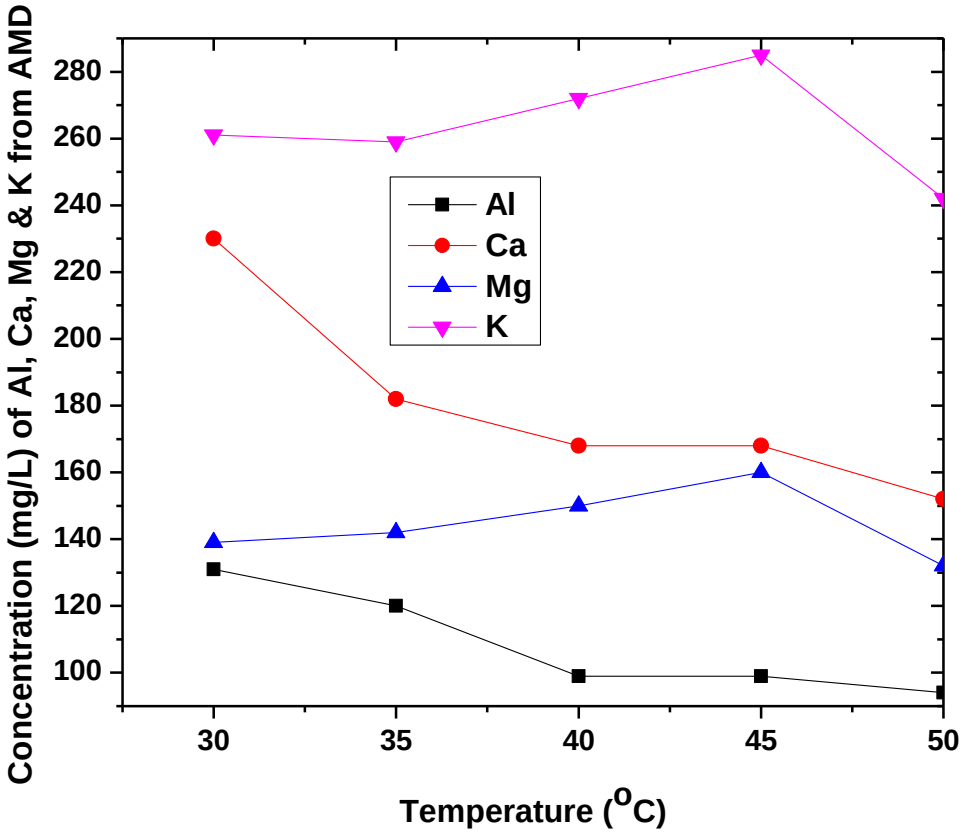

Figure 5. 19: Effect of temperature on the composition of the supernatant arising from the treatment of Penstock AMD solution with green tea extract. Experimental conditions: AMD volume=50 mL, AMD pH=2.14, dosage (of green tea extract)=50 mL solution of 0.5 g green tea extract, temperature=30-50 ^{O}C, agitation speed=250 rpm, and contact time=24 hours (n=3).

As the temperature rose above 30 ^{0}C , the concentration of Al, Ca, Mg, and K in the Penstock AMD varied slightly. Increasing the temperature from 30 ^{0}C to 50 ^{0}C result in an increase in the extent of the extraction of Al and Ca. However, when the temperature was increased from 30 ^{0}C

to 45 ^{0}C, the extent of the extraction of K and Mg decreased, which later increased when a higher temperature of 50 ^{0}C was used. This is because temperatures between 30 ^{0}C to 45 ^{0}C favoured the leaching of K and Mg from green tea extract that went into solution with AMD, thereby decreasing its removal from AMD.

5.2.17 Effect of temperature on the removal of Mn, Na, Zn, Si, Ni, Co, or Sr from AMD

The removal of Mn, Na, Zn, Si, Ni, Co, or Sr from the Penstock AMD, and their initial and final corresponding concentrations in the Penstock AMD were Si (28 mg/L), Mn (85 mg/L), Na (33 mg/L), Zn (9.8 mg/L), Si (28 mg/L), Ni (1.2 mg/L), Co (1.1 mg/L), or Sr (0.8 mg/L)

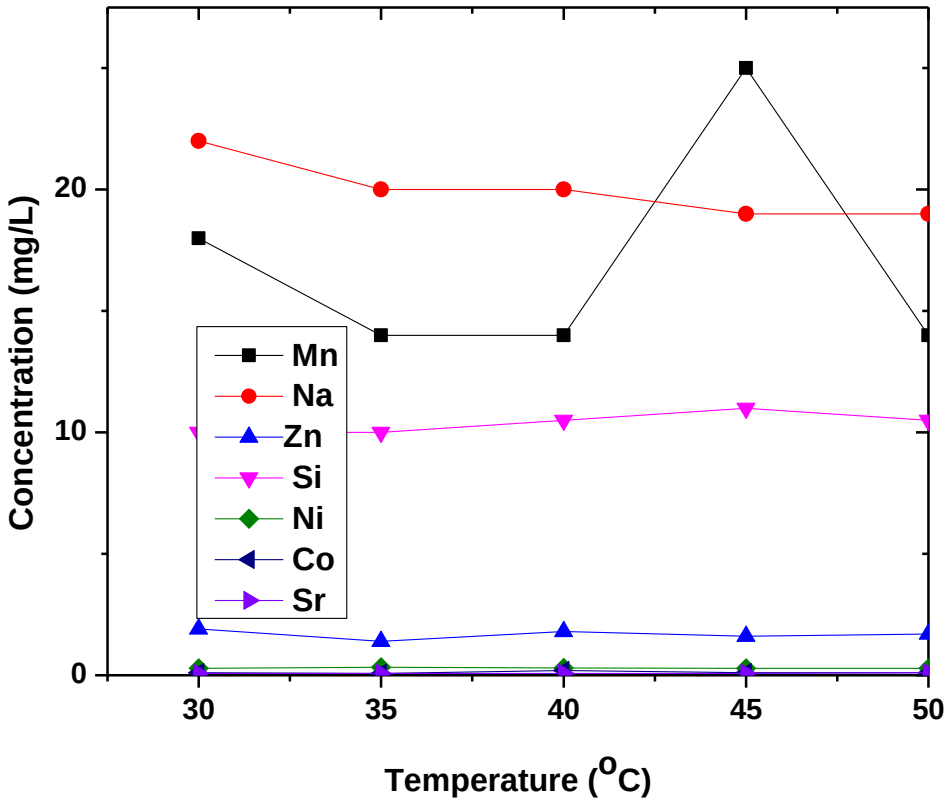

Figure 5. 20: Effect of temperature on the composition of the supernatant arising from the treatment of Penstock AMD solution with green tea extract. Experimental conditions applied: AMD volume=50 mL, AMD pH=2.14, dosage (of green tea extract)=50 mL solution of 0.5 g green tea extract, temperature=30-50 ^{o}C, agitation speed=250 rpm, and contact time=24 hours (n=3).

Figure 5.20 shows that when a dosage of 0.5 g of green tea extract was used to treat AMD, the effect of temperature on the extent of extraction of these metals (Mn, Na, Zn, Si, Ni, Co, or Sr) from the Penstock AMD was negligible, especially for minor and trace elements. The extent of Mn removal from AMD increased slightly when the temperature was increased from 30 to 35 degrees and decreased when the temperature was increased from 40 to 45 degrees. The extent of extraction of Mn was similar when the temperature was further increased to 50 degrees. This suggests that temperatures above 30°C were not beneficial for the removal of these metals from AMD.

5.2.18 Effect of temperature on the removal of SO^{2-}_4

Temperature was optimized during the treatment of the Penstock AMD solution. The trend of sulphate removal from AMD was observed. As shown in Table 4.1, the initial concentration of sulphate in the AMD sample prior to treatment was 11500 mg/L. The effect of temperature on sulphate concentration in the AMD solution was analysed using the IC and ICP analytical techniques described in sections 3.4.4 and 3.4.6 respectively. Figure 5.9 depicts the removal of sulphate concentrations from AMD.

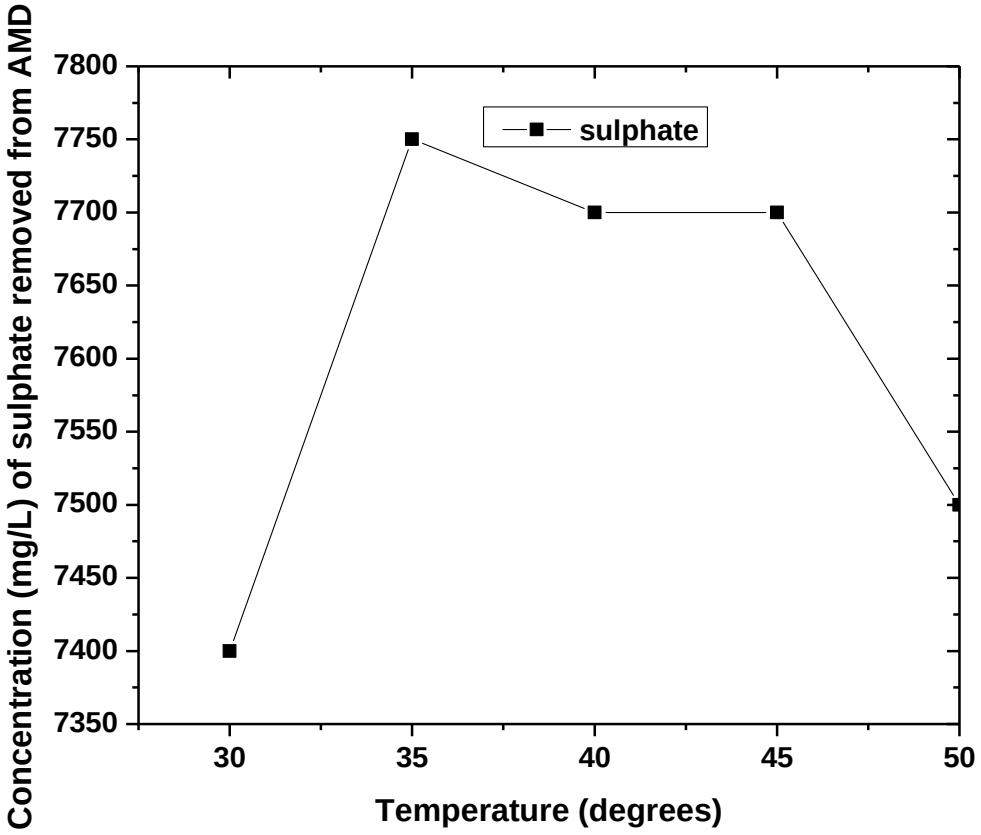

Figure 5. 21: Effect of temperature on the concentration of sulphate arising from the treatment of AMD solution P with green tea extract. Experimental conditions applied: AMD volume=50 mL, AMD pH=2.14, dosage (of green tea extract)=50 mL solution of 0.5 g green tea extract, temperature=30-50 ^{o}C, agitation speed=250 rpm, and contact time=24 hours (n=3).

The influence of temperature on the amount of sulphate extracted from AMD using green tea extract is shown in Table 5.21. A temperature of 30 ^{o}C was found to be optimal for sulphate reduction. Higher temperatures above 30 ^{o}C (from 35 to 50 degrees) decreased sulphate removal from the AMD solution (see 5.21). This is because the solubility of most sulphate salts increases with an increase in temperature due to increase in kinetic energy of particles in solution.

5.2.19 Effect of temperature on metal and sulphate percentage removal from AMD

This section returns to Table 5.7, but this time the data is presented as percentage removal.

Table 5. 8: Percentage removal of iron from the Penstock AMD solution: Effect of temperature on the composition of the supernatants generated from treating AMD with green tea extract.

Component	Percentage removal as a function of temperature				
	30ºC	**35 ºC**	**40 ºC**	**45 ºC**	**50 ºC**
Fe	78	89	90	91	91
Al	64	67	73	76	74
Ca	54	64	67	67	70
Mn	79	83	83	70	84
Mg	63	62	60	57	64
Si	64	64	62	61	62
Cu	40	50	50	50	60
Zn	81	86	82	83	82
Mo	ND	50	ND	ND	ND
Ni	76	73	75	77	77
Co	91	93	82	91	91
Sr	90	90	90	91	88
Na	33	39	39	42	42
Sulphate	35	33	33	33	35

5.2.20 The percentage removal of minor and major elements from AMD

The percentage removal of major and minor elements (Fe, Al, Ca, Mg, Mn, Si, or Zn) from AMD using different temperatures and green tea extract as a reductant is shown in Figure 5.21. The initial concentrations of these elements are shown in Table 5.8: Fe (4000 mg/L), Al (367 mg/L), Ca (503 mg/L), Mg (376 mg/L), Mn (85 mg/L), Si (28 mg/L), and Zn (9.8 mg/L). The experimental strategy of this process was as follows. Experimental conditions applied: AMD volume=50 mL, AMD pH=2.14, dosage (of green tea extract)=50 mL solution of 0.5 g green tea extract, temperature=30-50 ºC, agitation speed=250 rpm, and contact time=24 hours (n=3).

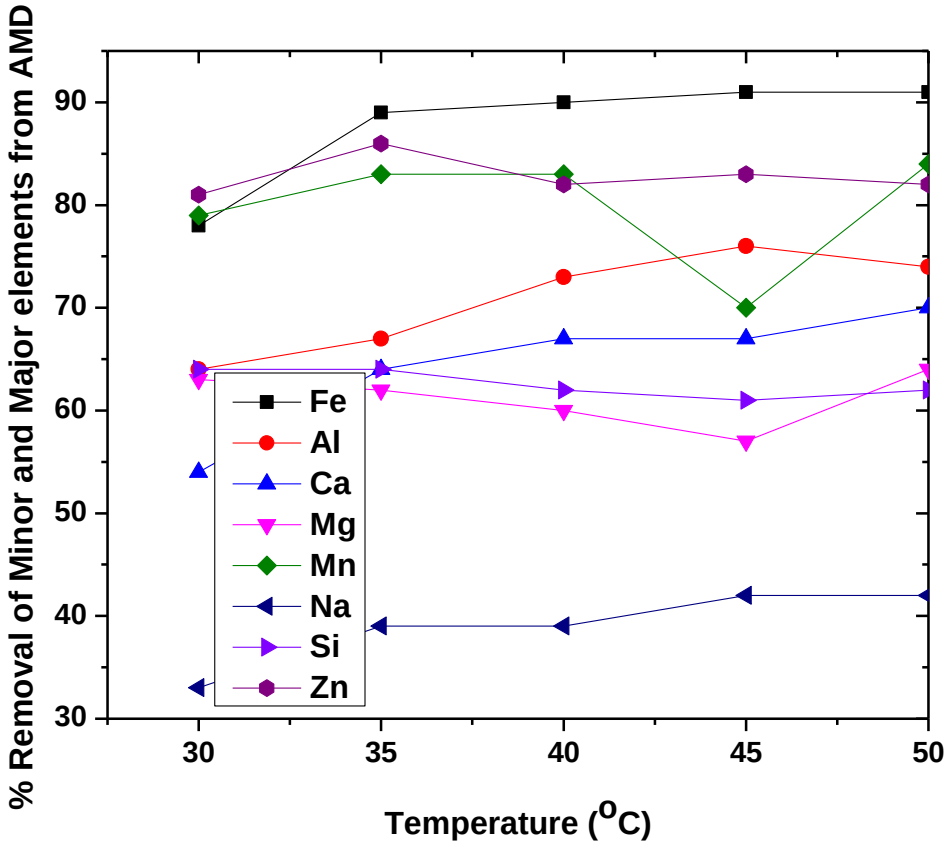

Figure 5. 22: Effect of temperature on the percentage removal of major and minor elements arising from the treatment of AMD solution P with green tea extract. Experimental conditions applied: AMD volume=50 mL, AMD pH=2.14, dosage (of green tea extract)=50 mL solution of 0.5 g green tea extract, temperature=30-50 ^{o}C, agitation speed=250 rpm, and contact time=24 hours (n=3).

The general trend of major and minor elements extracted from the Penstock AMD using different temperatures and green tea extract as a reductant is shown in Figure 5.22 for Fe, Al, Ca, Mg, Mn, Na, Si, and Zn. The highest percentages of minor and major elements removed from the Penstock AMD sample are as follows: Fe (91%), Al (76%), Ca (70%), Mg (64%), Mn (84%), Na (42%), Si (64%), and Zn (86%). In most cases, increasing the temperature of the raw AMD solution from 30 to 50 ^{o}C did not have a significant effect on the major and minor components that co-precipitated with Fe in the AMD sample (see Figure 5.22). This demonstrates that temperatures beyond 30 ^{o}C did not improve the removal of elements from AMD significantly.

5.2.7.2 The percentage removal of trace elements from AMD

The initial concentration of trace elements that were removed from AMD during AMD treatment using a dosage of 0.5 g of green tea extract in a 50 mL solution and varying temperatures are Ni (1.2 mg/L), Co (1.1 mg/L), Sr(0.8 mg/L), or Cu (0.1 mg/L).

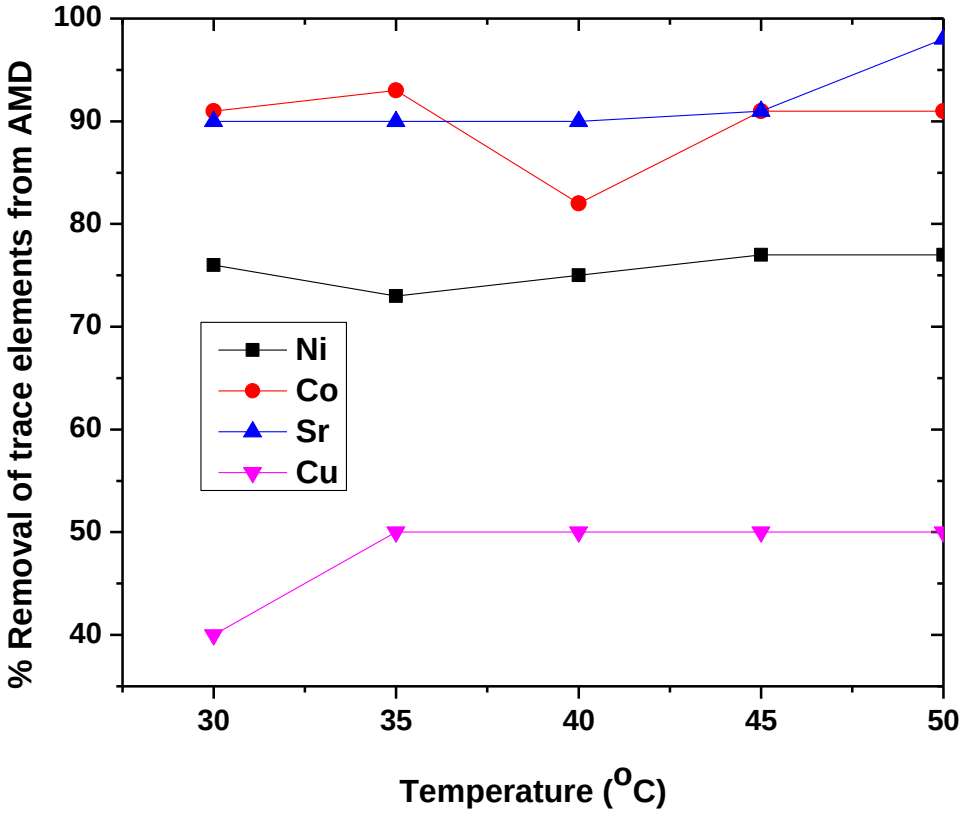

Figure 5. 23: Effect of temperature on the percentage removal of major and minor elements arising from the treatment of Penstock AMD solution with green tea extract. Experimental conditions applied: AMD volume=50 mL, AMD pH=2.14, dosage (of green tea extract)=50 mL solution of 0.5 g green tea extract, temperature=30-50 ^{o}C, agitation speed=250 rpm, and contact time=24 hours (n=3).

Figure 23 shows that the effect of temperature above 30 ^{o}C on the extent of trace metal extraction was relatively minor as the increase in treatment temperature from 30 ^{o}C to 50 ^{o}C resulted in a very slight increase in percentage removal.

5.2.21 The percentage removal of sulphate from AMD

Temperature was optimized during the treatment of the Penstock AMD sample to produce nano-iron particles. In this line of investigation, the trend of sulphate removal from AMD was observed. The initial concentration of sulphate in the AMD sample prior to treatment was 11500 mg/L, as shown in Table 4.1.

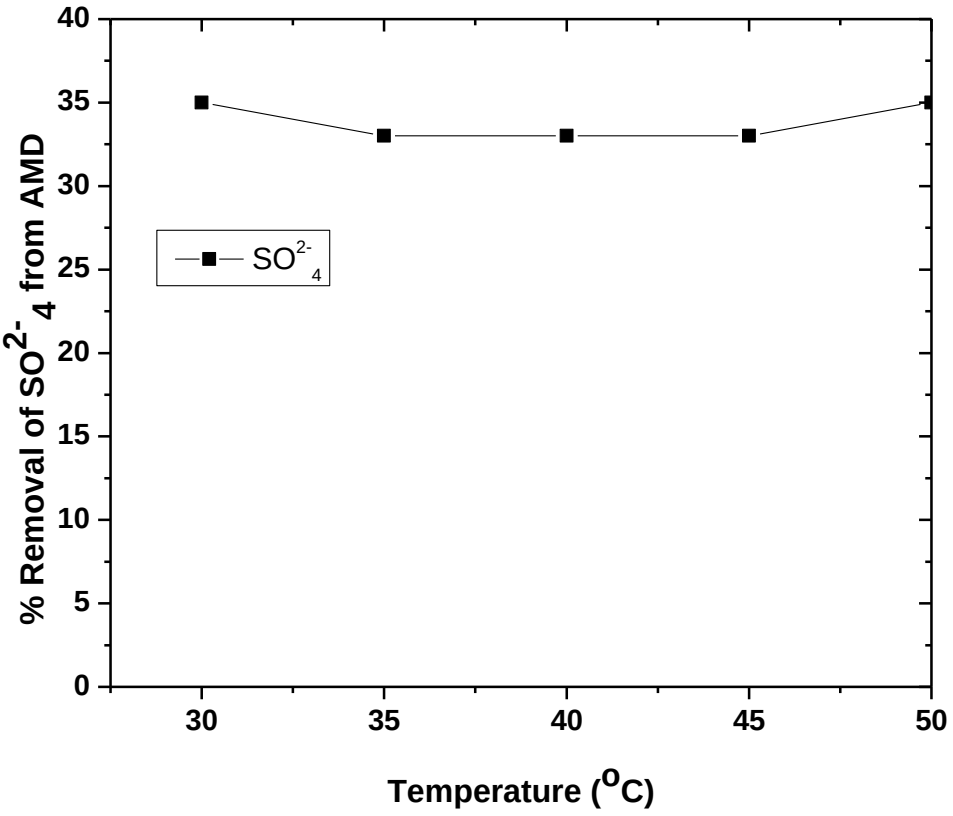

Figure 5. 24: Effect of temperature on the percentage removal of sulphate and minor elements arising from the treatment of AMD Penstock Solution with green tea extract. Experimental conditions applied: AMD volume=50 mL, AMD pH=2.14, dosage (of green tea extract)=50 mL

solution of 0.5 g green tea extract, temperature=30-50 ^{o}C, agitation speed=250 rpm, and contact time=24 hours (n=3).

As shown in Figure 5.24, sulphate was not significantly reduced from AMD using various temperatures and green tea extract as a reductant. The temperature change during AMD treatment with green tea extract resulted in a negligible change in sulphate removal. Maximum sulphate removals were observed to be 35% at a temperature of 35 ^{o}C. This study also shows that higher temperatures (above 35 ^{0}C) used for sulphate reduction in the Penstock AMD were a waste of energy because no real sulphate reduction trend was observed (see Table 5.24).

5.2.22 Contact time optimisation

The treatment of the Penstock AMD using green tea extract was performed at different contact times of 4, 8, 12, 16, 20, and 24 hours at an extract dosage of 0.5 g of green tea extract (in 50 mL deionised) / 50 mL AMD to investigate the effect of contact time on the removal of metal and sulphate from solution. The effect of contact time on the concentration of metals and sulphate in AMD is shown in Table 5.9 and Figures 5.25-5.28.

5.2.23 Effect of contact time on metal and sulphate removal from AMD

The effect of increasing contact time from 4 to 24 hours on the removal of metals and sulphate from the Penstock AMD was investigated using a green tea extract dosage of 0.5 g (in 50 mL deionised water) / 50 mL AMD. The effect of contact time on the concentration of metals and sulphate in the Penstock AMD is shown in Table 5.9 and Figures 5.25-5.28.

Table 5. 9: Effect of contact time on the composition of supernatants from the treatment of the Penstock AMD with green tea extract. Experimental conditions applied: AMD volume=50 mL, AMD pH=2.14, dosage of reductant=0.5 g of green tea extract (in 50 mL of deionised water), agitation speed=250 rpm, and temperature=45^{o}C.

Parameter	**Feed (mg/L)**	Concentration of elements (mg/L) from AMD as a function of time					
		4 hrs	8 hrs	12 hrs	16 hrs	20 hrs	24 hrs
Fe	4002	450	375	375	375	375	375
Al	367	183	170	125	120	120	120
Ca	503	230	193	178	178	178	178
Mn	85	34	26	13	13	13	13
Mg	376	207	164	152	148	146	146
Si	28	14	11	11	11	11	11
Cu	0.1	0.07	0.06	0.06	0.05	0.05	0.05
Zn	9.8	4.0	2.0	1.0	1.0	1.0	1.2
Mo	0.1	0.05	0.04	0.04	0.04	0.04	0.04
Ni	1.2	0.5	0.4	0.3	0.3	0.3	0.3
Co	1.1	0.5	0.4	0.3	0.3	0.3	0.3
Sr	0.84	0.3	0.18	0.1	0.09	0.08	0.08
K	ND	236	240	245	245	265	280
Na	33.1	27	27	25	23	20	20
Sulphate	11500	6849	6714	7527	6981	7028	7239

5.2.24 Effect of Contact Time on the concentration of Fe, Al, Ca, Mg and Zn from AMD

The results of the effect of contact time on the removal of Fe, Al, Ca, Mg, or Zn from the Penstock AMD are shown in Figure 5.25. The initial concentration (mg/L) of these elements (Fe, Al, Ca, Mg, or Zn) in the Penstock AMD were 4000 mg/L, 367 mg/L, 503 mg/L, 376 mg/L, or 9.8 mg/L respectively.

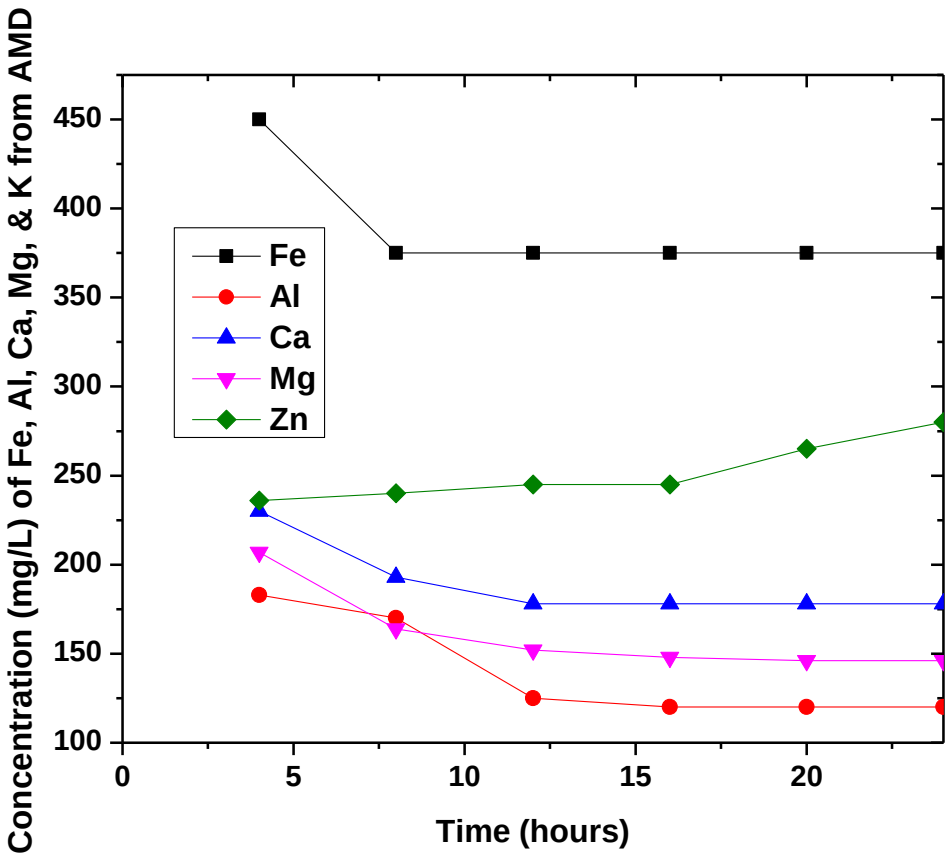

Figure 5. 25: Effect of retention time on the concentration of Fe, Al, Ca, Mg, or Zn arising from the treatment of Penstock AMD solution with green tea extract. Experimental conditions applied: AMD volume=50 mL, AMD pH=2.14, dosage of reductant=0.5 g of green tea extract (in 50 mL of deionised water), temperature=45^{o}C, agitation speed=250 rpm, (n = 3).

The results in Figure 5.25 show that increasing the retention time from 4 to 12 hours had no real effect on the concentrations of most metals, including Fe, Ca, Mg, Al, Mg, Si, Zn, and Mn, with longer retention times having no effect on the concentrations in the treatment supernatants (see Figure 5.25), except for K, whose concentration increased as the retention time increased from 4 to 24 hours. It is noteworthy that the optimum contact time for the precipitation of the target element Fe was 8 hours. This because no change of Fe removal was observed beyond 8 hours to 24 hours. This could be attributed to the nature of their covalent bonding or redissolution of the target element at higher retention time.

5.2.25 Effect of contact time on the concentration of Mn, Na, Zn, Si, Ni, Co or Sr from AMD

During the treatment of the Penstock AMD (50 mL) with 50 mL of green tea containing 0.5 g of green tea extract, the contact time was varied. The initial concentrations of some of the metals removed from the Penstock AMD solution were Mn (85 mg/L), Na (33.1 mg/L), Zn (9.8 mg/L), Si (28 mg/L), Ni (1.2 mg/L), Co (1.1 mg/L), or Sr (0.84 mg/L).

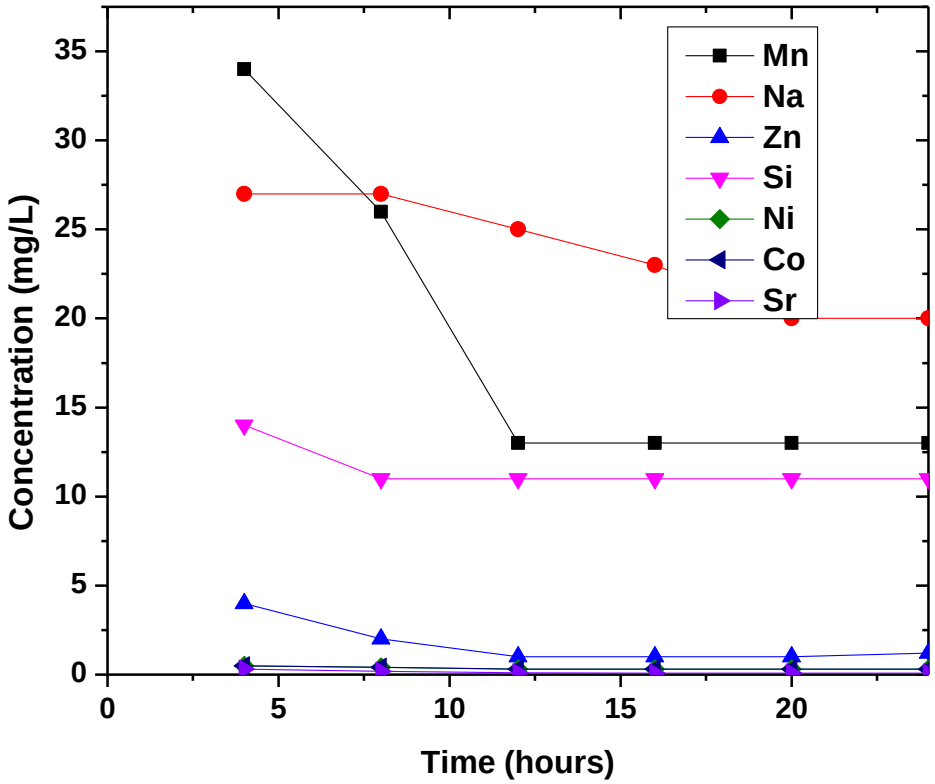

Figure 5. 26: Effect of retention time on the concentration of Mn, Na, Zn, Si, Ni, Co, or Sr arising from the treatment of Penstock AMD solution with green tea extract. Experimental conditions applied: AMD volume=50 mL, AMD pH=2.14, dosage of reductant=0.5 g of green tea extract (in 50 mL of deionised water), temperature=45^{o}C, agitation speed=250 rpm (n = 3).

Figure 5.26 shows the effect of reaction contact time on the removal of Mn, Na, Zn, Si, Ni, Co, or Sr from AMD. In most cases, the highest removal of metals was observed when a contact time of 12 hours was used to treat the Penstock AMD (see 5.26).

5.2.26 Effect of contact time on the concentration of SO^{2-}_4 from AMD

The initial concentration of sulphate in the AMD solution prior to optimization of the AMD treatment process using contact time was 11500 mg/L.

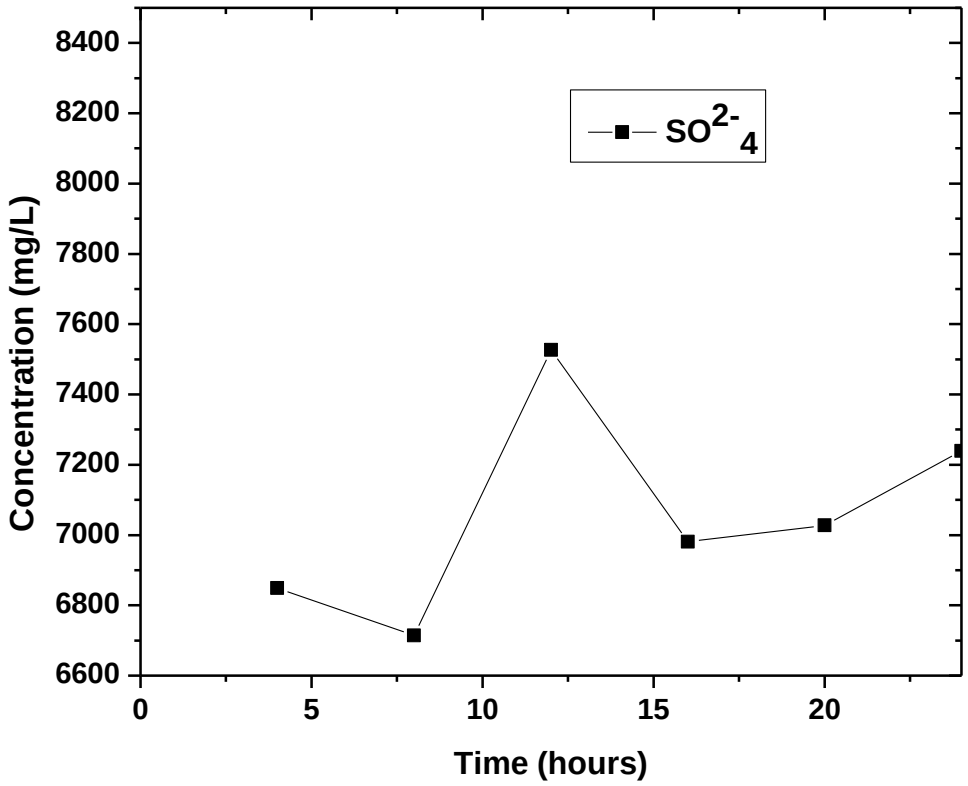

Figure 5. 27: Effect of retention time on the concentration of SO^{2-}_4 arising from the treatment of AMD solution P with green tea extract. Experimental conditions applied: AMD volume=50 mL, AMD pH=2.14, dosage of reductant=0.5 g of green tea extract (in 50 mL of deionised water), temperature=35^{o}C, agitation speed=250 rpm (n = 3).

The effect of contact time on the removal of sulphate from AMD using 50 mL of 0.5 g of green tea extract solution as a reductant is shown in Figure 5.27. After 8 hours of contact time, the highest sulphate removal was 6849 mg/L, and at levels between 7666 and 7000 mg/L, the sulphate concentration in the AMD solution increased.

5.2.27 Effect of contact time on percentage removal of metal and sulphate from AMD

The data in Table 5.9 was revisited, but this time were presented as percentage removal in Table 5.10.

The effect of varying reaction contact time from 4 hours to 24 hours on the percentage removal of metals and sulphate from the Penstock AMD solution was investigated. Experimental conditions applied: AMD volume=50 mL, AMD pH=2.14, dosage of reductant=0.5 g of green tea extract (in 50 mL of deionised water), agitation speed=250 rpm, and temperature=35^{o}C.

Table 5.10 presents the effect of contact time on the percentage removal of components from AMD using green tea.

Table 5. 10: Effect of reaction contact time on the percentage removal of components from AMD treated with green tea extract. Experimental plan: AMD volume=50 mL, AMD pH=2.14, dosage of reductant=0.5 g of green tea extract (in 50 mL of deionised water), agitation speed=250 rpm, and temperature=45^{o}C.

Parameter	**Feed (mg/L)**	Percentage removal of elements (mg/L) from AMD as a function of time					
		4 hrs	8 hrs	12 hrs	16 hrs	20 hrs	24 hrs
Fe	4000	89	91	91	91	91	91
Al	367	50	53	66	67	67	67
Ca	503	54	62	65	65	65	65
Mn	85	60	70	84	84	84	84
Mg	376	45	56	60	61	61	61
Si	28	50	61	61	61	61	61
Cu	0.1	30	40	40	50	50	50
Zn	9.8	59	80	90	90	90	88
Mo	0.1	50	60	60	60	60	60
Ni	1.2	58	67	75	75	75	75
Co	1.1	54	64	73	73	73	73
Sr	0.84	64	79	79	89	90	90
Na	33.1	18	18	24	31	40	40
Sulphate	11500	40	42	36	39	39	37

5.2.28 Effect of contact time on the percentage removal major elements

Figure 5.28 depicts the effects of reaction contact time on the percentage removal of Fe, Al, Ca, and Mg from the Penstock AMD. The initial concentrations (mg/L) of these elements in the Penstock AMD were 4000 mg/L, 367 mg/L, 503 mg/L, and 376 mg/L respectively. The experimental conditions used to carry out this plan were as follows: AMD volume=50 mL, AMD pH=2.14, dosage of reductant=50 mL of green tea containing 0.5 g of green tea extract, agitation speed=250 rpm and temperature=45^{o}C (n = 3).

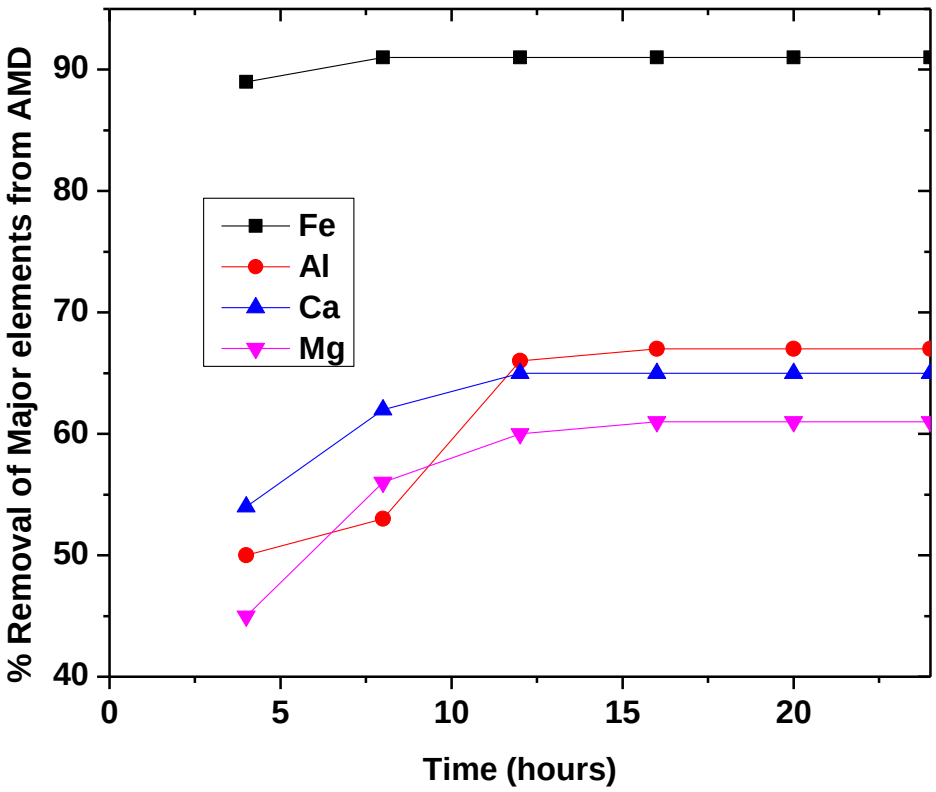

Figure 5. 28: Effect of contact time on percentage removal of Fe, Al, Ca, or Mg from Penstock AMD solution with green tea extract. Experimental conditions applied: AMD volume=50 mL, AMD pH=2.14, dosage of reductant=0.5 g of green tea extract (in 50 mL of deionised water), agitation speed=250 rpm, and temperature=35^{o}C (n = 3).

Figure 5.28 shows that as the reaction contact time increased from 4 to 12 hours, the percentage removal of metals from AMD increased. The highest removal of Al, Ca, or Mg was observed when a reaction contact time of 12 hours was used. The removal of Al, Ca, or Mg from AMD remained stable when the reaction contact time was further increased from 12 to 24 hours. However, the optimum contact time for the removal of Fe from AMD was observed to be 8 hours. Increasing the reaction contact time from 8 to 24 hours to remove Fe from AMD produced comparable results.

5.2.29 Effect of contact time on the percentage removal of minor elements

During the treatment of AMD with green tea extract (0.5g (in 50 mL solution) / 50mL AMD), the reaction contact time was optimized. Figure 5.23 depicts the percentage removal of these elements in the AMD sample over time.

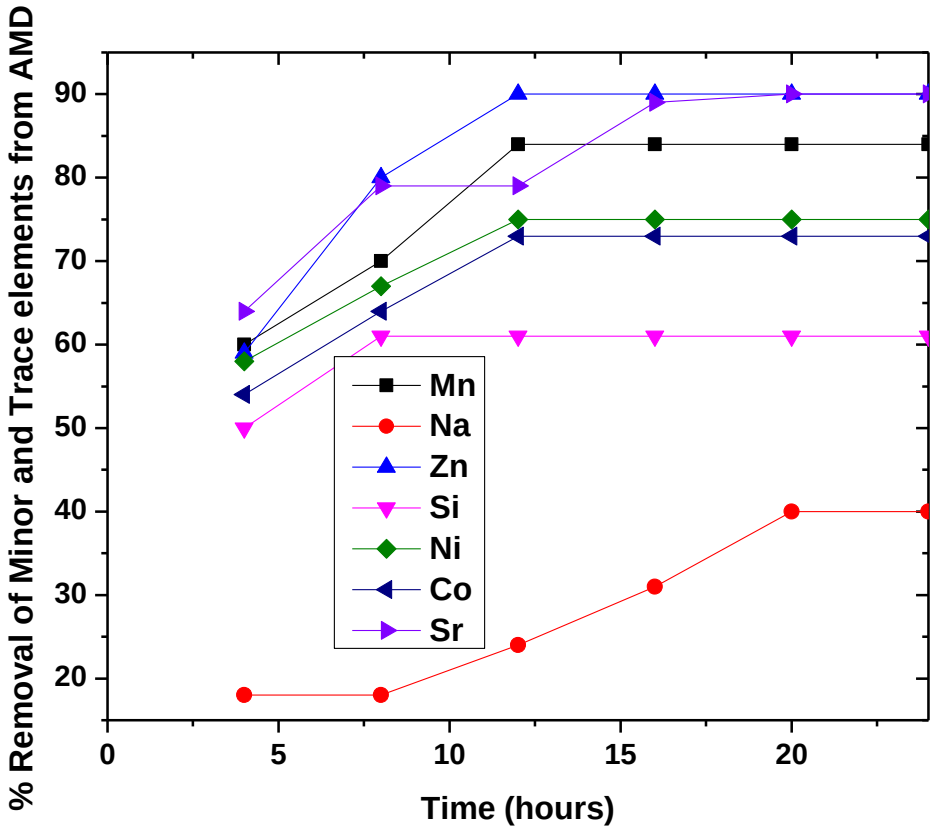

Figure 5. 29: Effect of contact time on the percentage removal of Mn, Na, Zn, Si, Ni, Co, or Sr from Penstock AMD solution with green tea extract. Experimental conditions applied: AMD volume=50 mL, AMD pH=2.14, dosage of reductant=0.5 g of green tea extract (in 50 mL of deionised water), agitation speed=250 rpm, and temperature=45 ^{o}C (n = 3).

Figure 5.29 shows a similar percentage removal trend of major and minor elements from AMD solution. In most cases, the optimum removal of minor and trace elements from AMD was found to be between 8-12 hours. However, the optimum removal of Na was observed after 20 hours of reaction time.

5.2.30 Effect of contact time on the percentage removal of sulphate

Figure 5.30 depicts the effect of contact time on the percentage removal of sulphate from AMD when treated with optimum reaction contact time and temperature.

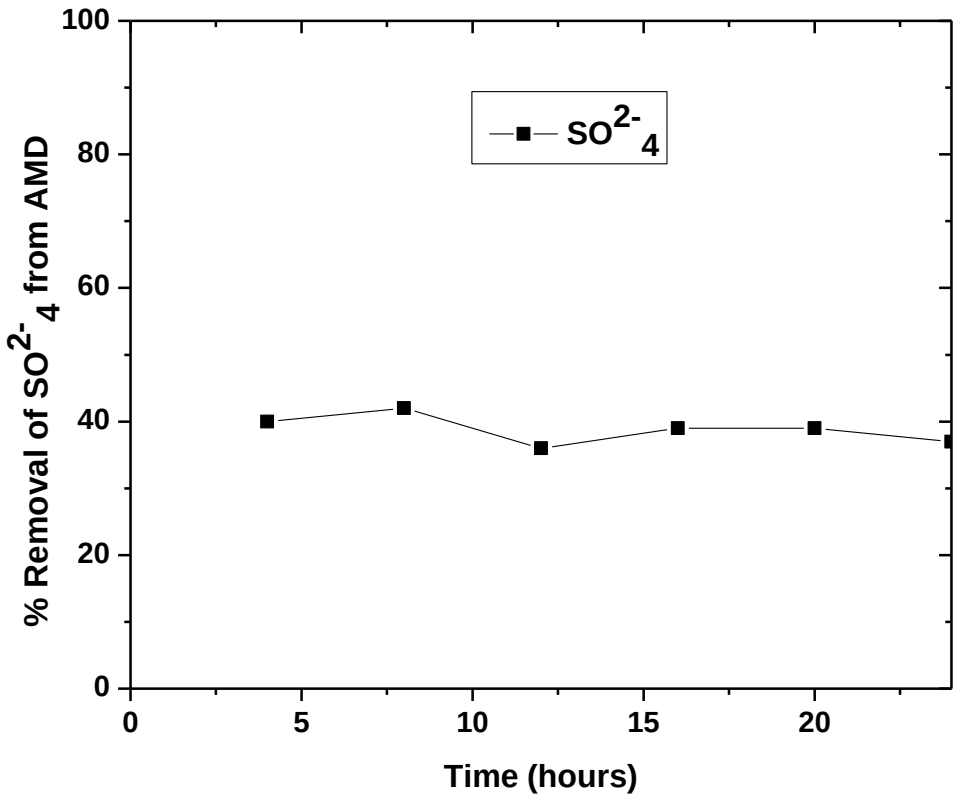

Figure 5. 30: Effect of retention time on the extent of extraction of SO^{2-}_4 from AMD solution P with green tea extract. Experimental conditions applied: AMD volume=50 mL, AMD pH=2.14, dosage of reductant=0.5 g of green tea extract (in 50 mL of deionised water), agitation speed=250 rpm, and temperature=45 ^{o}C (n = 3).

Figure 5.30 show that sulphate extraction remains relatively constant over the entire time period studied, with the extent of sulphate removal varying between 37% and 41%.

5.3 SUMMARY

Reductants such as sodium borohydride and green tea extract can be used to synthesize nano-iron particles from iron-rich AMD. Raw Penstock AMD samples were treated with reductants such as sodium borohydride or green tea extract, which improved AMD quality while avoiding sludge generation to produce nano-iron particles. The use of these reductants in the treatment of AMD removed a significant amount of metals from mine water that co-precipitated with Fe. However, treating AMD with sodium borohydride or green tea extract significantly increased the concentrations of Na and B in the sodium borohydride-treated AMD and K in the green tea-treated AMD. The increased concentration of these elements in the AMD solution is problematic and requires additional research. In line with this investigation, there is no literature describing the use of sodium borohydride or green tea extract as reductants for removing metals from raw AMD prior to liming or neutralization. This study also showed that the use of sodium borohydride as a reductant to produce nano-iron particles from AMD outperforms the use of green tea extract as a reductant to produce nano-iron particles from AMD, but the increased concentration of B and Na left in the treated sodium borohydride AMD solution is problematic. In Chapter 6, the quality of the precipitates produced by the treatment of the Navigation Penstock AMD with sodium borohydride or green tea extract is presented and discussed in detail.

CHAPTER 6

SYNTHESIS AND CHARACTERISATION OF AMD-BASED NANO-IRON PARTICLES

6.0 Introduction

The synthesis, characterization and catalytic testing of nano-iron particles produced from the Penstock AMD sample collected from the Navigation coal mine are presented and discussed in this chapter. The first section (section 6.1) presents and discusses the synthesis of nano-iron particles from AMD using a chemical reductant (sodium borohydride). Section 6.2 presents and discusses the characterization of nano-iron particles synthesized from AMD using an environmentally friendly reductant (green tea extract). Section 6.3 presents and discusses the catalytic testing of nano-iron particles synthesized from AMD in the decolourization of methylene blue. The Navigation Penstock AMD sample was used as a source of ferric iron salt for nano-iron synthesis using sodium borohydride or green tea extract as reductants.

6.1 Reductants used for nano-iron synthesis

The purpose of using sodium borohydride or green tea extract as a reductant to synthesize AMD-based nano-iron particles via a redox process was to determine and evaluate a more direct approach as well as the product quality formed from the AMD sample with the two reductants. Table 6.1 shows a list of synthesized nano-iron particles, experimental conditions, and labels.

Table 6. 1: AMD-based nano-iron particles, experimental conditions, and code names (label)

Sample	Parameter	Label
Field Penstock AMD	Collected and stored in an airtight container that was preserved at 4 ^{o}C	AMD
Sodium borohydride AMD-based nano-iron particles	Vol. of AMD (100 mL), pH of AMD (2.14), vol. of $NaBH_4$ (50 mL), concentration of $NaBH_4$ (0.1-0.7 M), reaction time (80 minutes), agitation speed (300 rpm)	SBNI
Green tea AMD-based nano-iron particles	Vol. of AMD (50 mL), vol. of green tea (50 mL), pH of AMD=2.14, mass of green tea (0.1-0.7 g in 50 mL solution), temperature (30-50 ^{o}C) reaction time (4-24 hours), agitation speed (300 rpm)	GTNI

6.2 Characterization of AMD-based nano-iron particles synthesized from AMD using sodium borohydride

The characterization of nano-iron particles (SBNI) synthesized from AMD using sodium borohydride is presented and discussed in this section. The following experimental conditions were used to synthesize the nano-iron particles from AMD: AMD volume (100 mL), AMD pH (2.14), $NaBH_4$ volume (100 mL), $NaBH_4$ concentration (0.1-0.7 M), reaction time (80 minutes), speed (300 rpm). The results are presented in section 6.2.1 to 6.2.5.

6.2.1 Synthesized nano-iron particle mineralogy

XRD was used to investigate the mineralogy of nano-iron particles (SBNI) synthesized from AMD using sodium borohydride as a reductant. The XRD results of the synthesized nano-iron particles are shown in Figure 6.1.

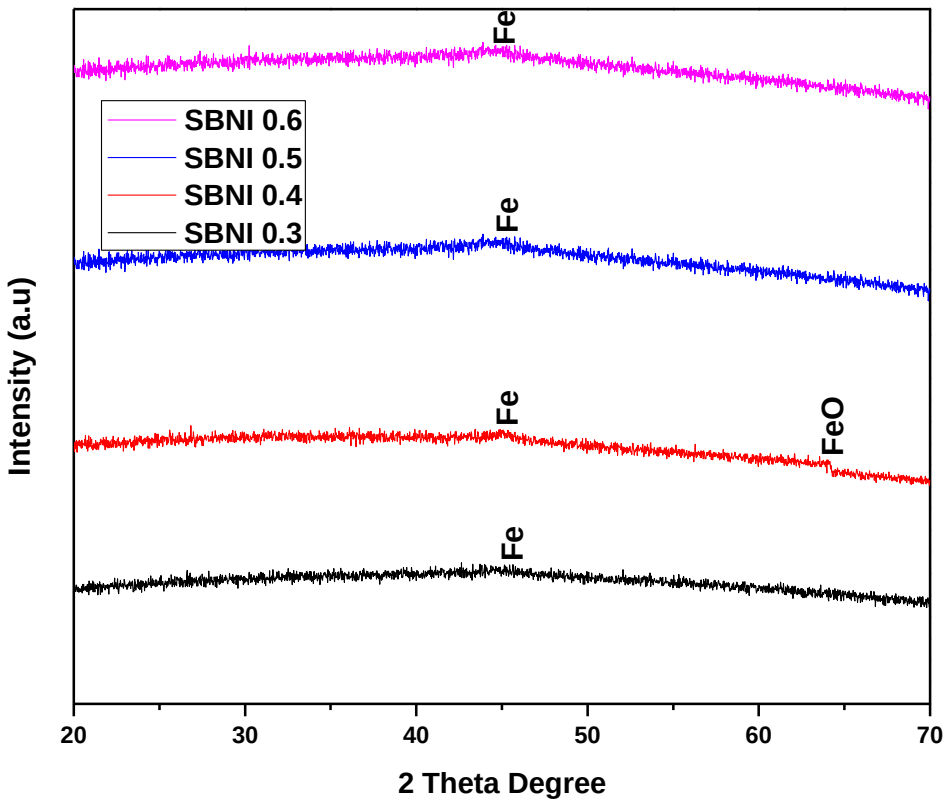

Figure 6. 1: XRD spectra of nano-iron particles (pure Fe=Fe^0 and FeO) extracted from field Penstock AMD using 0.3 M, 0.4 M, 0.5 M, and 0.6 M sodium borohydride solutions. Experimental conditions applied: vol. of AMD (100 mL), pH of AMD (2.14), vol. of $NaBH_4$ (50 mL), concentration of $NaBH_4$ (0.3-0.6 M), reaction time (80 minutes), speed (250 rpm)

Figure 6.1 shows that the AMD-based synthesized nano-iron particles have similar XRD diffraction patterns for all feed solutions, with identical peak matches from 2θ 10° to 70°. The presence of iron oxide (FeO) and pure zerovalent Fe nanoparticles (Fe^0) is confirmed by the broad diffraction peaks observed at 44.8° and 66° 2θ. The broad XRD peaks representing zerovalent iron nanoparticles are consistent with previous studies (Mahmoud et al. 2020; Alegbe et al., 2019; Badmus et al., 2018b; Afsheen et al., 2018). It is also noteworthy that there were no peaks observed above 70° 2 Theta on the XRD scan of the nano-iron powder samples.

6.2.2: Morphology and elemental composition of nano-iron particles synthesized from field AMD samples using sodium borohydride

This section describes the morphology of nano-iron synthesized from the Penstock AMD samples using sodium borohydride as a reductant. The EDS technique was used to determine the elemental composition of the synthesized nano-iron particles. Figure 6.2 shows SEM micrographs of nanoparticles derived from Penstock AMD solutions. According to these micrographs, the generated nano-iron particles were in the nano-size range, with a spherical, bead-like structure. Wang & and Zhang (1997) reported on similar nano-iron shapes. While the morphologies of the solids synthesized from the Penstock AMD were similar, the particle size distribution appeared to differ. The STEM particle size measurement corroborated this.

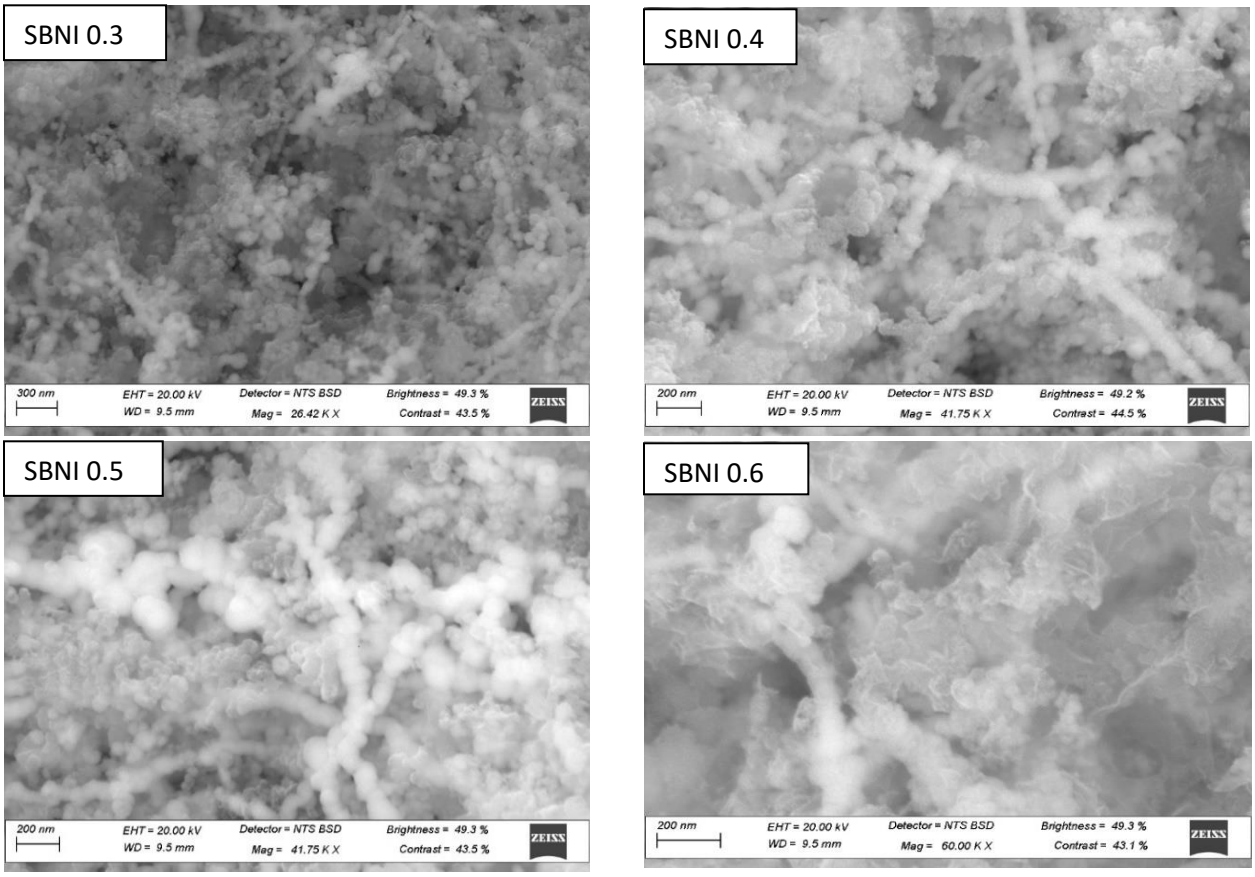

Figure 6. 2: Nano-iron extraction from AMD solutions using 0.3 M, 0.4 M, 0.5 M, and 0.6 M sodium borohydride solutions. SEM micrographs of nano-iron particles synthesized from Penstock AMD solutions: Experimental condition: vol. of AMD (100 mL), pH of AMD (2.14), vol.

of $NaBH_4$ (50 mL), concentration of $NaBH_4$ (0.3-0.6 M), reaction time (80 minutes), agitation speed (300 rpm)

The EDS spectra of the nano-iron products are presented in Figure 6.3, and the quantitative results are presented in Table 4.1.

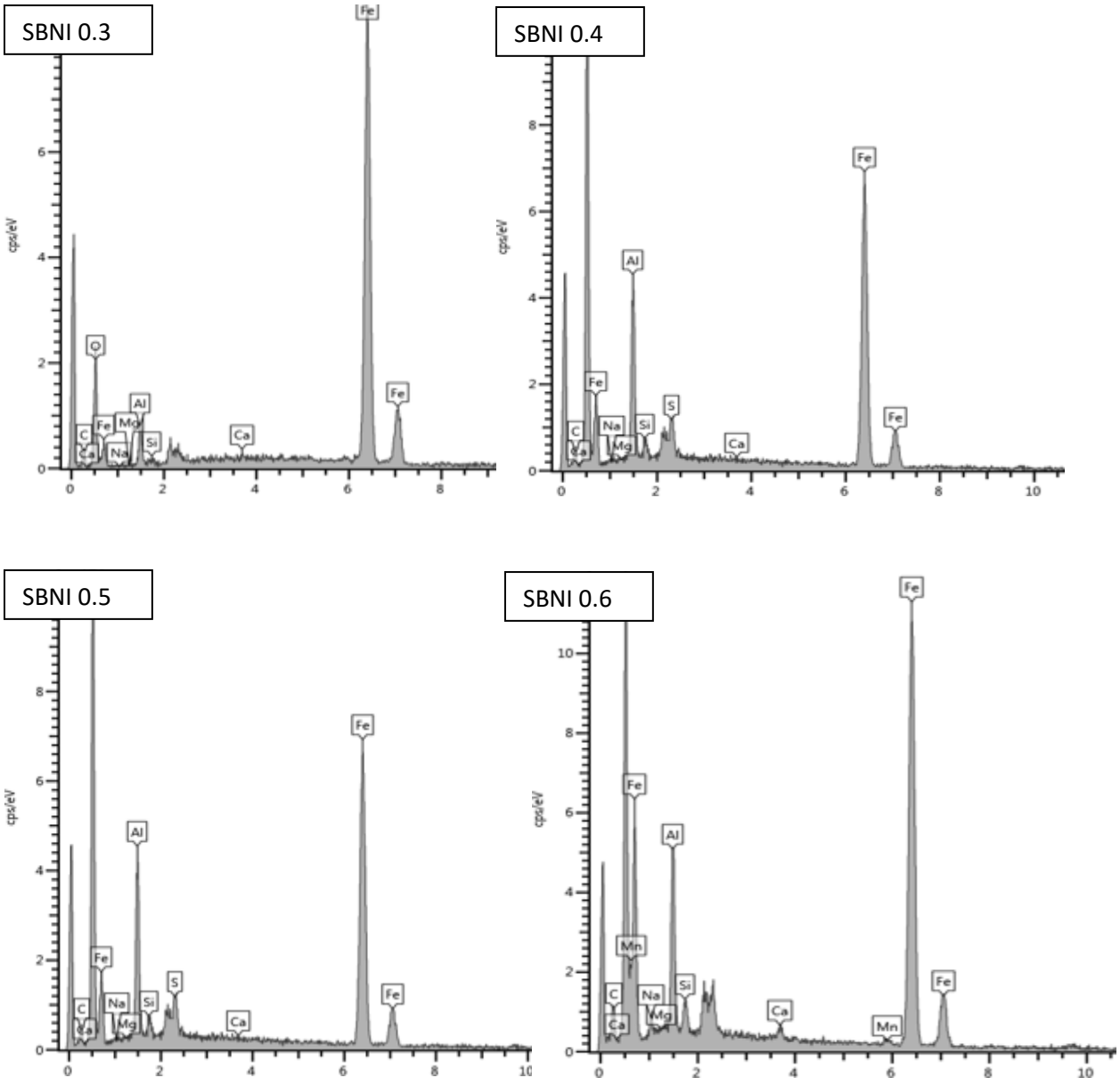

Figure 6. 3: EDS spectra of nano-iron particles synthesized from Penstock AMD using 0.3 M, 0.4 M, 0.5 M, or 0.6 M of sodium borohydride solution. Experimental conditions applied: vol. of AMD (100 mL), pH of AMD (2.14), vol. of $NaBH_4$ (50 mL), concentration of $NaBH_4$ (0.1-0.7 M), contact time (80 minutes), temperature=25 ^oC, and agitation speed (300 rpm)

The EDS results confirm that the synthesized nano-iron particles were mainly composed of Fe metal and its compounds (70-75 atomic weight percent), with minor amounts of Al (3.3-8.9 atomic weight percent) and Ca (0.43-0.58 atomic weight percent) and traces of Na, Mg, Si, and S. These findings are consistent with the compositions of the treated AMD solutions, which revealed significant co-extraction of Al and other metals.

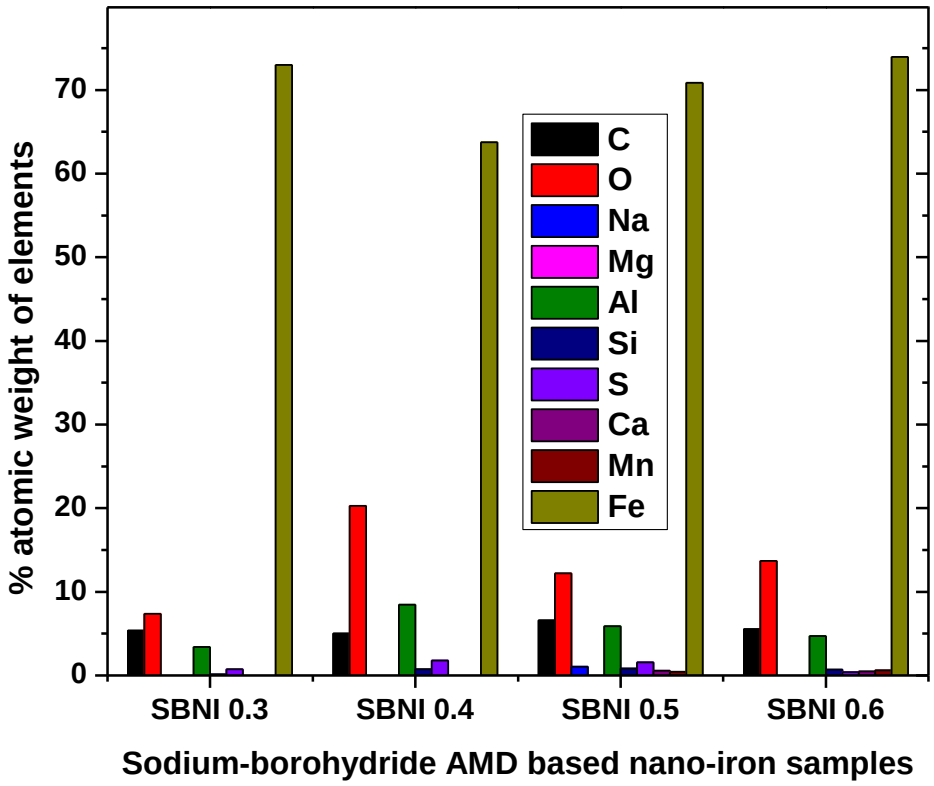

Figure 6. 4: Elemental composition of nano-iron particles synthesized from the Penstock AMD using 0.3 M, 0.4 M, 0.5 M, or 0.6 M of sodium borohydride solution. Experimental conditions applied: vol. of AMD (100 mL), pH of AMD (2.14), vol. of $NaBH_4$ (50 mL), concentration of $NaBH_4$ (0.1-0.7 M), contact time (80 minutes), temperature=25 ^oC, and speed (300 rpm)

6.2.3: STEM Morphology and size distribution of nano-iron particles synthesized from field Penstock AMD samples

STEM analytical technique and Image J software tool were used to confirm the average particle size, morphology, and crystallinity of the synthesized nano-iron (SBNI 0.3, SBNI 0.4, SBNI 0.5, and SBNI 0.6) particles. Figure 7.3 shows the results of the synthesized nano-iron particles from the Penstock AMD using varying concentrations of sodium borohydride as a reductant.

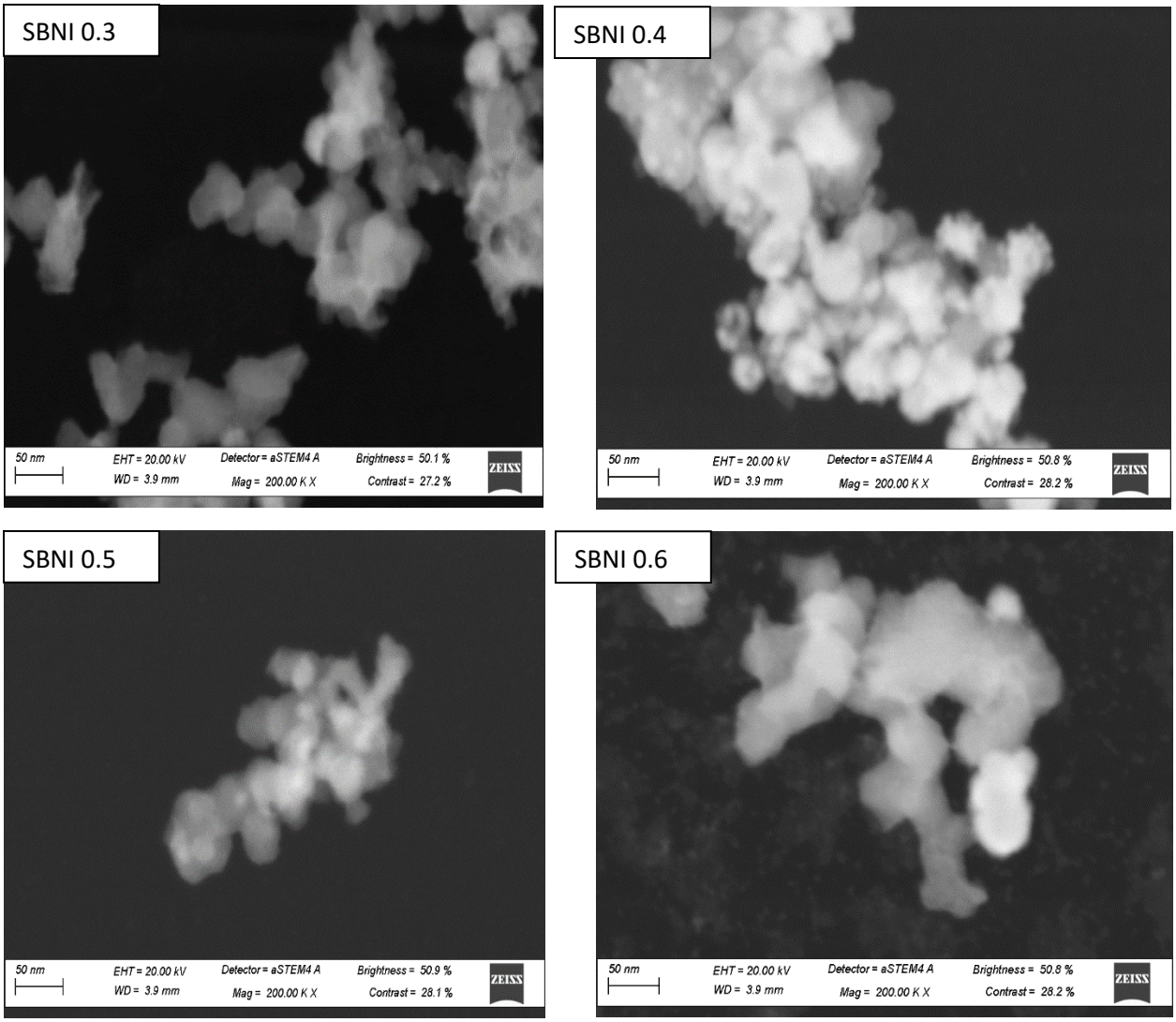

Figure 6. 5: STEM micrographs of nano-iron particles synthesized from the Penstock AMD using varying concentrations of sodium borohydride solution (0.3 M, 0.4 M, 0.5 M, and 0.6 M). Experimental conditions applied: vol. of AMD (100 mL), pH of AMD (2.14), vol. of $NaBH_4$ (50 mL),

concentration of $NaBH_4$ (0.1-0.7 M), contact time (80 minutes), temperature=25 ^oC, and speed (300 rpm).

The STEM morphology in Figure 6.5 revealed spherical, chainlike, nano-iron particles (SBNI 0.3, SBNI 0.4, SBNI 0.5 and SBNI 0.6) synthesized from the Penstock AMD. These results confirm the morphological structure observed in Figure 6.2 by SEM analysis and are consistent with literature reports (Alegbe et al., 2019). According to Alegbe et al. (2019), the spherical shape of the synthesized nano-iron particles is characteristic of nano-iron particles synthesized by precipitation. The STEM results of SBNI 0.3, SBNI 0.4, SBNI 0.5 and SBNI 0.6 also showed evidence of agglomeration, and this could be attributed to the drying process during sample preparation for STEM or due to the particles' high surface energy.

The size distribution histograms of nano-iron particles synthesized from field Penstock AMD using sodium borohydride are shown in Figure 6.5. SBNI 0.3 nano-iron particles ranged in particle size from 20 to 70 nm, with an average particle size of 43 nm. The nano-iron particles in the SBNI 0.4 sample ranged in size from 30 to 60 nm, with an average particle size of 44 nm. Nano-iron particles in the SBNI 0.5 sample ranged from 30 nm to 80 nm, with an average particle size of 55 nm, whereas nano-iron particles in the SBNI 0.6 sample ranged from 40 nm to 100 nm, with an average of 62 nm. These findings support the SEM and STEM micrographs, which revealed different particle sizes when viewed physically. It is worth noting that as the concentration of sodium borohydride (M) in the Penstock AMD solution increased from 0.3 to 0.6 M to precipitate nano-iron, the average particle size of the Fe nanoparticles increased (see Figure 6.6).

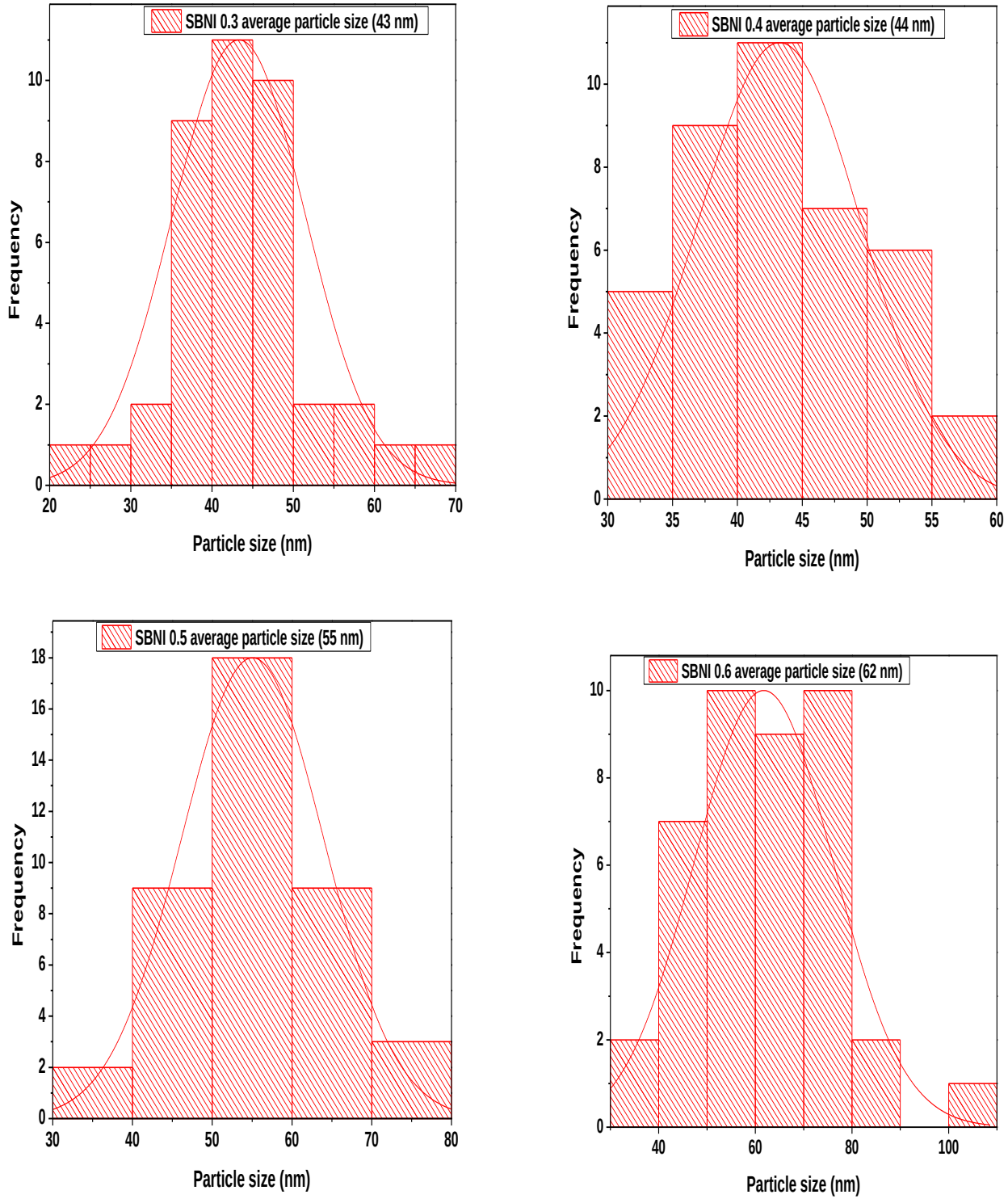

Figure 6. 6: Crystal size distribution of nano-iron particles (SBNI 0.3, SBNI 0.4, SBNI 0.5, or SBNI 0.6) synthesized from AMD sample P with sodium borohydride

In summary, Figure 6.6 proved that as the concentration (M) of sodium borohydride that was used as a reductant to precipitate Fe increased in solution, the particle size of the nano-iron particles increased.

6.2.4 FTIR spectra of synthesized nano-iron particles from field AMD

As stated in Chapter 3, Fourier transform infrared spectroscopy (FTIR) was performed on the nano-iron products to provide information on chemical bonding, molecular structure, and functional groups. Figure 6.6 shows the FTIR spectra of the synthesized nano products.

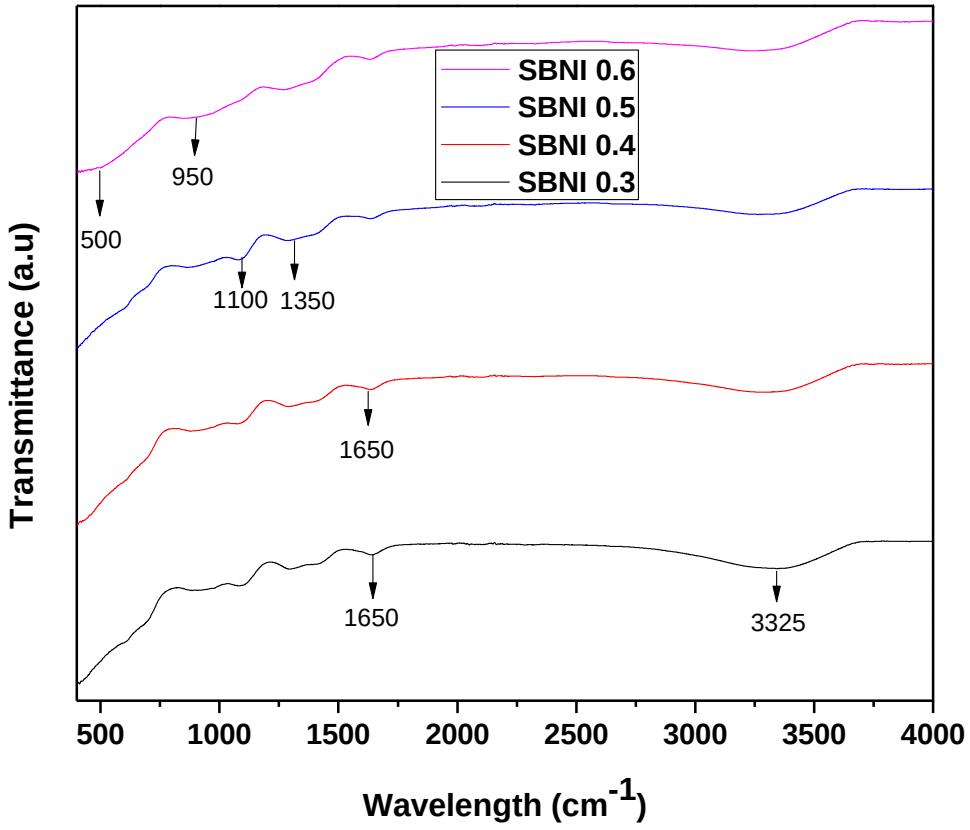

Figure 6. 7: FTIR spectra of nano-iron made from the Penstock AMD using 0.3 M, 0.4 M, 0.5 M, and 0.6 M sodium borohydride solution.

Figure 6.6 depicts all the structural vibrational bands observed on the FTIR spectra of scanned synthesized nano-iron particles from the Penstock AMD, and Table 6.2 summarizes and presents these vibrational bands.

Table 6. 2: Extraction of nano-iron from AMD solutions 0.3 M, 0.4 M, 0.5, or 0.6 M sodium borohydride solutions: structural vibrational bands for (SBNI 0.3-0.6) nano-iron particles.

	Samples Name
Vibration band (cm^{-1})	SBNI (0.3-0.6))
500	Fe-O bending
950	Fe-O stretch
1100	Fe-O stretch
1350	C-O stretch
1650	O-H bending
3325	O-H stretch

The FTIR spectra of synthesized nano-iron particles SBNI 0.3-0.6 in Figure 6.7 were scanned between 400 cm-1 and 4000 cm^{-1}. The absorption spectra of the AMD synthesized nano-iron particles SBNI 0.3, SBNI 0.4, SBNI 0.5, and SBNI 0.6 showed peaks at 500 cm-1 to 3325 cm-1. Ramalakshmi and Sundrarajan (2011) reported that the bands of nano-iron around 360 and 570 cm-1 corresponded to the bending and stretching vibrations of Fe-O bonds, which are characteristic of the crystalline lattice of magnetite. The current nano-iron particles show similar bands of FeO between 500 and 1100 cm-1. The absorption spectra at 3325 cm-1 and 1650 cm-1 are allocated to the stretching and bending vibrations of O-H in water, which is present on the surface of the nanoparticles (Sundrarajan et al., 2012; Roonasi, 2007).

6.3. Characterization of AMD-based nano-iron particles synthesized from AMD using green tea

The characterization of nano-iron particles (GTNI) synthesized from AMD using green tea extract is presented and discussed in this section. The following experimental conditions were used to synthesize the nano-iron particles from AMD: vol. of AMD (50 mL), vol. of green tea (40 mL), pH

of AMD=2.14, mass of green tea (0.1-0.7 g), temperature (30-50 ^{o}C), reaction time (4-24 hours), agitation speed (300 rpm). The results are presented in section 6.3.1 to 6.3.5.

6.3.1 Synthesized nano-iron particle mineralogy

XRD was used to investigate the mineralogy of nano-iron particles (SBNI) synthesized from AMD using green tea as a reductant. The XRD results of the synthesized nano-iron particles are shown in Figure 6.1, as the dosage of green tea was varied.

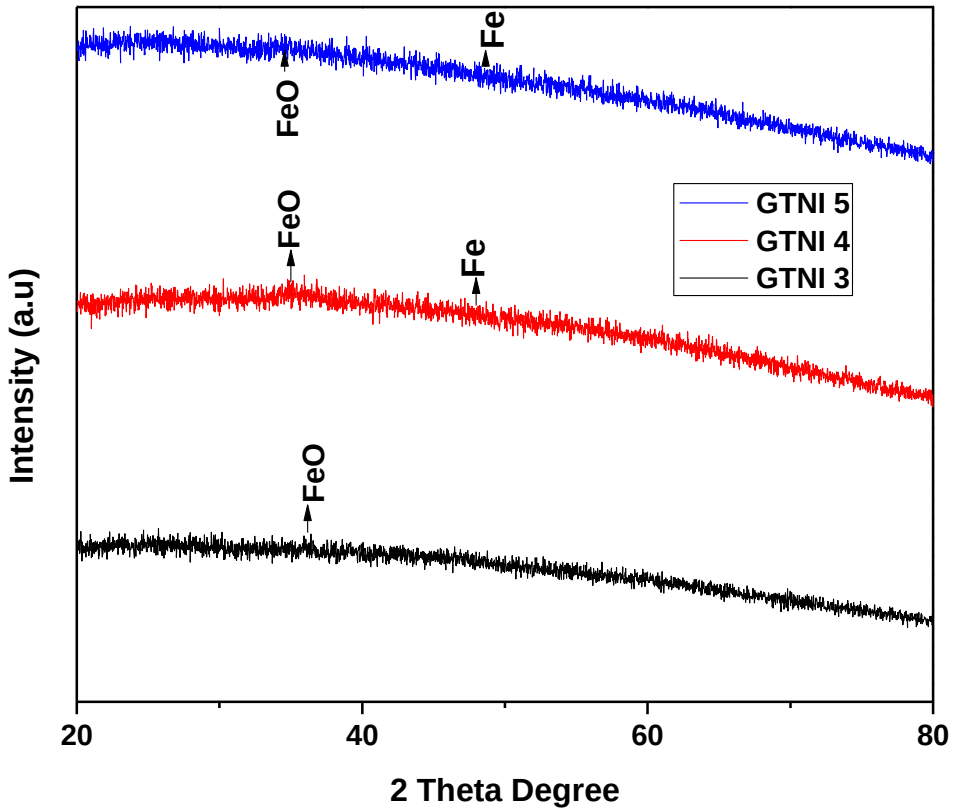

Figure 6. 8: XRD pattern of extracted nano-iron particles (pure Fe=Fe^{0} and FeO) from the Penstock AMD using green tea extract as a reductant. Experimental conditions applied: vol. of AMD (50 mL), pH of AMD=2.14, dosage of reductant=50 mL solution made from 0.3 g, 0.4 g, and 0.5 g of powdered green tea extract, temperature (35 ^{o}C), reaction time (12 hours), and agitation speed (250 rpm).

Figure 6.8 shows the diffraction pattern of nano-iron particles (GTNI 3, GTNI 4, or GTNI 5) synthesized from the Penstock AMD using different dosages of aqueous green tea extract. GTNI 4 and GTNI 5 had similar diffraction pattern spectra at 35^{o} and 44.5^{o}, except for GTNI 3, whose peaks were slightly less prominent. However, the very low peaks observed on the XRD spectra of the synthesized AMD-based nano-iron particles (GTNI3, GTNI4, or GTNI5) indicate the presence of nano-size range particles with short-range order. All the peaks in the XRD pattern can be attributed to a mixture of Fe=Fe^{0} and FeO. The JCPDS file was used to identify the C diffraction angles on the spectrum where the characteristic peaks of a particular mineral phase can be seen. The slightly more prominent diffraction peak on the spectra was observed at 35^{o} to be FeO nanoparticles, while the slightly less prominent diffraction pattern of GTNI 3, GTNI 4, or GTNI 5 was observed at the reflection angle of 44.5^{o} and was identified as pure Fe (Fe^{0}), which indicates the presence of zerovalent iron (Lu et al., 2007b).

The presence of both zerovalent iron (Fe^{0}) and iron oxide (FeO) nanoparticles in crystalline mineral phases are indicated by spectral peaks indexed at angle 2 Theta of 44.5° and 35.1° for all samples (Li & Zhang, 2006; Lu et al., 2007b; R. Yuvakkumar et al., 2011; Y. P. Sun et al., 2006). The diffraction peak for FeO nanoparticles was slightly more prominent than the diffraction peak for zerovalent nano Fe particles. This could be attributed to the green tea extract having a lower ferric reducing antioxidant power (FRAP) compared to sodium borohydride and thus being unable to significantly reduce Fe in the AMD solution from a higher oxidation state to a lower oxidation state. The nano-iron particles, on the other hand, were very stable due to their enclosure in polyphenol. It should also be noted that no peaks were observed above 60 degrees 2 Theta on the XRD spectra. This study is unique in that it is a proof-of-concept study that shows how a green reductant can be used to synthesize nano-iron particles from raw AMD solutions prior to neutralization with lime, thereby extracting iron and reducing costs. The literature that cited nano-iron synthesis from AMD used caustic soda and sulfuric acid to generate the ferric ion solution before using ammonium hydroxide (Wei & Viadero, 2007), and Cheng et al. (2011) reported the recovery of nano-iron from synthetic AMD using fuel cell technologies. Alegbe et al. (2019) used an alkali and acid approach to generate ferric iron solution before synthesizing magnetic iron nanoparticles known as magnetite with sodium borohydride. Alegbe et al. (2019) used sodium borohydride to synthesize nano-iron from AMD.

6.3.2: Morphology and elemental composition of nano-iron particles synthesized from field AMD samples using green tea extract

The morphology of nano-iron synthesized from field Penstock AMD samples using green tea extract as a reductant is described in this section. The elemental composition of the synthesized nano-iron particles was determined using the EDS technique. Figure 6.1 depicts a scanning electron micrograph of nanoparticles derived from Penstock AMD solutions.

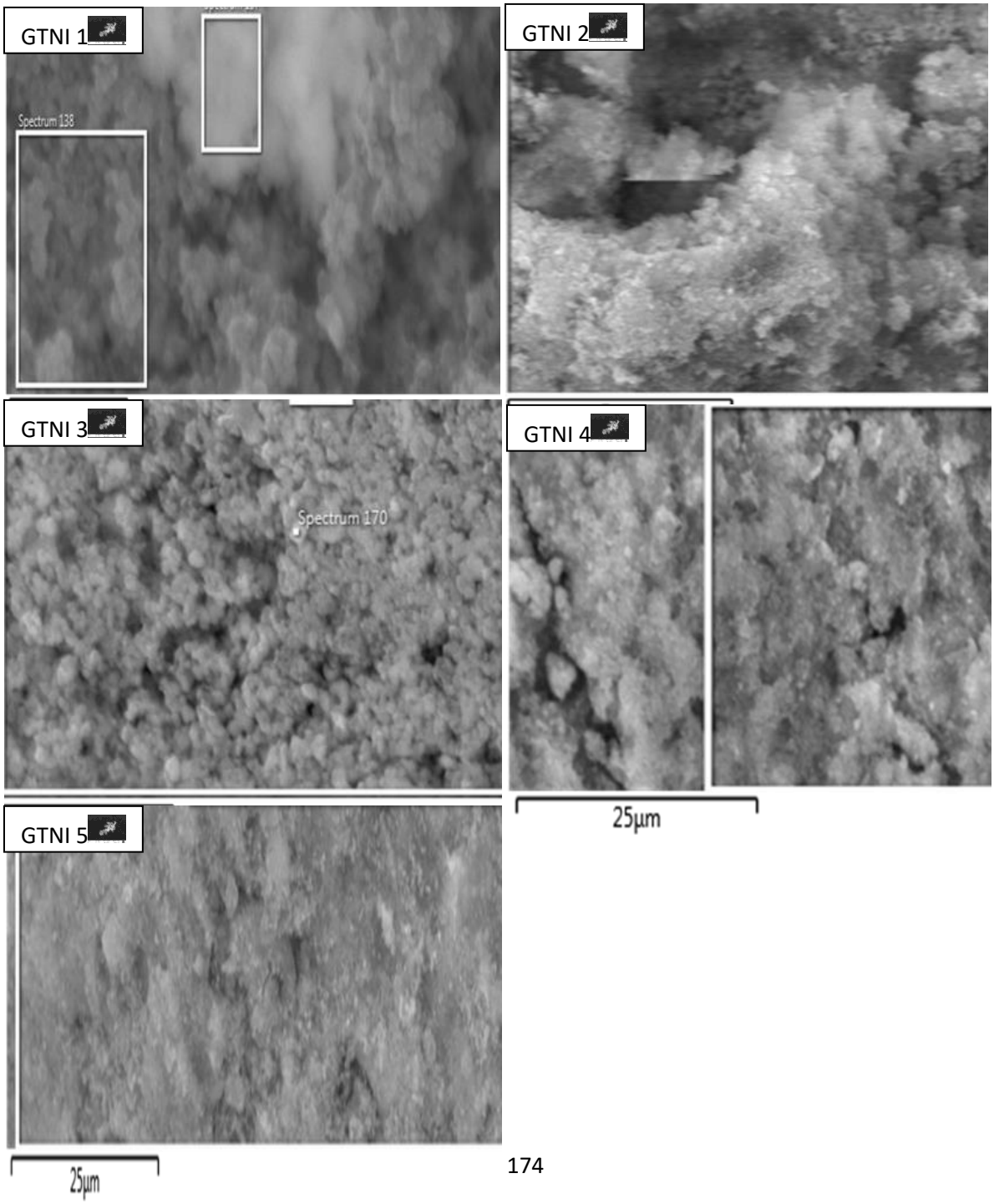

Figure 6. 9: SEM micrographs of nano-iron particles extracted from the Penstock AMD solutions using aqueous green tea extract. Experimental conditions applied: vol. of AMD (50 mL), pH of AMD=2.14, dosage of reductant=40 mL solution made from 0.3 g, 0.4 g, or 0.5 g of powdered green tea extract, temperature (35 ^{o}C), reaction time (12 hours), and agitation speed (250 rpm).

The SEM images of the nano-iron particles were difficult to analyse for their morphology, thus a further investigation was done using STEM analysis. This provided a clearer image for morphological interpretation and particle size distribution. Figure 6.9 presents the EDS spectra of the AMD-based nano-iron particles used for SEM analysis.

The EDS spectra of the nano-iron products are presented in Figure 6.9, and the quantitative results were presented in Table 4.1.

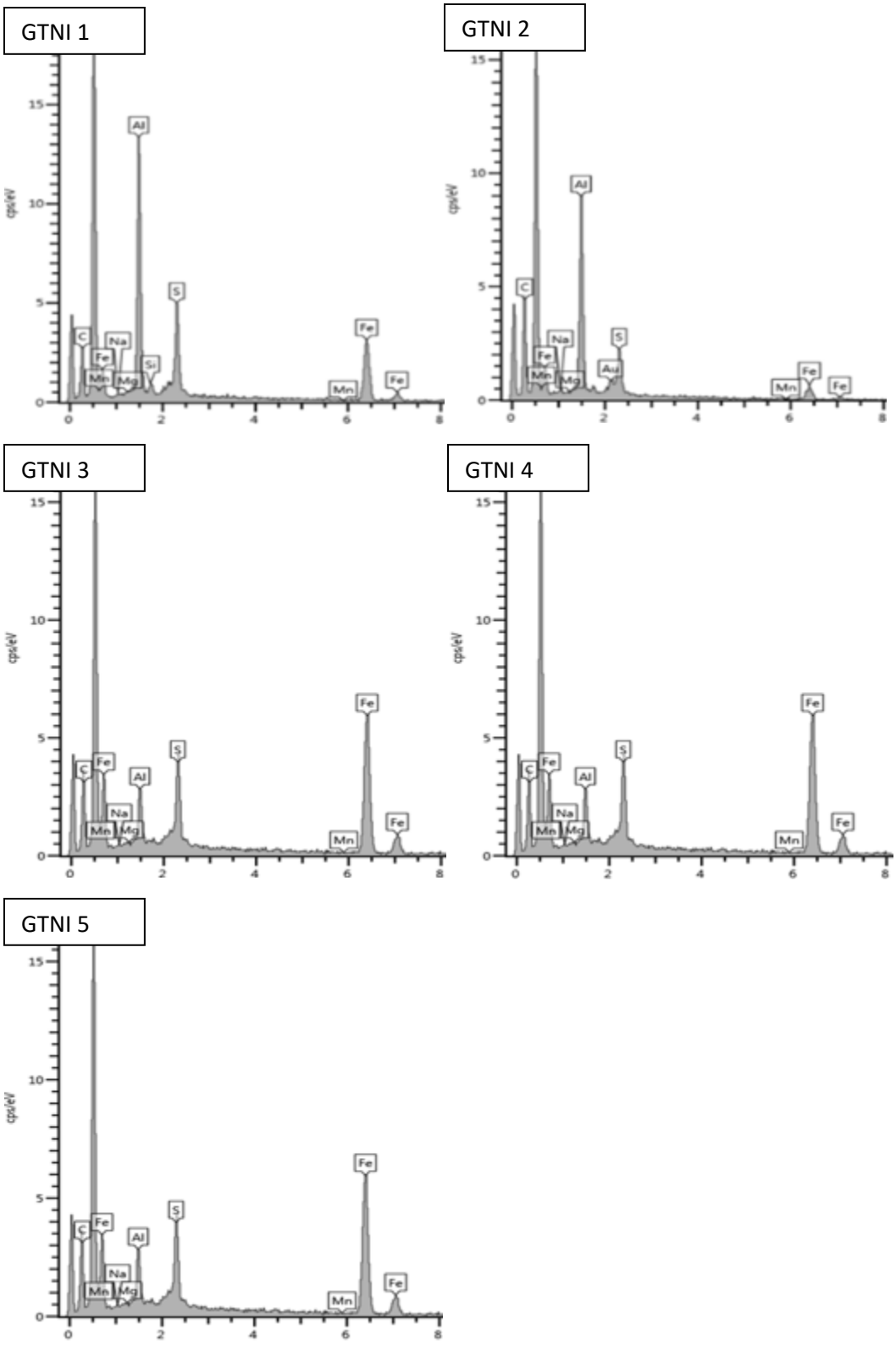

Figure 6. 10: EDS spectra of nano-iron particles synthesized from the Penstock AMD solutions using green tea extract as a reductant. Experimental conditions applied: vol. of AMD (50 mL), pH

of AMD=2.14, dosage of reductant=40 mL solution made from 0.3 g, 0.4 g, or 0.5 g of powdered green tea extract, temperature (35 ^{o}C), reaction time (12 hours), and agitation speed (250 rpm).

The EDS results show that the synthesized nano-iron particles co-precipitated with other elements such as Al etc. When a lower dosage of 0.1 g or 0.2 g of green tea extract was used to treat the Penstock AMD, the precipitation of Al was more favoured than that of Fe. However, when higher dosages of the reductant were used for the treatment of AMD the precipitation of nano Fe was dominant (refer to Figure 6.9 or Table 6.2). Figure 6.10 presents a bar chart of the percentage composition of elements in GTNI 1 - GTNI 5.

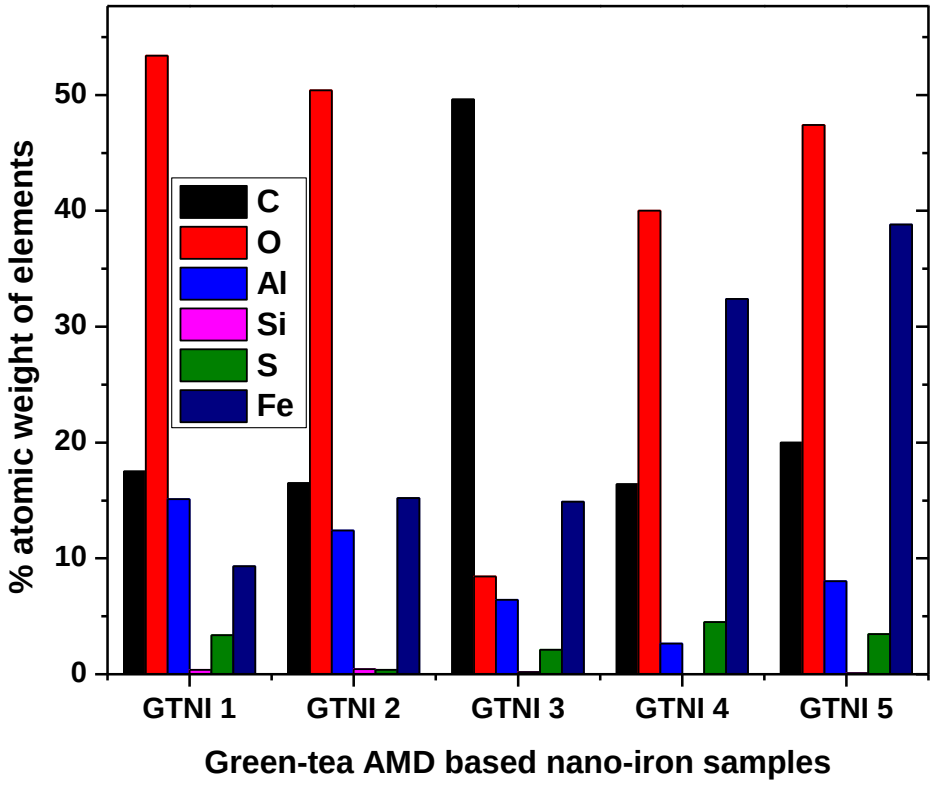

Figure 6. 11: Percentage elemental composition of nano-iron particles (GTNI 1 - GTNI 5) synthesized from the Penstock AMD with green tea extract. Experimental conditions applied: vol. of AMD (50 mL), pH of AMD=2.14, dosage of reductant=40 mL solution made from 0.3 g, 0.4 g, and 06.5 g of powdered green tea extract, temperature (35 ^{o}C), reaction time (12 hours), and agitation speed (250 rpm).

Figure 6.11 confirms that the percentage atomic weight of elements in the AMD-based nano-iron samples (GTNI 1, GTNI 2, GTNI 3, GTNI 4, and GTNI 5) included C, O, Al, Si, S, and Fe, but the percentage atomic weight of these elements varied across samples. Weng et al., (2013) reported similar elemental composition of nano-iron particles when the authors synthesized nano-iron particles from reagent-grade iron salt using green tea extract. Huang et al., (2014) also reported similar elemental composition when the author synthesized nano-iron particles from reagent grade Fe salt using various tea extracts. Elements such as S, Si, or Al found in the green synthesis of nano-iron particles (GTNI) from AMD could have come from the AMD feedstock. The C and O found in the composition of the nano-iron particles could be attributed to the carbonyl groups of polyphenols and other C-containing molecules of the green tea extract (Shahwan et al., 2011). It should be noted that EDS analysis is not an accurate method for measuring elemental composition because some of the elements that co-precipitated with Fe in small or trace amounts during nano-iron extraction from AMD using green tea extract were not detected; thus, EDS cannot measure traces of elements.

6.3.3 Scanning transmission electron microscopy (STEM): morphological and size distribution analysis of nano-iron particles generated using green tea extract.

The particle size, morphology, and crystallinity of the synthesized AMD-based nano-iron particles were further confirmed using STEM analysis and the results at various dosages of green tea extract are presented in Figure 6.12.

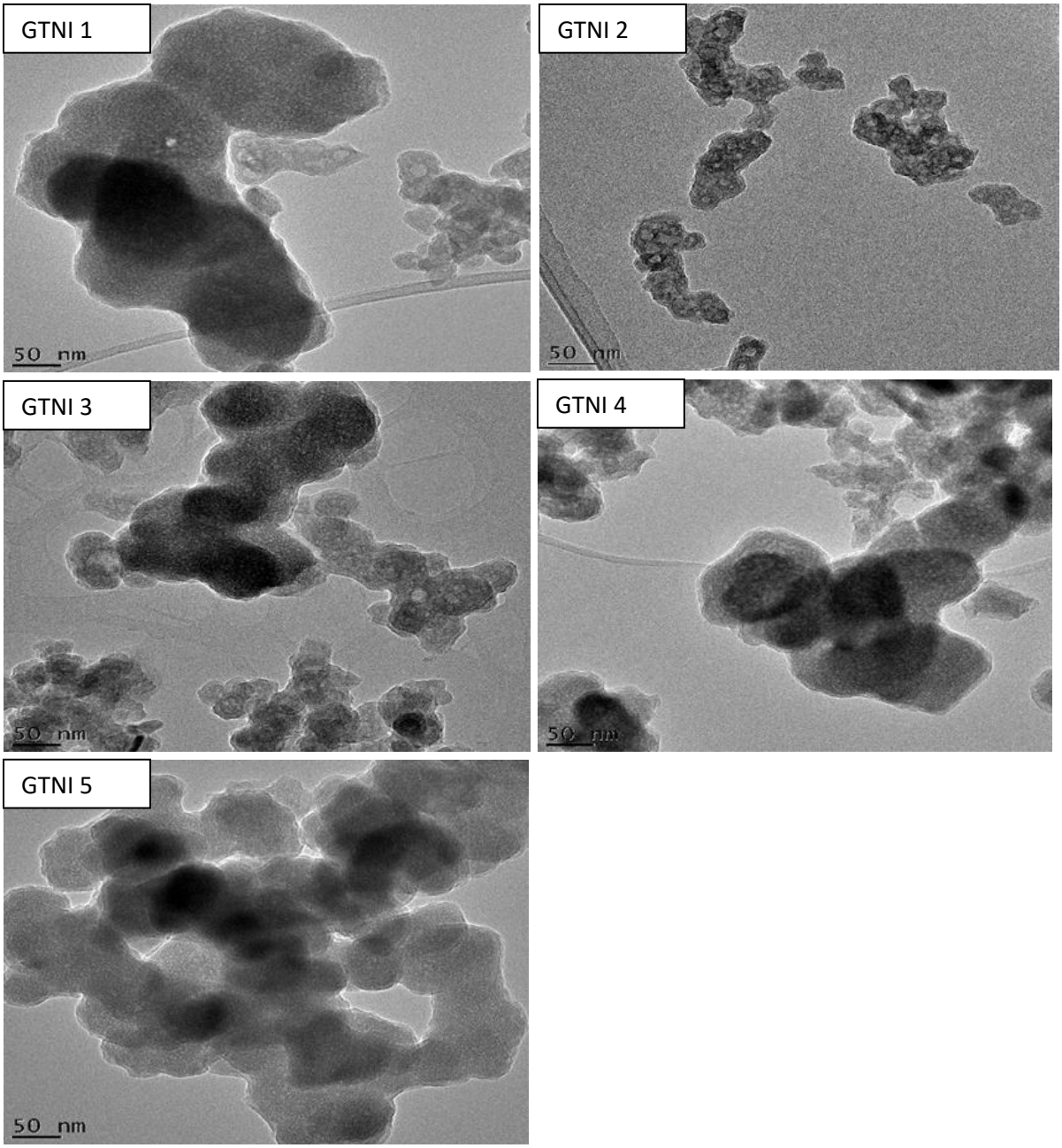

Figure 6. 12: STEM micrographs of GTNI1, GTNI2, GTNI3, GTNI4, or GTNI5 nano-iron particles synthesized from AMD using green tea extract as a reductant. Experimental conditions applied: vol. of AMD (50 mL), pH of AMD=2.14, dosage of reductant=50 mL solution made from 0.3 g, 0.4 g, or 0.5 g of powdered green tea extract, temperature (35 ^{o}C), reaction time (12 hours), and agitation speed (250 rpm).

To assess the morphology and calculate the average particle size of the green synthesized nano-iron particles (GTNI1, GTNI 2, GTNI 3, GTNI 4, and GTNI 5) from AMD, STEM analysis was

conducted. The STEM morphology of the synthesized nano-iron particles is shown in Figure 6.11. The morphology of GTNI 1, GTNI 2, GTNI 3, GTNI 4, and GTNI 5 revealed that the nano-iron particles were spherical in shape and evenly distributed. Zhu et al. (2018) reported the synthesis of similar well-dispersed nano-iron particles using green tea and reagent-grade iron salt. The dispersion of these nano-iron particles can be attributed to the natural organic coating, which can improve nanoparticle stability and facilitate nanoparticle dispersion (Ghosh et al., 2012). The spherical shape of the nano-iron particles obtained in this study was consistent with previous findings (Zhu et al., 2009). Figure 6.11 presents the particle size distribution and the average particle size of the spherical nano-iron particles (GTNI1, GTNI2, GTNI3, GTNI4, or GTNI5)

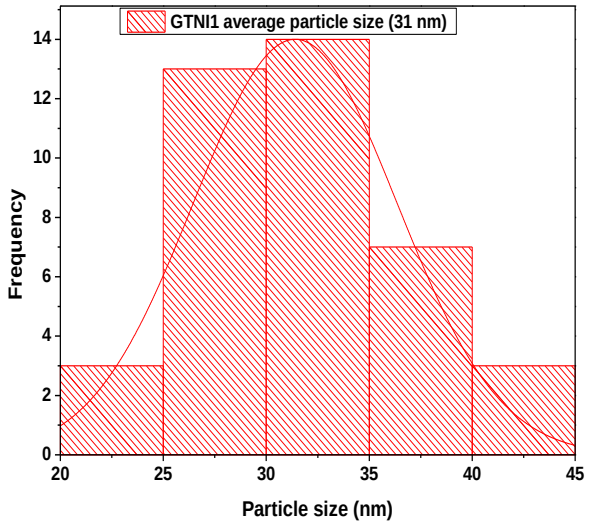
GTNI1 average particle size (31 nm)
Frequency
Particle size (nm)

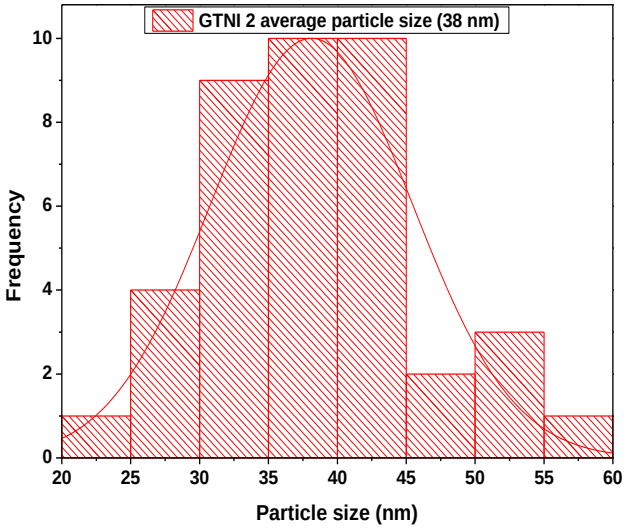
GTNI 2 average particle size (38 nm)
Frequency
Particle size (nm)

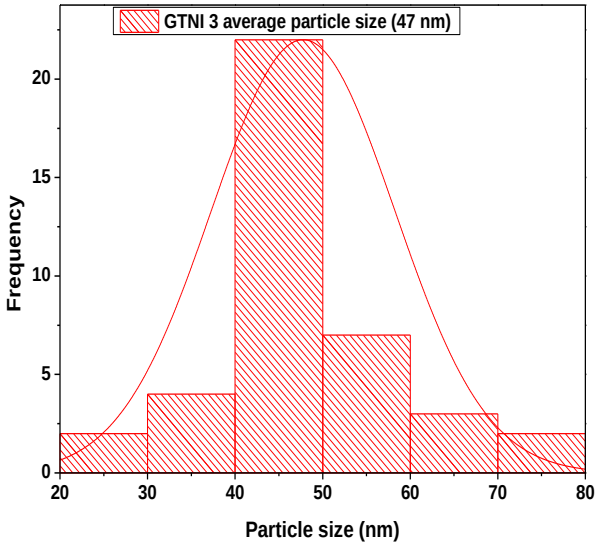
GTNI 3 average particle size (47 nm)
Frequency
Particle size (nm)

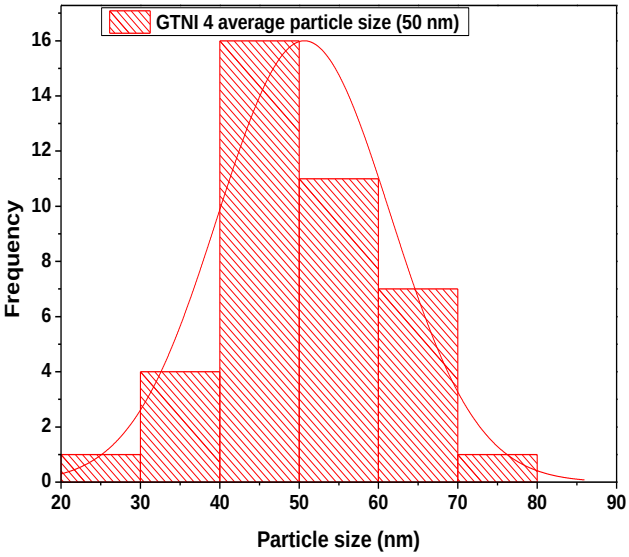
GTNI 4 average particle size (50 nm)
Frequency
Particle size (nm)

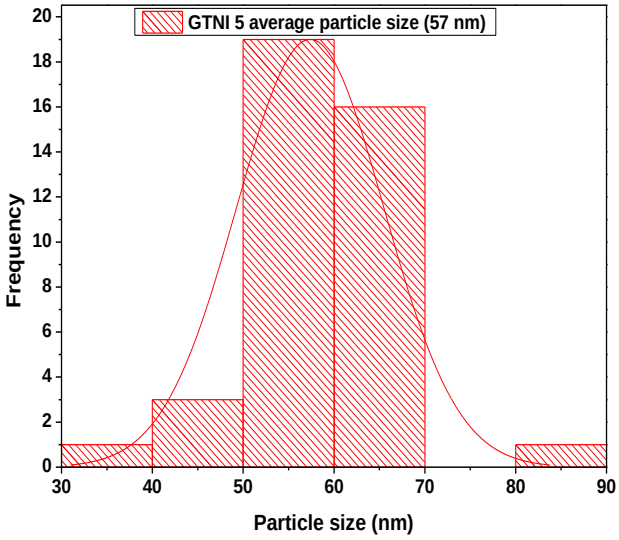
GTNI 5 average particle size (57 nm)
Frequency
Particle size (nm)

Figure 6. 13: Particle size distribution of nano-iron particles (GTNI1, GTNI2, GTNI3, GTNI4, and GTNI5) synthesized from the Penstock using aqueous green tea extract.

The size distribution histograms of nano-iron particles synthesized from the field Penstock AMD using aqueous green tea extract are shown in Figure 6.13. GTNI 1, GTNI 2, GTNI 3, GTNI 4, and GTNI 5 nano-iron particles had average particle sizes of 31 nm, 38 nm, 47 nm, 50 nm, and 57 nm respectively as the dosage of green tea extract used to synthesize nano-iron from the Penstock AMD solution increased. These findings corroborate the size obtained from SEM and STEM micrographs, which revealed different particle sizes when viewed physically. It is worth noting that as the dosage of green tea extract in the Penstock AMD solution increased from 0.1 to 0.5 g to precipitate nano-iron, the average particle size of the nano-iron particles increased. This can be attributed to the increase in the polyphenolic content surrounding the precipitated iron when the dosage of reductant used to reduce iron from the AMD solution increased. (Huang et al., 2014) reported the production of nano-iron particles from Oolong tea extracts and reagent-grade Fe salt having average particle size between 40-50 nm, which is well within the range of nano-iron particles produced in this study.

6.2.4 Fourier transform infrared spectroscopy (FTIR)

The structural analysis of the green tea synthesized nano-iron particles from the Penstock AMD with assigned code names GTNI, GTNI2, GTNI3, GTNI4, and GTNI5 are presented in Figure 6.13.

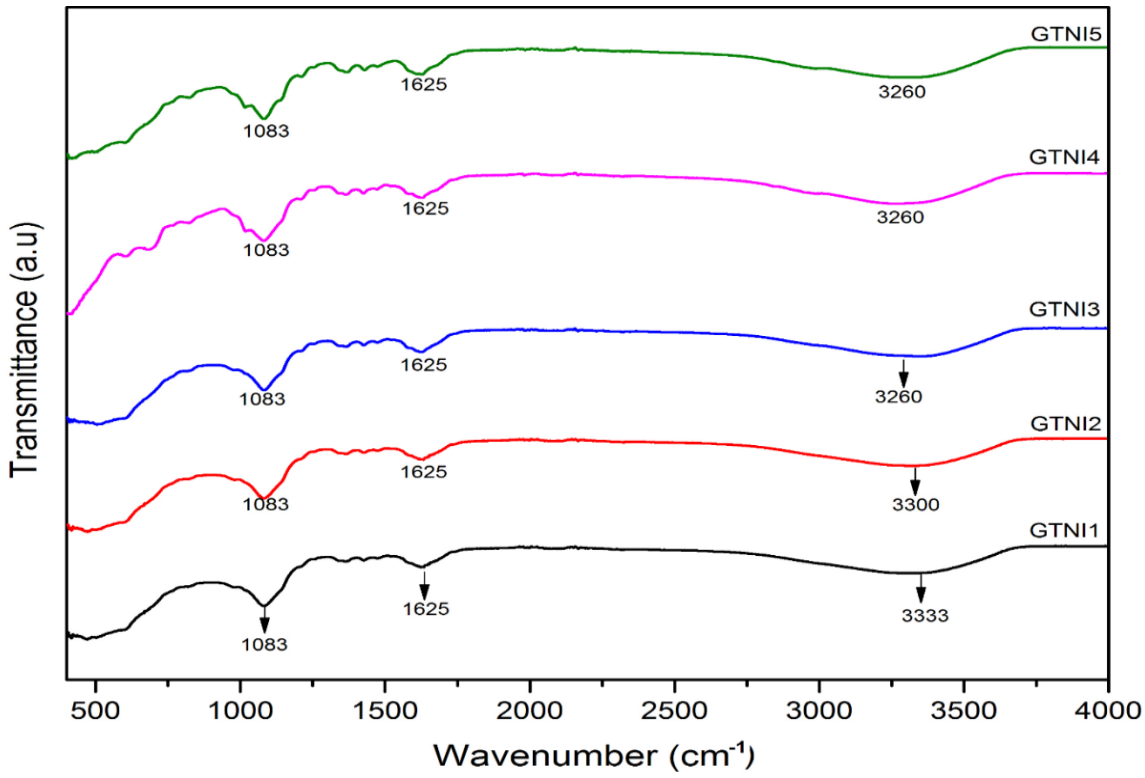

om the

The vibrations of polyphenolic compounds in the green tea-derived nano-iron particles from AMD were observed across all spectra (GTNI1, GTNI2,GTNI3, GTNI4, and GTNI5). The OH stretching vibration was observed at 3000 to 3333 cm^{-1} on all the samples. The broad OH spectrum indicates the contribution of benzylic OH from the polyphenolic content of the plant extract (Ashokkumar & Ramaswamy, 2014; Liu & Zhang, 2014). The less prominent peak on the spectra indicates the vibrations of aromatics and moisture from air. The second most pronounced peak at 1625 cm^{-1} on the spectra of the samples could be assigned to aromatic skeletal vibrations. This indicates the binding of polyphenolic compounds to the active surfaces of the plant derived nano-iron particles and suggested the presence of aromatic compounds (Badmus et al., 2018c). Its intensity confirms the presence of Fe-O complex as previously reported (Sathishkumar et al., 2018; Wang, 2013). In this line of investigation, the asymmetric, symmetric, and C-O stretching peaks observed at 1200, 1392, and 1082 respectively were present on all the coded samples. The carbonyl sugar base of the tea extract acts as a surface modifier of the synthesized nano-iron particles that prevents agglomeration and in its right proportion enhances the catalytic activity of the nano-iron.

6.5 Summary

The comparison of the nano-iron particles prepared from sodium borohydride with the nano-iron particles prepared with green tea extract shows that the sodium borohydride chemical reductant is a straightforward way to extract iron from the AMD solutions and form nanoparticles. Its FRAP strength was considerably higher than the tea extracts, making it much more effective for preparing the nano-iron particles. However, the particle sizes were larger than those prepared with the tea extracts, with borohydride-reduced nanoparticles being up to 62 nm whereas the tea extract nanoparticle sizes were in the range of 31-57 nm. This size difference was evident from the XRD spectra as well, with the borohydride nano-iron XRD spectra displaying some bulk metal long range crystallite ordering whereas the nanoparticles made from the tea had no long-range metal ordering and appeared amorphous. The EDS results showed that nano-iron particles prepared using sodium borohydride had a high Fe content between 63-74 wt % but other elements present in AMD were co-precipitated with the iron. Whereas when the tea extracts were used, the nanoparticles were coated by the polyphenols as could be deduced from the high carbon content shown by EDS and the relatively lower iron content, which ranged from 9-38 weight % depending on the extract dosage applied. The FTIR results confirmed that the sodium borohydride-reduced nano-iron was not fully in a zerovalent form, whereas in the case of the plant extracts, the spectral bands from the polyphenols were evident, acting as a surface modifier of the synthesized nano-iron particles that prevented agglomeration, as was evident from STEM.

CHAPTER 7

AMD NEUTRALISATION

7.0 Introduction

The neutralization of the Penstock AMD samples, before and after pre-treatment with reductants is presented and discussed in this chapter. This chapter is subdivided into three sections. The first section (section 7.1) presents and discusses the neutralization of the Penstock AMD with lime only. The second section (Section 7.2) presents and discusses the neutralization of the Penstock AMD after it was pre-treated with sodium borohydride to remove Fe from the solution. The third section presents and discusses the neutralization of the Penstock AMD after it was pre-treated with green tea extract to remove Fe from the solution.

7.1 Neutralisation agents used

The purpose of using hydrated lime for the neutralization of the field Penstock AMD, both before and after pre-treatment with sodium borohydride or green tea extract, was to assess the effect of lime dosage and pH on the removal of metals and salts and the characteristics of the sludges formed. The second reason for using hydrated lime in the neutralization process was that it is cost-effective compared to other neutralization agents.

Table 7. 1: Neutralisation of AMD, experimental conditions, and code names (label)

Sample	Parameter	Label
Field Penstock AMD	Vol. of AMD (500 mL), mass of lime (5.5-6 g), mixing time (120 min), speed (300 rpm)	Raw AMD
Field Penstock AMD pre-treated with sodium borohydride	Vol. of AMD (250 mL), mass of lime (1.5-2 g), mixing time (120 min), speed (300 rpm)	supernatant 1
Field Penstock AMD pre-treated with green tea extract	Vol. of AMD (250 mL), mass of lime (1.25, 1.75, 2.25, or 2.75g), mixing time (120 min), speed (300 rpm)	supernatant 2

Table 7.1 shows the experimental conditions that were used during the neutralization test work of the Penstock AMD samples, before and after pre-treatment.

7.2 Lime neutralization of Penstock AMD without pre-treatment

The results of the lime neutralization of the Raw Penstock AMD solutions are presented in this section.

7.2.1 pH and redox potential profile

The effect of 11 and 12 g/L of lime upon pH and redox potential trends in the neutralization of AMD over time is presented in Figure 7.1. As a reminder, 5.5 g or 6 g of lime corresponding to 11 or 12 g/L was used as optimum lime dosages for the neutralization of the Penstock AMD after 120 minutes to obtain the required pH for AMD neutralization.

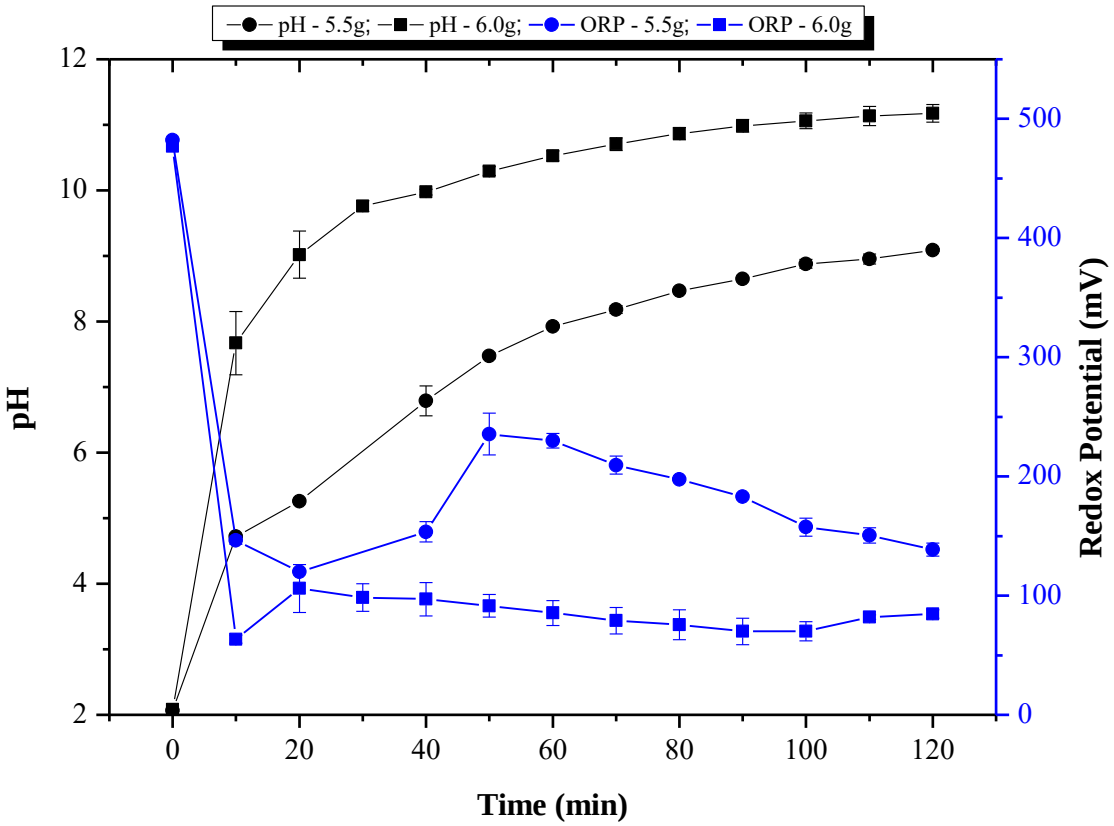

Figure 7. 1: pH and redox potential (ORP) of untreated Penstock AMD after neutralization with 11 g/L (■) and 12 g/L (●) of lime

The trends in Figure 7.1 show that pH increases rapidly from the initial value of 2.14 in the first 30 minutes after lime addition and then more gradually from 30 to 120 minutes. A maximum average pH of 9.1 and 11.2 was obtained after 120 minutes at lime additions of 5.5 g (11 g/L) and 6 g (12 g/L) respectively. The redox potential shows a significant decline from an average of 483 and 477 mV to 147 or 64 mV after 10 minutes of treatment of 500 mL AMD with 5.5 g and 6 g of lime addition respectively. The redox potential continued to fluctuate before settling at values of 146 mV and 85 mV after 120 minutes at lime additions of 5.5 g or 6 g respectively.

7.2.2 Composition of the neutralisation effluents

The compositions of the effluent obtained from the neutralization of 500 mL of Penstock AMD solution with 5.5 g (11 g/L) or 6 g (12 g/L) lime are presented in Table 7.2, and the extent of removal of selected components through precipitation is presented in Figure 7.2.

Table 7. 2: Composition of effluent from the neutralization of untreated Penstock AMD with lime to pH 9.1 (11 g/L lime) and pH 11.2 (12 g/L lime). T= 120 minutes

Parameters	**Units**	**Raw AMD**	Neutralization effluent concentrations as a function of lime dosage (mg/L)	
			11 g/L lime	12 g/L lime
Anions				
Sulphate	mg/L	11500	2790	1730
Nitrate	mg/L	2.13	ND	ND
Chloride	mg/L	10.2	ND	ND
Major Metals				
Fe	mg/L	4003	0.02	0.04
Ca	mg/L	495	560	580
Mg	mg/L	433	226	1.14
Al	mg/L	388	0.48	2.23
Mn	mg/L	83.2	0.30	0.04
K	mg/L	0.98	2.20	2.82
Minor metals				
Na	mg/L	48.8	47.5	54.6
Si	mg/L	46.6	0.40	0.30
Zn	mg/L	9.50	BDL	BDL
Trace elements				
As	mg/L	0.03	BDL	BDL
B	mg/L	0.40	BDL	BDL
Ba	mg/L	0.16	0.00	0.00
Cd	mg/L	0.01	0.00	0.00
Co	mg/L	1.07	BDL	BDL
Cr	mg/L	0.05	BDL	BDL
Cu	mg/L	0.08	BDL	BDL
Hg	mg/L	0.00	BDL	BDL
Mo	mg/L	0.00	BDL	BDL
Ni	mg/L	1.07	BDL	BDL
Pb	mg/L	0.02	BDL	BDL
Sb	mg/L	0.00	0.00	0.00
Sr	mg/L	0.64	0.69	0.63
Se	mg/L	0.00	BDL	BDL
Sn	mg/L	0.00	0.00	0.00
V	mg/L	0.04	BDL	BDL

Where: ND or 0.00 = not determined; BDL = below detection limits

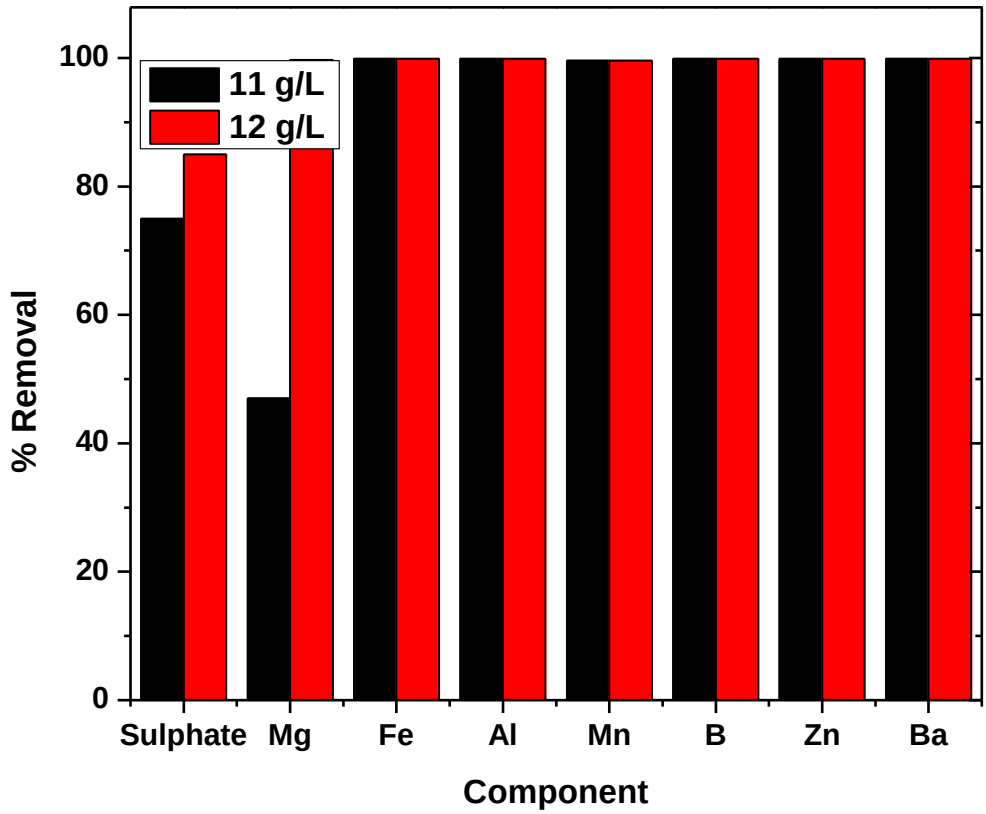

Figure 7. 2: Extent of removal of components from untreated 500 mL Penstock AMD solution after treatment with lime to pH 9.1 (11 g/L lime) or pH 11.2 (12 g/L lime) for 1 hour 20 minutes.

The results indicate that neutralisation with lime to pH 9.1 (11 g/L lime dosage) resulted in >99% removal of metals Fe, Al, Mn, Zn, B and Ba, but only partial removal of Mg (50%) and sulphate (77%) and negligible removal of Na. The effluent solution comprised mainly of residual sulphate (2788 mg/L), Ca (560 mg/L), Mg (226 mg/L) and Na (48 mg/L), with traces of K (2.2 mg/L) and < 0.5 mg/L Al, Mn, and Si. The addition of further lime (12 g/L or 12000 mg/L) to increase the pH to 11.2 enhanced the removal of Mg to >99% and sulphate removal to 85%, resulting in corresponding effluent concentrations of 1.14 mg/L and 1728 mg/L respectively. Raising the pH also resulted in slightly lower effluent Mn concentrations (0.04 mg/L) but higher soluble Al concentrations (2.82 mg/L). In both cases, neutralisation with lime resulted in an increase in the concentration of soluble K (2-3 mg/L) in comparison to the feed AMD (1 mg/L). This increase can

be attributed to the presence of K in the hydrated lime (≤ 500 ppm). Both effluents also contained slightly higher concentrations of Ca (560-580 mg/L) than the feed AMD solution (~ 500 mg/L). Mass balance calculations indicated that between 90% and 91% of the total initial Ca (including the Ca added as lime and the Ca in the AMD feed) was removed in the form of precipitates during neutralisation.

7.2.3 Composition of the neutralisation residue generated from AMD after treatment with lime

Neutralisation of 500 mL of the Penstock AMD solution with 5.5 g or 6 g lime resulted in the formation of 14.2 g (28.4 g/L) or 14.9 g (29.8 g/L) of total precipitate formation respectively. The compositions of the residues obtained from the neutralisation of 500 mL of the Penstock AMD solution with 5.5 g (11 g/L) and 6 g (12 g/L) lime are presented in figure 7.3.

The results in Table 7.3 indicate that the residues at both pH values are comprised predominantly of sulphate (~ 38%), calcium (16-17 %) and iron (11-13%), with lesser amounts of Al (1.3 %), Mg (0.9-1.4 %) and traces of Si (0.1-0.3 %), Mn (0.2-0.3 %) and Na (0.1-0.2 %). Qualitative XRD analysis of neutralisation residues prepared over a range of lime additions and pH values (9.1 or 11.2) show the predominance of gypsum ($CaSO_4 \cdot 2H_2O$) in the residues, with evidence of iron oxyhydroxide, goethite (FeOOH), and ettringite ($Ca_6Al_2(SO_4)_3(OH)_{12} \cdot 26H_2O$). If all the precipitated sulphate in the two residues presented in Table 7.3 is present as gypsum and the iron as amorphous ferric hydroxide ($Fe(OH)_3$), this would equate to concentrations of approximately 67% gypsum and 22-24% ferric hydroxide. Parity calculations indicate that the remaining 9-11% of the residue is likely to be made up of hydroxides of Al ($Al(OH)_3$, at approximately 3.7%, Mg ($Mg(OH)_2$, at approximately 3.5 % and 4.3 % at 11 g/L and 12 g/L lime addition respectively; and possibly calcite ($CaCO_3$), at approximately 1.4 % and 3.7 % at 11 g/L and 12 g/L lime addition respectively. The residue is also likely to contain traces of $Mn(OH)_2$ (~ 0.4%) and amorphous SiO_2 (0.4-0.5 %).

Table 7. 3: Composition of residue from the neutralisation of raw Penstock AMD solution with lime to pH 9.1 (11 g/L lime) and pH 11.2 (12 g/L lime), t=120 minutes.

Component	Residue concentration (%)	
	11 g/L lime (pH 9.1)	12 g/L lime (pH 11.2)
Sulphate	37.9	37.7
Ca	16.3	17.1
Fe	12.5	11.2
Al	1.31	1.30
Mn	0.26	0.23
Mg	0.85	1.40
Si	0.12	0.25
K	0.00	0.00
Na	0.20	0.14

7.2.4 Mineralogy of the neutralisation residue generated from AMD after treatment with lime

Figure 7.3 shows the XRD spectra of the mineralogical phase composition of the residue separated from the supernatant after neutralization.

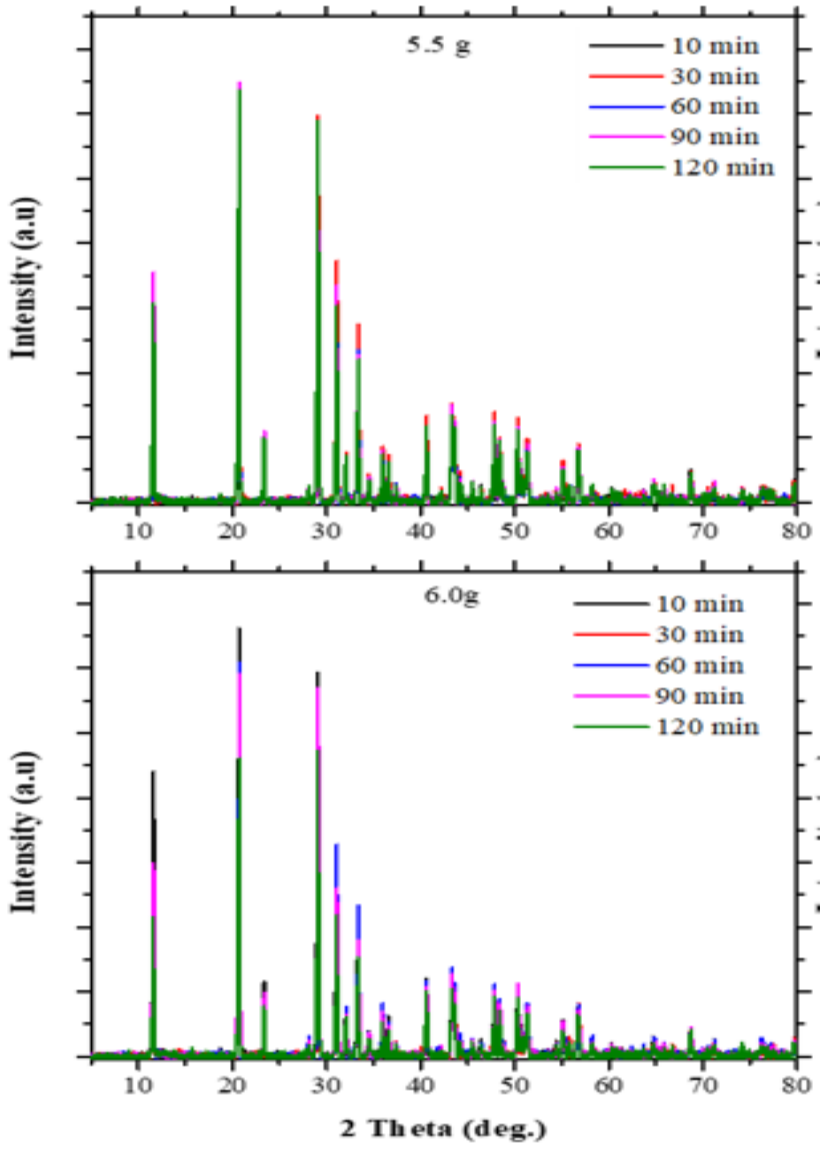

Figure 7. 3: XRD pattern of neutralization residues generated from raw 500 mL Penstock AMD after treatment with lime to pH 9.1 (11 g/L lime) or pH 11.2 (12 g/L lime).

The XRD results in Figure 7.3 revealed that the major crystalline mineral phase present in the resulting residue from mixing lime with AMD after 10, 30, 60, 90 and 120 minutes was gypsum ($CaSO_4 \cdot 2H_2O$) with evidence of ettringite ($Ca_6Al_2(SO_4)_3(OH)_{12} \cdot 26H_2O$), oxyhydroxide and goethite peaks.

7.3 Lime neutralization of Penstock AMD after nano-iron removal using sodium borohydride

The results of the neutralization tests performed on the Penstock AMD solution after pre-treatment with 0.6 M sodium borohydride solution are summarized in this section.

7.3.1 pH and redox potential profile

Figure 7.4 shows the pH and redox potential profiles of the neutralization of AMD pre-treated with an optimum dosage of 0.6 M sodium borohydride solution to remove iron. As a reminder, 250 mL of Penstock AMD was pre-treated with 0.6 M sodium borohydride to remove iron from solution before being neutralized (limed) for 120 minutes using 1.5 g, or 2 g of lime, which corresponds to 6 g of lime per litre of AMD (6 g/L,) or 8 g of lime per litter of AMD (8 g/L) respectively.

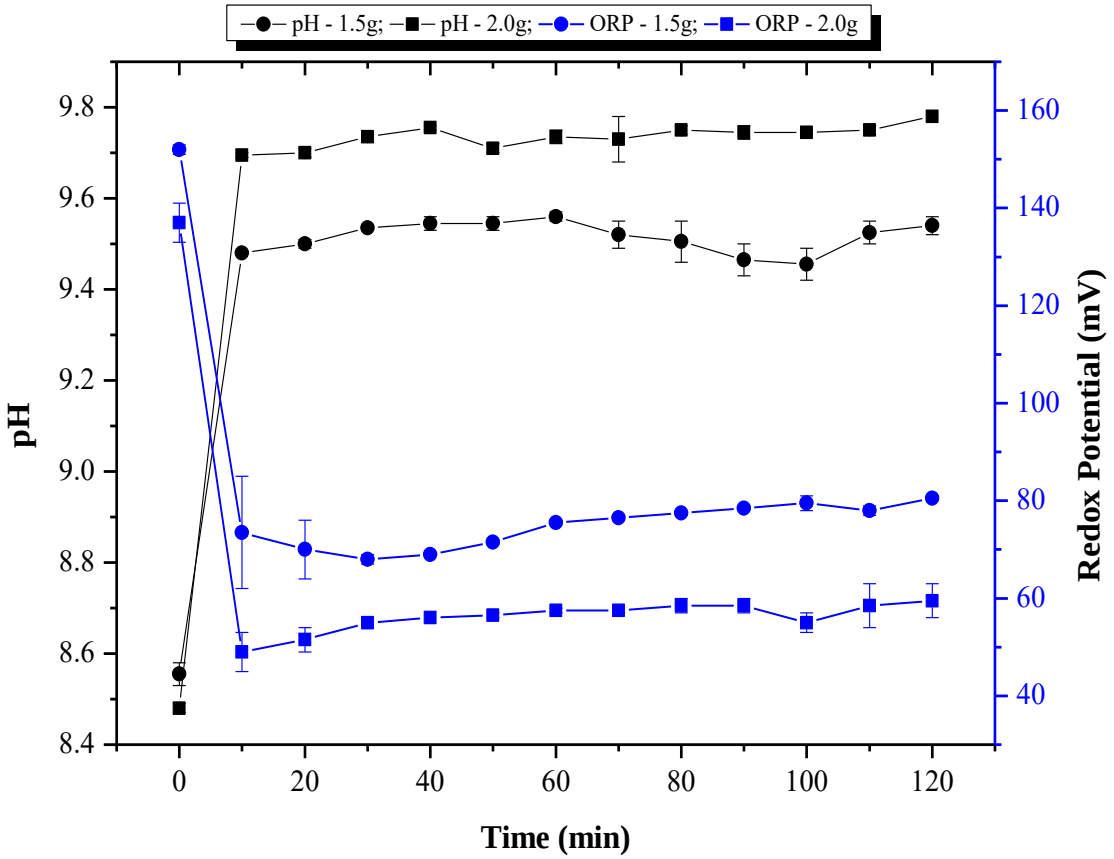

Figure 7. 4: pH and redox potential (ORP) profiles of 250 mL AMD supernatant after pre-treatment of AMD with sodium borohydride to remove iron from solution followed by neutralisation with 6 g/L (●) or 8 g/L (■) of lime respectively.

Figure 7.4 shows that after pre-treating AMD with sodium borohydride to remove iron from the solution, followed by the addition of 1.5 g (6 g/L) lime to the generated supernatant, the initial pH (8.6) of the supernatant increases to 9.5 within the first 10 minutes and remains relatively stable over the entire 120-minutes period. A similar trend is observed when 2 g (8 g/L) lime was added, with the pH rising to 9.7 within 10 minutes and then gradually increasing to 9.8 over the 2-hour retention period.

In the case of 1.5 g (6 g/L) lime addition, redox potentials drop from initial values of 152 mV to 74 mV in the first 10 minutes, with the redox potential gradually increasing to 81 mV over the 120 minutes retention period. Similar trends were observed at 2 g (8 g/L) lime addition with the redox potential dropping from an initial value of 137 mV to 49 mV, before gradually increasing to 60 mV.

7.3.2 Composition of the neutralisation effluents

Table 7.4 shows the composition of the effluent obtained from using 1.5 g (6 g/L) or 2 g (8 g/L) of lime to neutralize 250 mL of AMD pre-treated with 0.6 M sodium borohydride solution, and the extent of removal of selected components through lime precipitation is presented in Figure 7.5

Consistent with previous tests (See Chapter 5), treatment of the raw AMD solution with sodium borohydride results in > 99% removal of Fe along with Al, Zn and Ba, as well as partial removal of Mn (72%), Ca (37%) and Mg (22%). Sodium borohydride treatment also results in 9.5% sulphate removal from solution. The supernatant from the sodium borohydride treatment has a pH of 8.5 and contains major quantities of sulphate (10400 mg/L), Na (5005 mg/L) and B (2194 mg/L), minor quantities of Ca (313 mg/L), Mg (338 mg/L) and Mn (23 mg/L), as well as trace quantities of K (0.4 mg/L), Si (4 mg/L) and Al (0.5 mg/L).

As indicated in Figure 7.4, subsequent neutralisation of the pre-treated supernatant with lime resulted in further removal of residual Fe (33% or 100 % at 1.5 g (6 g/L) or 2 g (8 g/L) lime respectively); Al (23 % or 70 % at 1.5 g (6 g/L) or 2 g (8 g/L) lime addition respectively); Mn (52 % or 75 % at 1.5 g (6 g/L) or 2 g (8 g/L) lime respectively); Mg (17 % and 35 % at 1,5 g (6 g/L) or

2 g (8 g/L) lime respectively); sulphate (7% and 13 % at 1.5 g (6 g/L) and 2 g (8 g/L) lime respectively); as well as partial removal of B (26 % and 42 % at 1.5 g (6 g/L) and 2 g (8 g/L) lime respectively). In all cases, the extent of removal increased on increasing the lime dosage from 1,5 g (6 g/L) to 2 g (8 g/L), with corresponding lower concentrations in the treated effluent. Nevertheless, the effluent solutions still contained elevated concentrations of sulphate (9600 mg/L and 9100 mg/L at 1.5 g (6 g/L) and 2 g (8 g/L) lime respectively); Na (5800 mg/L and 5200 mg/L at 1.5 g (6 g/L) and 2 g (8 g/L) lime respectively); B (1664 mg/L and 1262 mg/L at 1.5 g (6 g/L) or 2 g (8 g/L) lime respectively); and Ca (1254 mg/L or 1144 mg/L at 1.5 g (6 g/L) and 2 g (8 g/L) lime respectively); minor quantities of Mg (280 mg/L and 220 mg/L at 1,5 g (6 g/L) and 2 g (8 g/L) lime respectively); and Mn (11.5 mg/L and 5.8 mg/L at 1.5 g (6 g/L) and 2 g (8 g/L) lime respectively). Neutralisation of AMD pre-treated with sodium borohydride resulted in an increase in the concentration of sodium, calcium and potassium relative to the feed supernatant, with mass balance calculations indicating that approximately 63% and 86% of the total initial Ca (including the Ca added as lime and the Ca in the pre-treated supernatant) is removed in the form of precipitates during neutralisation at 1.5 g (6 g/L) and 2 g (8 g/L) lime addition respectively. The relatively high concentration of Ca in the solution could possibly be due to the formation of the calcium borate ion $[Cabe(OH)_4]+$ which is reported to form in alkaline solutions of Ca and B (Tsai & Lo, 2015). Complex formation stabilises ions in solution, retarding precipitate formation. Since the purity of lime was 95%, the excess Na and K in the solution could be due to impurities in the lime. Table 7.4 shows the neutralization results of AMD pre-treated with sodium borohydride solution.

Table 7. 4: Neutralisation of AMD pre-treated with sodium borohydride solution to pH 9.2 (6 g/L lime) and 9.8 (8 g/L lime): composition of neutralisation effluent (t=120 minutes).

Parameters	Units	Raw AMD	Treatment Supernatant	Neutralisation effluent concentration as a function of lime dosage	
				6 g/L lime	8 g/L lime
Anions					
Sulphate	mg/L	11500	10400	9600	9100
Nitrate	mg/L	2.13	ND	ND	ND
Chloride	mg/L	10.2	ND	ND	NA
Major Metals					
Fe	mg/L	4003	0.06	0.04	BDL
Ca	mg/L	495	313	1254	1144
Mg	mg/L	433	338	280	220
Al	mg/L	388	0.53	0.41	0.16
Mn	mg/L	83.2	23.6	11.5	5.76
K	mg/L	0.98	5.93	8.55	7.33
Minor metals					
Na	mg/L	48.8	5005	5805	5177
Si	mg/L	46.6	4.03	0.78	0.28
Zn	mg/L	9.47	0.00	0.01	0.00
Trace elements					
As	mg/L	0.03	0.00	0.00	0.00
B	mg/L	0.40	2194	1664	1262
Ba	mg/L	0.16	0.00	0.00	0.00
Cd	mg/L	0.01	BDL	BDL	BDL
Co	mg/L	1.07	BDL	BDL	BDL
Cr	mg/L	0.05	BDL	0.01	0.02
Cu	mg/L	0.08	BDL	0.01	BDL
Hg	mg/L	0.00	0.00	0.00	0.00
Mo	mg/L	0.00	BDL	0.02	0.00
Ni	mg/L	1.07	0.01	0.14	0.00
Pb	mg/L	0.02	BDL	BDL	BDL
Sb	mg/L	0.00	0.00	0.00	0.00
Sr	mg/L	0.64	0.37	0.53	0.47
Se	mg/L	0.00	0.00	0.00	0.00
Sn	mg/L	0.00	BDL	BDL	BDL
V	mg/L	0.04	0.00	0.00	0.00

Where ND=not determined and BDL=Below detection limit

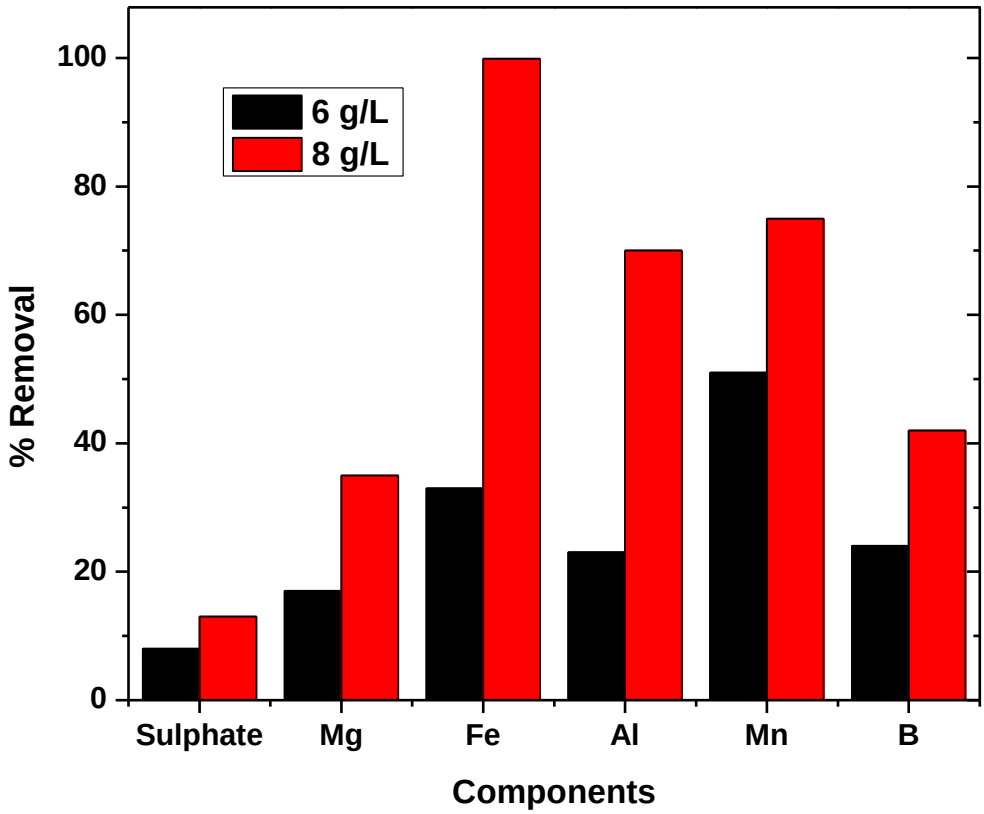

Figure 7. 5: Extent of removal of components during AMD neutralisation with lime after pre-treatment using sodium borohydride to pH 9.2 (6 g/L lime) or pH 9.8 (8 g/L lime). T= 120 minutes.

The net removal of elements from the raw AMD solution through sodium borohydride and subsequent neutralisation with lime is presented in Figure 7.5 (see discussion in section 7.3.2)

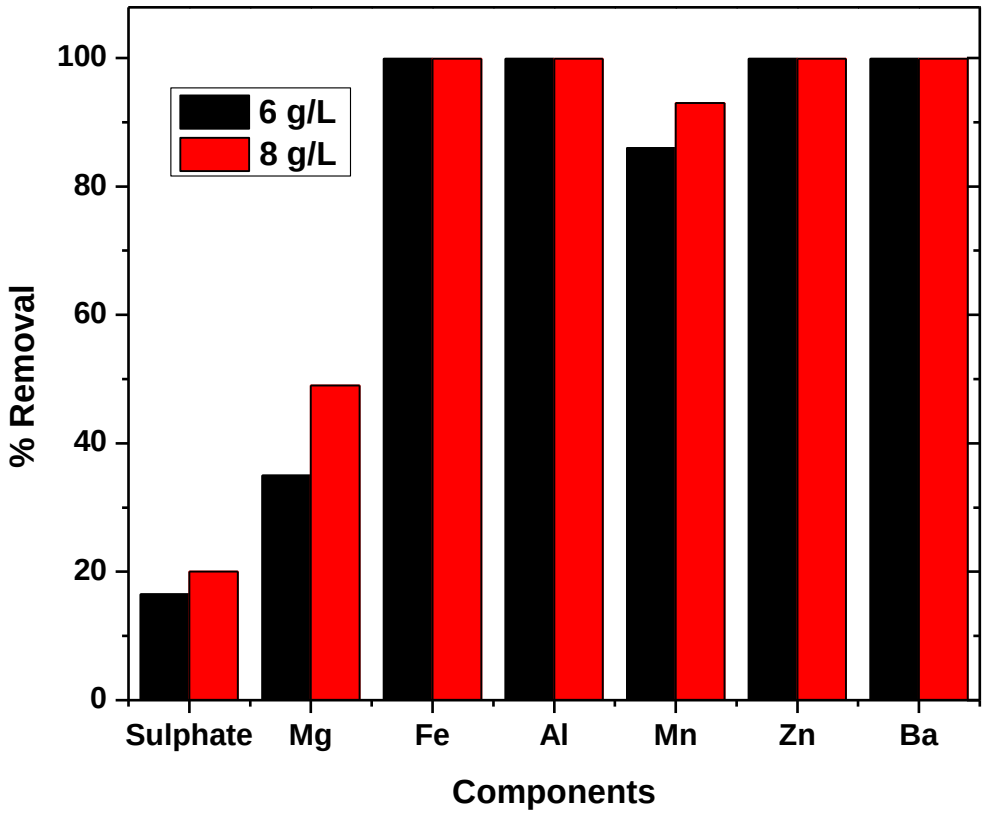

Figure 7. 6: Overall extent of removal of components after sodium borohydride pre-treatment and subsequent neutralisation of 250 mL Penstock AMD solution with lime to pH 9.2 (6 g/L lime) and pH 9.8 (8 g/L lime). T= 120 minutes.

The difference between the extent of removal of components from AMD pretreated sodium borohydride solution followed by neutralization with lime (Figure 7.7) and the overall extent of removal of components from AMD pretreated with sodium borohydride solution followed by liming (7.8) is that the extent of removal was calculated using the initial concentration of elements in the pre-treated AMD solution, and the final concentration of elements after liming the pre-treated AMD solution. However, the overall extent of removal was calculated using the initial concentration of elements in the raw AMD solution, and the final concentration of elements after the raw AMD solution was pre-treated with sodium borohydride solution, followed by neutralization with lime.

Overall, treatment of the Penstock AMD solution with sodium borohydride and lime (to pH values < 10) resulted in > 99.9 % removal of Fe, Al, and Zn, as well as significant removal of Ba (>98%) and Mn (86% or 93% at lime addition of 6 g/L or 8 g/L respectively). However, removal of Mg (35% and 49% at 1.5 g (6 g/L) and 2 g (8 g/L) lime respectively), and sulphate (8% or 13% at 1.5 g (6 g/L) or 2 g (8 g/L) lime respectively) was only partial, whilst Na, Ca, B and K concentrations in the treated solution were much higher than in the raw feed (see Table 7.4).

7.3.3. Composition of the neutralisation effluents

The neutralisation of sodium borohydride pre-treated Penstock AMD with 1.5 g (6 g/L), or 2 g (8 g/L) lime resulted in the formation of 2.2g (9 g/L) or 3.6 g (15 g/L) of total precipitate formation respectively.

Table 7. 5: Composition of residue from the lime neutralisation of 250 mL Penstock AMD pre-treated with sodium borohydride to pH 9.2 (6 g/L lime) or pH 9.8 (8 g/L lime).

	Residue concentration (%)	
	6 g/L lime (pH 9.2)	8 g/L lime (pH 9.8)
S	8.3	9.2
Ca	20.2	22.5
Fe	0.50	0.02
Al	0.31	0.00
Mn	0.31	0.29
Mg	1.20	1.40
Si	3.15	0.24
K	0.04	0.04
Na	1.01	0.76

The results in Table 5-4 indicate that the residues at both pH values are comprised mainly of calcium (20-23%) with sulphate (8-9%) and lesser amounts of Si (0.2-3%), Na (0.8-1%), Mg (1.2-1.4%) and Mn (0.3%). In contrast to the results from the lime neutralisation of raw AMD, the

residues contained relatively low quantities of sulphate, corresponding to gypsum contents of only 15-17 % and accounting for only 17-18% of the Ca content in the residues. Whilst boron is reported to form several stable calcium borate precipitates upon neutralisation with lime (Remy et al., 2005; Yilmaz et al., 2012; Tsai & Lo, 2015), the relatively high residual concentrations in the neutralisation effluent indicate that the boron concentrations in the residues would have been relatively low. It is possible that most of the calcium in the precipitate was present as the relatively insoluble calcite ($CaCO_3$), with the dissolved carbonate having been formed through the entrainment of air during rigorous agitation of the relatively small volume of supernatant used in the neutralisation experiment. Whilst the presence of this species still needs to be confirmed, mass balance calculations indicate that the residues might have contained 42% and 46% calcite in the case of 1.5 g (6 g/L) and 2 g (8 g/L) lime dosage respectively. Calcite has a lower solubility than gypsum and hence will form preferentially in the presence of carbonate ions

7.3.4 Advantages and drawbacks of AMD pre-treatment using sodium borohydride before neutralisation with lime.

To recap, 250 mL of iron-rich AMD was treated for 80 minutes with a 0.6 M sodium borohydride solution. The supernatant obtained after AMD treatment with sodium borohydride was then neutralized for 120 minutes using 1.5 or 2 g of lime. The benefit of using sodium borohydride to treat AMD was that zerovalent nano-iron particles, a value-added product, were synthesized from a waste material in a straightforward manner, reducing neutralization costs. However, the supernatant produced contained high levels of sulphate, sodium, and boron. This will have an impact on the ultrafiltration and reverse osmosis processes. According to this study, nearly half the amount of lime used to neutralize raw AMD was used to neutralize AMD pre-treated with sodium borohydride (see Table 7.1). This procedure also reduced neutralization costs. Nevertheless, the treated effluent still contained high levels of sulphate, sodium, boron, and calcium.

7.4 Lime neutralisation of Penstock AMD after nano-iron removal using green tea

The results of the neutralization tests performed on the Penstock AMD solution after pre-treatment with 0.5 g of green tea extract (in its solution form) are summarized in this section.

7.4.1 pH and redox potential profile

The effect of the dosage of lime on the pH and redox trends over time is shown in Figure 7.4. To recap, 250 mL of Penstock AMD was pre-treated with 0.5 g of green tea extract (in its solution form) to remove iron before being neutralized (limed) for 120 minutes using 1.25 g, 1.75 g, 2.25 g, and 2.25 g of lime, which corresponded to 5 g/L, 7 g/L, 9 g/L, or 11 g/L respectively.

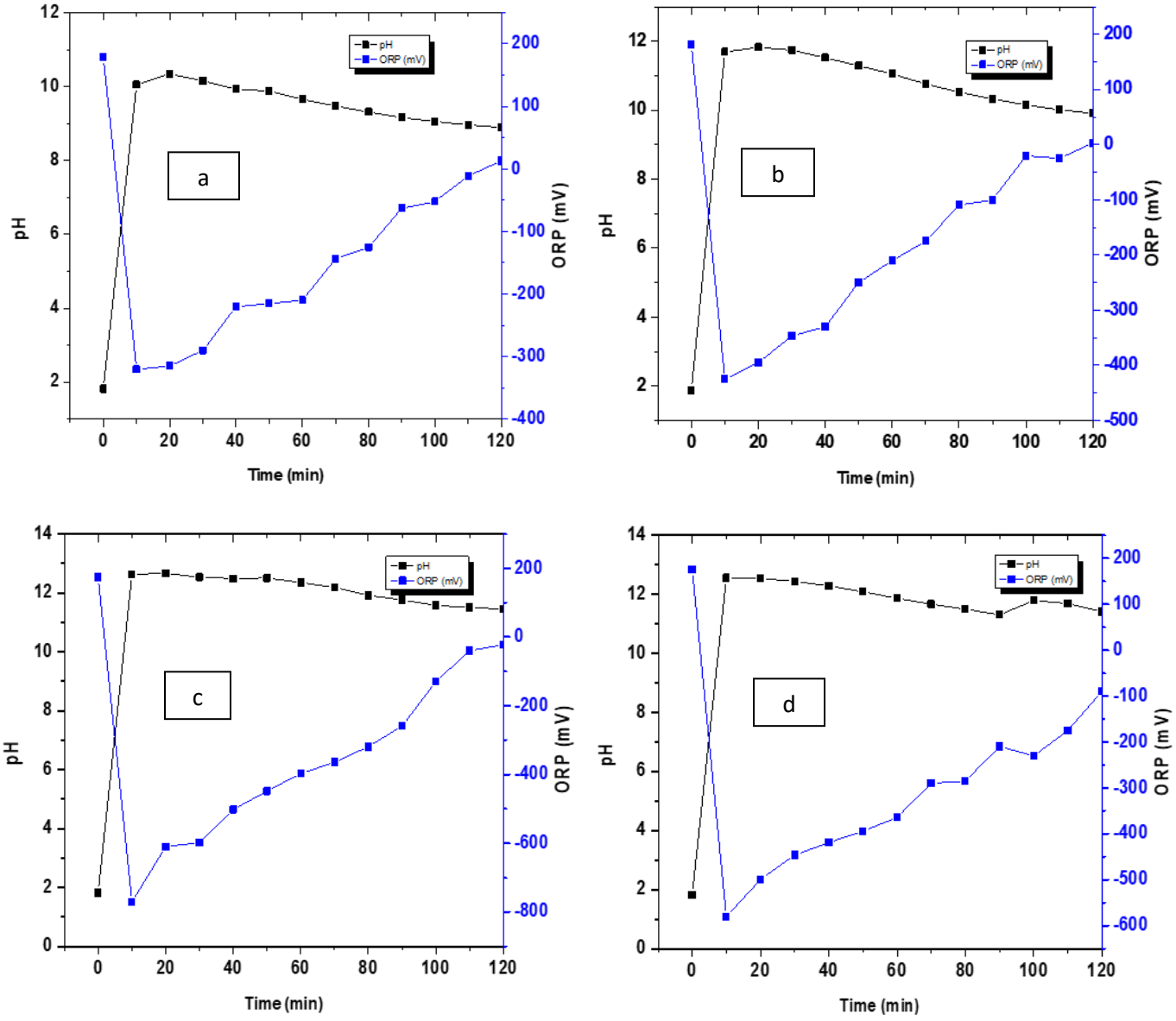

Figure 7. 7: pH and redox potential (ORP) profiles of 250 mL of AMD solution pre-treated with sodium borohydride solution to remove iron followed by neutralisation using (a) 1.25, (b) 1.75, (c) 2.25, and (d) 2.75 g of lime (that corresponds to 5 g/L, 7 g/L, 9 g/L, or 11 g/L) respectively.

The results in Figure 7.6 show that even though the pH of AMD pre-treated with green tea was more acidic (1.81) than that of the as-received AMD (2.14), the pH of the pre-treated AMD increased significantly in the first 10 minutes of liming (pH=10.1, 11.7, 12.6 or 12.6) corresponding to lime dosages of 1.25, 1.75, 2.25, or 2.75 respectively. In all cases, this was followed by a gradual decrease in pH over the subsequent 100-minute retention period. Similarly, the redox potentials of the solutions dropped rapidly from an initial value of 177 mV to -320 mV, -425 mV, -580 mV, and -770 mV at 1.25, 1.75, 2.25, and 2.75 g of lime addition to pre-treated AMD respectively, but then increased considerably over the period of 10 to 120 minutes.

7.4.2 Composition of the neutralisation effluents

Table 7.6 shows the compositions of the effluent obtained from the neutralization of 250 mL of AMD after pre-treatment with green tea extract; meanwhile the extent of removal of selected components through precipitation is presented in Figure 7.7. As a reminder, 1.25, 1.75, 2.25, and 2.75 g of lime was used for the neutralization of 250 mL of AMD pre-treated with 0.5 g of green tea extract (in solution form). Pre-treated AMD neutralization time was 120 minutes.

Table 7.6: Neutralisation of AMD pre-treated with green tea extract solution to pH 8.9 (5.0 g/L lime), pH 9.9 (7 g/L lime), pH 11.4 (9.0 g/L lime) and pH 11.5 (11 g/L lime).

				Neutralisation effluent concentrations as a function of lime dosage (mg/L)			
Parameters	**Units**	**Raw AMD**	**Supernatant**	5.0 g/L lime	7 g/L lime	9 g/L lime	11 g/L lime
pH		2.1	1.8	8.89	9.91	11.42	11.45
Electrical conductivity (EC)	mS/cm	2900					
Redox potential	mV	448	177	13	3	-90	-22
Anions							
Sulphate	mg/L	11500	7820	2914	2027	3249	3070
Nitrate	mg/L	2.13	1.4	0.20	0.76	1.50	0.24
Chloride	mg/L	10.2	11.2	16.5	16.9	16.3	16.1
Major Metals							
Fe	mg/L	4002	420	0.08	0.54	9.70	13.7
Ca	mg/L	494	178	1067	1264	1339	1288
Mg	mg/L	432	142	48.4	9.60	1.10	1.00
Al	mg/L	388	120	1.05	3.8	0.69	0.22
Mn	mg/L	83.2	13.0	0.44	0.06	0.22	1.56
Na	mg/L	48.81	19.0	29.7	32.3	29.7	31.8
Si	mg/L	46.56	10.0	0.30	0.20	0.70	1.30
Zn	mg/L	9.47	1.30	0.09	0.04	0.01	0.01
Trace elements							
As	mg/L	0.03	BDL	BDL	BDL	BDL	BDL
Be	mg/L	BDL	BDL	BDL	BDL	BDL	BDL
Cd	mg/L	0.01	BDL	BDL	BDL	BDL	BDL
Cr	mg/L	0.05	BDL	BDL	BDL	BDL	BDL
Cu	mg/L	0.08	0.05	0.01	0.02	0.02	0.03
Li	mg/L	0.03	BDL	BDL	BDL	BDL	BDL
Mo	mg/L	0.03	0.04	BDL	BDL	BDL	BDL
Ni	mg/L	1.07	0.3	0.16	0.13	0.11	0.18
P	mg/L	BDL	1.20	0.30	0.60	0.60	0.60
Pb	mg/L	0.01	BDL	BDL	BDL	BDL	BDL
Si	mg/L	46.6	10.0	0.30	0.20	0.70	1.30
Sr	mg/L	0.57	0.08	0.63	0.67	0.99	1.36
Th	mg/L	BDL	BDL	BDL	BDL	BDL	BDL
Ti	mg/L	0.01	BDL	BDL	BDL	BDL	BDL
Y	mg/L	BDL	BDL	BDL	BDL	BDL	BDL
Zr	mg/L	0.01	BDL	BDL	BDL	BDL	BDL

BDL = Below detection limit

Consistent with previous tests (see Chapter 5), treatment of the raw AMD solution with a solution of 0.5 g of green tea extract was found to result in approximately 89% Fe removal, 86% Zn removal and 84% Mn removal, along with substantial amounts of Si (78%), Al (69%), Mg (67%), Ca (64%) and Na (64%). Green tea extract removal also resulted in the removal of 32% of the soluble sulphate. The supernatant generated from pre-treatment of AMD with green tea had an acidic pH of 1.8 and still contained significant quantities of sulphate, along with major elements such as Fe (420 mg/L), Ca (178 mg/L), Mg (142 mg/L), Al (120 mg/L), and minor trace quantities of Mn (13 mg/L), Si (10 mg/L), Na (19 mg/L), P (1.2 mg/L) and Zn (1.3 mg/L). As indicated in Figure 7.7, subsequent neutralisation of the pre-treated supernatant resulted in the removal of sulphate to much lower levels than were obtained with sodium borohydride and further precipitation of Fe (>99% in all cases), Al (>99% in all cases), Zn (93% to > 99%), Mn (88% to >99%), Mg (66% to > 99%), Si (87-93%), and partial removal from the solution of sulphate (58-74%). An increase in the final pH from 8.9 (5 g/L lime) to 9.9 (7 g/L lime) resulted in an increase in the extent of removal of Mg from solution significantly (from 66% to 93%), whilst also increasing the extents of Mn and Zn precipitation from 96% and 93% respectively, to > 99%. Additional lime dosage to a pH value of 11.5 (9 g/L lime) further increased the extent of Mg removal to >99%. A lime dosage of 11 g/L, corresponding to a final pH of 11.5, resulted in a slight decrease in the extent of precipitation of some metals including Mn, Si and, to a lesser extent, Fe. This decrease can probably be attributed to the formation of stable oxyanion species at elevated pH values. The major components in the effluents treated with 7 g/L and 9 g/L lime were sulphate (2027-3249 mg/L) and Ca (1067-1264g/L), with minor amounts of Na (32-30 mg/L), and traces of Fe (0.54-9.7 mg/L), Mg (9.6-1.1 mg/L), Al (0.7-4 mg/L), Mn (0.06-0.2 mg/L), Si (<1 mg/L), Zn (<0.05 mg/L), Ni (0.1 mg/L) and Sr (0.7-1 mg/L). Neutralisation resulted in an increase in the calcium concentration relative to the feed supernatant, with mass balance calculations indicating that approximately 61% and 78% of the total initial Ca (including the Ca added as lime and the Ca in the pre-treated supernatant) was removed in the form of precipitates during neutralisation.

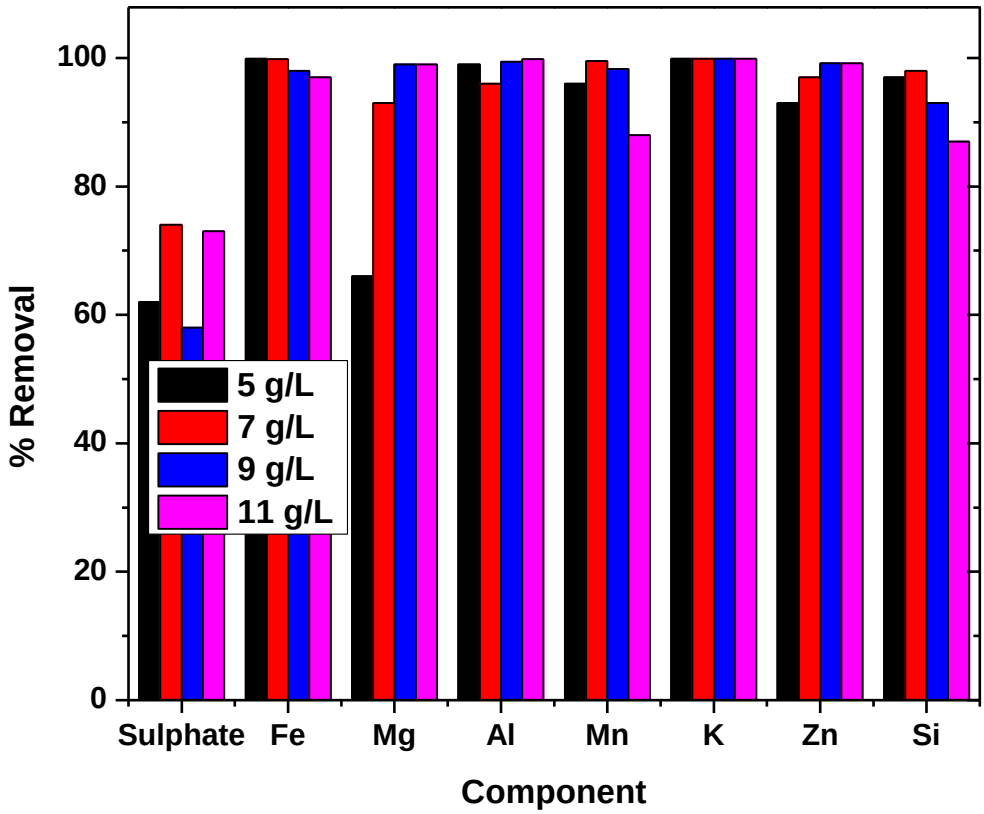

Figure 7. 8: Extent of removal of components from AMD pre-treated with a 0.5 g of green tea extract (in its solution form) followed by neutralisation of 250 mL Penstock AMD with lime to pH 8.9 (5 g/L lime), pH 9.9 (7 g/L lime), pH 11.4 (9 g/L lime) and pH 11.5 (11 g/L lime).

The liming of pre-treated Penstock AMD with green tea (to pH values > 10) results in effective removal (>99 %) of Mg, Fe, Al, Mn, K, Zn and Si. The highest removal of sulphate (74 %) was observed at pH 9.9 (5 g/L). However, removal of Mg was dependent on the pH of the neutralisation with relatively high pH values (>11) and lime dosages (9 g/L) being required to achieve > 99% Mg removal from solution (equivalent to a residual concentration of ≤ 1 mg/L).

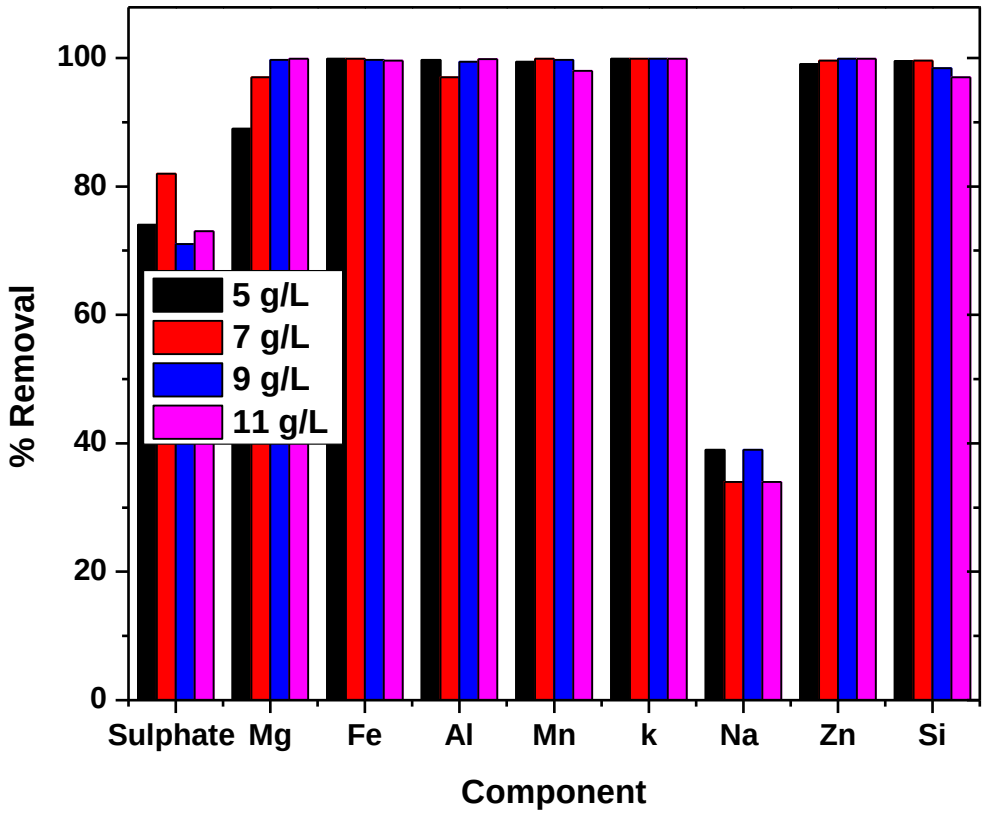

Figure 7. 9: Overall extent of removal of components from AMD pre-treated with a 0.5 g of green tea extract (in its solution form) followed by neutralisation of 250 mL Penstock AMD with lime to pH 8.9 (5 g/L lime), pH 9.9 (7 g/L lime), pH 11.4 (9 g/L lime) and pH 11.5 (11 g/L lime).

The net removal of elements from the raw Penstock AMD solution through green tea extract treatment and subsequent neutralisation with lime is presented in Figure 7.9.

As a reminder, the difference between the extent of removal of components from AMD pretreated with green tea followed by liming (Figure 7.9) and the overall extent of removal of components from AMD pretreated with green tea followed by liming (7.8) is that the extent of removal was calculated using the initial concentration of elements in the pre-treated AMD solution and the final concentration of elements after liming the pre-treated AMD solution; whereas the overall extent of removal was calculated using the initial concentration of elements in the raw AMD solution and

the final concentration of elements after the raw AMD was pre-treated with green tea followed by liming.

Overall, treatment of Penstock AMD solution with a solution of green tea extract and lime (to pH values > 10) resulted in effective removal (>99.9 %) of Mg Fe, Al, Mn, K, Zn and Si, as well as significant removal of sulphate (72-82%) and, to a lesser extent, Na (42-44%). However, removal of Mg was dependent on the pH of the neutralisation with relatively high pH values (>11) and lime dosages (9 g/L) being required to achieve > 99% Mg removal from solution (equivalent to a residual concentration of ≤ 1 mg/L). As a reminder, when 0.6 M sodium borohydride solution was used to pre-treat 250 mL field Penstock AMD solution prior to lime neutralization using 1.5 g (6 g/L) or 2 g (8 g/L) of lime, a large amount of Na (5805 mg/L or 5177 mg/L) and B (1664 mg/L or 1262 mg/L) was left in solution and small amount of sulphate was removed. In line with this investigation, when 0.5 g of powdered green tea extract in its solution form was used to pre-treat AMD prior to lime neutralization, effective removal of sulphate and K was observed.

7.4.3 Composition of the neutralisation residues

The neutralisation of the green tea pre-treated Penstock AMD with 1.25 g (5 g/L), 1.75 g (7 g/L), 2,25 g (9 g/L) and 2.75 g (11 g/L) lime resulted in the formation of 3.1 g (6.4 g/L), 3.8 g (15 g/L), 4.7 g (18 g/L) and 5.6 (22 g/L) of total precipitate formation respectively, approximately 21-31% of that obtained from raw AMD. The compositions of the neutralization residues obtained are presented in Table 7.7. In the same line of investigation, more precipitate was formed when AMD pre-treated with green tea was neutralized using different dosages of lime than when sodium borohydride pre-treated AMD was neutralized using different dosages of lime. Overall, precipitates formed when raw AMD was neutralized with lime were significantly higher than precipitates formed when raw AMD was pre-treated with green tea or sodium borohydride prior to neutralization with lime. This could be due to the fact that raw AMD contains high levels of sulphate, iron and other major and minor elements, which co-precipitate with the gypsum sludge during the lime neutralization process, increasing the mass of sludge generated. On the other hand, AMD pre-treated with sodium borohydride or green tea removed sulphate, iron and other major and minor elements from the AMD solution, reducing the mass of precipitate generated during the lime neutralization process (see section 7.2.2, 7.3.3, and 7.4.3).

Table 7. 6: Composition of residue from the neutralisation of green tea pre-treated Penstock AMD using 5 g/L, 7 g/L, 9 g/L or 11 g/L for 120 minutes

Component	Residue concentration (%)			
	5 g/L lime	7 /L lime	9 g/L lime	11 g/L lime
S	25.6	24.5	22.2	19.5
Ca	21.4	22.9	25.9	29.1
Fe	2.78	3.00	2.75	2.60
Al	1.11	0.76	0.98	0.80
Mn	0.11	0.12	0.32	0.36
Mg	0.30	1.60	1.42	1.29
Si	0.11	0.10	0.14	0.15
K	0.02	0.01	<0.01	0.02
Na	0.12	0.03	0.13	0.15

The results in Table 7.6 indicate that the residues at all pH values are comprised predominantly of sulphate (19-26 %) and calcium (21-29 %), with lesser amounts of Fe (2.6-3.0 %), Al (0.8-1.1 %), Mg (0.3-1.3 %) and traces of Si (0.1-0.15 %), Mn (0.1-0.4 %) and Na (0.1-0.2 %). The sulphate content decreased (from 26 % to 20 %) and the calcium concentrations increased (from 21 % to 29 %) on increasing the lime dosage from 5 g/L to 11 g/L. Parity calculations based on the sulphate contents indicates a gypsum content of 44-46 %, 40-44 %, 34-40 % and 28-34 % at lime additions of 5 g/L, 7 g/L, 9 g/L and 11 g/L respectively, depending on whether Al was present as aluminium hydroxide or ettringite. Calculations indicate furthermore that gypsum formation only accounted for only 47%, 40%, 32% and 23% of the Ca in the residue at lime dosages of 5 g/L, 7 g/L, 9 g/L and 11 g/L respectively. As in the case of the residues from the neutralisation of solutions pre-treated with sodium borohydride, it is possible that the remaining Ca was present in the form of calcite ($CaCO_3$) formed through the entrainment of CO_2, with calculations showing possible calcite concentrations of 27-28 %, 32-34 %, 41-44 %, and 52-56 % at lime dosages of 5 g/L, 7 g/L, 9 g/L and 11 g/L respectively. The increase in gypsum content and decrease in calcite content as the lime dosage increased from 5 g/L to 11 g/L is consistent with the sulphate and calcium content trends. Iron contents were consistent with ferric hydroxide contents of between 4.9 and 5.3 % in all cases. Solid Al compounds amounted to 2.4 % to 5.7 %, depending on whether

these existed as aluminium hydroxide ($Al(OH)_3$) or ettringite ($Ca_6Al_2(SO_4)_3(OH)_{12}•26H_2O$). (and amorphous SiO_2 (0.4-0.5 %).

As a reminder, 250 mL of iron-rich AMD was treated for 80 minutes with a 0.5 g sodium borohydride solution. The supernatant obtained after AMD treatment with green tea extract was then neutralized for 120 minutes using 1.25 g, 1.75 g, 2.25 g, or 2.75 g of lime. The benefit of using green tea extract to treat AMD was that nano-iron particles, a value-added product, were synthesized from a waste material reducing neutralization costs. However, the supernatant produced contained an increased concentration of K. This will have an impact on the ultrafiltration and reverse osmosis processes. According to this study, nearly half the amount of lime used to neutralize raw AMD was used to neutralize AMD pre-treated with green tea extract (see Table 7.7). This procedure also reduced neutralization costs.

7.5 Summary

A comparison of lime dosage (Table 7.8) indicates that the pre-removal of iron through treatment with the AMD solutions reduced the amount of lime required to achieve any specific pH value.

Table 7. 7: pH as a function of lime addition during the neutralisation of AMD samples before and after pre-treatment to recover nano-iron

Lime Addition (g/L)	pH
Raw AMD	
11	9.1
12	11.2
AMD pre-treated with NaBH4	
6	9.2
8	9.8
AMD pre-treated with green tea extract	
5	8.9
7	9.9
9	11.4
11	11.5

In all cases, neutralisation to pH values > 9 resulted in effective removal (> 99%) of Fe, Al, Mn, Ba, and Zn. Although Mg removal at pH values < 11 was only partial (≤ 50%), this increased to > 99% at pH values > 11. However, whilst between 72% and 85% precipitation of sulphate occurred during neutralisation of the raw AMD and AMD pre-treated with green tea extract, neutralisation of the AMD solution after $NaBH_4$ treatment resulted in only 7-13% sulphate precipitation. The effluent from the neutralisation of AMD pre-treated with $NaBH_4$ not only still contained elevated levels of sulphate, but also high levels of residual sodium and boron which might adversely affect the subsequent ultrafiltration and reverse osmosis treatment processes (Figure 7.9).

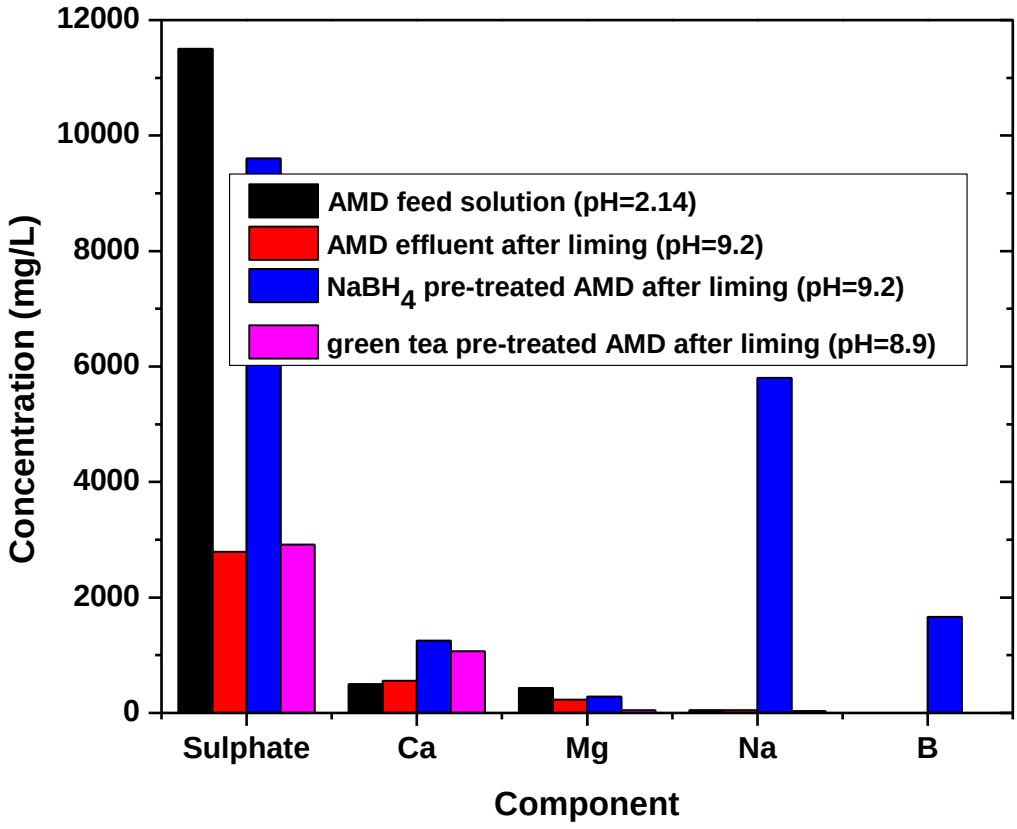

Figure 7. 10: Comparison of the concentrations of key components in the AMD feed and neutralisation effluents with pH values of 8.9-9.2 (T= 120 minutes).

In Figure 7.10, key components such as sulphate, Ca, Mg, Na, or B, in the solution of AMD feed, AMD feed after liming, NaBH4 pretreated AMD after liming, or green tea pretreated AMD after

liming are compared. It was observed that the neutralization of green tea pre-treated AMD solution using lime was more effective in the reduction of sulphate compared to the neutralization of sodium borohydride pre-treated AMD with lime. This could be attributed to the fact that during the neutralization of pre-treated green tea AMD solution, the mechanism that allows gypsum ($CaSO_4.2H_2O$) formation was favoured over the formation of carbonate in solution to produce calcite ($CaCO_3$), lowering the concentration of sulphate in solution. In terms of Ca concentration, it was noted that pre-treated AMD solutions after neutralization had a higher Ca concentration than feed AMD or feed AMD after neutralization. The increase in Ca concentration in all cases was caused by Ca being released from lime during neutralization. The high concentrations of Na and B observed in the sodium borohydride ($NaBH_4$) pre-treated AMD solution was caused by the release of Na and B from sodium borohydride (NaBH4) reductant after iron precipitation in the solution. The concentration of key components in the residues derived from the neutralization of raw AMD and AMD pre-treated (with sodium borohydride and green tea) solutions is shown in Table 7.8.

Table 7. 8: Concentrations of key components in the residues derived from the neutralisation of AMD solution P before and after pre-treatment (t = 120 minutes)

Component	Content in the neutralisation residue as a function of final pH (%)						
	Raw AMD		AMD treated with $NaBH_4$		AMD treated with green tea extract		
	pH 9.1	pH 11.2	pH 9.2	pH 9.8	pH 8.9	pH 9.9	pH 11.4
Fe	12.5	11.2	0.5	0.02	2.8	3.0	2.8
Ca	16.3	17.1	20.2	22.5	21.4	22.9	25.9
Sulphate	37.9	37.7	8.3	9.2	25.6	24.5	22.2
Gypsum[1]	67.9	67.5	14.9	16.5	45.8	44.0	39.8
Calcite[1]	1.4	3.7	42.0	46.6	26.7	31.8	41.7

1. Calculated on the assumption that all sulphate is present as gypsum ($CaSO_4.2H_2O$), and the remaining calcium is present as calcite ($CaCO_3$)

A comparison of the contents of the key components in the neutralisation residues derived from the Penstock AMD, both before and after pre-treatment is shown in Table 7.9. Whilst the pre-treatment of the AMD results in a considerable decrease in the Fe content of the neutralisation residues, pre-treatment did not give rise to residues with higher gypsum content, as reflected by the lower sulphate contents. This could possibly be attributed to the preferential formation of

calcite due to carbonate formation as a result of CO_2 entrainment during the laboratory-scale neutralisation tests. Mass balance calculations show that the calcite content increases as the lime dosage (and hence the final pH) increase for any given feed solution, with calcite formation being more prevalent during the neutralisation of AMD solutions pre-treated with sodium borohydride. The factors influencing CO_2 entrainment and/or carbonate formation could include chemical factors such as alkalinity as well as physical factors such as agitation speed and/or volume of solution. The effect of these factors would require further investigation.

CHAPTER 8

APPLICATION OF AMD-BASED NANO-IRON PARTICLES

8.0 Introduction

This chapter discusses the treatment of simulated methylene solution using SBNI 0.6 or GTNI 0.5 iron nanoparticles synthesised from AMD.

8.1 Catalytic testing of nano-iron particles synthesized from AMD.

The degradation of organic dye from textile wastewater has been tested using conventionally synthesized nano-iron particles from reagent grade iron salt (Badmus et al., 2018b). Several studies have been published on the use of various nanoparticles, optimal pH, catalyst mass, and contact time for this process (Abdelfatah et al., 2021; Darezereshki et al., 2022). In this study, nano-iron particles synthesized from an iron-rich AMD solution were tested for methylene blue decolorization. The main aim of this test work was to determine if the nano-iron particles synthesized from AMD were active. The AMD catalysts used in the catalytic testing process were assigned code names such as SBNI 0.6 and GTNI 0.5. SBNI 0.6 represents nano-iron particles synthesized from AMD using sodium borohydride under optimal experimental conditions, whereas GTNI 0.5 represents nano-iron particles synthesized from AMD using green tea extract under optimal experimental conditions. Further optimization is required for this process.

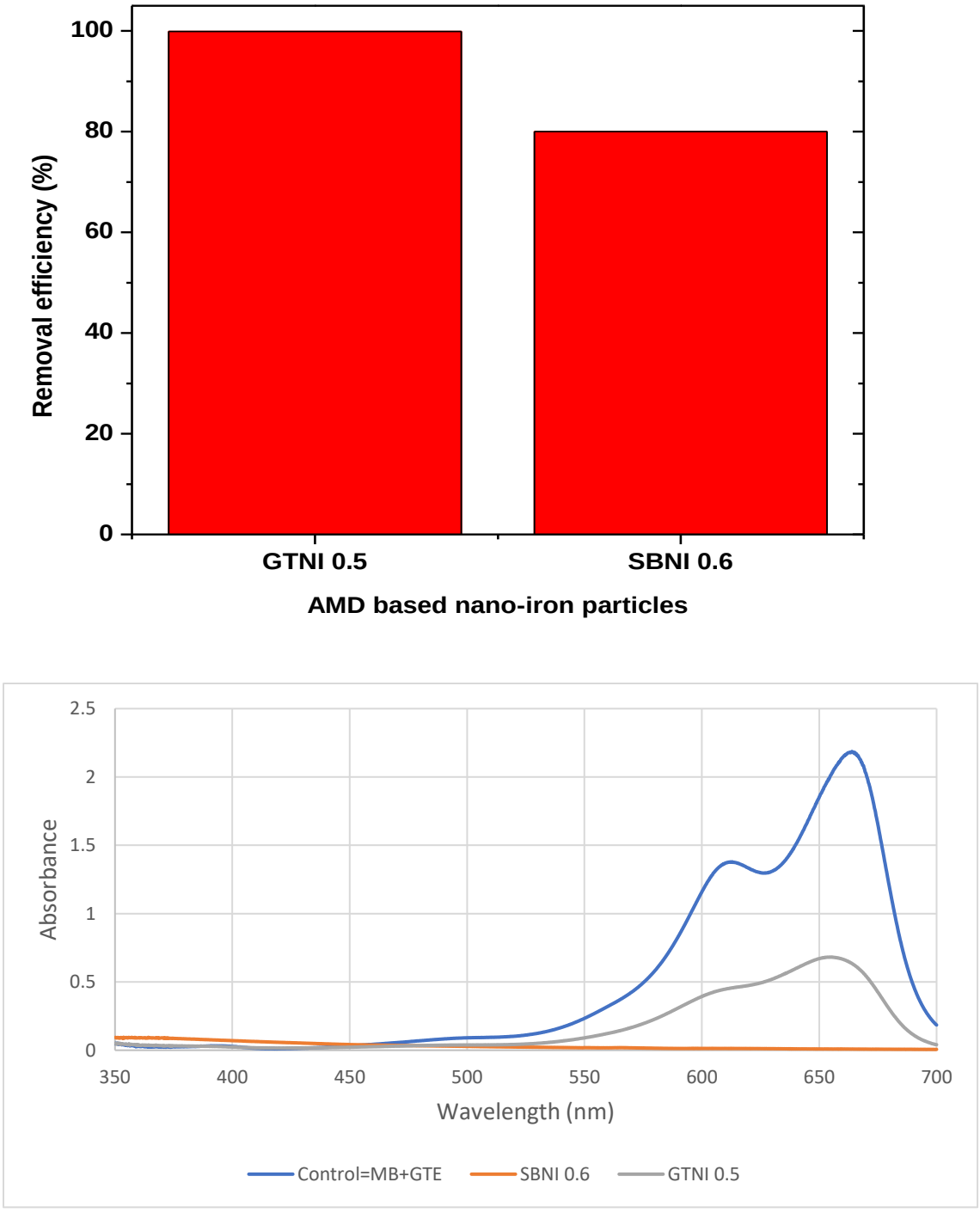

Figure 8. 1: Catalytic activity of GTNI 0.5 or SBNI 0.6 in the treatment of methylene blue . Experimental condition: volume of methylene blue (10 ppm)=100 mL, pH=5 mg, mass of catalyst (SBTNI 0.6 or GTNI =0.5 mg)=5 mg, contact time=120 minutes. MB=methylene blue, GTE=green

tea extract, SBNI=sodium borohydride synthesized nano-iron particles, GTNI=green tea synthesized nano-iron particles.

Figure 8.1 shows that SBNI 0.6 performed efficiently, with 99.9% removal efficiency of methylene blue (10 ppm, 100 mL) from methylene blue contaminated water after 120 minutes, followed by 80% removal efficiency with GTNI 0.5. The green tea extract used to synthesize GTNI 0.5 nano-iron particles from AMD acted as a surface modifier, thus enhancing air stability, and preventing particle agglomeration. However, its removal efficiency of methylene blue in the contaminated solution was lower (80%) compared to SBNI 0.6 (99.9%). This is due to polyphenolic substances coating the active sites of GTNI 0.5 during its synthesis. However, this section (8.1) proves that the AMD based nano-iron catalysts (SBNI 0.6 and GTNI 0.5) were active in the removal of methylene blue from a contaminated solution.

CHAPTER 9

CONCLUSIONS AND RECOMMENDATIONS

9.0 Introduction

The discussions, key findings, and conclusions from the previous chapters are presented in this chapter. This chapter also outlines the recommendations and possible future work of this study. This chapter is broken down into ten sections. Section 9.1 provides an overview of the research. Section 9.2 discusses analysis of feedstock materials. Section 9.3 discusses the extraction and characterization of nano-iron from AMD. Section 9.4 discusses the use of a chemical reductant (sodium borohydride) in the synthesis of nano iron particles and the treatment of AMD. Section 9.5 describes the use of green tea extract as an environmentally friendly reductant in the synthesis of nano-iron particles and the treatment of AMD. Section 9.6 discusses the characterisation techniques used to analysed the synthesised nano-iron particles and their corresponding supernatants. Section 9.7 discusses the neutralisation and characterisation of treated effluents and solid product. Section 9.8 discusses the novelty of the research findings. Section 9.9 discusses concluding remarks of the research findings. Section 9.10 discusses recommendation for future work.

9.1 Overall review

The research aims and objectives provide detailed information about the raw materials used and the finished products derived from waste materials. The feedstock materials used in this study (AMD and pre-treated AMD) were deemed not to be environmentally friendly. The raw materials were analyzed (using ICP and ICP-OES) to determine their quality and the potential environmental impact or benefits. AMD was used as a source of ferric iron salt reagent, which was used to synthesize nano-iron particles. Reductants such as sodium borohydride and green tea extract were used to treat the AMD samples in order to remove dissolved metals in the mine water. The iron in the AMD solution was successfully converted to nano-iron particles during the cleaning process with the reductants (sodium borohydride and green tea extract). The nano-iron particles were analyzed using x-ray diffraction (XRD), scanning electron microscopy-energy dispersion spectroscopy (SEM-EDS), as well as Image J particle size analysis. The characterized AMD-based nano-iron particles were applicable for the degradation of methylene blue in solution.

The supernatant (pre-treated AMD) generated as a result of extracting iron from the AMD solution was characterized using ion chromatography (IC) and inductively coupled plasma-optical emission spectroscopy (ICP-OES) prior to neutralization using lime. Neutralized pre-treated AMD solutions (neutralization effluents) were characterized using IC and ICP-OES. The results of all the feedstock materials, synthesis, and treatments were used to make a conclusive statement about this study.

9.2 Analysis of feedstock materials (raw materials)

The pH, EC, TDS, DO, IC, and ICP-OES were used to characterize the as-received AMD samples collected from the Navigation coal mining sites. This revealed that the quality of the AMD samples was poor as they did not meet the qualifications for potable water. It also revealed that the major cations and anions found in the AMD solution were Fe, Al, Ca, Mn, Mg, and sulphate respectively. The AMD solutions were unsuitable for industrial, agricultural, or mining processes, among other things. However, the Navigation Penstock AMD sample was selected for the production of nano-iron particles using reductants because of its availability, richness in iron (III) ions, and for economic reasons. After iron removal from AMD, the pH, ICP, and ICP-OES analytical techniques were used to characterize the pre-treated AMD solutions. The AMD pre-treated solutions using reductants (sodium borohydride and green tea extract) were used as feedstock for lime neutralization. The generated neutralization effluents were characterized using IC, and ICP-OES, while their corresponding solid products were analyzed using XRF.

9.3 Incorporation of nano-iron extraction into the AMD treatment circuit

Two different classes of reductants were used to treat AMD, which is a chemical reductant (sodium borohydride) and an environmentally friendly reductant (green tea extract). Sodium borohydride or green tea extract was successful in removing soluble metal ions from the AMD sample. Sodium borohydride was more effective in the removal of metal ions such as Fe, Al, Zn, and Mn from the AMD sample. This could be attributed to the fact that sodium borohydride had higher FRAP and DPPH values (see tables 4.17 and 4.18), thus making it more reactive. However, even though green tea extract had a FRAP and DPPH value almost 4 times less than sodium borohydride, it could remove more Mg and Ca from the AMD sample. This could be because temperature had more influence on the reduction mechanism of these metals than their

corresponding FRAP and DPPH values. Sodium borohydride was able to remove over 99% of the target element (Fe), Al, and Zn as opposed to 89% of Fe removed using green tea as a reductant. During the treatment of AMD solution using sodium borohydride or green tea extract, the colour of the AMD solution changed from yellow to colourless or yellowish green respectively. The treated mine water failed to reach the target for potable water according to World Health Organization guidelines. However, these treated samples could be used for mining, irrigation, and construction.

9.4 Sodium borohydride as a chemical reductant

At a sodium borohydride dosage of 22 g/L, the treatment of AMD using sodium borohydride resulted in the successful removal of iron (99.9% removal in 80 minutes). Other metals effectively removed (>99%) included Al, Zn, Ba, Ni, and Co, together with partial removal of Mn (56-83%), Ca (37%), and Mg (22%). The resulting products were iron-pure (70-80%), with minor amounts of Al (5-7%) and Ca (1.1-1.3%), as well as traces of Mg, Na, Si, and S. The particle size distribution of the nano-iron product was mostly within the desired range of 100 nm, though agglomeration aided the formation of clusters, thereby increasing particle size in some circumstances. The morphology of the synthesized nanoparticles that were described in this study as having a chainlike structure was consistent with nano-iron from reagent-grade iron salt in the literature. Also, aligning with the literature, nano-iron particles synthesized from sodium borohydride are highly unstable and oxidize quickly when exposed to air. Despite being depleted in Fe, aluminum, and other metals, the AMD solution treated with sodium borohydride contained significantly more B (up to 2.2 g/L) and Na (1–5 g/L), as well as a higher pH (5-9) value than the raw AMD. Contrary to predictions, the neutralization of the sodium borohydride pre-treated AMD solution to pH values of 9.2–9.8 did not remove a significant amount of sulphate (about 15%), which led to high sulphate as well as elevated levels of Na and B compared to untreated AMD. Most likely, the low levels of gypsum product formation during lime neutralization were caused by CO_2 attenuation and dissolving in the NaOH-containing supernatant solutions. This made calcite form more than gypsum.

9.5 Green tea extract as an environmentally friendly reductant

The removal of Fe from AMD using polyphenols (green tea extract) was discovered to be dependent on the extract dosage, temperature, and retention time. The optimum recovery of Fe occurred when a dosage of green tea extract, 0.5 g/L of AMD, a retention time of 12 hours, and a temperature of 30 were applied. The removal of Fe from AMD using green tea was not as effective compared to sodium borohydride, yielding a maximum Fe extraction of 89%. This was consistent with its lower antioxidant activity. Other elements that co-precipitated during AMD treatment with green tea extract included Al (69%), Mg (61%), Ca (65%), Na (40%), Mn (84%), Zn (90%), Co (73%), and sulphate (39%). The synthesized nano-iron product from AMD was characterized as being amorphous and coated with a polyphenolic compound. This was consistent with the high stability of the nano-iron product under air. The iron content of the synthesized green tea nano-iron product was significantly lower (9–38 weight%) than that of sodium borohydride due to its high organic content. The particles of the nano-iron product had an average particle size that was between 31 and 57 nm, which was smaller than the nano-iron particles gotten from sodium borohydride, indicating that polyphenol complexation prevents particle agglomeration. Even though the green tea treated AMD solutions contained less sulphate and more metals than the as-received raw AMD feedstock, the concentrations of P, K, and to a certain degree Se, were higher as a result of the elements present in the green tea extract. In addition, the treated AMD solution had a slightly lower pH (1.8 vs. 2.1), making it more acidic compared to the as-received AMD solution.

9.6 Characterization techniques used to analyze the synthesized nano-iron particles and their corresponding supernatants

The synthesized nano-iron particles from AMD were characterized using XRD, SEM-EDS, STEM, FTIR, or Image J particle size measurement in order to measure the quality of the nano-iron particles. This revealed that the quality of the nano-iron particles was comparable with quality synthesized nano-iron particles cited in literature. The XRD analytical technique was used to reveal the mineralogy of the synthesized nano-iron particles by showing broad peaks of FeO and pure Fe on the XRD spectra. The SEM analytical technique was used to disclose the morphology, size and distribution of the AMD based nano-iron particles. The SEM-EDS revealed that the major metals and non-metals that co-precipitated with the nano-iron particles synthesized with sodium

borohydride were Al, S, Si, Ca, Na, Mn, and Mg; whereas in the case of nano-iron particles synthesized from AMD using green tea, the major metal and non-metals that co-precipitated with Fe were Al, Si, and S. It worth noticing that the SEM-EDS analytical technique is not an accurate method that is normally used to measure elemental composition on solid samples as only spots on the sample are measured for elemental composition. The STEM analytical technique was used to obtain a clearer morphology so that the Image J particle size measurement tool could be used to obtain the average particle size of the nano-sized particles. Finally, the structural vibrations of the nano-iron particles were revealed using the FTIR analytical technique.

The supernatant generated as a result of removing iron from solution using reductants was characterized using IC and ICP-MS to obtain the elemental composition of the pre-treated AMD solution. IC was used to measure the concentration of non-metals such as sulphate, nitrate, and chloride whereas ICP-MS was used to identify and measure the concentration of major, minor and trace metals such as Fe, Al, Ca, Mg, Si, Mn, or Zn, etc., thus revealing the quality of the pretreated solution prior to lime neutralization.

9.7 Neutralization and characterization of treated effluents and solid products

This study used AMD pre-treated with sodium borohydride or green tea extract (to remove iron from solution) for its neutralization test work using lime. The pre-treated AMD and treated effluents were characterized using pH, redox potential (ORP), IC (inductive coupled plasma), and inductively coupled plasma-optical mass spectroscopy (ICP-MS). Their corresponding solid residues were characterized using XRF analytical technique. These analytical techniques were performed to assess the quality of AMD and treated effluents. The maximum pH of AMD pre-treated with sodium borohydride prior to lime neutralization were pH 9.5 and 9.8 at lime addition of 1.5 g (6 g/L) and 2 g (8 g/L) respectively whereas the pH of AMD pre-treated with green tea extract prior to lime neutralization was achieved at pH 8.9 and 9.9 at lime addition of 1.25 (5 g/L) and 1.75 (7 g/L). The mass of lime used for direct neutralization of AMD to achieve pH values (9.1 or 11.2) was almost twice the amount of lime used to achieve the same pH when the AMD was pre-treated with sodium borohydride or green tea extract. The pre-treatment of AMD prior to lime neutralization significantly lowered the amount of lime used for the process. The treated effluents of raw and pretreated AMD contained low concentrations of metals except for Ca, Na, or B, whose concentration increased after neutralization. The corresponding solid residue of pre-treated AMD after lime neutralization was made up of calcite and gypsum. The solid residue of

AMD pretreated with sodium borohydride prior to neutralization contained calcite (42% or 46%) and gypsum (14.9% or 16.5%) at pH (9.2 or 9.8) and lime addition of 1.5 g (6 g/L) or 2 g (8 g/L), whereas the solid residue after neutralization of AMD pretreated with green tea extract contained calcite (26.7% or 31.8%) and gypsum (45.8% or 44.0%) at pH (9.2 or 9.8) and lime addition of 1.25 (5 g/L) or 1.75 (7 g/L). However, direct neutralization of AMD produced high gypsum sludge that contained calcite (1.4 or 3.4%), and gypsum (67.9 or 67.5%)) at pH (9.1 or 11.2) and lime addition of 5.5 (11 g/L) and 6 (12 g/L).

9.8 Novelty of the research findings

Several studies have reported the synthesis of nano-iron particles from reagent-grade iron salts (such as $FeCl_2$, $FeSO_4$, or $FeNO_3)_3$, etc.), using sodium borohydride or environmentally friendly reductants such as plant extracts. One study shifted from using reagent-grade iron salts in the synthesis of nano-iron particles and reported the use of AMD (a waste material) as a source of ferric or ferrous ions in the synthesis of nano-iron particles using sodium borohydride. The use of sodium borohydride (a chemical reductant) in the synthesis of nano-iron particles from either reagent-grade iron salts or AMD is not environmentally friendly. Based on previous research that reported the synthesis of iron nanoparticles, this study developed two novel approaches to extracting value from AMD, a waste material that pollutes or harms the environment. These approaches include:

- A novel approach was used to synthesize quality nano-iron particles from AMD using an environmentally friendly reductant such as green tea extract. The quality of these nano-iron particles were compared with the quality of nano-iron particles synthesized from AMD using sodium borohydride.

- A novel approach to synthesizing nano-iron particles from AMD using an environmentally friendly reductant (green tea extract) and a chemical reductant (sodium borohydride) prior to lime neutralization of their corresponding supernatant was conducted. This method not only cut down on the cost of treating AMD but also improved the quality of the mine water, making it suitable for discharge. Even though the sludge obtained when pre-treated AMD was neutralized contain a low amount of gypsum, it could be used to improve soil fertility.

In summary, a value-added product was synthesized from AMD, and the amount of lime used to neutralize the pre-treated AMD was cut down to almost half compared to the lime used to neutralize raw AMD. Furthermore, the generated sludge could be used for agricultural purposes.

9.9 Concluding remarks

While this research revealed the technical feasibility of obtaining nano-iron from raw AMD, the use of a chemical reductant (sodium borohydride) is likely to be costly and results in effluents with high levels of sodium and boron, which may have a negative effect on the downstream neutralization of lime and the reverse osmosis processes. The approach of green reductants, such as green tea extract, appears to be more cost-effective and effective, producing relatively stable nano-iron particles as well as producing a purer gypsum product during successive neutralization. However, the residual presence of polyphenols in the feed and its negative effects on the process of reverse osmosis, together with the effectiveness of the nano-iron product for downstream water treatment, requires further investigation. Furthermore, the green tea extract used in this study was not as successful as the chemical reductant, sodium borohydride, in removing iron and other metals. Because green tea extracts do not completely remove metals such as iron and aluminum, the subsequent neutralization residue is unlikely to be pure enough for the production of high-value products like gypsum board. Nonetheless, the improved purity may make the sludge suitable for construction purposes (e.g., cement brick or cement production) or as feedstock to the Gyp-SLiM or related process for the production of higher-value magnesite, limestone, and sulphur. The applications, together with present uncertainties and knowledge gaps, will necessitate a more comprehensive feasibility study on the different ways to recover valuable products from AMD.

9.10 Recommendations

The following recommendations are made based on the outcomes and results of this study

- More scientific testing should be done to examine the feasibility of utilizing polyphenolic plant extracts to produce iron nanoparticles from AMD. This should involve the distribution and stability of polyphenols in pre-treated AMD, the availability of substitute, and

potentially more effective green reductants, locally. The feasibility of using iron nanoparticles for the treatment of downstream water, and the properties of the resulting neutralization residue.should be further investigated.

REFERENCES

Abdelfatah, A.M., Fawzy, M., Eltaweil, A.S. & El-Khouly, M.E. 2021. Green Synthesis of Nano-Zero-Valent Iron Using Ricinus Communis Seeds Extract: Characterization and Application in the Treatment of Methylene Blue-Polluted Water. ACS Omega, 6(39): 25397–25411.

Adeleye, A.S., Conway, J.R., Garner, K., Huang, Y., Su, Y. & Keller, A.A. 2016. Engineered nanomaterials for water treatment and remediation: Costs, benefits, and applicability. Chemical Engineering Journal, 286: 640–662.

Adriano, D.C., Page, A.L., Elseewi, A.A., Chang, A.C. & Straughan, I. 1980. Utilization and Disposal of Fly Ash and Other Coal Residues in Terrestrial Ecosystems: A Review. Journal of Environmental Quality, 9(3): 333–344.

Afsheen, S., Tahir, M.B., Iqbal, T., Liaqat, A. & Abrar, M. 2018. Green synthesis and characterization of novel iron particles by using different extracts. Journal of Alloys and Compounds, 732: 935–944.

Akcil, A. & Koldas, S. 2006. Acid Mine Drainage (AMD): causes, treatment and case studies. Journal of cleaner production, 14(12–13): 1139–1145.

Akinwekomi, V., Maree, J.P., Zvinowanda, C. & Masindi, V. 2017. Synthesis of magnetite from iron-rich mine water using sodium carbonate. Journal of Environmental Chemical Engineering, 5(3): 2699–2707.

Alegbe, M.J., Ayanda, O.S., Ndungu, P., Fatoba, O.O., Nechaev, A. & Petrik, L.F. 2018. Assessment of the physical and chemical qualities of brine and the application of nano zerovalent iron for the treatment of brine effluent.

Alegbe, M.J., Ayanda, O.S., Ndungu, P., Nechaev, A., Fatoba, O.O. & Petrik, L.F. 2019. Physicochemical characteristics of acid mine drainage, simultaneous remediation and use as feedstock for value added products. Journal of Environmental Chemical Engineering, 7(3): 103097.

Alexander, W. v & Ristow, N. 2010. Ambient Temperature Ferrite Process: Adapting the laboratory-scale process to treat acid mine drainage Report to the Water Research Commission.

Ali, A., Moghal, B. & Sivapullaiah, P. v. 2011. Role of Gypsum in the Strength Development of Fly Ashes with Lime. Journal of material in civil engineering, 23(2): 197–206.

de Almeida Silva, R., Jean, ·, Salomé, C., Menezes, S., Fabrício, ·, Lopes, A., Ana, ·, Kirchheim, P., Andre, I. & Schneider, H. 2017. Synthesis of a Goethite Pigment by Selective Precipitation of Iron from Acidic Coal Mine Drainage. Mine Water and the Environment, 36: 386–392.

de Almeida Silva, R., Secco, M.P., Lermen, R.T., Schneider, I.A.H., Hidalgo, G.E.N. & Sampaio, C.H. 2019. Optimizing the selective precipitation of iron to produce yellow pigment from acid mine drainage. Minerals Engineering, 135: 111–117.

Amaral Filho, J.R., Firpo, B.A., Broadhurst, J.L. & Harrison, S.T.L. 2020. On the feasibility of South African coal waste for production of 'FabSoil', a Technosol. Minerals Engineering, 146: 106059.

Annandale, J.G., Beletse, Y.G., Stirzaker, R.J., Bristow, K.L. & Aken, M.E. 2009. Is irrigation with coal-mine water sustainable? In International Mine Water Conference. 337–342.

Ashokkumar, R. & Ramaswamy, M. 2014. Phytochemical screening by FTIR spectroscopic analysis of leaf extracts of selected Indian medicinal plants. International journal of Current Microbiology and applied Sciences, 3(1): 395–406.

Ashraf, W. & Mian, A.A. 2008. Levels of selected heavy metals in black tea varieties consumed in Saudi Arabia. Bulletin of environmental contamination and toxicology, 81(1): 101–104.

Azushima, A. 2003. Azushima, A. (2003). Trend of Ultrafine grained steel. In Proceedings of the 24th Symposium on Technology on Plasticity. 53–60.

Azushima, A., Kopp, R., Korhonen, A., Yang, D.Y., Micari, F., Lahoti, G.D., Groche, P., Yanagimoto, J., Tsuji, N., Rosochowski, A. & Yanagida, A. 2008. Severe plastic deformation (SPD) processes for metals. CIRP Annals, 57(2): 716–735.

Azzie, B.A.-M. 2002. Coal mine waters in South Africa: Their geochemistry, quality and classification. University of Cape Town.

Badmus, K.O., Coetsee-Hugo, E., Swart, H. & Petrik, L. 2018a. Synthesis and characterisation of stable and efficient nano zero valent iron. Environmental Science and Pollution Research, 25(24): 23667–23684.

Badmus, K.O., Coetsee-Hugo, E., Swart, H. & Petrik, L. 2018b. Synthesis and characterisation of stable and efficient nano zero valent iron. Synthesis and characterization of stable and efficient nano zerovalent iron, 25(24): 23667–23684.

Bae, S., Gim, S., Kim, H. & Hanna, K. 2016. Effect of NaBH4 on properties of nanoscale zero-valent iron and its catalytic activity for reduction of p-nitrophenol. Applied Catalysis B: Environmental, 182: 541–549.

Banks, D., Younger, P.L. & Dumpleton, S. 2012. The Historical Use Of Mine-Drainage And Pyrite-Oxidation Waters In Central And Eastern England, United Kingdom. Hydrogeology Journal 1992 4:4, 4(4): 55–68. https:

Barrie, J.D. & Hallberg, K.B. 2005. Acid mine drainage remediation options: a review. Science of the total environment, 338(1–2): 3–14.

de Beer, M., Maree, J.P., Liebenberg, L. & Doucet, F.J. 2014. Conversion of calcium sulphide to calcium carbonate during the process of recovery of elemental sulphur from gypsum waste. Waste Management, 34(11): 2373–2381.

Benzaazoua, M., Marion, P., Picquet, I. & Bussière, B. 2004. The use of pastefill as a solidification and stabilization process for the control of acid mine drainage. Minerals Engineering, 17(2): 233–243.

Benzie, I.F.F. & Strain, J.J. 1996. The Ferric Reducing Ability of Plasma (FRAP) as a Measure of "' Antioxidant Power "': The FRAP Assay. Analytical biochemistry, 239: 70–76.

Bjureby, E., Britten, M., Cheng, I., Kazmierska, M., Mezak, E., Munnik, V., Nandi, J., Pennington, S., Rochon, E., Schulz, N., Shahab, N., Vincent, J., Wei, M. & Short, R. 2009. The True Cost of Coal. How people and the planet are paying the price for the world's dirtiest fuel. International Nuclear Information System, 46(5).

Bowell, R., Smith, K.S., Plumlee, G.S., Hageman, P.L. & Kleinmann, R. 2016. Metal Recovery from Mine Waters: Feasibility and Options – an Example Assessment from the Colorado Mineral Belt, USA. In Proceedings IMWA 2016 Freiberg Germany. 1263–1266.

Broadhurst, J., Filho, J.A., Moyo, A., Nwaila, P., Sampa N'gandu, H., Shongwe, B., Sibanda, L., Stander, H.-M. & Harrison, S. 2019c. Resource Efficient and Socially Responsible Approaches for the Integrated Management of Mine Waste: Understanding the Risks, Opportunities, Enablers and Barriers Report to the Water Research Commission.

Cairncross, E., Kisting, S.K., Liefferink, M. & van Wyk, D. 2013. Case study on Extractive Industries prepared for the Lancet Commission on Global Governance, South Africa.

Cao, J., Clasen, P., Research, W.Z.-J. of M. & 2005, undefined. 2005. Nanoporous zero-valent iron. Journal of Materials Research, 20(12): 3238–3243.

Cayuela, A., Benítez-Martínez, S. & Soriano, M.L. 2016. Carbon nanotools as sorbents and sensors of nanosized objects: The third way of analytical nanoscience and nanotechnology. TrAC Trends in Analytical Chemistry, 84: 172–180.

Chadwick M. J, H.N.H. and L.N. eds. 2013. Environmental Impacts of Coal Mining & Utilization: A Complete Revision of environmental implications of expanded coal utilization. Elsevier.

Chen, Y., Yu, M., Xu, J., Chen, X. & Shi, J. 2009. Differentiation of eight tea (Camellia sinensis) cultivars in China by elemental fingerprint of their leaves. Journal of the Science of Food and Agriculture, 89(14): 2350–2355.

Cheng, S., Jang, J.H., Dempsey, B.A. & Logan, B.E. 2011. Efficient recovery of nano-sized iron oxide particles from synthetic acid-mine drainage (AMD) water using fuel cell technologies. Water Research, 45(1): 303–307.

Chibuike, G.U. & Obiora, S.C. 2014. Heavy Metal Polluted Soils: Effect on Plants and Bioremediation Methods. Applied and Environmental Soil Science, 2014.

Chugh, Y.P., Biswas, D. & Deb, D. 2002. Underground placement of coal processing waste and coal combustion by-products based paste backfill for enhanced mining economics. Southern Illinois University (US).

Cogho, V.E. & van Niekerk, A.M. 2009. Optimum coal mine reclamation project. In International Mine Water Conference. 19–23.

Colling, A.V., Menezes, J.C.S.D.S. & Schneider, I.A.H. 2011. Bioprocessing of pyrite concentrate from coal tailings for the production of the coagulant ferric sulphate. Minerals Engineering, 24(11): 1185–1187.

Cornell, R.M. & Schwertmann, U. 2003. The iron oxides: structure, properties, reactions, occurrences and uses. John Wiley & Sons.

Costa, M.C., Martins, M., Jesus, C. & Duarte, J.C. 2008. Treatment of acid mine drainage by sulphate-reducing bacteria using low-cost matrices. Water, air, and soil pollution, 189(1): 149–162.

Cundy, A.B., Hopkinson, L. & Whitby, R.L.D. 2008. Use of iron-based technologies in contaminated land and groundwater remediation: A review. Science of The Total Environment, 400(1–3): 42–51.

Darezereshki, E., Ali, ·, Vakylabad, B., Pourseyedi, S., Zarea, · Elham & Moravvej, Z. 2022. Methylene Blue Degradation Over Green Fe 3 O 4 Nanocatalyst Fabricated Using Leaf Extract of Rosmarinus officinalis. Topics in catalysis: 1–14.

Demirezen, D. & Aksoy, A. 2006. Heavy metal levels in vegetables in Turkey are within safe limits for Cu, Zn, Ni and exceeded for Cd and Pb. Journal of Food Quality, 29(3): 252–265.

Dumett, Miguel A, Keener, James P, Dumett, M A & Keener, J P. 2014. Mathematical Biology The pyrite iron cycle catalyzed by Acidithiobacillus ferrooxidans. J. Math. Biol, 69: 449–467.

Durand, J.F. 2012. The impact of gold mining on the Witwatersrand on the rivers and karst system of Gauteng and North West Province, South Africa. Journal of African Earth Sciences, 68: 24–43.

Duruibe, J.O., Ogwuegbu, M.O.C. & Egwurugwu. 2007. Heavy metal pollution and human biotoxic effects. International Journal of Physical Sciences, 2(5): 112–118.

Eisler, R. 2004. Arsenic hazards to humans, plants, and animals from gold mining. Springer New York. https://link.springer.com/chapter/10.1007/0-387-21729-0_3 4 October 2022.

Evangelou, V.P. (Bill) & Zhang, Y.L. 2009. A review: Pyrite oxidation mechanisms and acid mine drainage prevention. Review in Environmental Science and Technology, 25(2): 141–199.

Feng, D., Aldrich, C. & Tan, H. 2000. Treatment of acid mine water by use of heavy metal precipitation and ion exchange. Minerals Engineering, 13(6): 623–642.

Fernandez, P.L., Pablos, F., Mart\in, M.J. & Gonzalez, A.G. 2002. Multi-element analysis of tea beverages by inductively coupled plasma atomic emission spectrometry. Food Chemistry, 76(4): 483–489.

Ferrara, L., Montesano, D. & Senatore, A. 2001. The distribution of minerals and flavonoids in the tea plant (Camellia sinensis). Il farmaco, 56(5–7): 397–401.

Ficklin, W.H., Plumlee, G.S., Smith, K.S. & Mchugh, J.B. 1992. Geochemical classification of mine drainages and natural drainages in mineralized areas. In International symposium on water-rock interaction. 381–384.

Gall, J.E., Boyd, R.S. & Rajakaruna, N. 2015. Transfer of heavy metals through terrestrial food webs: a review. Environmental Monitoring and Assessment, 184(4): 1–21.

Gillham, R.W. & O'Hannesin, S.F. 1994. Enhanced degradation of halogenated aliphatics by zero-valent iron. Ground water, 32(6): 958–969.

Gitari, W.M., Fatoba, O.O., Petrik, L.F. & Vadapalli, V.R.K. 2009. Leaching characteristics of selected South African fly ashes: Effect of pH on the release of major and trace species. Journal of Environmental Science and Health, 44(2): 206–220.

Gitari, W.M., Petrik, L.F., Etchebers, O., Key, D.L. & Okujeni, C. 2008. Utilization of fly ash for treatment of coal mines wastewater: Solubility controls on major inorganic contaminants. Fuel, 87(12): 2450–2462.

Gitari, W.M., Petrik, L.F., Key, D.L. & Okujeni, C. 2011a. Interaction of acid mine drainage with Ordinary Portland Cement blended solid residues generated from active treatment of acid mine drainage with coal fly ash. Journal of Environmental Science and Health, 46(2): 117–137.

Gunther, P., M.W. and V.N.A., 2006. A sustainable mine water treatment initiative to... - Google Scholar. In Water in Mining Conference. 14–16.

Gunther, P. & Naidu, T. 2008. Mine water reclamation—towards zero disposal. In In WISA Biennial Conference, Johannesburg, South Africa.

Gunther, P., W, Mey. & and A. Van Niekerk. 2006. Gunther P, Mey W and Van Niekerk A (2006) A sustainable mine water treatment initiative to provide portable water to a South African city-A public private partnership. In water in Mining Conference (pp. 14-16).

Halstead, W.J. 1986. Use of fly ash in concrete. NCHRP Synthesis of Highway Practice, (127).

Han, W.Y., Shi, Y.Z., Ma, L.F. & Ruan, J.Y. 2005. Arsenic, cadmium, chromium, cobalt, and copper in different types of Chinese tea. Bulletin of environmental contamination and toxicology, 75(2): 272–277.

Harrison, S., Broadhurst, J., van Hille, R., Oyekola, O., Bryan, C., Hesketh, A. & Opitz, A. 2010a. A systematic approach to sulphidic waste rock and tailings management to minimize acid rock drainage formation. Report to the water research commission.

Hedin, R., Environmental, H. & Hedin, R.S. 2003. Land Contamination & Reclamation. Land contamination and Reclamation, 11(2): 93–98.

Hedin, R.S., Watzlaf, G.R. & Nairn, R.W. 1994. Passive Treatment of Acid Mine Drainage with Limestone. Journal of Environmental Quality, 23(6): 1338–1345.

Herlekar, M., Barve, S. & Kumar, R. 2014. Plant-mediated green synthesis of iron nanoparticles. Journal of Nanoparticles, 2014.

Hoag, G.E., Collins, J.B., Holcomb, J.L., Hoag, J.R., Nadagouda, M.N. & Varma, R.S. 2009. Degradation of bromothymol blue by 'greener'nano-scale zero-valent iron synthesized using tea polyphenols. Journal of Materials Chemistry, 19(45): 8671–8677.

Hota, P. & Behera, B. 2015. Coal mining in Odisha: An analysis of impacts on agricultural production and human health. The Extractive Industries and Society, 2(4): 683–693.

Huang, L., Weng, X., Chen, Z., … M.M.-S.A.P. & 2014, undefined. 2014. Green synthesis of iron nanoparticles by various tea extracts: comparative study of the reactivity. Molecular and Biomolecular Spectroscopy, 130: 295–301.

Hutton, B., Kahan, I., Naidu, T. & Gunther, P. 2009a. Operating and maintenance experience at the Emalahleni water reclamation. In International Mine Water Conference, pretoria South Africa. 415–430.

Jaganyi, D. & Wheeler, P.J. 2003. Rooibos tea: equilibrium and extraction kinetics of aspalathin. Food chemistry, 83(1): 121–126.

Johnson, D.B. 2003a. Chemical and microbiological characteristics of mineral spoils and drainage waters at abandoned coal and metal mines. Water, Air, and Soil Pollution: Focus, 3(1): 47–66.

Johnson, D.B. & Hallberg, K.B. 2005a. Acid mine drainage remediation options: a review. Science of The Total Environment, 338(1–2): 3–14.

Jomova, K. & Valko, M. 2011. Advances in metal-induced oxidative stress and human disease. Toxicology, 283(2–3): 65–87.

Kalombe, R.M., Ojumu, T.V., Katambwe, V.N., Nzadi, M., Bent, D., Nieuwouldt, G., Madzivire, G., Kevern, J. & Petrik, L.F. 2020. Treatment of acid mine drainage with coal fly ash in a jet loop reactor pilot plant. Minerals Engineering, 159: 106611.

Karthikeyan, D.K., Nagarajan, D.N. & Sivaprakasam, D.S. 2019. Study on Innovative Building Materials Used in Fly Ash Bricks Manufacturing with Various Mix Proportion. IRE journals, 2(9): 68–75.

KootbodienOO T, M.A. and M.N. 2012. Heavy metal contamination in a school vegetable garden in Johannesburg. South Africa Medical Journal, 102(4): 226–227.

Koralegedara, N.H., Pinto, P.X., Dionysiou, D.D. & Al-Abed, S.R. 2019. Recent advances in flue gas desulfurization gypsum processes and applications – A review. Journal of Environmental Management, 251: 109572.

Kuang, Y., Wang, Q., Chen, Z., Megharaj, M. & Naidu, R. 2013. Heterogeneous Fenton-like oxidation of monochlorobenzene using green synthesis of iron nanoparticles. Journal of colloid and interface science, 410: 67–73.

Kucera, J., Bouchal, P., Lochman, J., Potesil, D., Janiczek, O., Zdrahal, Z. & Mandl, M. 2013. Ferrous iron oxidation by sulfur oxidizing Acidithiobacillus ferrooxidans and analysis of the process at the levels of transcription and protein synthesis. Antonie Van Leeuwenhoek, 4(103): 905–919.

Kumar, K.M., Mandal, B.K., Kumar, K.S., Reddy, P.S. & Sreedhar, B. 2013. Biobased green method to synthesise palladium and iron nanoparticles using Terminalia chebula aqueous extract. Spectrochimica Acta Part A: Molecular and Biomolecular Spectroscopy, 102: 128–133.

Kumar Mishra, M. & Rao Karanam, U.M. 2006. Geotechnical characterization of fly ash composites for backfilling mine voids. Geotechnical and Geological Engineering, 24(6): 1749–1765.

LeFevre, S.R. & Sharpe, W.E. 2002. Acid stream water remediation using limestone sand on bear run in southwestern Pennsylvania. Restoration Ecology, 10(2): 223–236.

Li, L., Fan, M., Brown, R.C., van Leeuwen, J., Wang, J., Wang, W., Song, Y. & Zhang, P. 2010. Synthesis, Properties, and Environmental Applications of Nanoscale Iron-Based Materials: A Review. Critical Reviews in Environmental Science and Technology, 36(5): 405–431.

Li, X.Q. & Zhang, W.X. 2006. Iron nanoparticles: The core-shell structure and unique properties for Ni(II) sequestration. Langmuir, 22(10): 4638–4642.

Lin, J., Weng, X., Dharmarajan, R. & Chen, Z. 2017. Characterization and reactivity of iron-based nanoparticles synthesized by tea extracts under various atmospheres. Chemosphere, 169: 413–417.

Liu, A. & Zhang, W. 2014. Fine structural features of nanoscale zero-valent iron characterized by spherical aberration corrected scanning transmission electron microscopy (Cs-STEM). Analyst, 139(18): 4512–4518.

Lopes, D. v, Sillanpää, M. & Wolkersdorfer, C. 2016. Nitrate reduction in real mine water using zero-valent iron (ZVI) and iron waste. In Proceeding of International Congress of MINING Meets Water-Conflicts and Solutions (IMWA). 11–15.

López-Téllez, G., Barrera-Díaz, C.E., Balderas-Hernández, P., Roa-Morales, G. & Bilyeu, B. 2011. Removal of hexavalent chromium in aquatic solutions by iron nanoparticles embedded in orange peel pith. Chemical Engineering Journal, 173(2): 480–485.

Lottermoser, B.G. 2007. Mine wastes (second edition): Characterization, treatment, environmental impacts. Springer Berlin Heidelberg.

Lourenco, M. & Curtis, C. 2021. The influence of a high-density sludge acid mine drainage (AMD) chemical treatment plant on water quality along the blesbokspruit wetland, South Africa. Water SA, 47(1): 35–44.

Lu, L., Ai, Z., Li, J., Zheng, Z., Li, Q. & Zhang, L. 2007a. Synthesis and Characterization of Fe-Fe 2 O 3 Core-Shell Nanowires and Nanonecklaces. Crystal growth & Design, 7(2): 459–464.

Madzivire, G., Petrik, L.F., Gitari, W.M., Ojumu, T. v. & Balfour, G. 2010. Application of coal fly ash to circumneutral mine waters for the removal of sulphates as gypsum and ettringite. Minerals Engineering, 23(3): 252–257.

Mahmoud, A.S., Farag, R.S. & Elshfai, M.M. 2020. Reduction of organic matter from municipal wastewater at low cost using green synthesis nano iron extracted from black tea: Artificial intelligence with regression analysis. Egyptian Journal of Petroleum, 29(1): 9–20.

Makanjuola, S.A. 2017. Influence of particle size and extraction solvent on antioxidant properties of extracts of tea, ginger, and tea--ginger blend. Food science \& nutrition, 5(6): 1179–1185.

Malik, J., Szakova, J., Drabek, O., Balik, J. & Kokoska, L. 2008. Determination of certain micro and macroelements in plant stimulants and their infusions. Food chemistry, 111(2): 520–525.

Mangena, S.J. & Brent, A.C. 2006. Application of a Life Cycle Impact Assessment framework to evaluate and compare environmental performances with economic values of supplied coal products. Journal of Cleaner Production, 14(12–13): 1071–1084.

Masindi, V., Chatzisymeon, E., Kortidis, I. & Foteinis, S. 2018. Assessing the sustainability of acid mine drainage (AMD) treatment in South Africa. Science of the Total Environment, 635: 793–802.

Mativenga, P.T., Marnewick, A. & others. 2018. Water quality in a mining and water-stressed region. Journal of cleaner production, 171: 446–456.

Matlock, M.M., Howerton, B.S. & Atwood, D.A. 2002. Chemical precipitation of heavy metals from acid mine drainage. Water Research, 36(19): 4757–4764.

Mbhele, N.R., van der Merwe, W., Maree, J.P. & Theron, D. 2009. Recovery of sulphur from waste gypsum. In International Mine Water Conference. 622–630.

McCarthy, T.S. and P.K. 2009. Coal mining of the highveld and its implications for future water quality in the Vaal river system. In International Mine Water Conference. 19–23.

McKenzie, J.S., Jurado, J.M. & De Pablos, F. 2010. Characterisation of tea leaves according to their total mineral content by means of probabilistic neural networks. Food Chemistry, 123(3): 859–864.

Mehra, A. & Baker, C.L. 2007. Leaching and bioavailability of aluminium, copper and manganese from tea (Camellia sinensis). Food Chemistry, 100(4): 1456–1463.

Menezes, J., Silva, R.A., Arce, I.S. & Schneider, I.A.H. 2010. Production of a poly-alumino iron sulphate coagulant by chemical precipitation of a coal mining acid drainage. Minerals Engineering, 23(3): 249–251.

Menezes, J.C.S.S., Silva, A.R.A., Arce, A.I.S. & Schneider, I.A.H. 2009a. Production of a Poly-ferric Sulphate Chemical Coagulant by Selective Precipitation of Iron from Acidic Coal Mine Drainage. Mine Water and the Environment, 28(4): 311–314.

Merovich, G.T. & Petty, J.T. 2007. Interactive effects of multiple stressors and restoration priorities in a mined Appalachian watershed. Hydrobiologia, 575(1): 13–31.

Migliorini, M., Pigino, G., Bianchi, N., Bernini, F. & Leonzio, C. 2004. The effects of heavy metal contamination on the soil arthropod community of a shooting range. Environmental Pollution, 129(2): 331–340.

Misra, M., Yang, K. & Mehta, R.K. 1996. Application of fly ash in the agglomeration of reactive mine tailings. Journal of Hazardous Materials, 51(1–3): 181–192.

MoDiselle M. 2012. Review of the sulphur industry in the Republic of South Africa, 2012. Department of Mineral Resources, Pretoria.

Mogashane, T.M., Maree, J.P., Mujuru, M. & Mphahlele-Makgwane, M.M. 2020. Technologies that can be Used for the Treatment of Wastewater and Brine for the Recovery of Drinking Water and Saleable Products. John Wiley & Sons, Ltd.

Moghaddam, M.A., Mahvi, A.H., Asgari, A.R., Yonesian, M. & others. 2008. Determination of aluminum and zinc in Iranian consumed tea. Environmental monitoring and assessment, 144(1): 23–30.

Mohapatra, M. & Anand, S. 2010. Synthesis and applications of nano-structured iron oxides/hydroxides--a review. International Journal of Engineering, Science and Technology, 2(8).

Morais. S, C.F.G. and P.M.D.L. 2012. Environmental Health: Emerging Issues and Practice - Google Books. Environmental health-Emerging issues and practice, 10(1): 227–245.

Morin, K.A. & Hutt, N.M. 2001. Environmental geochemistry of minesite drainage: practical theory and case studies, digital edition.

Mossion, A., Potin-Gautier, M., Delerue, S., Le Hécho, I. & Behra, P. 2008. Effect of water composition on aluminium, calcium, and organic carbon extraction in tea infusions. Food Chemistry, 106(4): 1467–1475.

Mpode Ngole-Jeme, V. & Fantke, P. 2017. Ecological and human health risks associated with abandoned gold mine tailings contaminated soil.

Mueller., N.C. and N.B. 2010. Nano zero valent iron – The solution for water and soil remediation? Report of the Observatory NANO.

Müller, N.C. & Nowack, B. 2010. Nano zero valent iron—The solution for water and soil remediation. Report of the Observatory NANO: 1–34.

Munnik, R. & Pulles, W. 2009. The implementation of the recently developed best practice guidelines for water resource protection in the South African mining industry. In International Mine Water Conference. 22–28.

Naicker, K., Cukrowska, E. & McCarthy, T.S. 2003. Acid mine drainage arising from gold mining activity in Johannesburg, South Africa, and environs. Environmental Pollution, 122(1): 29–40.

Naik, N., Bahadure, B., Res, C.J.-Int.J.Comput.Eng. & 2014, undefined. 2014. Strength and durability of fly ash, cement and gypsum bricks. Int. J, Comput, Res, 4(5): 1–4.

Neculita, C.-M., Zagury, G.J. & Bussière, B. 2007. Passive Treatment of Acid Mine Drainage in Bioreactors using Sulfate-Reducing Bacteria. Journal of Environmental Quality, 36(1): 1–16.

Ngole-Jeme, V.M. & Fantke, P. 2017. Ecological and human health risks associated with abandoned gold mine tailings contaminated soil. PLOS ONE, 12(2): e0172517.

Nowack, B. 2010. Pollution Prevention and Treatment Using Nanotechnology. Nanotechnology, 2: 1–15.

Oakes, J.S. 2013. Investigation of iron reduction by green tea polyphenols for application in soil remediation.

O'Carroll, D., Sleep, B., Krol, M., Boparai, H. & Kocur, C. 2013. Nanoscale zero valent iron and bimetallic particles for contaminated site remediation. Advances in Water Resources, 51: 104–122.

Oelofse, S.H.H., Hobbs, P.J., Rascher, J. & Cobbing Csir, J.E. 2007. The pollution and destruction threat of gold mining waste on the Witwatersrand-A West Rand case study. In 10th International Symposium on Environmental issues and waste management in Energy and Mineral Production (SWEMP). 11–13.

Okamoto, M., Kobayashi, T. & Sakamoto, M. 2006. Physical properties of sediments deposited in the minewater from a closed coal mine. In Proceedings of the 10th Congress of the International Assoc for Engineering Geology and the Environment (Electronic resource), Nottingham, UK. Electronic optical disks (CD-ROM).

Palarski, J. 1993. The use of Fly Ash, tailings, rock and binding agents. In In Proc. Minfill. 403–408.

Parbs, A. & Birke, V. 2005. State-of-the-art report and inventory on already. EURODEMO.

Petrik, L., Burgers, C., Gitari, W., Surender, D., Reynolds, K., Ellendt, A., Etchebers, O., Kumar Vadapalli, V.R., Key, D. & Iwuoha, E. 2006. Stability and neutralisation capacity of potential mine backfill material formed by neutralisation of fly ash and acid mine drainage. In Final Report submitted to Water Research Commission K5.

Petty, J.T., Fulton, J.B., Strager, M.P., Merovich, G.T., Stiles, J.M. & Ziemkiewicz, P.F. 2010. Landscape indicators and thresholds of stream ecological impairment in an intensively mined Appalachian watershed. Journal of the North American Benthological Society, 29(4): 1292–1309.

Pohl, P. & Prusisz, B. 2007. Fractionation analysis of manganese and zinc in tea infusions by two-column solid phase extraction and flame atomic absorption spectrometry. Food Chemistry, 102(4): 1415–1424.

Pulles, W., Juby, G.J.G. & Busby, R.W. 1992. Development of the Slurry Precipitation and Recycle Reverse Osmosis (SPARRO) Technology for Desalinating Scaling Mine Waters. Water Science and Technology, 25(10): 177–192.

Pullin, H., Springell, R., Parry, S. & Scott, T. 2017. The effect of aqueous corrosion on the structure and reactivity of zero-valent iron nanoparticles. Chemical Engineering Journal, 308: 568–577.

R. Yuvakkumar, v. Elango, v. Rajendran & and N, K. 2011. Yuvakkumar, R., Elango, V., Rajendran, V., and Kannan

Ram, L.C. & Masto, R.E. 2014. Fly ash for soil amelioration: A review on the influence of ash blending with inorganic and organic amendments. Earth-Science Reviews, 128: 52–74.

Randall, D. G., Nathoo, J. & Lewis, A.E. 2011. A case study for treating a reverse osmosis brine using Eutectic Freeze Crystallization—Approaching a zero waste process. Desalination, 266(1–3): 256–262.

Rao, A., Bankar, A., Kumar, A.R., Gosavi, S. & Zinjarde, S. 2013. Removal of hexavalent chromium ions by Yarrowia lipolytica cells modified with phyto-inspired Fe0/Fe3O4 nanoparticles. Journal of contaminant hydrology, 146: 63–73.

Rashid, U., Bot, P.J., Farooq, M. & Anwar, F. 2008. Appraisal of heavy metals in different vegetables grown in the vicinity of an industrial area Appraisal of heavy metal contents in different vegetables grown in the vicinity of an industrial area. Pak. J. Bot, 40(5): 2099–2106.

Reddy, K.R., Kadlec, R.H., Flaig, E. & Gale, P.M. 1999. Critical Reviews in Environmental Science and Technology Phosphorus Retention in Streams and Wetlands: A Review Phosphorus Retention in Streams and Wetlands: A Review. Critical Reviews in Environmental Science and Technology, 29(1): 83–146.

Remy, P., Muhr, H., Plasari, E. & Ouerdiane, I. 2005. Removal of boron from wastewater by precipitation of a sparingly soluble salt. Environmental Progress, 24(1): 105–110.

Roonasi, P. 2007. Adsorption and Surface Reaction Properties of Synthesized Magnetite Nano-Particles. Doctoral dissertation, Luleå tekniska universitet).

Rösner, T. & van Schalkwyk, A. 2000. The environmental impact of gold mine tailings footprints in the Johannesburg region, South Africa. Bull Eng Geol Env, 59: 137–148.

Samuel, N. 2009. Establishing effective , appropriate and applicable technologies in treating contaminated surface water as part of a rehabilitation strategy for the princess dump in roodeport, west of Johannesburg.

Scheetz, B.E. & Earle, R. 1998a. Utilization of fly ash. Current Opinion in Solid State and Materials Science, 3(5): 510–520.

Scheetz, B.E. & Earle, R. 1998b. Utilization of fly ash. Current Opinion in Solid State and Materials Science, 3(5): 510–520.

Schippers, A., Jozsa, P.-G. & Sand, W. 1998. Short contribution Evaluation of the ef®ciency of measures for sulphidic mine waste mitigation. Applied microbiology and biotechnology, 49(6): 698–701.

Schutte, C. 2018. Value added utilisation possibilities of coal combustion products in South Africa. Doctoral dissertation, North-West University).

Seenivasan, S., Manikandan, N., Muraleedharan, N.N. & Selvasundaram, R. 2008. Heavy metal content of black teas from south India. Food control, 19(8): 746–749.

Sekar, S., Zintchem, A.A.E.A., Keshri, J., Kamika, I. & Momba, M.N.B. 2014. Bacterial profiling in brine samples of the Emalahleni Water Reclamation Plant, South Africa, using 454-pyrosequencing method. FEMS microbiology letters, 359(1): 55–63.

Setman, D., Schafler, E., Korznikova, E. & Zehetbauer, M.J. 2008. The presence and nature of vacancy type defects in nanometals detained by severe plastic deformation. Materials Science and Engineering: A, 493(1–2): 116–122.

Shahwan, T., Sirriah, S.A., Nairat, M., Boyac\i, E., Ero\uglu, A.E., Scott, T.B. & Hallam, K.R. 2011. Green synthesis of iron nanoparticles and their application as a Fenton-like catalyst for the degradation of aqueous cationic and anionic dyes. Chemical Engineering Journal, 172(1): 258–266.

Sharma, R. & Lall, N. 2014. Antibacterial, antioxidant activities and cytotoxicity of plants against Propionibacterium acnes. South African Journal of Science, 110(11–12): 01–08.

Shen, F.-M. & Chen, H.-W. 2008. Element composition of tea leaves and tea infusions and its impact on health. Bulletin of Environmental Contamination and Toxicology, 80(3): 300–304.

Shi, Z., Nurmi, J.T. & Tratnyek, P.G. 2011. Effects of nano zero-valent iron on oxidation- reduction potential. Environmental science \& technology, 45(4): 1586–1592.

Shoumkova, A.S. 2011. Magnetic separation of coal fly ash from Bulgarian power plants. Waste management & research, 29(10): 1078–1089.

Silva, R. de A., Secco, M.P., Lermen, R.T., Schneider, I.A.H., Hidalgo, G.E.N. & Sampaio, C.H. 2019. Optimizing the selective precipitation of iron to produce yellow pigment from acid mine drainage. Minerals Engineering, 135: 111–117.

Silva, R.D.A., Castro, C.D., Vigânico, E.M., Petter, C.O. & Schneider, I.A.H. 2012. Selective precipitation/UV production of magnetite particles obtained from the iron recovered from acid mine drainage. Minerals Engineering, 29: 22–27.

Simate, G.S. & Ndlovu, S. 2014. Acid mine drainage: Challenges and opportunities. Journal of Environmental Chemical Engineering, 2(3): 1785–1803.

Skousen, J., Yang, J.E., Lee, J.-S. & Ziemkiewicz, P. 2013. Geosystem Engineering Review of fly ash as a soil amendment. International journal of environment research and public health, 5(5): 450–456.

Sobolev, D. & Begonia, M.F.T. 2008. Effects of Heavy Metal Contamination upon Soil Microbes: Lead-induced Changes in General and Denitrifying Microbial Communities as Evidenced by Molecular Markers. International Journal of Environmental Research and Public Health 2008, Vol. 5, Pages 450-456, 5(5): 450–456.

Steed, V.S., Suidan, M.T., Gupta, M., Miyahara, T., Acheson, C.M. & Sayles, G.D. 2000. Development of a Sulfate-Reducing Biological Process To Remove Heavy Metals from Acid Mine Drainage. Water Environment Research, 72(5): 530–535.

Stumm, W. and J.J.M. 2012. Aquatic Chemistry: Chemical Equilibria and Rates in Natural Waters - Werner Stumm, James J. Morgan

Sun, J., Xie, X., Bi, H., Zhu, C., Wan, N., Huang, J., Nie, M., Li, D. & Sun, L. 2017. Solution-assisted ultrafast transfer of graphene-based thin films for solar cells and humidity sensors. Nanotechnology, 28(13): 1–7.

Sun, Y.P., Li, X. qin, Cao, J., Zhang, W. xian & Wang, H.P. 2006. Characterization of zero-valent iron nanoparticles. Advances in Colloid and Interface Science, 120(1–3): 47–56.

Sundrarajan, M., Chemistry, M.R.-E.-J. of & 2012, undefined. 2012. Novel cubic magnetite nanoparticle synthesis using room temperature ionic liquid. E-Journal of Chemistry, 9(3): 1070–1076.

Suresh, Y., Annapurna, S., Singh, A.K. & Bhikshamaiah, G. 2014. Green synthesis and characterization of tea decoction stabilized copper nanoparticles. Int. J. Innov. Res. Sci. Eng. Technol, 3(4): 11265–11270.

Tavakoli, A., Sohrabi, M. & Kargari, A. 2007. A review of methods for synthesis of nanostructured metals with emphasis on iron compounds. Chemical Papers, 61(3): 151–170.

Taylor, S. & Maphorogo, E.A. 2015. 104: Mining, Environmental, Pollution And Public Health challenges in Johannesburg.

Tchuldjian, H., Mcraktchiyska, M., Kamenova-Jouhimenko, S., Georgieva, V. & Mineva, & Y. 1994. Fly Ash Addition to Soils and its Influence on Some Properties of Soils and Biological Productivity of Plants. Biotechnology & Biotechnological Equipment, 8(2): 32–37.

Tiwari, B.K., Muthukumarappan, K., O' Donnell, C.P. & Cullen, P.J. 2008. Modelling colour degradation of orange juice by ozone treatment using response surface methodology. Journal of Food Engineering, 88(4): 553–560.

Tsai, H.C. & Lo, • S L. 2015. Boron recovery from high boron containing wastewater using modified sub-micron Ca(OH) 2 particle. International Journal of Environmental Science and Technology, 12(1): 161–172.

Tutu, H., McCarthy, T.S. & Cukrowska, E. 2008. The chemical characteristics of acid mine drainage with particular reference to sources, distribution, and remediation: The Witwatersrand Basin, South Africa as a case study. Applied Geochemistry, 23(12): 3666–3684.

Vadapalli, V.R.K., Fester, V., Petrik, L. & Slatter, P. 2014. Effect of fly ash size fraction on the potential to neutralise acid mine drainage and rheological properties of sludge. Desalination and Water Treatment, 52(37–39): 6947–6955.

Venkateswarlu, S., Rao, Y.S., Balaji, T., Prathima, B. & Jyothi, N.V. v. 2013. Biogenic synthesis of Fe3O4 magnetic nanoparticles using plantain peel extract. Materials Letters, 100: 241–244.

Vermeulen, P.D., Usher, B.H. & van Tonder, G.J. 2008. Determination of the Impact of Coal Mine Water Irrigation on Groundwater Resources Report to the Water Research Commission.

Vigânico, E.M., Colling, A.V., Silva, R.D.A. & Schneider, I.A.H. 2011. Biohydrometallurgical/UV production of ferrous sulphate heptahydrate crystals from pyrite present in coal tailings. Minerals Engineering, 24(11): 1146–1148.

Vishnoi, H., Bodla, Ramesh B, Kant, R. & Bodla, R B. 2018. Green tea (camellia sinensis) and its antioxidant property: a review. Int J Pharm Sci Res, 9(5): 1723–1736.

Wang, C.-B. & Zhang, W. 1997. Synthesizing nanoscale iron particles for rapid and complete dechlorination of TCE and PCBs. Environmental science & technology, 31(7): 2154–2156.

Wang, Z. 2013. Iron complex nanoparticles synthesized by eucalyptus leaves. ACS Sustainable Chemistry \& Engineering, 1(12): 1551–1554.

Watzlaf2, G.R. 1988. Chemical Inhibition of iron-oxiozing bacteria in waste rock sulfide tailings and effect on water quality 1. In The proceedings of Mine Drainage and Surface Mine Reclamation. 109–116.

Wei, X., Viadero Jr, R.C. & Buzby, K.M. 2005. Recovery of iron and aluminum from acid mine drainage by selective precipitation. Environmental Engineering Science, 22(6): 745–755.

Wei, X. & Viadero, R.C. 2007. Synthesis of magnetite nanoparticles with ferric iron recovered from acid mine drainage: Implications for environmental engineering. Colloids and Surfaces A: Physicochemical and Engineering Aspects, 294(1–3): 280–286.

Welna, M., Szymczycha-Madeja, A. & Pohl, P. 2013. A comparison of samples preparation strategies in the multi-elemental analysis of tea by spectrometric methods. Food research international, 53(2): 922–930.

Weng, X., Huang, L., Chen, Z., Megharaj, M. & Naidu, R. 2013. Synthesis of iron-based nanoparticles by green tea extract and their degradation of malachite. Industrial Crops and Products, 51: 342–347.

Wieder, R. and L.G. 1982. Modification of acid mine drainage in a freshwater wetland. Paper at Symp on Wetland of the unglaciated Appalachian Region.

Wu, W., He, Q. & Jiang, C. 2008. Magnetic iron oxide nanoparticles: synthesis and surface functionalization strategies. Nanoscale research letters, 3(11): 397.

Wu, W., Quanguo, A.E., Ae, H. & Jiang, C. 2008. Magnetic Iron Oxide Nanoparticles: Synthesis and Surface Functionalization Strategies. Nano Scale Research Letters, 3(11): 397–415.

Yaacob, W., Kamaruzaman, N., Eng, A.R.-Chem. & 2012, undefined. 2012. Development of nano-zero valent iron for the remediation of contaminated water. Chem. Eng, 28.

Yilmaz, A.E., Boncukcuoğlu, R., Bayar, S., Fil, B.A. & Kocakerim, M.M. 2012. Boron removal by means of chemical precipitation with calcium hydroxide and calcium borate formation. Korean Journal of Chemical Engineering 2012 29:10, 29(10): 1382–1387.

Zaal, S. & Sheridan, C. 2015. Permeable Concrete with Bio-Reactive Layers to Target Heavy Metals and Sulfates in Acid Mine Drainage. In 10th ICARD-IMWA Annual Conference, Santiago, Chile.

Zhang, G., Shen, Z., Liu, M., Guo, C., Sun, P., Yuan, Z., Li, B., Ding, D. & Chen, T. 2006. Synthesis and Characterization of Mesoporous Ceria with Hierarchical Nanoarchitecture Controlled by Amino Acids. The journal of physical chemistry, 110(50): 25782–25790.

Zhang, W. 2003. Nanoscale iron particles for environmental remediation: an overview. Journal of nanoparticle Research, 5(3–4): 323–332.

Zhu, F., Ma, S., Liu, T. & Deng, X. 2018. Green synthesis of nano zero-valent iron/Cu by green tea to remove hexavalent chromium from groundwater. Journal of Cleaner Production, 174: 184–190.

Zhu, H., Jia, Y., Wu, X. & Wang, H. 2009. Removal of arsenic from water by supported nano zero-valent iron on activated carbon. Journal of Hazardous Materials, 172(2–3): 1591–1596.

van Zyl, H.C., Maree, J.P., van Niekerk, A.M., van Tonder, G.J. & Naidoo, C. 2001. Collection, treatment and re-use of mine water in the Olifants River Catchment. Journal of the Southern African Institute of Mining and Metallurgy, 101(1): 41–46.